PRECIPITATION BEHAVIOUR OF CALCIUM PHOSPHATE – A MODEL FOR HARD TISSUE MINERALISATION

Alfred T.-C. Wong

Brasenose College

A thesis submitted for the degree of Doctor of Philosophy

in the University of Oxford

Trinity Term 1993

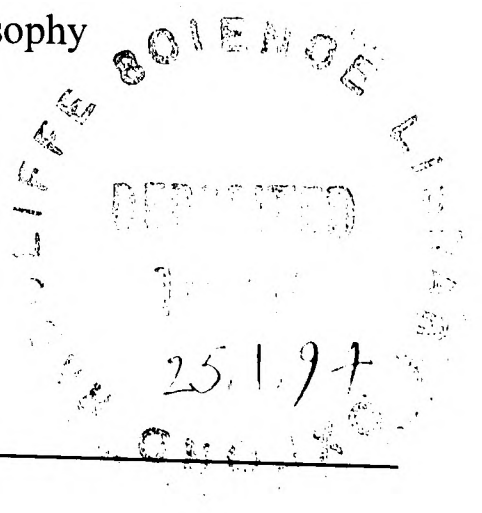

ABSTRACT

Precipitation behaviour of calcium phosphate – a model for hard tissue mineralisation

A.T.-C. Wong **Doctor of Philosophy**

Brasenose College, Oxford **Trinity Term, 1993**

Various aspects of the precipitation behaviour of calcium phosphate in aqueous media have been investigated using seeded growth in conjuction with constant-volume and constant-composition techniques under different physical and chemical conditions. In each case, precipitation was allowed to proceed for up to seven days. The solid precipitates thus obtained were characterised by means of scanning electron microscopy, powder X-ray diffractometry and wavelength dispersive spectroscopy.

During these precipitation experiments, the formation of the thermodynamically most stable and most supersaturated phase was invariably preceded by the appearance of less supersaturated precursor phase(s). These precursors subsequently underwent step-wise phase transformation into more stable phases. The preferred precursor and the rates of precipitation and phase transformation were dependent on the physical conditions and the chemical composition of the calcifying medium.

Under physiological conditions, precipitation experiments were also carried out with the addition of certain non-collagenous bone-specific bio-chemicals. Phosphoserine dramatically accelerated the precipitation of a large quantity of small plate-like crystals, while osteonectin and phosphatidylserine induced the formation of quasi-cubic crystals at a slow rate. Bone protein extract displayed the strongest inhibitory effect on calcification. Bovine serum albumin showed signs of being irreversibly adsorbed to the crystal surface, thereupon inducing a high degree of calcium deficiency in the precipitate stoichiometry.

Using a number of phosphorylated amino acids of different molecular masses, it was found that the processes of precipitation and phase transformation were facilitated by organic molecules whose phosphoryl functional groups were sterically accessible and highly electronegative. However, the acceleration brought about by the presence of a phosphorylated amino acid was maximised at an optimum concentration. The existence of such an optimum was very likely to be consequent of the competition for free calcium ions by the ongoing complexation and precipitation reactions.

A model has also been developed to describe and predict the precipitation behaviour of calcium phosphate. The model is based on the Avrami-Johnson-Mehl expression for three-dimensional nucleation and growth processes. Appropriate modifications to the original equation have been made, in order to adapt to this multi-ionic aqueous system. The resulting model has been found to describe the actual precipitation process accurately. It has also been applied to systems in which organic additives were present, and has again furnished predictions closely resembling the behaviour as observed experimentally.

Preface

The work described in this thesis was undertaken by the author in the Department of Materials at the University of Oxford between October 1990 and September 1993, under the supervision of Dr. J. T. Czernuszka, and supported by a Rhodes Scholarship. It is original except where reference to the work of others is acknowledged in the text.

No part of this thesis has previously been submitted for a degree at this or any other university. Various parts of the work have been published as follows:-

Clarke, K.I.; Wong, A.T.-C.; Czernuszka, J.T.; Dowling, B.; Triffitt, J.T. (1991):
"Crystallographic aspects of the growth of calcium phosphate on type I collagen and hydroxyapatite"
Bioceramics, **4**, 107.

Wong, A.T.-C.; Czernuszka, J.T. (1992):
"Effects of non-collagenous matrix proteins, fatty acid derivatives, etc. on the nucleation and growth of calcium phosphate on hydroxyapatite"
Mat. Res. Soc. Symp. Proc., **252**, 49.

Czernuszka, J.T.; Mathers, N.J.; Clarke, K.I.; Wong, A.T.-C. (1992):
"Mechanical properties of collagen / calcium phosphate composites"
Trans. World Biomat. Cong., **5**, 190.

Clarke, K.I.; Graves, S.E.; Wong, A.T.-C.; Francis, M.J.O.; Triffitt, J.T.; Czernuszka, J.T. (1993):
"Investigation into the formation and mechanical properties of a bioactive material based on collagen and calcium phosphate"
J. Mat. Sci.: Mat. Med., **4**, 107.

Wong, A.T.-C.; Czernuszka, J.T. (1993):
"Constant-composition study of the precipitation behaviour of calcium phosphate in the presence of non-collagenous bio-chemicals"
Mat. Res. Soc. Symp. Proc., in press.

Wong, A.T.-C.; Czernuszka, J.T. (1993):
"Prediction of precipitation and transformation behaviour of calcium phosphate in aqueous media"
Mat. Res. Soc. Symp. Proc., in press.

Wong, A.T.-C.; Czernuszka, J.T. (1993):
"Transformation behaviour of calcium phosphate: 1. Theory and modelling"
Coll. Surf. A: Physicochem. Eng. Aspects, in press.

Wong, A.T.-C.; Czernuszka, J.T. (1993):
"Transformation behaviour of calcium phosphate: 2. Experimental verification of theoretical predictions"
Coll. Surf. A: Physicochem. Eng. Aspects, to be submitted.

Acknowledgements

Just a brief(!) and informal note to those who have helped to keep me (in)sane throughout the past three years.

Dr. Jan Czernuszka - Jan, what can I say? You're without doubt the coolest supervisor I've ever known (especially with that unpronounceable surname of yours)! I don't know how you did it, but you've put up with my in(s)anity and my stubbornness during those mind-boggling discussions for three years. I hope I haven't scared you away from supervising new D.Phil. students! Dziękuję za pomoc.

Sir Anthony Kenny, the Rhodes Trustees and everybody at Rhodes House - Thanks for the scholarship [not forgetting those (generous!) conference grants] and the prestige. You have all made me feel very much at home here in Oxford. I hope I have lived up to the expectation and the reputation of the Scholarships.

Prof. Sir Peter Hirsch and Prof. Richard Brook - Thanks for taking the risk and letting me spend three enjoyable years in the Materials Department.

Former members of the Biomaterials Group - Karen Clarke, Dave Haddow, Nigel Leyland and Jon Thompson (co-inventor of "me number-crunching and me delamination"!). However, for some mysterious reason, they have all left and are having a better time elsewhere!

Chris Bowen and Surinder Kooner - fellow materials scientists with whom I have spent endless hours (not) having highly intellectual conversations in the common room or elsewhere. (Now that I've mentioned the two of you, when's the next dinner party?)

The original and the not-so-original "Boring Graduates" of Brasenose College - Adrian E. (This one's for you: $\#VI^{Maj7}$ - don't say I can't remember your favourite chord!), Matthias (mad biochemist and poet!), Chan (ek, mmm, ek...), Neil (Karaoke sometime?!), Craig (the rampant Scotsman), Nigel (on whom I can always rely to offer me a good cup of tea and his much treasured chocolate fingers), Robert (more British than Québecois - Not!), Graham (qui a besoin d'une femme! Ooh la la!), Adrian M. (Yo DJ, pump up the vibe!) and Danny (a.k.a. Chakadeva! - hit those high notes, muvva!). Life will never be the same without this "boring" possé.

"Dr." Chester Ho - my "most bestest" friend for God knows how long. (Actually 13 years and still counting!) Thanks for having the same sense of humour and taste (if any) in music as mine, and for the countless phone conversations which have been so mindlessly hilarious that it's scary! One thing I'm sure: you'll NEVER find me inside an operating theatre with a doctor remotely as crazy as you, Chester!

My parents and sisters - for being tolerant and supportive, and for simply being themselves! Madness does run in the family and is definitely hereditary - beware!

CONTENTS

Chapter 1
INTRODUCTION

In recent years, calcium phosphate has attracted major research effort in the field of biomaterials because it has shown promising potential as a substitute material for natural hard tissues, i.e. bones and cartilages. Since calcium phosphate is a natural constituent of bone, a sound knowledge of its precipitation behaviour is vital for a better understanding of the physiological mineralisation process, of which little is known at present. Also, the manufacture of a bone replacement material incorporating calcium phosphate also requires the same essential information. However, due to the complexity of the physical and chemical properties of various calcium phosphate phases, experimental results obtained by different researchers have often been confusing and contradictory.

The uncertainty concerning the precipitation behaviour of calcium phosphate arises from its possible existence in a number of solid phases and the high complexation potential of both calcium and phosphate ions in solution. These factors make the precipitation phenomenon extremely sensitive to changes in physical and chemical conditions during the reaction. Consequently, it has always been difficult to devise precipitation experiments which furnish reliable and reproducible results.

Since the precipitation behaviour is closely related to the physiological mineralisation process and the manufacture and application of a novel class of hard-tissue replacement material, it is also necessary to imitate the physiological condition as closely as possible in experimental studies. A main concern is the interaction between certain biological chemicals and calcium phosphate. These bio-chemicals may be responsible for controlling the strengthening and the rejuvenation of natural bone mass through their effects on the precipitation and dissolution rates of calcium phosphate minerals. However, the addition of organic chemicals into the calcifying media during precipitation experiments inevitably introduce further complexity into the system. Hence, there has been until now no systematic investigation in the exact rôles assumed by these bone-specific bio-chemicals.

There is, therefore, a real necessity to clarify the confusion over the precipitation behaviour of calcium phosphate and to examine the effects exerted by certain chemicals on the process. An experimental study has thus been performed. In the following chapters, the background of this study, the experimental approach, the results and their implication on the *in vivo* and *ex vivo* calcification phenomena will be discussed in detail. An attempt has also been made to develop a model, which takes into account the prevailing thermodynamic and kinetic factors, in order to describe and predict the precipitation behaviour in the intricate calcium phosphate system.

Chapter 2
THE RÔLE OF CALCIUM PHOSPHATE IN BIOMATERIALS RESEARCH

In this chapter, the reasons for the choice of calcium phosphate as a hard tissue replacement material will be discussed, with reference to the structure of natural bone, the requirements for a suitable substitute material and the processes of *in vivo* and *in vitro* mineralisation. Special emphasis will be put on the chemistry of calcium phosphate and its *ex vivo* precipitation behaviour in aqueous media. The effects of certain bio-chemicals on the calcification process will also be covered.

2.1 Bone

Bone is a unique form of living connective tissue in that it is extremely stiff and hard. This mechanical strength can be attributed to the deposition of a mineral phase within a relatively soft organic matrix.

2.1.1 Functions of bone

Bone serves multiple purposes. It constitutes the rigid skeleton of the body, but at the same time enhances mobility by acting as attachment sites for muscles and tendons. Also, it provides protection for various vital organs such as the heart, the brain, the lungs, etc. Its mechanical properties enable bone to perform these functions satisfactorily. Moreover, due to its high mineral content, bone serves as a reservoir of ions to maintain mineral homœostasis within the body (Vaughan 1981).

2.1.2 Constituents of bone

Bone mass can be divided into matrix material and minerals. Table 2.1 shows the average composition of bovine cortical bone, but the exact values vary appreciably with age, health condition, etc.

The organic bone matrix consists of collagen, the most abundant protein in metazoan animals due to its occurrence as a principal constituent of soft and hard tissues (Miller 1984). Collagen

Table 2.1 Composition of bovine cortical bone (Vaughan 1981)

Component	Percentage by weight (%)
Water	9.1
Inorganic mineral	68.8
Organic:	22.1
Collagen	19.5
Non-collagenous constituents: *including*	2.6
Chondroitin 4-sulphate	0.18
Bone sialoprotein	0.17
Glycoprotein	0.08
Albumin	0.06
Lipids	1.03
Peptides	0.12
Others	0.90

(*Greek: "to produce glue"*) is the major macromolecule of most connective tissues. The structure of collagen, like any other protein, is determined by the folding and the sequence of its amino acid chain. Each collagen molecule, about 3000 Å long and only 15 Å in diameter, is a left-handed triple helix comprising three sub-chains, each containing about 1000 amino acid residues. Collagen molecules then aggregate to form collagen microfibrils. Hodge & Petruska (1963) suggested a prototype model for the structure of collagen microfibrils (Figure 2.1). Collagen molecules, 4.4*D* in length, where *D* (approximately 690 Å) is the principal low-angle meridianal X-ray Bragg spacing of hydrated fibrils, are longitudinally staggered with respect to each other by the distance*D* (or some integral multiple thereof). Thus, fibrils have regions of different lateral geometry - 0.6*D* (414 Å) long regions in which "holes" are localised and 0.4 *D* (276 Å) long regions (the zone of molecular

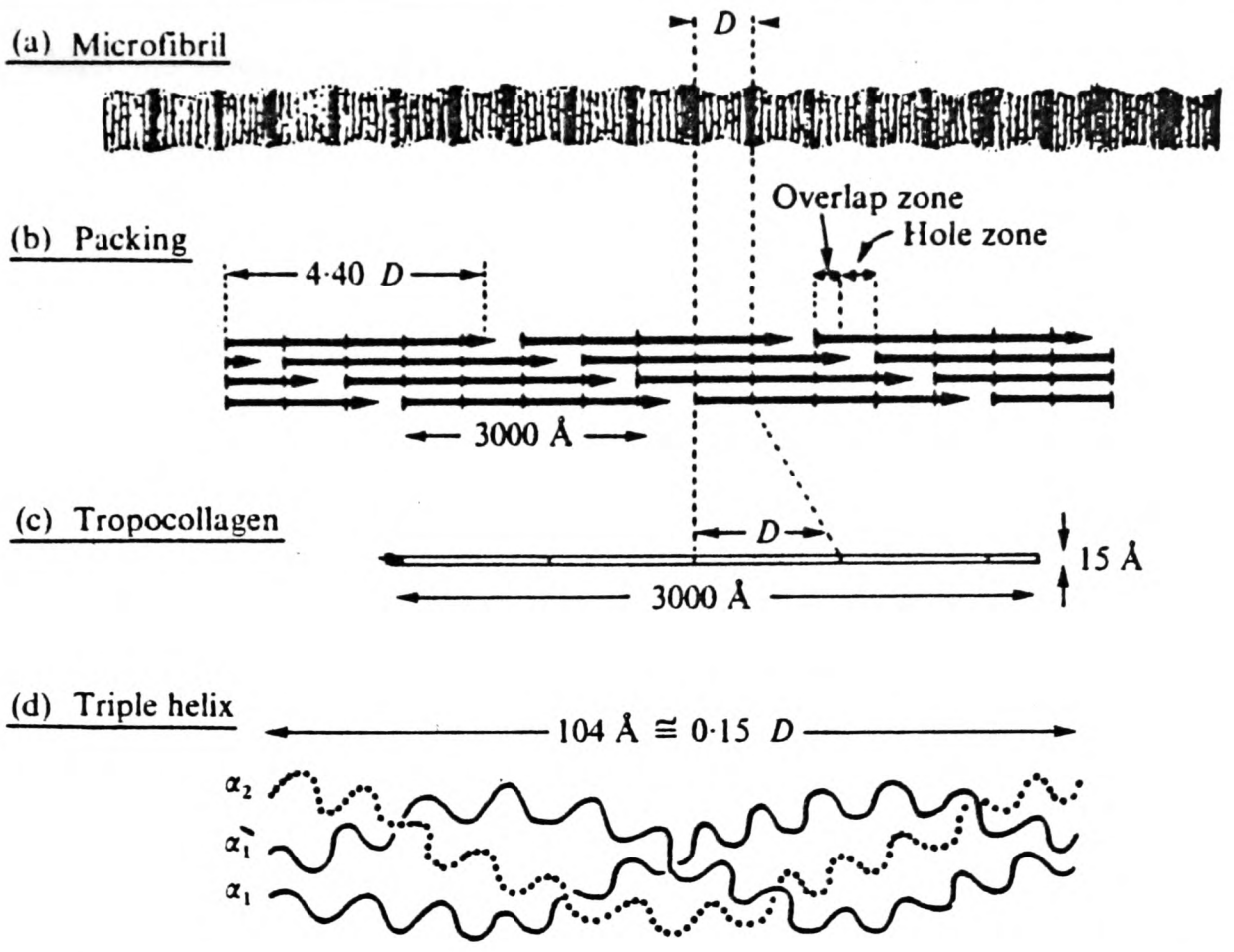

Figure 2.1 Diagrammatic representation of the structure of collagen (Vaughan 1981)

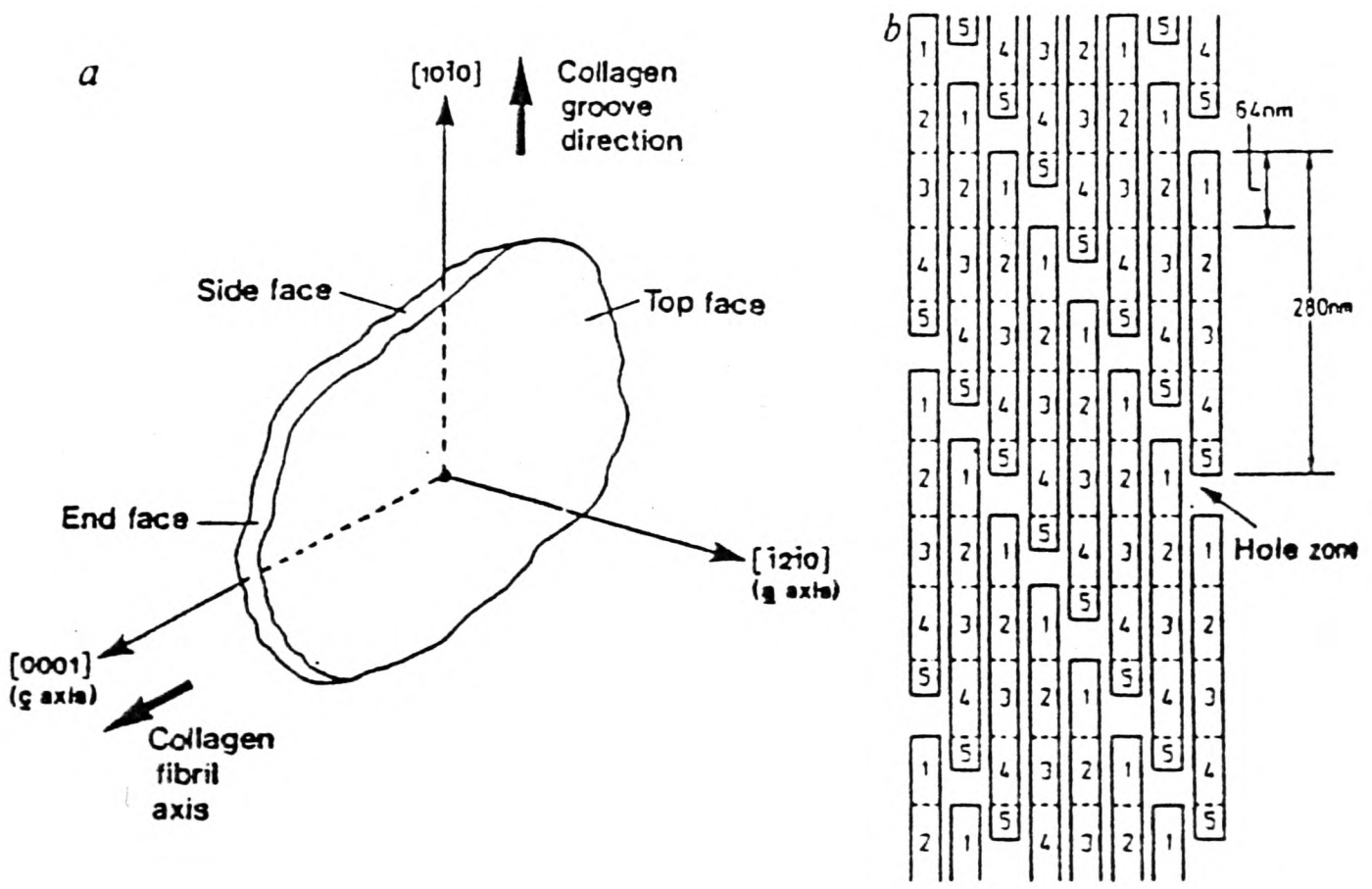

Figure 2.2 The relationship between the crystallographic properties of hydroxyapatite crystals and the pre-organisation of collagen fibrils. (*a*) The **a** ([$\bar{1}2\bar{1}0$]) and **c** ([0001]) axes of a plate-like HAP crystal are aligned perpendicular and parallel to the collagen fibril axis respectively; (*b*) The "quarter-stagger" model of collagen in planar form (Mann 1988).

overlap) in which molecular segments are more uniformly packed. These "holes" may act as nucleation sites for mineral deposition (see Sections 2.3 and 2.4).

Calcium phosphate is the predominant constituent of bone mineral. It is present as a mixture of hydroxyapatite crystals and a non-crystalline phase. There are also traces of carbonate, sodium, magnesium and fluoride. There is a close relationship between the collagen structure and the form and orientation of the calcium phosphate mineral which may find its place in the "holes" in the collagen fibrils (Figure 2.2).

2.2 Biomaterials for hard tissue replacement

Any non-drug substances suitable for inclusion in biological systems in order to augment or replace the functions of bodily tissues or organs can be regarded as biomaterials. To be acceptable as a biomaterial, a substance must exhibit the appropriate mechanical properties and be biocompatible, i.e. it must interact with the host in a non-toxic, controlled and predictable manner (Fuller & Rosen 1986).

Very stringent requirements need to be satisfied before a material can be considered a potential substitute for bone (Thomas & Cook 1985, Bonfield 1987). Obviously, it has to be biocompatible in the body environment (37 °C, *p*H 7.4). Mechanically, it must be able to withstand physiological forces without fracture due to either short-term overloading or long-term fatigue and stress. A high enough interfacial shear strength for the implant system to withstand load must be achieved immediately after implantation and maintained throughout the entire service life. Tribological characteristics are also important at joints. Throughout the years, different materials have been used, with different levels of success. They can be broadly classified into two categories - bioinert and bioactive materials.

2.2.1 Bioinert materials

A material is bioinert if it does not or almost does not influence the adjacent tissue biochemically after implantation, i.e. the leakage of ions or other matter from the implant into the surrounding tissue is well below detectability by the cells and bears no systematic effects. Materials which react with the surrounding may still be bioinert if the reaction products at the interface are

instantly and efficiently absorbed by the body fluids so that the surface of the implant is virtually covered in its entirety by natural body substances (Heimke 1989).

Owing to this extremely low reactivity, bioinert materials exert no biochemical influence on cell differentiation and proliferation (Heimke 1989). Hence, they provide a minimal stimulus to inflammation and the subsequent generation of soft fibrous reparative tissue (Williams 1991). Also, there is no biochemical information given to the cells about the presence of the implant which is consequently camouflaged against the host's immune system (Heimke 1989). However, since there is no reaction between the implant and the host, the substitute component needs to be bonded to the skeletal system of the host through the aid of additional adhesives.

Typical examples of bioinert bone replacement materials include inert metals and alloys, e.g. titanium. Traditionally, metallic materials were considered to be the only suitable candidates because they possess adequate strength and rigidity. They are also ductile and formable. As a result, not only can implants come in all shapes and sizes, they are also capable of accommodating minor adjustments during surgery. However, metals do present practical drawbacks. In particular, the very rigidity becomes a liability after implantation. Since metals are stiffer than natural bone, they tend to bear the brunt of any load placed on the bone as a result of load transfer in order to maintain equal strains. Now, bone is constantly undergoing remodelling and resorption which are cell-mediated processes controlled by a number of factors, including the stress level. An increase in the stress level normally stimulates bone growth and strengthening through the deposition of more mineral on the collagen network. Hence, stress shielding by the metallic implant subjects the bone to a sub-normal stress level or an altered stress pattern, leading to the preferential resorption of bone mass. As a consequence of this upset of equilibrium, the bone loses its mineral phases and is therefore weakened (Williams 1991). Eventually the bone shrinks, resulting in the loosening of the implant. The only remedy to this problems is by a revision surgery in which the original implant is replaced by a bigger substitute component. Unfortunately, this essentially becomes a vicious circle and it is impossible to avoid expensive and traumatic revisions which need to be performed on a regular basis.

2.2.2 Bioactive materials

This other group of biomaterials behave completely differently from the previous type. They play an active part in controlling the tissue response (Williams 1991). They enhance attachment at the interface by chemically bonding onto the tissue surface in the sense of a gluing effect, but without the addition of an adhesive (Hence & Wilson 1985, Katthagen 1987, Heimke 1989). Materials such as Bioglasses, coral and calcium phosphate have found progressively wider use in the orthopædic field. In cases where resorption of the implant is favoured, the body should be able to assimilate the implant, consequently resorbing and replacing the material with living cells, so that it may eventually survive and grow as if it were natural.

Calcium phosphate ceramics exhibit promising potential in this respect since their elementary component is present in bone naturally (Lavernia & Schönung 1991). *In vivo* and *in vitro* tests have shown that they bond with bone through the deposition of hydroxyapatite almost on the whole of the ceramic surface (Thomas & Cook 1985, Higashi *et al.* 1986, van Blitterswijk *et al.* 1990, Lavernia & Schönung 1991). This is apparently a normal bone-cementing mechanism which does not interfere with the deposition of mineral in nearby bone (Fuller & Rosen 1986). In fact, organic matter can be detected down to a depth of several crystal layers along grain boundaries (Osborn 1985). There is the prospect of continuing favourable bone medelling, rather than bone loss (Bonfield 1987). In addition, there are neither inflammatory nor rejection responses (Fuller & Rosen 1986). However, the main disadvantage of these ceramics is that calcium phosphate is too brittle to be used as a monolithic solid in joint prostheses (Williams 1991). When compared to the mechanical properties of natural bone, these ceramics exhibit lower ultimate strength, higher elastic modulus, less satisfactory fatigue life and they fail in a brittle manner (Lavernia & Schönung 1991). In order to exploit the high bioactivity of calcium phosphate, bioactive composites containing calcium phosphate have thus attracted a large amount of interest in biomaterials research.

2.3 Collagen / calcium phosphate biocomposites

Apart from living cells and water, collagen and calcium phosphate are the main constituents of bone. A composite incorporating the two should therefore exhibit excellent bio-properties

necessary for a bone substitute material. In order to synthesise a biomaterial which mimics the qualities of natural hard tissues, it is essential to understand the biological mineralisation process.

2.3.1 In vivo hard tissue mineralisation

There is at present no unified theory of the mechanism of bone mineralisation. In general, the theories of tissue mineralisation fall into three categories (Betts *et al.* 1981, Vaughan 1981):-

- *Raising the $[Ca^{2+}] \times [PO_4^{3-}]$ ionic product locally to levels at which spontaneous precipitation of mineral would occur.*

  The $[Ca^{2+}] \times [PO_4^{3-}]$ ionic product in circulating body fluids is below the level needed for spontaneous precipitation which, therefore, does not occur. As early as in 1923, Robison suggested that the enzyme alkaline phosphatase could hydrolyse phosphate esters and produce an excess of free inorganic phosphate ions, thereby elevating the $[Ca^{2+}] \times [PO_4^{3-}]$ ionic product at specific calcification centres to a degree required to produce precipitation. The elevation of this enzyme in bone is still regarded as a marker of active tissue mineralisation and its level in plasma is used as an indication of active bone metabolism. Posner (1978) suggested that in bone matrix the calcium-binding proteins may also be involved in raising the ionic product locally. Glimcher (1984), however, dismissed this idea of homogeneous nucleation because heterogeneous nucleation must have occurred on extraneous particles within the fluid phase before the point of unstable equilibrium for spontaneous homogeneous nucleation to take place. Moreover, spontaneous nucleation should result in random precipitate distribution, but this does not agree with experimental findings.

- *Provision of substances which would create nucleating sites or remove barriers to these sites*

  The precipitation of sparingly soluble salts involves nucleation followed by growth (Glimcher 1959). In Section 2.1.2, the close relationship between the collagen structure and the orientation of mineral crystals has already been pointed out. This relationship is independent of any direct physical contact with a solid phase of calcium phosphate located between the fibrils. In fact, it is the specific aggregation state of native type collagen fibrils that produces the volume

of space and the electrochemical and stereochemical distribution of the side chain groups, which together constitute a nucleation site (Glimcher 1984).

- *Presence of substances which prevent mineral formation and must be removed or rendered inactive to permit calcification.*

  Posner (1978) suggested that magnesium, which is largely present in bone as an intracellular ion, exerts a powerful effect in preventing the formation of apatite crystals. He also pointed out that very large proteoglycan molecules can somehow delay or prevent apatite precipitation. Fleisch & Neuman (1961) discovered that inorganic pyrophosphates can also inhibit the precipitation of any form of calcium phosphate in general. These barriers must be removed in order that calcification can proceed successfully.

2.3.2 In vitro collagen calcification

Most of the quantitative studies of collagen mineralisation have been made in solutions highly supersaturated with respect to a number of calcium phosphate phases. As might have been predicted from the intimate ultrastructural relationship between the collagen fibrils and the mineral phase of bone, native type reconstituted collagen fibrils and extensively demineralised and extracted particles of bone, consisting almost wholly of collagen fibrils, were found to be potent nucleation catalysts for the formation of apatite crystals (Glimcher*et al.* 1957, Glimcher 1959). The discovery that aggregates of collagen macromolecules into fibrils which were structurally different from the native form failed to nucleate calcium phosphate crystals from identical metastable solutions of calcium phosphate aptly demonstrated that the exquisite and specific property of nucleation catalysis resides in the special way which collagen macromolecules are assembled in native type fibrils. Electron microscopy of the *in vitro* samples showed that mineral particles were not randomly disposed within the collagen but were instead located within the "hole zone" regions of the fibrils and were distributed at regular intervals along the axial period. This is analogous to the configuration of the actual *in vivo* mineralisation product in bone. The study of *in vitro* calcification is, however, complicated by the intricate phase and solution chemistries of calcium phosphate, both of which have been the subject of investigation for a long time.

2.4 Chemistry of calcium phosphate

Owing to its promising prospects in orthopædic applications, calcium phosphate has become a major area of scientific research. Unfortunately, the development of this biomaterial has encountered plenty of difficulties. One of the main reasons is the highly complex phase and solution chemistries of this class of sparingly soluble inorganic compounds, about which high degrees of uncertainty still remain.

2.4.1 Phase chemistry

There are many different possible phases of calcium phosphate, due to the existence of phosphate radicals with different degrees of ionisation. These solid phases exhibit completely different physical and biochemical properties, and thus their suitabilities as hard tissue replacement materials vary dramatically. In order to select the most desirable candidates, it is necessary to establish a sound understanding of the phase chemistry of calcium phosphate.

§ Stoichiometric calcium phosphate

The existence in the form of numerous different phases makes calcium phosphate a very complex family of inorganic compounds. Amongst the various phases, three can be obtained in aqueous media in crystalline form. They are, in the order of increasing Ca/P atomic ratio: dicalcium phosphate dihydrate (DCPD), $CaHPO_4 \cdot 2H_2O$; octacalcium phosphate (OCP), $Ca_8H_2(PO_4)_6 \cdot 5H_2O$ or $Ca_4H(PO_4)_3 \cdot 2.5H_2O$; and hydroxyapatite (HAP), $Ca_{10}(PO_4)_6(OH)_2$ or $Ca_5(PO_4)_3(OH)$. The molecular structures of these three phases are shown in Figure 2.3, and their crystallographic properties are summarised in Table 2.2. Except in an extremely acidic environment (e.g. when $pH < 1$), HAP is thermodynamically the most stable, and thus the least soluble, phase over an extensive range of conditions.

It can be seen from Table 2.2 that the unit-cell parameters - b, c, α and β - are almost the same for OCP and HAP, revealing a possible layer type compatibility between these two structures. This hypothesis (Brown *et al.* 1957) has been confirmed (Brown *et al.* 1962), with evidence strongly supporting the view that the two salts contain structurally related layers parallel to (100), as shown in Figure 2.4 (Brown *et al.* 1981).

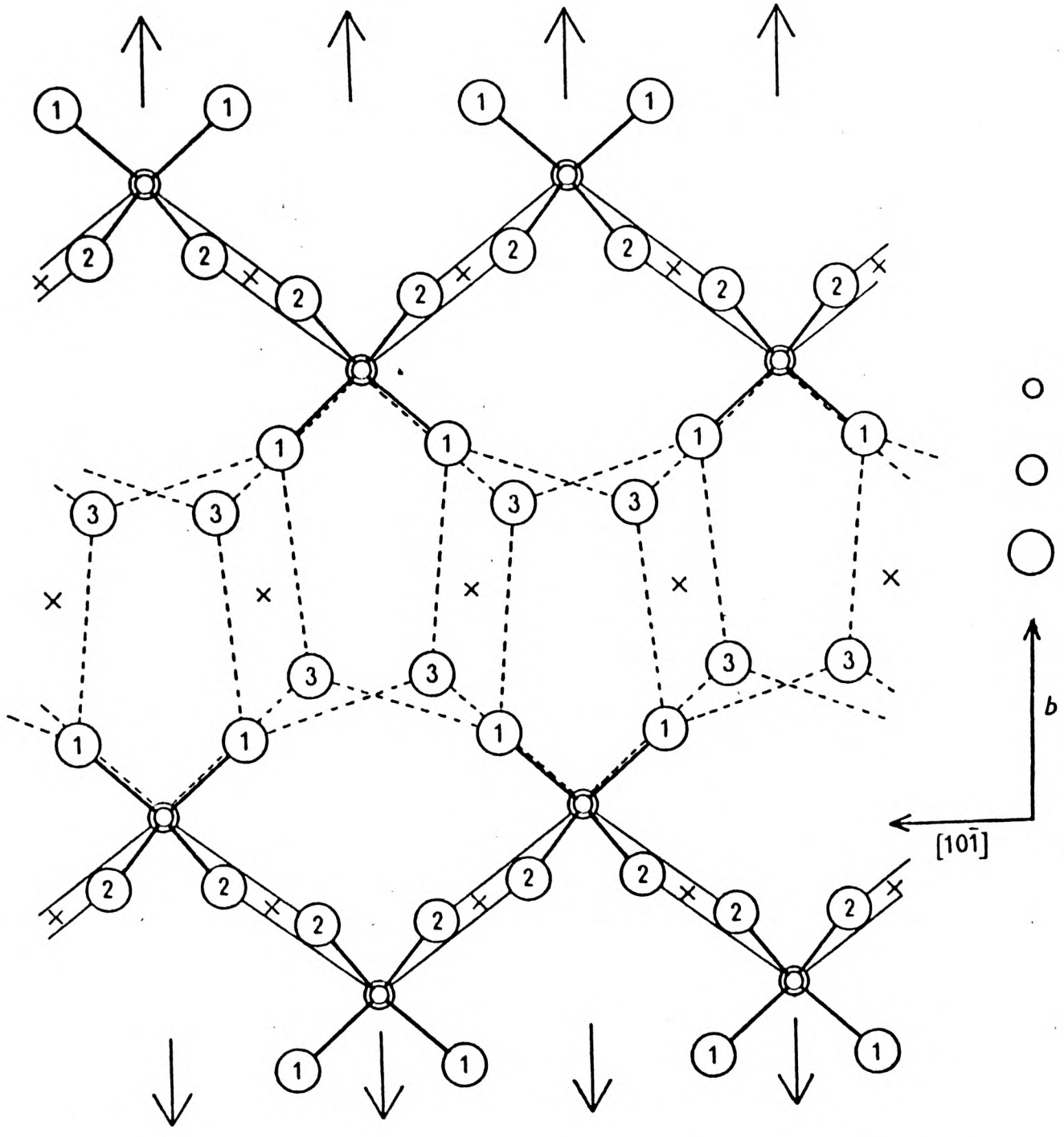

Atomic parameters:

Ca	(30/120, 99/120, 0)
P	(30/120, 39/120, 0)
O_1	(30/120, 46/120, 24/120)
O_2	(59/120, 32/120, 12/120)
O_3	(20/120, 112/120, 32/120)

Figure 2.3(a) Projection of the structure of DCPD on the plane perpendicular to [101] (Beevers 1958)

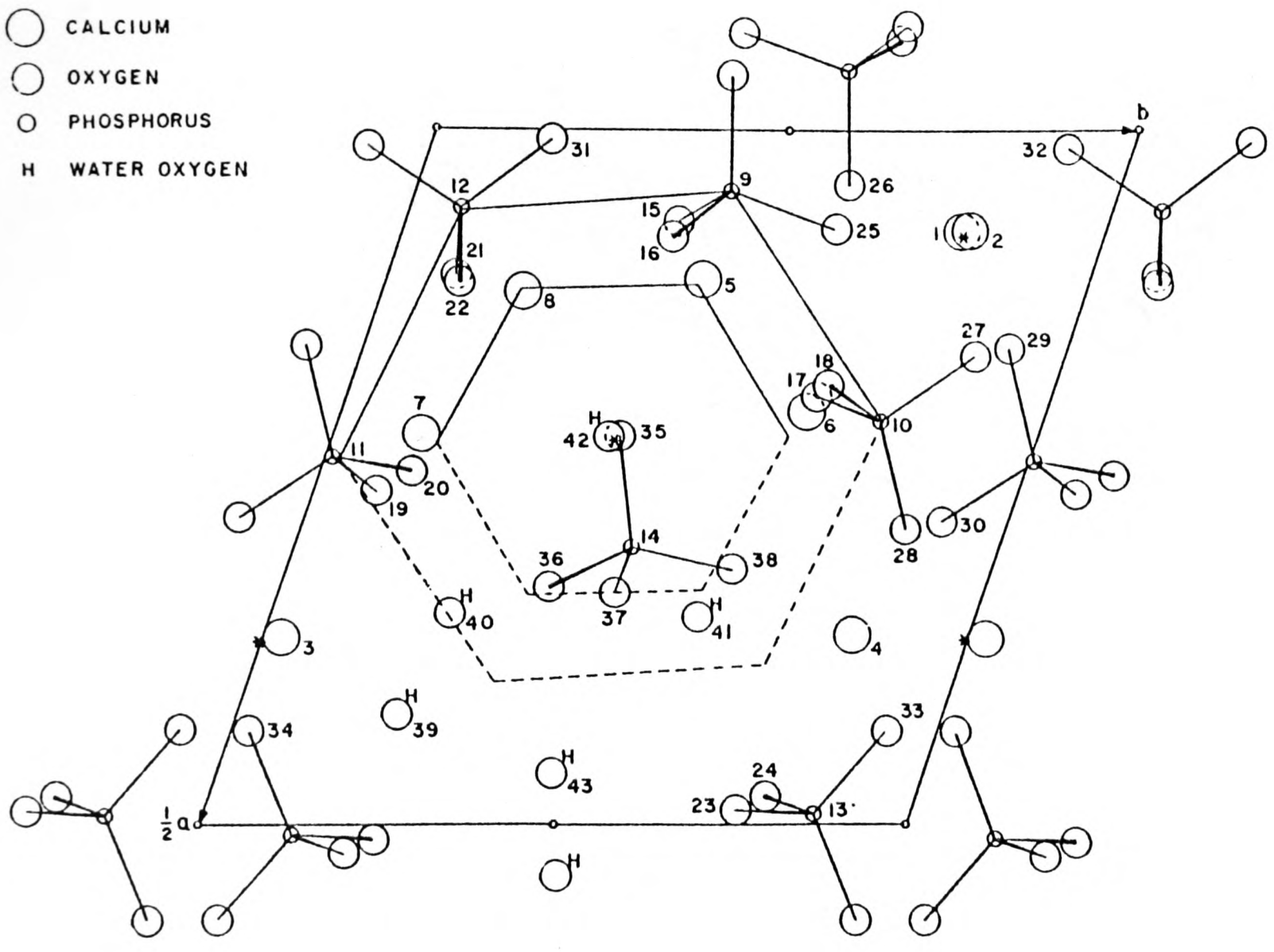

Figure 2.3(b) Projection of the structure of OCP on the x-y plane (Brown *et al.* 1962)

Atomic Positions of Octacalcium Phosphate

Atom number	Parameter x	y	z
Ca(1)	0·0717	0·7929	0·0048
Ca(2)	0·0702	0·8055	0·5029
Ca(3)	0·3660	0·0246	0·0226
Ca(4)	0·3628	0·8339	0·5313
Ca(5)	0·1071	0·4490	0·7617
Ca(6)	0·2016	0·6600	0·2745
Ca(7)	0·2178	0·1250	0·7697
Ca(8)	0·1153	0·2006	0·2606
P(9)	0·0431	0·4473	0·2576
P(10)	0·2073	0·7703	0·7749
P(11)	0·2348	0·0096	0·2736
P(12)	0·0562	0·0708	0·7577
P(13)	0·4922	0·8646	0·2668
P(14)	0·3001	0·4748	0·2455
O(15)	0·0638	0·3836	0·0744
O(16)	0·0751	0·3835	0·4312
O(17)	0·1897	0·6638	0·5986
O(18)	0·1812	0·6769	0·9556
O(19)	0·2589	0·0867	0·0798
O(20)	0·2452	0·1271	0·4356
O(21)	0·1031	0·0981	0·5766
O(22)	0·1072	0·1030	0·9404
O(23)	0·4891	0·7499	0·1045
O(24)	0·4803	0·7856	0·4661
O(25)	0·0693	0·6141	0·2600
O(26)	0·0386	0·6095	0·7360
O(27)	0·1600	0·8727	0·7506
O(28)	0·2852	0·8573	0·7889
O(29)	0·1547	0·9172	0·2606
O(30)	0·2803	0·9085	0·3103
O(31)	0·0075	0·1677	0·7543
O(32)	0·0133	0·9075	0·7606
O(33)	0·4317	0·9276	0·2311
O(34)	0·4332	0·0284	0·7404
O(35)	0·2187	0·4045	0·2111
O(36)	0·3272	0·3791	0·3976
O(37)	0·3335	0·4730	0·0520
O(38)	0·3153	0·6280	0·3236
O(39)	0·4212	0·2259	0·2577
O(40)	0·3481	0·2501	0·8202
O(41)	0·3506	0·6046	0·7244
O(42)	0·2205	0·3886	0·7743
O(43)	0·4618	0·4718	0·6508

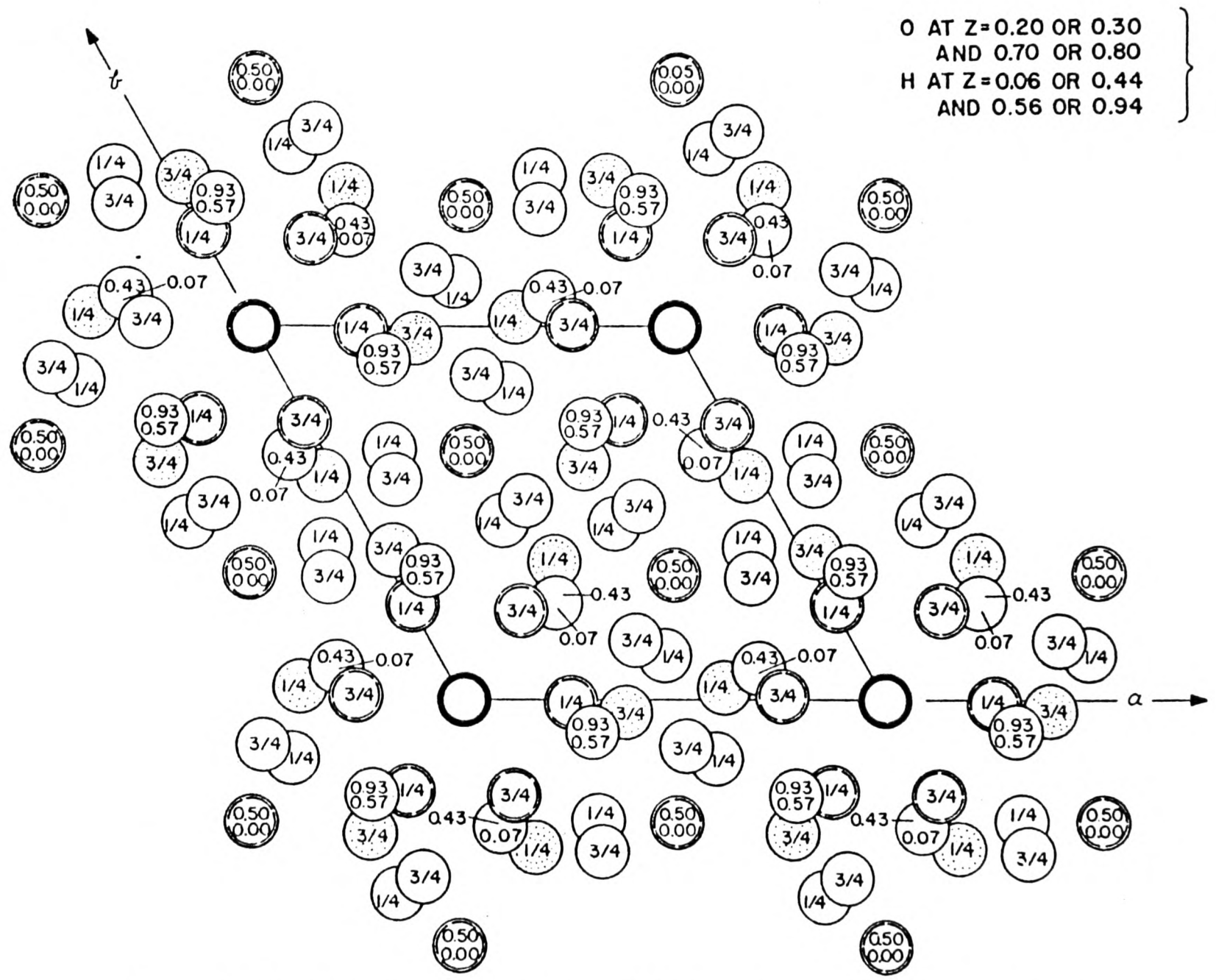

Figure 2.3(c) Projection of the structure of HAP on the x-y plane (Kay *et al.* 1964)

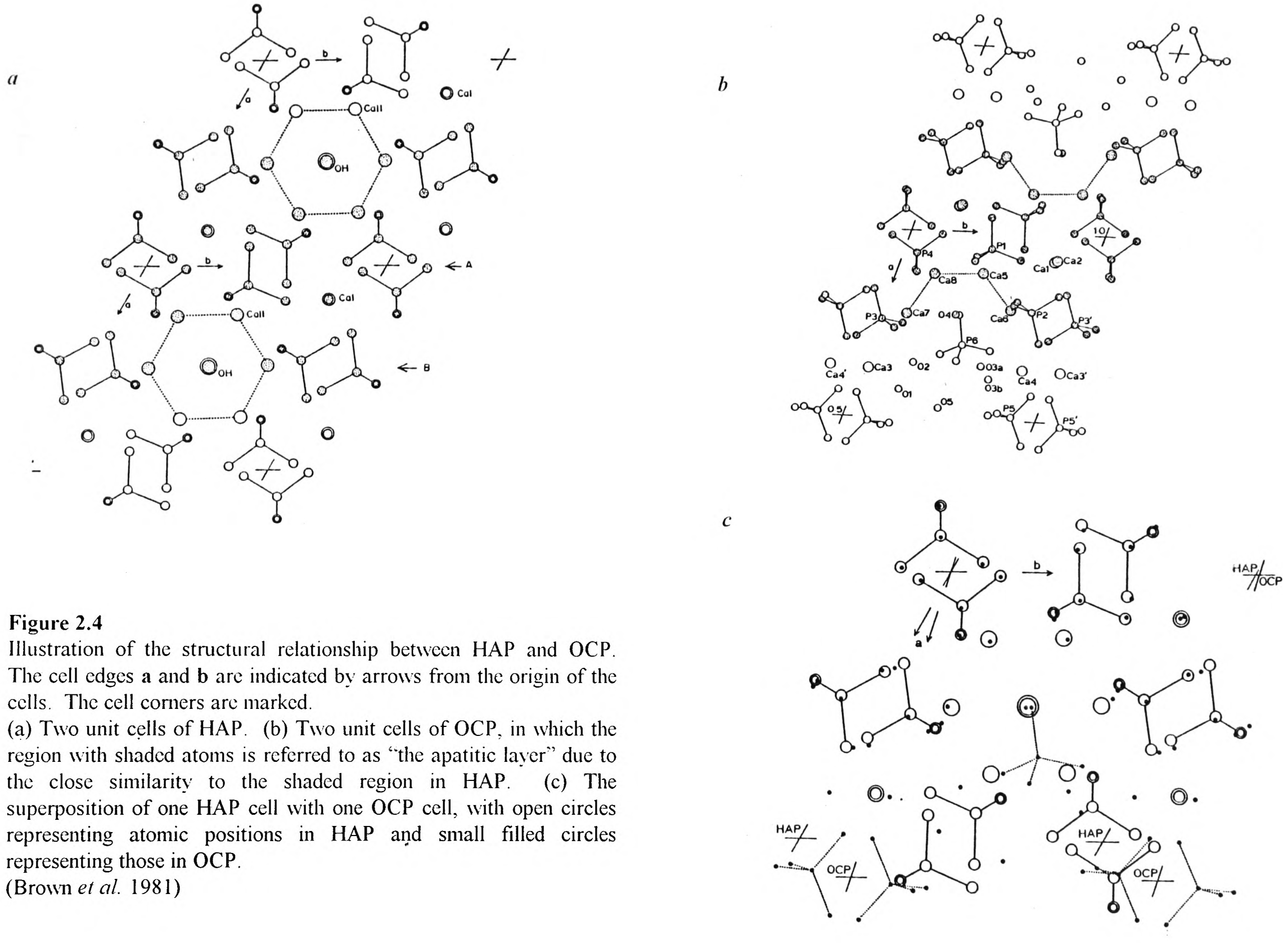

Figure 2.4
Illustration of the structural relationship between HAP and OCP. The cell edges **a** and **b** are indicated by arrows from the origin of the cells. The cell corners are marked.
(a) Two unit cells of HAP. (b) Two unit cells of OCP, in which the region with shaded atoms is referred to as "the apatitic layer" due to the close similarity to the shaded region in HAP. (c) The superposition of one HAP cell with one OCP cell, with open circles representing atomic positions in HAP and small filled circles representing those in OCP.
(Brown *et al.* 1981)

Table 2.2 Lattice characteristics of DCPD, OCP, HAP

	DCPD (Beaver *et al.* 1958)	**OCP** (Brown *et al.* 1981)	**HAP** (Posner *et al.* 1958)
System	Monoclinic	Triclinic	Hexagonal
Space group	I2/a	$P\bar{1}$	$P6_3/m$
a (Å)	5.812	19.715	9.432
b (Å)	15.180	9.534	9.432
c (Å)	6.239	6.839	6.881
α	90°	90.14°	90°
β	116.42°	92.52°	90°
γ	90°	108.67°	120°

A reliable way of determining the identity of a sample of calcium phosphate crystal is by powder X-ray diffraction. Figure 2.5 shows the theoretical X-ray diffraction peak patterns for perfect DCPD, OCP and HAP crystals. The DCPD pattern is very different from the other two, and is characterised by its distinctive (020) and (040) peaks. However, owing to their crystallographic similarities, the diffraction patterns of OCP and HAP are quite similar, particularly within the intermediate 2θ range of 15°-50°. In order to distinguish between the two, it is necessary to locate the peaks which are unique to each of the crystal structures. For OCP, there are a few characteristic low-angle peaks - (010), (020) and (110); whereas for HAP, the pattern is marked by a pair of close but discrete (212) and (310) peaks plus its high-angle peaks (at values of 2θ beyond the (004) peak) which are absent in the OCP pattern. These characteristic peaks will be used to identify the calcium phosphate precipitate obtained in experiments described later in this thesis.

In addition to these crystalline phases, an unstable amorphous phase of calcium phosphate (ACP) has been precipitated as a precursor solid phase (Eanes *et al.* 1965, Newseley 1966, Betts & Posner 1974). This phase is characterised by the absence of definite peaks in the X-ray diffraction

Figure 2.5 Theoretical X-ray diffraction peak patterns for perfect DCPD, OCP and HAP crystals

STOE Powder Diffraction System

2-AUG-93

DCPD - JCPDS powder diffraction file 11 293

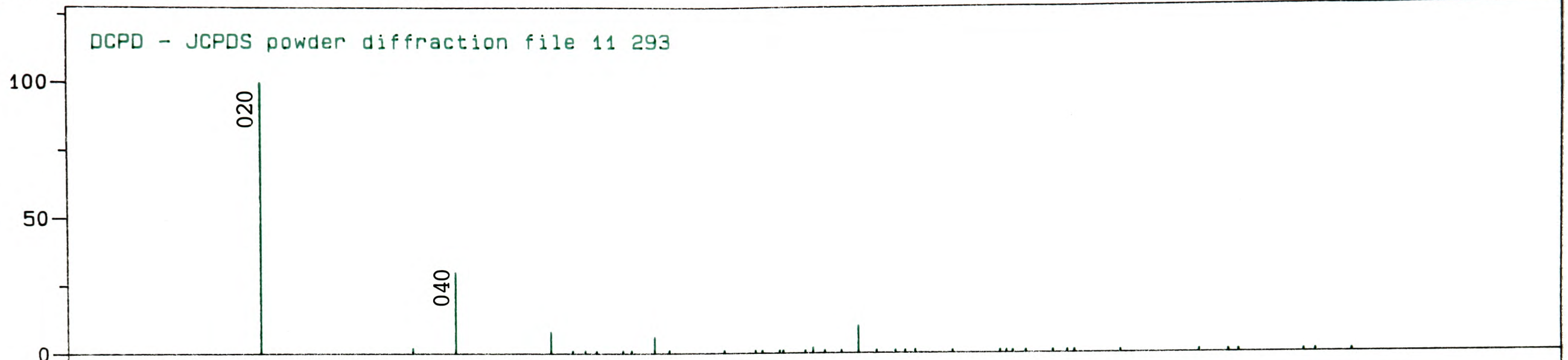

OCP - JCPDS powder diffraction file 26 1056

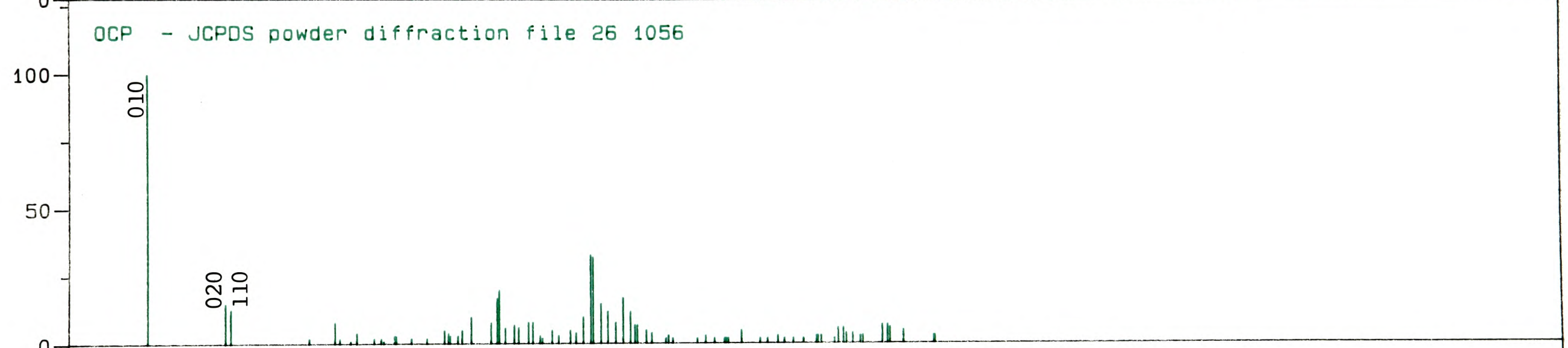

HAP - JCPDS powder diffraction file 9 432

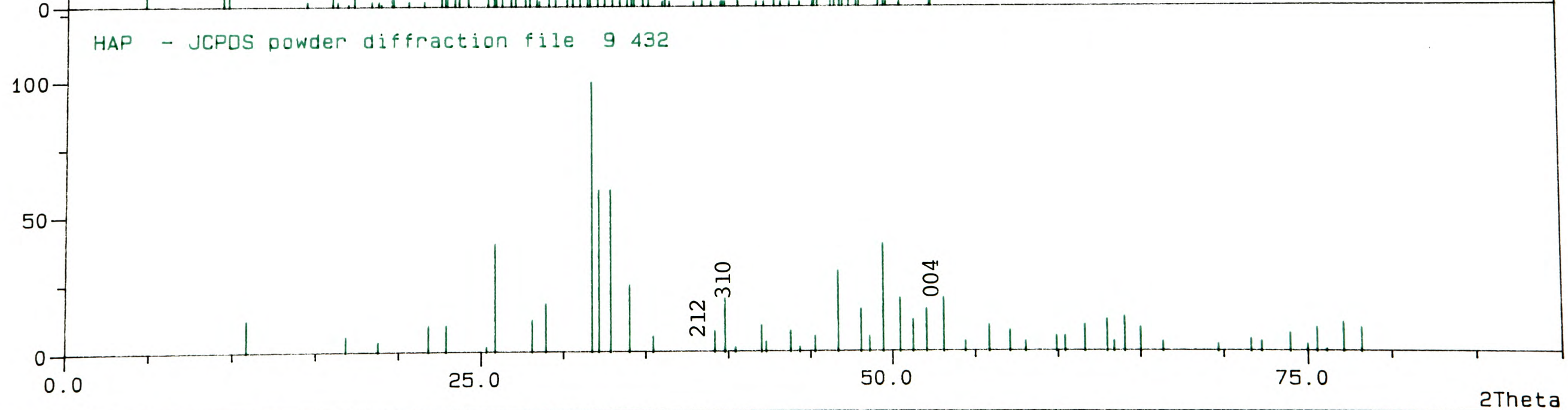

pattern, a low resolution in the infra-red absorption spectra, a spheroidal appearance in electron micrographs and some degree of short-range order in the radial distribution pattern in diffraction studies (Nancollas 1989).

§ Bone mineral

The physiological condition is bracketed well within the limits between which HAP is the most stable phase in terms of thermodynamics. Indeed, HAP is the phase which bone mineral resembles most closely. However, in spite of the structural similarities, bone apatite is characterised by the distinctive lack of crystal and chemical perfection and a high degree of internal disorder within crystals, i.e. biological apatite often exhibit a degree of non-stoichiometry and non-crystallinity. In fact, these intrinsic imperfections satisfy the teleological needs of bone mineral which has to be insoluble enough for physical stability, yet biochemically reactive enough to allow for normal resorption and redeposition needs (Posner *et al.* 1980). HAP is thermodynamically stable, while the non-stoichiometry and the lattice disorder provide the chemical driving force for structural perfection of the mineral crystal, thereby resulting in continuous replacement by new bone material. In addition to their intrinsic imperfection, these non-stoichiometric apatite crystals also have extremely small dimensions. As explained earlier, the deposition of bone mineral is restricted to certain "hole zones" along the collagen chains, and the maximum strengthening effect on the soft organic base network is therefore dictated by the dimensions of the mineral crystals in relation to these "holes". The size and shape of bone apatite crystals have been measured by direct visual observation through electron microscopy and by indirect calculations employing X-ray diffraction line-broadening (Eanes & Posner 1967, 1970, Posner 1978). The literature on this subject is confusing for several reasons (Posner *et al.* 1980). Size and shape of mineral particles change with species, age and health condition, and a single specimen contains a range of particle sizes and shapes (Betts *et al.* 1981). Also, different measuring techniques may yield different average values on polydisperse samples (Lundy & Eanes 1973). The two prevalent viewpoints consider bone apatite crystals to be either needle-like or, in contrast, plate-like. Posner (1978) found that the largest dimension of crystals never exceeds, on average, 400 to 500 Å, while the maxima of the two other dimensions are in the range of 200 to 300 Å and 25 to 50 Å respectively. Jackson *et al.* (1978), however, concluded that

bone mineral particles are plate-shaped, measuring 50 to 60 Å in the smallest dimension, while the largest dimension has a mean value of 320 to 360 Å, with a standard deviation of 130 to 190 Å and ranges up to about 1100 Å. The authors of both reports agreed that, in a given biological species, the crystal size is smaller at formation and increases in average size until maturity is reached, at which point there is a levelling of this growth process. Concomitant with the maturation of crystal size is an improvement in chemical perfection. The earliest bone crystal is deficient in calcium and hydroxide ions, but contained hydrogen ions (i.e. it is a more acidic form of calcium phosphate than hydroxyapatite); and the Ca/P molar ratio is in the range of 1.37 to 1.71 (Woodard 1962). With ripening, the bone crystal approaches, but never quite reaches, the stoichiometric HAP composition (Posner 1978).

Traces of iron, copper, lead, manganese, tin, aluminium, strontium and boron have been detected to be adsorbed to the bone matrix (Vaughan 1981). In addition, sodium, strontium and lead are capable of occupying the positions of calcium within the crystal lattice. Fluoride and chloride can chemically substitute for hydroxide, whereas carbonate can replace phosphate, although all these replacements are not strictly isomorphous, and more often than not, they create significant distortions within the crystal lattice. Lattice distortions are particularly prominent when, in order to attain a neutral balance in electrostatic charge, certain lattice ions need to be replaced by vacancies. Both the deficiency in calcium and hydroxide and the presence of alien ions activate bone mineral metabolically. They act as the driving force behind the improvement in crystal chemistry.

Well-defined crystalline apatite only accounts for less than 65% of the total mineral content, the rest of which is in the form of a non-crystalline calcium phosphate phase (Posner 1978, Glimcher 1984). The chemistry of this phase is not yet fully understood, but two contrasting theories have been proposed. One theory refers to this as an "amorphous" calcium phosphate phase. It has been reported to be present in both pre-osseous matrix and mature bone (Vaughan 1981). X-ray diffraction studies (Harper & Posner 1966, Termine & Posner 1967) indicated that this amorphous phase makes up approximately 40% of the mineral in the femurs of adult human, cow and rat. The molar Ca/P ratio is found to vary between 1.44 and 1.55 and it is thought to have a structure similar to that of ACP prepared synthetically (Posner *et al.* 1975). However, Glimcher (1984) found no evidence for the presence of an "amorphous" calcium phosphate phase. Instead, it was suggested

(Glimcher *et al.* 1981) that the difference in the X-ray diffraction patterns was due to the presence of highly imperfect calcium phosphate crystals which may be similar to DCPD or OCP. These phases have been found experimentally at the inception of *in vitro* mineralisation.

2.4.2 Solution chemistry

The solubility of any of the calcium phosphate phases in aqueous media is very low, but once it is dissolved, both the calcium and the phosphate ions participate extensively in complexation reactions, giving rise to the co-existence of a wide variety of charged and uncharged species, including Ca^{2+}, PO_4^{3-}, HPO_4^{2-}, $H_2PO_4^-$, $CaPO_4^-$, $CaHPO_4°$, $CaH_2PO_4^+$ and $CaOH^+$ (Zhang & Nancollas 1992). It becomes obvious that analytical studies of calcium phosphate precipitation in supersaturated solutions are extremely difficult as a result of all the different chemical equilibria established among the various ions and complexes. The formation of a particular phase depends on the availability of the appropriate lattice constituents, and is therefore affected by the chemical composition of the solution. The thermodynamic driving force for precipitation is known as supersaturation, which is the ratio between the product of the concentrations of the lattice ions in the solution and the solubility product of that phase. Now the solubilities of different phases can be graphically represented by solubility isotherms as in Figure 2.6. These isotherms show the variation

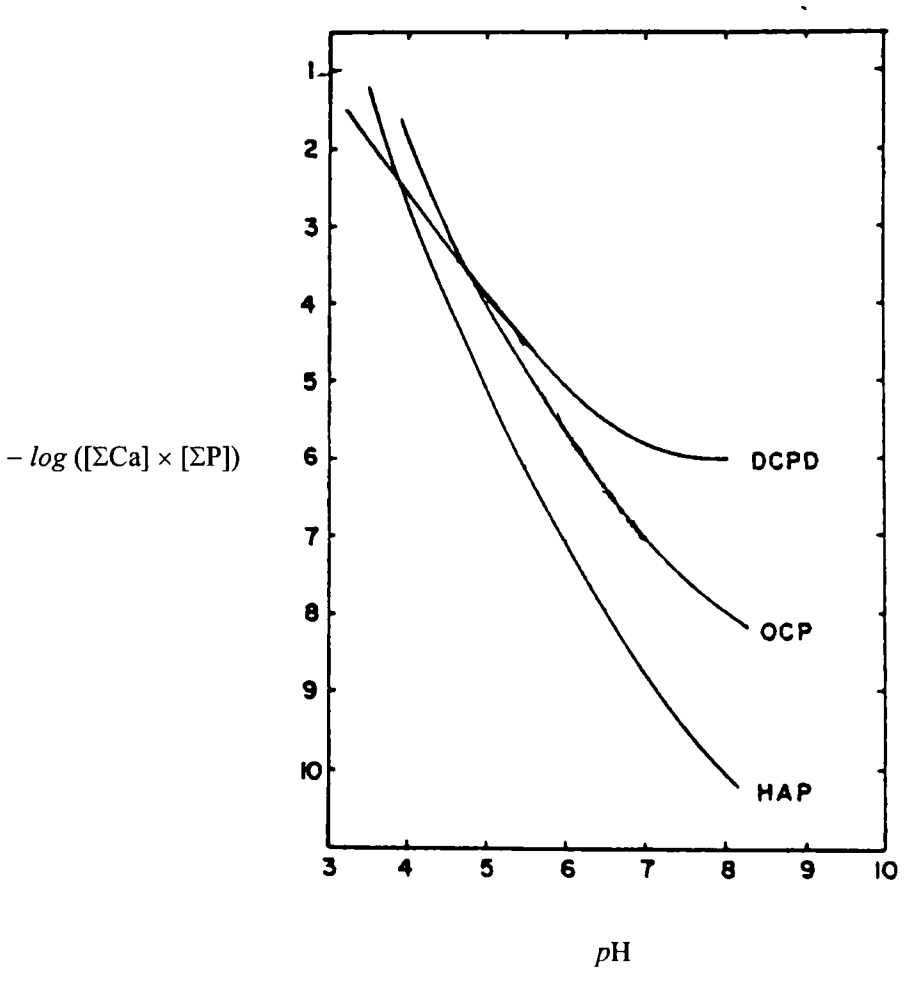

Figure 2.6
Plots of $-\ log\ ([\Sigma Ca] \times [\Sigma P])$ against *p*H in solutions saturated with respect to DCPD, OCP or HAP and containing 0.1 M KCl at 37 °C (Heughebaert & Nancollas 1984).

of the composition of an aqueous solution saturated with the various phases as a function of *p*H at a particular temperature, and any point above [below] a particular isotherm represents the composition of a solution which is supersaturated [undersaturated] with that phase. In order that the supersaturations can be evaluated, the exact concentration of each chemical species in the solution thus needs to be known. This requires the knowledge of the various chemical equilibria present within the solution. Detailed discussion on these inter-related equilibria will be given in Chapter 3.

2.5 Precipitation of calcium phosphate in aqueous media

The precipitation of calcium phosphate in aqueous solutions has been widely studied in the past under many different experimental conditions. In most of the cases, the mineralising solutions were considerably more supersaturated than typical biological media, in which the total calcium content is only around 1.9 to 2.6 mM (Berne & Levy 1988). Although it is most desirable to obtain HAP which is closest to bone mineral, the experimental precipitation of pure HAP has always been extremely difficult, despite the fact that the precipitation of HAP is in fact thermodynamically more favourable than that of any other phase under a wide range of conditions. Almost invariably, the formation of HAP is preceded by the emergence of precursor phases like DCPD and OCP, which subsequently transform to HAP after a certain induction period. This intricate precipitation and transformation phenomenon has been investigated by many researchers using a number of different techniques.

2.5.1 Spontaneous precipitation

Spontaneous precipitation requires the formation of nuclei of critical radius [$= -2\,\gamma_{SL} / \Delta G$, where γ_{SL} is the solid-liquid interfacial free energy and ΔG (which has a negative value) is the enthalpy of formation of the solid phase] (Pascoe 1978). Numerous kinetic studies have been made on the spontaneous precipitation of calcium phosphate in solutions containing lattice ions at concentrations considerably in excess of the solubility values (Nancollas *et al.* 1979, Arend *et al.* 1987). Precipitation was performed at the physiological *p*H of 7.4, with the starting total calcium content ranging from 0.3 mM to 0.1 M and the starting total phosphate content from 1 to 60 mM, and at 25 and 37 °C (Füredi-Milhofer *et al.* 1971, Brečević & Füredi-Milhofer 1972). Precipitates

isolated 24 hours after mixing were analysed. It was found that OCP was formed preferentially irrespective of the temperature. At 37 °C, due to rapid hydrolysis of OCP, apatitic calcium phosphate was obtained. It was also discovered that, as the total calcium and phosphate contents increased, the chance for DCPD formation became more likely.

Abbona *et al.* (1986, 1988, 1990) again carried out a range of spontaneous precipitation experiments at 25 °C, with the starting total calcium and phosphate contents ranging from 0.5 mM to 0.5 M, and a starting *p*H from 5.0 to 8.0. Invariably, the first precipitated phases were ACP and DCPD crystals. DCPD appeared first at low *p*H, whereas at higher *p*H ACP was first to precipitate, both accompanied by a drop in the *p*H. Ageing followed which led to the transformation to OCP and eventually HAP. It was also found that increasing the concentrations of calcium and phosphate reduced the *p*H at which nucleation commenced. Precipitation of OCP or HAP as first phases was never observed. This can be explained according to the classical nucleation theory, by considering that DCPD has a lower interfacial free energy than any of the other phases. DCPD also has the simplest chemical composition and the lowest number of atoms in the formula unit. Precipitation of DCPD and ACP, however, does leave the system in a metastable state, since the solution is still supersaturated with respect to the other phases, especially HAP. Therefore, these phases were found to be able to nucleate at a later stage. For ACP, since it is a non-equilibrium state, its instability impelled the evolution into a crystalline phase at a rate which was accelerated by high solution concentrations.

Boistelle & Valero-Lopez (1990) performed similar experiments at 37 °C and a *p*H range of 5.0 to 11.0. Parallel results were obtained, although they did report the nucleation of OCP and HAP at high *p*H's. Christoffersen *et al.* (1989), on the other hand, discovered the following sequences of transformation: at 15 °C, the formation of ACP was followed by DCPD; while at 30 and 42 °C, ACP was successively followed by OCP and calcium-deficient HAP.

It can be seen that a comparison of results of different spontaneous precipitation experiments is often confusing and inconclusive. Although attempts are usually made to control the mixing of reagent solutions, it is difficult to obtain reproducible results from spontaneous precipitation experiments since probabilistic nucleation of solid phases is likely to occur on foreign particles which are inevitably present in the solution. Moreover, this procedure suffers from the disadvantage that a

considerable amount of precipitation must have already taken place before the naked eye can detect any precipitate in the solution, making the experimental results somewhat questionable. Consequently, alternative methods need to be devised.

2.5.2 Seeded precipitation

Many of the above difficulties associated with spontaneous homogeneous precipitation can be avoided by studying the crystal growth of well-characterised seed crystals in metastable supersaturated solutions of calcium phosphate. Such solutions do not need to be as concentrated as those used in spontaneous precipitation experiments and their metastability can be maintained for periods of days. The kinetics of growth of the added seed material may then be studied by following the concentration changes in the fixed volume of solution as a function of time. Not only is this method capable of furnishing reproducible results, this model may also be closer to the physiological situation in which precipitation does take place on an existing solid surface.

It has been shown that constant-volume seeded precipitation experiments are consistently reproducible (Nancollas & Purdie 1964, Marshall & Nancollas 1969, Nancollas & Tomažić 1974). Precursors to the formation of HAP were obtained and verified to be DCPD at low*p*H values or OCP at high *p*H values. However, as the seeded precipitation process proceeds, the metastable solution becomes progressively more acidic and the dynamics of the reaction are constantly changing. From the solubility isotherms (Figure 2.6), it is clear that the solubilities, and hence the supersaturations, vary quite considerably with *p*H. As a result, it is impossible to continually maintain a high driving force in prolonged precipitation studies. Moreover, as the rate of *p*H drop is influenced by the solution composition and the precipitation rate, it is also very difficult to draw quantitative comparisons between constant-volume experiments performed under different experimental conditions. Thus, a means to monitor and control the solution *p*H must be devised in order to facilitate a more accurate assessment of the precipitation behaviour.

This has led to the development of the *p*H-stat method (Nancollas & Mohan 1970), where the *p*H of the calcifying solution is monitored and constantly adjusted to the starting value. Results from *p*H-stat experiments suggested that the overall precipitation reaction involves, in addition to the

formation of different phases of calcium phosphate, the concomitant redissolution of the thermodynamically unstable phases formed rapidly during the initial stage.

2.5.3 Constant-composition technique

Although the seeded crystallisation method has yielded high reproducibility and, in the case of the *p*H-stat technique, the proton activity can be held constant during the reaction, it still suffers from the disadvantage that the calcium and phosphate ionic concentrations decrease appreciably as the precipitation proceeds towards solubility equilibrium. During the course of the experiments, the supersaturated solutions are metastable with respect to various calcium phosphate phases which can form and subsequently redissolve as the concentrations in the solutions progressively decrease. Since the rate of change in solution concentration can become very slow as the reaction progresses, a relative analytical error of only a few per cent in the total calcium or the total phosphate content can preclude differentiation between the possible crystalline phases.

To overcome the problems associated with the change in solution composition during the precipitation process, the constant-composition technique has been developed (Tomson & Nancollas 1978). The basic principle is rather simple. Following the addition of well-characterised seed material to a stable supersaturated solution of calcium phosphate at the required *p*H, the concentrations of the lattice ions are monitored and maintained constant by the simultaneous addition of reagent solutions containing calcium, phosphate, hydrogen and hydroxide ions. This addition is triggered by any drop in the solution calcium content and/or any change in the solution*p*H, until the original composition is retained. A detailed explanation of the constant-composition technique is given later in Chapter 4.

An advantage of the constant-composition technique is the ability to select particular points on the solubility profile (Figure 2.6) for precipitation studies. Also, a relatively large extent of crystallisation can be achieved even at very low supersaturations (Nancollas 1989). Constant-composition experimental results (Tomson & Nancollas 1978, Heugheaert & Nancollas 1984) showed OCP to be the sole precursor phase to HAP in physiological conditions. After performing constant-composition experiments with solutions supersaturated only with respect to HAP,

Heughebaert *et al.* (1990) discovered the formation of a calcium- and hydroxide-deficient apatite with a Ca/P molar ratio of 1.57.

With the development of better techniques, in-depth studies of the precipitation behaviour of calcium phosphate have become increasingly more fruitful. However, owing to the complex chemistry of this family of inorganic compounds and its relevance in mineralisation processes, various aspects of the precipitation behaviour still require a lot of research efforts. It is vital that the phase transformation phenomenon is fully understood, and the effects of any external agents actively involved in physiological calcification must also be studied.

2.6 Effects of non-collagenous bio-chemicals on the precipitation of calcium phosphate

Although there is strong evidence in support of the native type of aggregation of the collagen macromolecules being necessary for the nucleation of a calcium phosphate solid phase within the hole zone regions of the fibrils, it cannot satisfactorily account for the rapidity of nucleus induction. *In vivo* and *in vitro* experiments have shown that it takes at least several weeks to initiate mineralisation within reconstituted collagen and decalcified bone, a rate much slower than biologically required. Now, for a condition to be biologically sufficient, it must enable an event to occur at a tempo consistent with biological functioning. So, even if the conditions in the extracellular fluids are adequate and stable, there may be other structural and chemical factors intimately related to the collagen fibrils, which, together with normal conditions in the extracellular fluid, constitute the necessary and biologically sufficient conditions for the heterogeneous nucleation of calcium phosphate (Glimcher 1984).

From the physiological, biochemical, structural and physicochemical points of view, a compound, in order to play a significant and positive rôle in the formation of the mineral phase, should ideally: (i) be synthesised by the cells of the tissue; (ii) be located ultrastructurally at the sites where mineralisation occurs; (iii) interact with the appropriate mineral ions constituting the inorganic crystals; and (iv) bind the ions in such a way that the bound ions remain reactive and can further interact with other inorganic ions to eventually form the inorganic crystals.

Certain bone-specific phosphoproteins have been found to satisfy all of these requirements (Glimcher 1984, Endo & Glimcher 1989). These proteins are present in natural hard tissues and their high phosphorus contents are consequent of the abundance of phosphorylated amino acid residues in their chemical structures. The most common of these residues are those of phosphoserine (SerP) and phosphothreonine (ThrP). Veis (1988) located the local collagen- and calcium-binding regions within molecules of phosphoproteins from bone and teeth. Since SerP is responsible for the phosphorus content of many phosphoproteins, some research effort has been dedicated to studying how SerP affects calcification on its own. Clarke (1991) showed that SerP not only promotes nucleation, but also suppresses growth, thus producing a large amount of small crystals.

However, not all phosphoproteins bear the same effects on the precipitation of calcium phosphate. Osteonectin (ONec), a bone-specific phosphoprotein characterised by Termine *et al.* (1981b), was found to bind both to HAP crystals and Type I collagen through different regions of the molecule and could therefore mediate the binding of HAP to collagen substrate. Collagen-bound ONec has a tendency to bond to calcium rather than phosphate ions in solution. However, more recent studies (Doi *et al.* 1989) showed that ONec itself, in the absence of collagen, actually retards and inhibits calcification. Glimcher (1984) also questioned the effects of ONec. The suggested rôle of ONec has been derived from the idea that it bonds strongly to collagen and to apatite crystals, but no reported data are available to indicate a specific binding of ONec by collagen. Similarly, the binding of ONec to already existing apatite crystals has little physicochemical meaning in terms of its involvement in the formation of the inorganic crystals.

Casein, another phosphoprotein containing a small amount of SerP residues, was actually found to inhibit the formation of calcium phosphate drastically (van Kemenade & de Bruyn 1989), although the SerP groups do act as nucleation centres and accelerate the early stages of precipitation. The adverse effect is due to the structure of the remainder of the protein chain.

Apart from phosphoproteins, there are also other organic compounds which can exert influence on the mineralisation process. Boskey (1989) studied the formation of calcium phosphate in a denatured collagen gel system and concluded that phospholipids, another family of bone-specific bio-chemicals, may promote calcification. Cardiolipin, a member of the phospholipid family, was found to affect *in vitro* calcification in a complicated manner, although in general it does somewhat

promote nucleation and growth (Dalas *et al.* 1989a). However, salivary phospholipids did not show signs of significantly inducing the nucleation and growth of calcium phosphate (Campbell & Nancollas 1991).

In contrast to potential calcification promoters, there are also a number of inhibitors. These inhibitors are necessary for the prevention of undesired precipitation of calcium phosphate in inappropriate locations in the body. Proteoglycans, for example, reduce the extent of calcification both in solutions and in gel systems (Boskey 1989). Inorganic ions, e.g. Mg^{2+}, are also capable of reducing the extent of crystallisation through the substitution at the Ca^{2+} sites in the apatite crystals (Blumenthal 1989).

Bio-chemicals may influence calcification through two mechanisms. Some of them, e.g. alkaline phosphatase, catalytically alter the local solution chemistry but are not actively involved in the actual calcification process. Catalysts serve the purpose of changing the thermodynamic barrier, i.e. the activation energy, of nucleation and growth. Alternatively, compounds may affect mineralisation by actively binding onto either collagen or one of the inorganic lattice ions, thus enhancing or inhibiting further bond formation depending on the nature of each particular compound. However, information concerning the actual reaction mechanism of different bio-chemicals is scarce and often contradictory. A sound knowledge of the effects of various bone-specific bio-chemicals is essential for both a better understanding of the physiological mineralisation process and the development of a superior bioactive bone replacement material.

2.7 Scope of the present project

Although a massive amount of effort has been put into the study of calcification and the effects of different bio-chemicals on the process, a number of fundamental questions still remain. There are at present no satisfactory explanations for the phasal preference of different precursor phases and the subsequent phase transformations during the precipitation of calcium phosphate. In addition, the way in which certain bio-chemicals affect the process is not yet fully understood either. This project, therefore, aims to clarify some aspects of these uncertainties and to derive a model which can hopefully describe the overall precipitation behaviour satisfactorily. The first part of the project dealt with the precipitation of calcium phosphate in purely ionic media. This was first

performed using the constant-volume technique and then, with the aid of the results from these preliminary experiments, carefully studied under constant-composition environments. Using the precipitation data furnished by the constant-composition experiments, a transformation model was then developed. Next, the effects of certain bone-specific bio-chemicals on the calcification process were studied and their impact on the transformation model was assessed.

Chapter 3
PRELIMINARY CONSTANT-VOLUME STUDIES OF CALCIUM PHOSPHATE PRECIPITATION IN PURELY IONIC MEDIA

Constant-volume experiments were performed since they had the advantage that, compared to other techniques, they did not require elaborate instrumentation while at the same time provided an opportunity to study various aspects of the precipitation behaviour. As the solution compositions were allowed to vary with time, results from these experiments should yield valuable information about the dependence of the precipitation characteristics on changes in *p*H and supersaturations with respect to different phases. Without such results, it would be impossible to devise intricate equipment and approach for more in-depth studies.

3.1 Materials and method

A typical precipitation experiment involved the introduction of substrates into a supersaturated calcium phosphate solution. Both components needed to be carefully prepared to ensure reliability of experimental results.

3.1.1 Substrates

§ Choice of substrates

The choice of substrates is important for the reliable control of any precipitation experiment. A suitable substrate needs to satisfy certain chemical and physical criteria. Chemically, it has to be inert and insoluble under the experimental conditions; whereas physically, accurate evaluation of parameters such as the specific surface area must be easily achieved. Also, subsequent treatments of solid samples may influence the choice of substrates.

Owing to the fact that the solution and phase chemistries of calcium phosphate are so complex, and that the potential for precipitation can be immensely affected by the presence of small amounts of alien ions, the substrate to be used in these experiments had to be a stable, insoluble and pure phase of calcium phosphate free from foreign ions (with the exception of hydrogen and

hydroxide ions which could be allowed for in aqueous media) to avoid any possibility of contamination. In a supersaturated aqueous medium, hydroxyapatite is the most insoluble and thermodynamically the most stable calcium phosphate and was thus chosen to be the substrate material.

The actual physical appearance of the substrates is also important for the accurate study of secondary precipitation. Precise evaluation of physical parameters such as the specific surface area is necessary for the standardisation of experiments in order that quantitative comparison can be carried out. Furthermore, it is also necessary to choose a form of substrate which is easy to be prepared and treated before and after the experiments. Substrates in dense pellet form have advantages over loose powder in both of these aspects because bulk materials are easier to handle and physical characterisation is a lot simpler. However, as dense substrates tend to sink to the bottom of reaction tanks, efficient stirring becomes crucial to ensure the uniformity of the working solutions. This was taken into consideration in the design of the experimental set-up.

§ Preparation of substrates

Synthetic hydroxyapatite powder obtained from Aldrich Chemicals was pressed in a 1 cm^2 hardened stainless steel die under a pressure of 200 MPa. The pellets were put in a furnace and subjected to the following temperature profile: from room temperature to 500 °C at a heating rate of 20 °C h^{-1}; kept at 500 °C for 10 hours for any trapped gases to escape; then heated up to 1100 °C at a rate of 50 °C h^{-1} and left to sinter for 168 hours; finally allowed to cool to room temperature at a rate of 100 °C h^{-1}. This resulted in a volumetric shrinkage of about 25%.

Next, to ensure a flat surface, each pellet was cold-mounted using Acryfix resin supplied by Struers and then polished in a Kent 3 polishing machine with successively finer diamond laps and cloths down to a tolerance of 1 μm to give a mirror finish. The pellets were then cleaned in distilled water using ultrasonics. Their actual dimensions and final finish were examined under a Nikon optical microscope. Cracked and imperfect specimens were disposed of. 150 satisfactory pellets were stored in a desiccator for future use.

3.1.2 Calcifying solutions

The preparation of calcifying solutions was a lot more complicated than that of the substrates because it was absolutely critical to control the solution composition precisely so that the supersaturation with respect to the various calcium phosphate phases could be known with exact accuracy. Since supersaturation is very sensitive to the ionic strength (see Section 3.2), it cannot be determined unless the ionic strength is stabilised with an additional neutral electrolyte which readily dissolves in the working solutions but is not involved in the actual precipitation process. Potassium chloride has widely been used as the background electrolyte and has shown outstanding inertness (Nancollas & Tomažić 1974). The concentration of the electrolyte should be such that the overall variations in ionic strength throughout the experiments is negligible.

Supersaturated calcium phosphate solutions were prepared based on the method described by Silverstone *et al.* (1981). 5.023 g of synthetic hydroxyapatite powder [$Ca_{10}(PO_4)_6(OH)_2$, molecular weight = 1004.64] having a calcium-to-phosphate molar ratio of 1.67 obtained from Aldrich Chemicals was added to 800 mℓ of distilled water. 2 mℓ doses of 0.1 M hydrochloric acid were introduced to the mixture until all the powder dissolved and the *p*H of the solution was around 3. The solution was then made up to 1 ℓ with distilled water and its *p*H was adjusted to the desired value by dissolving solid potassium hydroxide, giving rise to a stock solution with a total calcium content of 50 mM.

Aliquots of this stock solution were then appropriately diluted to the desired concentration and minor adjustments to the *p*H achieved by the addition of hydrochloric acid or potassium hydroxide. Finally, taking into account the total amount of potassium and chloride ions already present in the solution through the addition of hydrochloric acid and potassium hydroxide, a calculated weight of solid potassium chloride powder was dissolved to give a working solution with an ionic strength of 0.1 M.

Since solutions prepared in this way were supersaturated and metastable, it was necessary to make use of them within one week from production.

3.1.3 Experimental procedure

Table 3.1 shows the starting compositions and the temperatures of the solutions used in this

Table 3.1 Compositions and temperatures of working solutions

Expt. no.	Starting total calcium content (mM)	Starting *p*H	Temp. (°C)	Expt. no.	Starting total calcium content (mM)	Starting *p*H	Temp. (°C)
I-I	50	3.7	37	I-10	10	3.6	37
I-2			20	I-11			17
I-3			4	I-12			4
I-4	20	3.8	37	I-13	2	7.4	37
I-5			16	I-14			17
I-6			4	I-15			4
I-7	10	7.4	37	I-16		3.5	37
I-8			15	I-17			17
I-9			4	I-18			4

series of experiments. In each experiment, 250 mℓ of calcifying solution was placed in a glass chamber into which three polished hydroxyapatite substrates were introduced. The temperature was maintained constant either by means of a water bath or by storing the reaction chamber in a refrigerator. Nitrogen gas was bubbled first through distilled water and then into the working solution. This moisture-saturated nitrogen gas served two purposes - firstly, it eliminated any dissolved carbon dioxide gas; and secondly, it provided sufficient stirring to the system while preventing diminution of the reaction volume due to evaporation of water vapour, especially at high temperatures. The *p*H and the concentration of free (uncomplexed) Ca^{2+} ions were measured at regular intervals using a Jenway 3040 ion analyser with a combined glass *p*H electrode (Jenway PCP505) and a Ca^{2+} ion selective electrode (Radiometer F2002) coupled with a calomel reference electrode (RS 985-77). A temperature probe (Jenway PCT121) was also attached to the meter for the necessary corrections in the potentiometer outputs. Pre-experimental calibrations were performed using *p*H 4.0 and *p*H 7.0 buffers (obtained from BDH) for the *p*H electrode; and 0.001 M, 0.01 M, 0.1 M and 1 M solutions of calcium chloride (made from AnalaR grade $CaCl_2$ crystals obtained from BDH) for the Ca^{2+} and the reference electrodes.

The hydroxyapatite pellets were left in the solutions for 3 days and were then dried in a desiccator for at least 24 hours.

3.1.4 Precipitate characterisation

The solid precipitate was characterised by means of scanning electron microscopy (SEM), wavelength dispersive spectroscopy (WDS) and X-ray powder diffractometry (XRD).

For each experiment, one substrate sample was sputter-coated with gold and examined in a Hitachi S530 scanning electron microscope at a voltage between 20 and 25 kV. Another sample was carbon-coated for WDS by a Camebax Microprobe at an accelerating voltage of 10 kV and a corresponding interaction volume of about 10^{-14} m^3. The microprobe was pre-calibrated with apatite and potassium chloride standards for calcium, phosphorus, potassium and chlorine detection respectively*. The precipitate on the third sample was removed from the substrate with a razor blade for XRD. Powder diffraction using Cu Kα radiation was usually performed on a Philips PW-1050 diffractometer at a current of 20 mA and a voltage of 40 kV in reflection mode, but in the cases where the amount of solid precipitate obtained was particularly small (< 20 mg), high-resolution X-ray diffraction (HRXRD) was done on a STOE STADI P diffractometer in transmission mode which ran from a water-cooled rotating anode generator source at 6 kW+.

3.2 Calculation of supersaturation

Before any results can be interpreted, it is first necessary to explain how the supersaturations with respect to the various phases were calculated. The high tendency of calcium and phosphate ions to form complexes in aqueous solution has been briefly discussed in Section 2.4.2, and at this point, the chemical equilibria among these complexes must be analysed in detail for the correct evaluation of supersaturations. Furthermore, as there were numerous chared entities within the solutions, the actual mobility of these ions and complexes and thus the degrees of supersaturation were also influenced by electrostatic forces. These factors must be taken into consideration in order to obtain accurate values of ionic concentrations using potentiometric outputs from the meter.

3.2.1 Ionic activity

In a solution containing ions, the interaction among the solute particles extends over a much

* WDS was performed under the supervision and with the assistance of Mr. Chris Salter of the Department of Materials, University of Oxford.

+ HRXRD was kindly performed by Mr. Fred Wondre and Dr. Alison Roberts at the Clarendon Laboratory, University of Oxford.

longer range than in a solution containing uncharged molecules, owing to electrostatic forces. The result is that deviations from the ideal laws, which assume that each particle in the solution behaves independently of one another, occur at much lower concentrations in ionic solutions than in solutions of uncharged molecules. Fortunately, the long-range electrostatic interactions of ions in solution do not depend on the nature of the ions but only on their charges. These interactions are essentially the electrostatic attraction of ions of opposite charges, and hence in dilute solutions the actual activity of an ion is smaller than its concentration (Butler 1964). However, in more concentrated solutions, consequent of repulsive forces between ions of like charges, and because the water molecules which are coordinated to an ion in its primary hydration shell give the ion a rather large effective size, the activity may become enormous when the concentration reaches the point at which essentially all the water in solution is bound in the primary hydration shells of ions. Therefore, the necessity for making activity corrections becomes apparent, especially because the calcium phosphate system involves multi-valent ions which exhibit more pronounced effects than singly charged ions (Nancollas 1989).

The ratio of the activity over the actual concentration of an ion is known as the activity coefficient. By assuming that ions are point charges in a continuum of dielectric constant equal to that of the solvent, Debye and Hückel derived the theoretical form for the activity coefficient of an ion in dilute solutions from laws of electrostatics and thermodynamics. Davies (1962) modified the Debye-Hückel expression in order to give a better agreement with experimental data and arrived at the following expression for the activity coefficient of a single ion of charge$z$ (polarity disregarded) in a dilute solution:

$$-\log \chi_z = 1.825 \times 10^6 (\varepsilon T)^{-3/2} z^2 \left(\frac{\sqrt{I}}{1+\sqrt{I}} - 0.2\, I \right) \qquad ...(3.1)$$

where χ_z = activity coefficient of an ion with z units of charge;

I = ionic strength of the solution

$= \frac{1}{2} \sum_j [j]\, z_j^2$, $[j]$ being the molar concentration of species j;

z_j being the charge carried by species j;

ε = dielectric constant of solvent (= 78.54 for water);

T = absolute temperature.

A vast number of measurements have been made both in aqueous media and in solvents of other dielectric constants, and at different temperatures. In every case, Davies' version of the Debye-Hückel relation is obeyed within an error of ±1% provided that the ionic strength of the solution does not exceed 0.2 M (Nancollas & Tomažić 1974).

3.2.2 Ionic product and supersaturation

Whether a particular phase of calcium phosphate is going to precipitate under certain conditions depends on the availability of free and mobile ions to form that phase. This is expressed in terms of an ionic product (IP) of the activities of the constituent ions, i.e.:

$$IP^{DCPD} = ([Ca^{2+}] \chi_2) ([HPO_4^{2-}] \chi_2) = [Ca^{2+}] [HPO_4^{2-}] \chi_2^2$$

$$IP^{OCP} = ([Ca^{2+}] \chi_2)^4 ([H^+] \chi_1) ([PO_4^{3-}] \chi_3)^3 = [Ca^{2+}]^4 [H^+] [PO_4^{3-}]^3 \chi_1 \chi_2^4 \chi_3^3$$

$$IP^{HAP} = ([Ca^{2+}] \chi_2)^5 ([PO_4^{3-}] \chi_3)^3 ([OH^-] \chi_1) = [Ca^{2+}]^5 [PO_4^{3-}]^3 [OH^-] \chi_1 \chi_2^5 \chi_3^3 \quad ...(3.2)$$

The thermodynamic driving force behind precipitation is a function of supersaturation, β, which is the ratio between the ionic product as defined by Equation 3.2 and the equilibrium solubility product (K_{sp}) of each phase. Numerically,

$$\beta = \frac{IP}{K_{sp}} \quad ...(3.3)$$

The solubility product of each phase is defined as the activity product of the constituent ions in a solution which is in physical and chemical equilibrium with the solid phase of the solute. In other words,

for DCPD, $CaHPO_4 \cdot 2H_2O(s) \Leftrightarrow Ca^{2+}(aq) + HPO_4^{2-}(aq)$

$$K_{sp}^{DCPD} = ([Ca^{2+}] \chi_2)_{eq} ([HPO_4^{2-}] \chi_2)_{eq} \quad \text{(unit: } M^2\text{)}$$

for OCP,

$$Ca_4H(PO_4)_3 \cdot 2.5H_2O(s) \Leftrightarrow 4\,Ca^{2+}(aq) + H^+(aq) + 3\,PO_4^{3-}(aq)$$

$$K_{sp}^{OCP} = ([Ca^{2+}] \chi_2)_{eq}^4 ([H^+] \chi_1)_{eq} ([PO_4^{3-}] \chi_3)_{eq}^3 \qquad \text{(unit: } M^8\text{)}$$

for HAP,

$$Ca_5(PO_4)_3(OH)(s) \Leftrightarrow 5\,Ca^{2+}(aq) + 3PO_4^{3-}(aq) + OH^-(aq)$$

$$K_{sp}^{HAP} = ([Ca^{2+}] \chi_2)_{eq}^5 ([PO_4^{3-}] \chi_3)_{eq}^3 ([OH^-] \chi_1)_{eq} \qquad \text{(unit: } M^9\text{)}$$

...(3.4)

As solubility products are equilibrium properties, their values are only dependent on the temperature of the system. The relationships between the K_{sp} of various phases and temperature have been previously established as follows:

$$ln\ K_{sp}^{DCPD} = -\frac{8403.50}{T} + 41.863 - 0.09678\,T \qquad \text{(Gregory } et\ al.\text{ 1970)}$$

$$log\ K_{sp}^{OCP} = -\frac{3270.33}{T} + 60.836 - 0.09678\,T \qquad \text{(Frèche \& Heugheaert 1989)}$$

$$log\ K_{sp}^{HAP} = -\frac{8219.41}{T} - 1.6657 - 0.098215\,T \qquad \text{(McDowell } et\ al.\text{ 1977)}$$

(T: absolute temperature in K) ...(3.5)

If the value of β in Equation 3.3 for a particular phase exceeds 1, the solution is supersaturated with respect to that phase. This acts as the driving force for precipitation to take place in order to lower the ionic product so that thermodynamic equilibrium can be attained.

3.2.3 Ionic equilibria

In an aqueous medium, phosphate protonation and calcium phosphate ion-pair formation proceed to significant extents, producing a wide variety of charged entities within the solution. Additional ions are also present due to the dissociation of water and the introduction of external acids and bases. Again, inter-ionic equilibria need to be considered when determining the respective concentration of the individual ions and complexes. Listed here are the reactions and the corresponding equilibrium constants as functions of temperature:

$H_3PO_4 \Leftrightarrow H^+ + H_2PO_4^-$ $\quad log\, K_0 = -\frac{799.31}{T} + 4.5535 - 0.013486\, T$ (unit of K_0: M)

(Bates 1951)

$H_2PO_4^- \Leftrightarrow H^+ + HPO_4^{2-}$ $\quad log\, K_1 = -\frac{1979.50}{T} + 5.3541 - 0.019840\, T$ (unit of K_1: M)

(Bates & Acree 1943)

$HPO_4^{2-} \Leftrightarrow H^+ + PO_4^{3-}$ $\quad log\, K_2 = -\frac{2017.76}{T} - 1.5026 - 0.0136\, T$ (unit of K_2: M)

(Vanderzee & Quist 1961, Frèche & Heughebaert 1989)

$CaH_2PO_4^+ \Leftrightarrow Ca^{2+} + H_2PO_4^-$ $\quad ln\, K_3 = -\frac{19373}{T} + 122.81 - 0.1994\, T$ (unit of K_3: M)

(Gregory *et al.* 1970)

$CaHPO_4^\circ \Leftrightarrow Ca^{2+} + HPO_4^{2-}$ $\quad ln\, K_4 = -\frac{51090}{T} + 341.14 - 0.5880\, T$ (unit of K_4: M)

(Gregory *et al.* 1970)

$CaPO_4^- \Leftrightarrow Ca^{2+} + PO_4^{3-}$ $\quad log\, K_5 = -\frac{1156}{T} + 3.603 - 0.0208\, T$ (unit of K_5: M)

(Frèche & Heughebaert 1989)

$CaOH^+ \Leftrightarrow Ca^{2+} + OH^-$ $\quad log\, K_6 = -\frac{409.9}{T} + 2.8235 - 0.0090\, T$ (unit of K_6: M)

(Frèche & Heughebaert 1989)

$H_2O \Leftrightarrow H^+ + OH^-$ $\quad log\, K_w = -\frac{4471}{T} + 6.0875 - 0.01706\, T$ (unit of K_w: M^2)

(Harned & Owen 1958)

...(3.6)

3.2.4 *Electroneutrality*

Since all the reactants and starting materials were electrically neutral as a whole, the overall sum of all the charges within the reaction medium should be zero throughout the experiments (Harned & Owen 1958). Thus, at any instant,

$$2\,[Ca^{2+}] + [CaH_2PO_4^+] + [CaOH^+] + [H^+] + [K^+]$$
$$= 3\,[PO_4^{3-}] + 2\,[HPO_4^{2-}] + [H_2PO_4^-] + [CaPO_4^-] + [OH^-] + [Cl^-] \qquad ...(3.7)$$

3.2.5 *Calculation of ionic concentrations*

The activities of free H^+ and Ca^{2+} ions given by the *p*H and *p*Ca readings from the meters were used to work out the actual concentrations of these two ions in the solution:

$$[H^+] = 10^{-pH} / \chi_1$$
$$[Ca^{2+}] = 10^{-pCa} / \chi_2 \qquad ...(3.8)$$

The activity coefficients were dictated by the ionic strength of the solution, given by:

$$I = \frac{1}{2}\{ 4\,[Ca^{2+}] + 9\,[PO_4^{3-}] + 4\,[HPO_4^{2-}] + [H_2PO_4^{-}] + [CaH_2PO_4^{+}] + [CaPO_4^{-}] + [CaOH^{+}] + [H^{+}] + [OH^{-}] + [K^{+}] + [Cl^{-}] \} \quad ...(3.9)$$

However, as previously described, neutral KCl was deliberately dissolved in the solutions in abundance compared to all the other ions to stabilise the ionic strength to 0.1 M (±3%). (Fine adjustment in the exact evaluation of this stabilised ionic strength can be made by successive iterations using subsequently calculated concentrations of the various ions.) Substituting this value of I into Equation 3.1, the activity coefficients and hence $[Ca^{2+}]$ and $[H^{+}]$ were thus calculated.

Next, $[PO_4^{3-}]$ was deduced from Equation 3.7 by replacing the concentrations of the complexes with those of Ca2+, PO_4^{3-} and H+ ions and the equilibrium constants in Equation 3.6:

$$[PO_4^{3-}] = \frac{C_1\,[Ca^{2+}] + C_2}{C_3\,[Ca^{2+}] + C_4} \quad ...(3.10)$$

where

$$C_1 = K_1 K_2 K_3 K_5 (2 K_6 [H^{+}] + K_w)$$

$$C_2 = K_1 K_2 K_3 K_5 K_6 ([H^{+}]^2 + [H^{+}] [K^{+}] - [H^{+}] [Cl^{-}] - K_w)$$

$$C_3 = K_6 [H^{+}] (K_1 K_2 K_3 - K_5 [H^{+}]^2)$$

$$C_4 = K_3 K_5 K_6 [H^{+}] (3 K_1 K_2 + 2 K_1 [H^{+}] + [H^{+}]^2)$$

With $[Ca^{2+}]$, $[H^{+}]$ and $[PO_4^{3-}]$, the concentrations of the other ions and complexes were then calculated:

$$[HPO_4^{2-}] = [H^{+}]\,[PO_4^{3-}] / K_2$$

$$[H_2PO_4^{-}] = [H^{+}]^2\,[PO_4^{3-}] / K_1 K_2$$

$$[CaH_2PO_4^{+}] = [Ca^{2+}]\,[H^{+}]^2\,[PO_4^{3-}] / K_1 K_2 K_3$$

$$[CaHPO_4^{\circ}] = [Ca^{2+}]\,[H^{+}]\,[PO_4^{3-}] / K_2 K_4$$

$$[CaPO_4^{-}] = [Ca^{2+}]\,[PO_4^{3-}] / K_5$$

$$[CaOH^{+}] = [Ca^{2+}]\,K_w / [H^{+}]\,K_6$$

$$[OH^{-}] = K_w / [H^{+}] \quad ...(3.11)$$

These calculated values were substituted back into Equation 3.9 for iteration to yield a more accurate value of the ionic strength. Ionic concentrations and activity coefficients obtained using the final iterated value of I were used to evaluate the supersaturation with respect to the different phases of calcium phosphate by Equations 3.2, 3.3 and 3.5.

Apart from the individual concentrations, the total calcium and total phosphate contents were also of interest when analysing experimental results, as they were directly related to the amount of precipitate produced. Their values are respectively defined in Equation 3.12.

$$[\Sigma Ca] = [Ca^{2+}] + [CaH_2PO_4^{+}] + [CaHPO_4^{\circ}] + [CaPO_4^{-}] + [CaOH^{+}]$$

$$[\Sigma P] = [PO_4^{3-}] + [HPO_4^{2-}] + [H_2PO_4^{-}] + [CaPO_4^{-}] + [CaHPO_4^{\circ}] + [CaH_2PO_4^{+}] \quad ...(3.12)$$

All the above mathematical manipulation was handled by a dedicated FORTRAN computer programme specially written for this particular application.

3.2.6 *Effects of pH, solution composition and temperature on solubility and superaturation*

Extreme care must be taken when investigating the solubilities of various phases of calcium phosphate under different experimental conditions. Although equilibrium solubility products are dependent only on temperature (as discussed in Section 3.2.2), they merely indicate the activity products of specific ions in the solution. It is important to take into account the co-existence of other ions. Hence, the actual solubilities are in fact influenced by the various ionic equilibria listed in Equation 3.6, and in particular, the acidity of the solution which has a dramatic effect on the degree of phosphate protonation.

Using these equilibria, it is possible to represent graphically the variation of the solubilities of different phases at particular temperature in the form of solubility isotherms as in Figure 2.6 (Nancollas *et al.* 1989). Any solution whose composition is above a solubility isotherm is supersaturated with respect to that particular phase. Conversely, at a certain temperature, the degrees of supersaturation with respect to the three phases as functions of solution composition and*p*H can also be displayed in the style of three-dimensional isothermal surfaces (Figure 3.1). Similar sets of solubility isotherms and supersaturation surfaces can be constructed for different temperatures.

Figure 3.1(a) 3-dimensional representation of the supersaturation of calcium phosphate solutions with respect to DCPD at 37 °C. It is expressed in terms of the *p*H and the total ionic product of calcium and phosphate ions and complexes. The blue portion of the isothermal supersaturation surface corresponds to solutions undersaturated with respect to DCPD. Supersaturation calculation assumed an ionic strength of 0.1 M, and a [ΣCa]/[ΣP] value of 1.67.

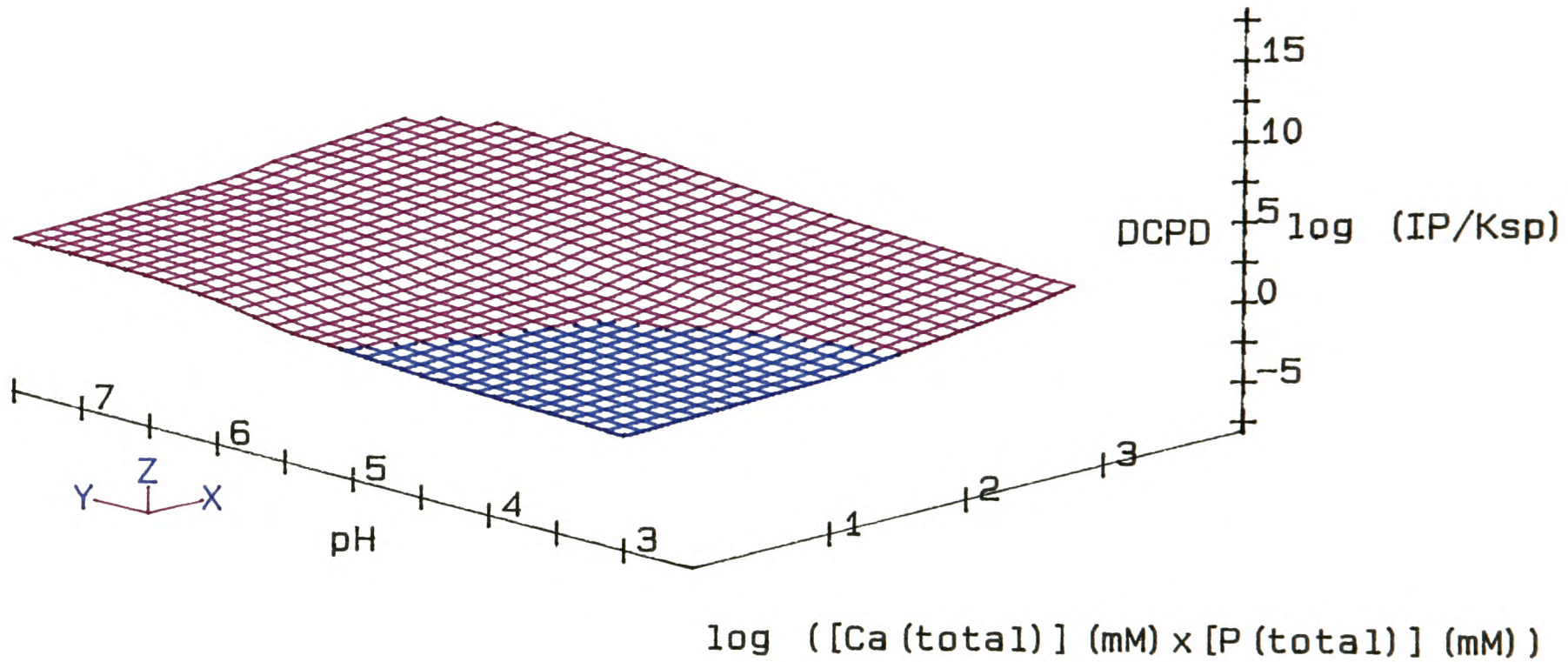

Figure 3.1(b) 3-dimensional representation of the supersaturation of calcium phosphate solutions with respect to OCP at 37 °C. It is expressed in terms of the *p*H and the total ionic product of calcium and phosphate ions and complexes. The dark blue portion of the isothermal supersaturation surface corresponds to solutions undersaturated with respect to OCP. Supersaturation calculation assumed an ionic strength of 0.1 M, and a [ΣCa]/[ΣP] value of 1.67.

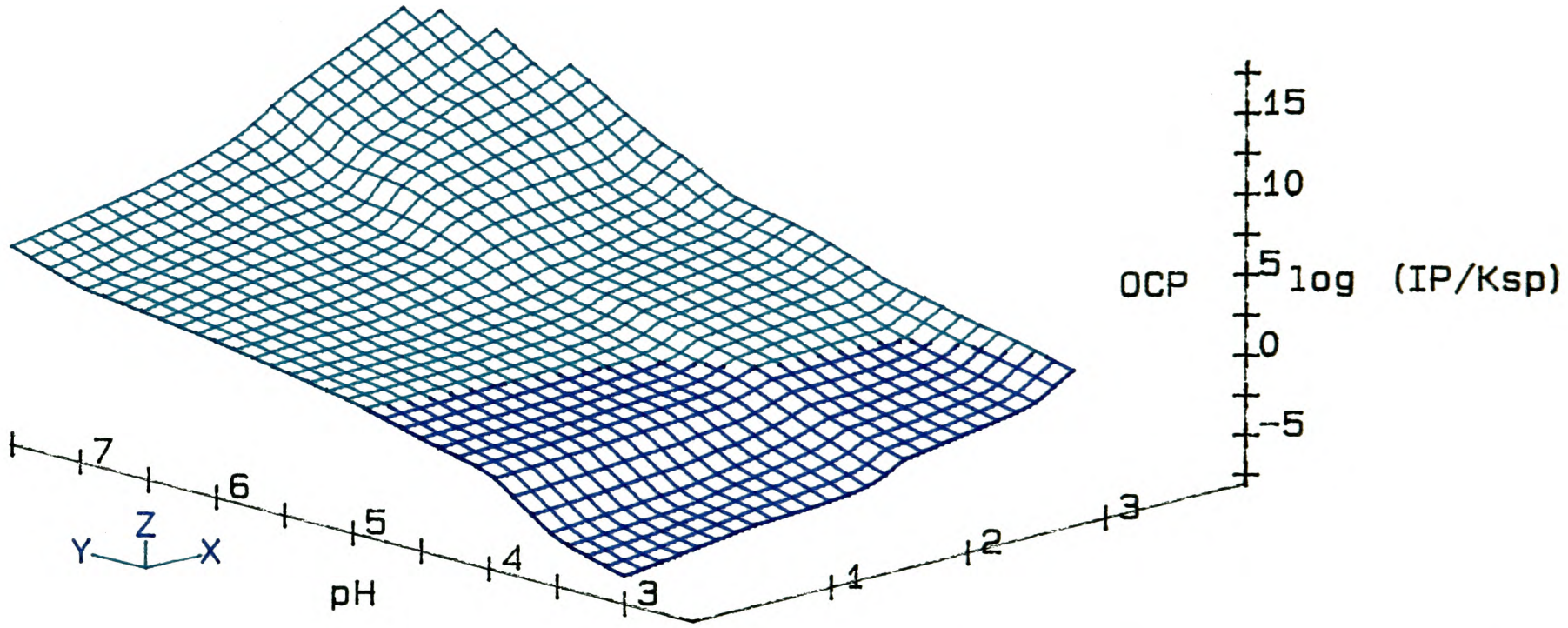

Figure 3.1(c) 3-dimensional representation of the supersaturation of calcium phosphate solutions with respect to HAP at 37 °C. It is expressed in terms of the *p*H and the total ionic product of calcium and phosphate ions and complexes. The blue portion of the isothermal supersaturation surface corresponds to solutions undersaturated with respect to HAP. Supersaturation calculation assumed an ionic strength of 0.1 M, and a [ΣCa]/[ΣP] value of 1.67.

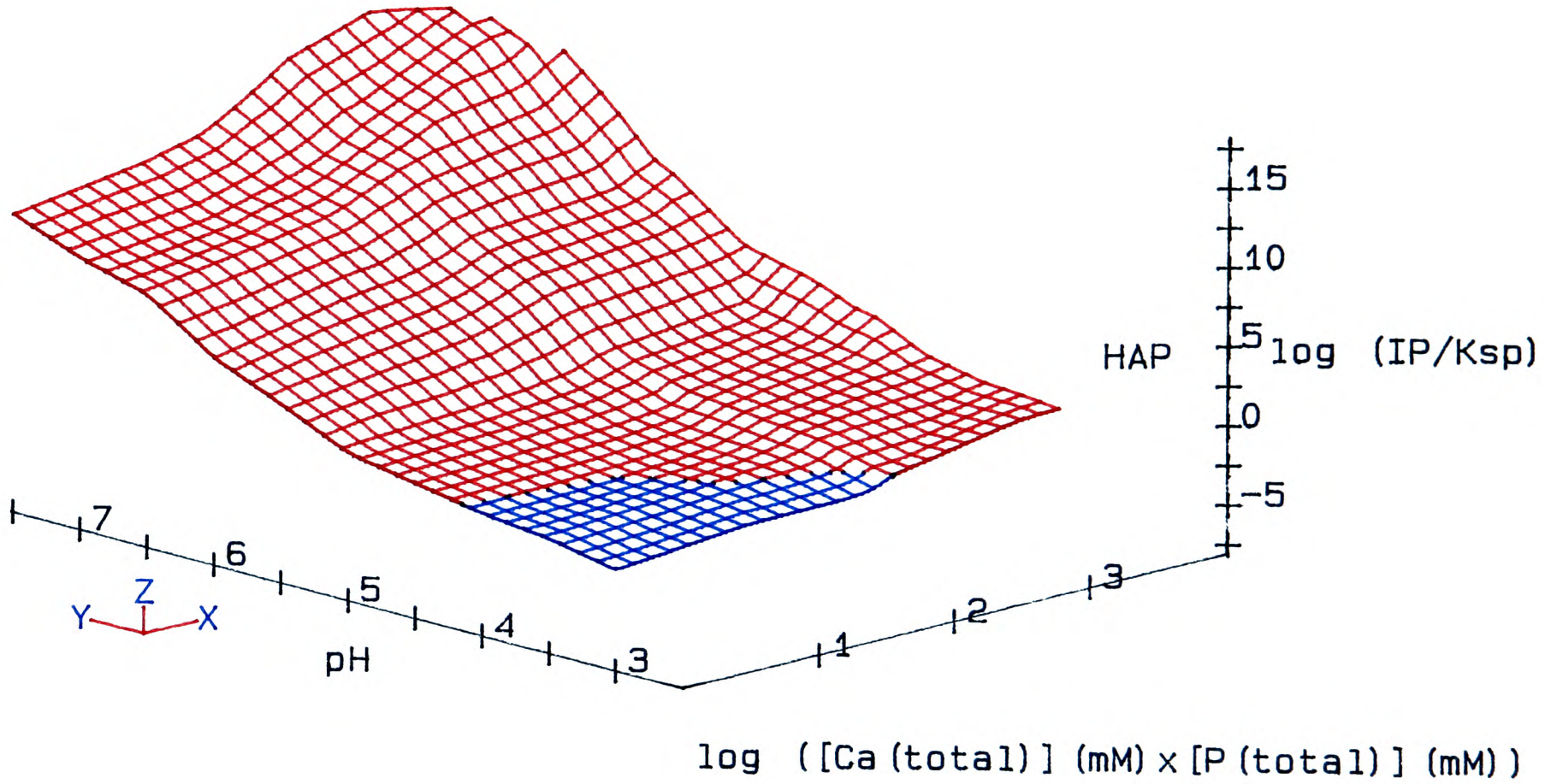

Figure 3.1(d) Superposition of the isothermal supersaturation surfaces of DCPD, OCP and HAP. It is clear that the sensitivity of the supersaturation (and hence the driving force for precipitation) towards changes in solution composition varies significantly with the different phases.

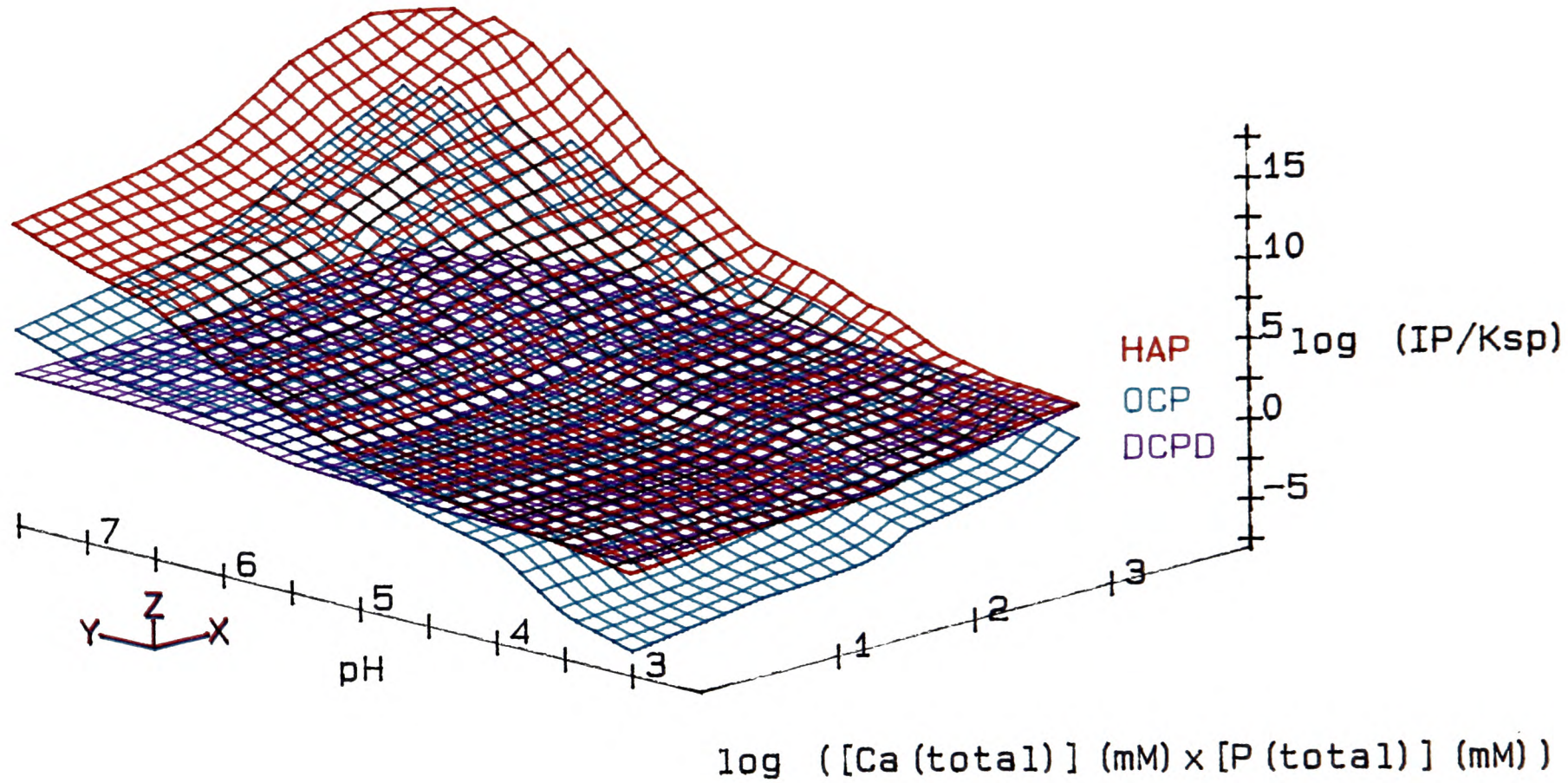

3.3 Results and discussion

Changes in solution composition, *p*H and temperature were found to affect the precipitation behaviour in a number of ways. The chemical composition, stoichiometry, crystallography and rate of formation are but a few examples of precipitate properties which were influenced. These effects will be discussed in this section in detail.

3.3.1 Rate of precipitation

Figure 3.2 shows the variations in *p*H and [ΣCa] (calculated from Ca^{2+} activity and *p*H) with time under different conditions. In all cases, both the measured Ca^{2+} activity and the *p*H dropped at a progressively slower rate. These decreases were indicative of reductions in the total contents of calcium and phosphate ions (i.e. the summation of free and complexed ions) respectively. Several trends are observed from these plots:

- *At the same temperature and initial pH, the overall precipitation rate increased with increasing initial calcium content.*

  As the only difference among the solutions was the amount of calcium phosphate solute, the thermodynamic solubilities of the different phases, which were determined by the temperature and acidity of the solutions, were identical at the inception of precipitation. Hence, with increased amounts of solute, the degrees of supersaturation increased accordingly and thus provided a greater potential gradient to drive the precipitation process.

- *At the same temperature and initial calcium content, the overall precipitation rate increased with increasing initial pH.*

  This effect was again directly related to the solubilities and thus the supersaturations of the various calcium phosphates. As previously mentioned, the inclusion of external acids or bases effectively shifted the inter-ionic equilibria, thereby affecting the chemical composition of a saturated solution at equilibrium. Referring to the solubility isotherms (Figure 2.6), it is obvious that at a constant temperature, calcium phosphates are more soluble in a more acidic medium; and correspondingly from the supersaturation surfaces (Figure 3.1), with the same amounts of solute, the degrees of supersaturation are lower as the *p*H decreases. Although

Figure 3.2

The graphs of *p*H and [ΣCa] of calcifying solutions against time for precipitation performed at different temperatures

(a) Experiments I-1 to I-3

(b) Experiments I-4 to I-6

(c) Experiments I-7 to I-9

(d) Experiments I-10 to I-12

(e) Experiments I-13 to I-15

(f) Experiments I-16 to I-18

(a)

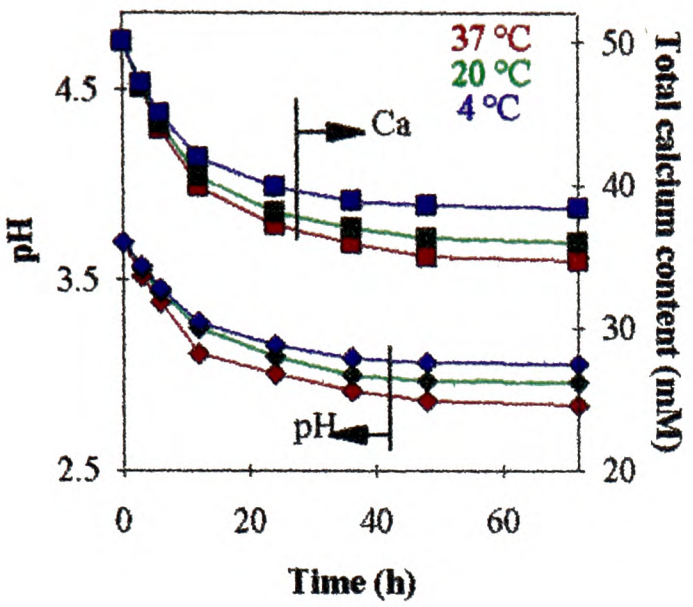
37 °C
20 °C
4 °C
Ca
pH
pH
Total calcium content (mM)
Time (h)
4.5
3.5
2.5
50
40
30
20
0
20
40
60

(b)

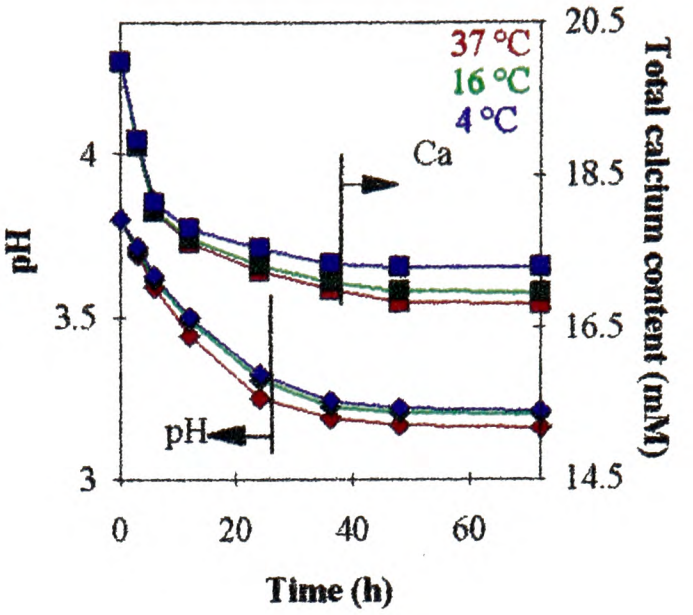
37 °C
16 °C
4 °C
Ca
pH
pH
Total calcium content (mM)
Time (h)
4
3.5
3
20.5
18.5
16.5
14.5
0
20
40
60

(c)

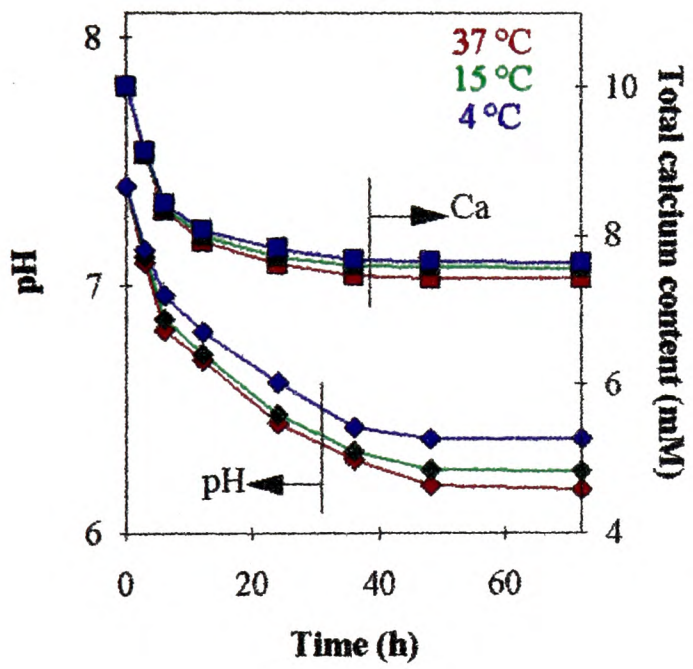
37 °C
15 °C
4 °C
Ca
pH
pH
Total calcium content (mM)
Time (h)
8
7
6
10
8
6
4
0
20
40
60

(d)

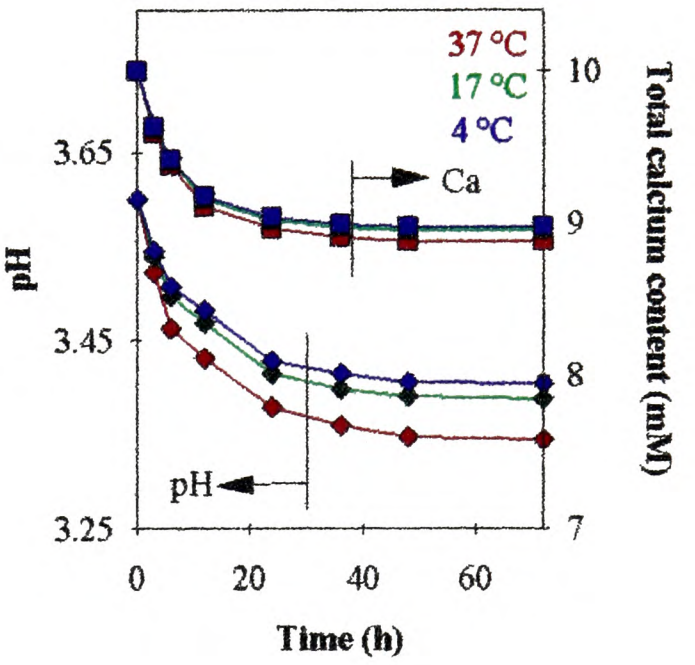
37 °C
17 °C
4 °C
Ca
pH
pH
Total calcium content (mM)
Time (h)
3.65
3.45
3.25
10
9
8
7
0
20
40
60

(e)

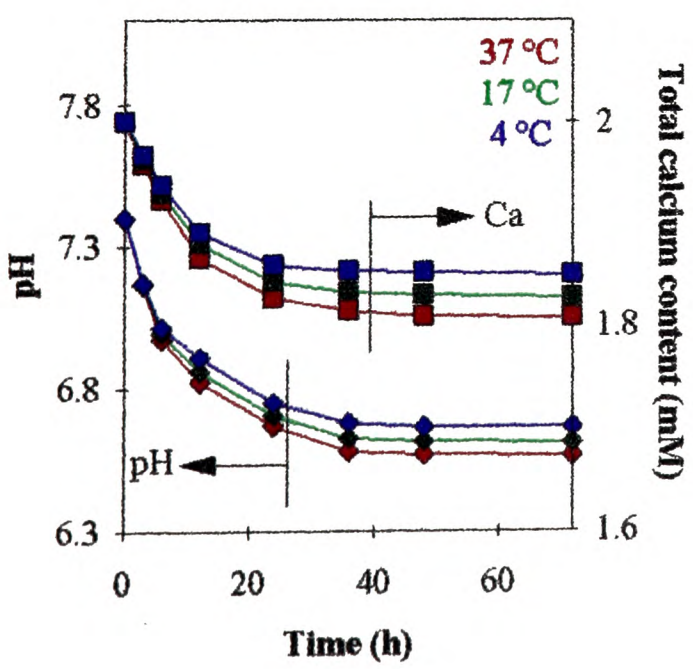
37 °C
17 °C
4 °C
Ca
pH
pH
Total calcium content (mM)
Time (h)
7.8
7.3
6.8
6.3
2
1.8
1.6
0
20
40
60

(f)

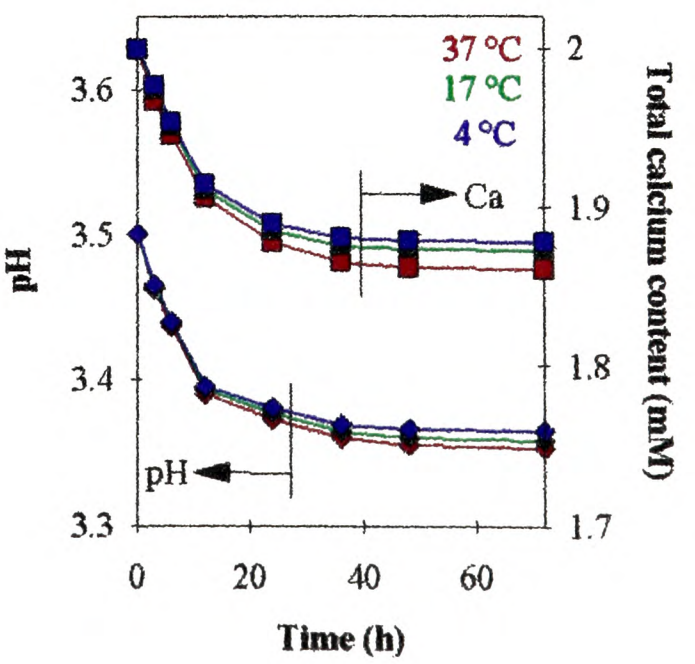
37 °C
17 °C
4 °C
Ca
pH
pH
Total calcium content (mM)
Time (h)
3.6
3.5
3.4
3.3
2
1.9
1.8
1.7
0
20
40
60

Figures 2.6 and 3.1 were constructed for a particular temperature, analogous trends are also exhibited over a range of temperature much wider than has been covered in these experiments. Hence, the difference in the precipitation rates at different solution acidities can be accounted for.

- *At the same initial pH and calcium content, the overall precipitation rate increased with increasing temperature.*

Both the dissolution and the precipitation of calcium phosphate were affected by changes in temperature. In general, for the dissolution of sparingly soluble inorganic salts, an increase in temperature facilitates the dissociation and solvation processes by lowering the activation energy barrier. As a result, the equilibrium solubility of calcium phosphate was in fact increased at higher temperatures leading to decreased supersaturations. Thus, if we only consider the influence of temperature on the thermodynamic driving force, precipitation should indeed be hindered at high temperatures, which is in contradiction to the present experimental results.

However, this adverse effect on thermodynamics was overcome by favourable kinetics. Precipitation involves the collision of appropriate ions, and at higher temperatures, ions become more energetic and mobile, thereby increasing the probability of the formation of precipitate. These kinetic effects changed in a manner so much faster than the thermodynamic effects that the overall precipitation rate was still significantly accelerated at higher temperatures.

3.3.2 Chemical composition of precipitate

The chemical compositions of the precipitates were analysed by XRD and WDS. XRD spectra were compared with theoretical peaks for DCPD, OCP and HAP. XRD patterns were used to identify the actual phase of the precipitate. WDS results provided information on the atomic ratio between Ca and P of each sample and, as the Ca/P ratio is unique to each calcium phosphate phase, the chemical composition of the precipitate could be compared to that of the XRD-matched phase. Owing to the presence of large amounts of KCl in the solution, the chlorine content in the precipitate was also analysed to find out if chloride substitution had occurred. The identity of the precipitate was verified by the calculated decrements in [ΣCa] and [ΣP] based on the Ca^{2+} activity and *p*H

Table 3.2 Constant-volume experimental results

Expt. no.	*p*H	Temp. (°C)	$[\Sigma Ca]_i$ (mM)	$[\Sigma Ca]_f$ (mM)	$[\Sigma P]_i$ (mM)	$[\Sigma P]_f$ (mM)	$\frac{[\Sigma Ca]_i-[\Sigma Ca]_f}{[\Sigma P]_i-[\Sigma P]_f}$	XRD phase identification	WDS atomic ratio Ca/P	K/Ca	Cl/Ca
I-1	3.7	37	50	42.97	30	22.90	**0.99**	**DCPD**	**1.02**	0.01	0.00
I-2	3.7	20	50	44.43	30	24.37	**0.99**	**DCPD**	**0.96**	0.02	0.03
I-3	3.7	4	50	44.92	30	24.82	**0.98**	**DCPD**	**0.97**	0.03	0.00
I-4	3.8	37	20	17.12	12	9.23	**1.04**	**DCPD**	**0.97**	0.03	0.00
I-5	3.8	16	20	17.51	12	9.25	**1.03**	**DCPD**	**1.01**	0.01	0.01
I-6	3.8	4	20	18.02	12	9.94	**0.96**	**DCPD**	**1.00**	0.01	0.00
I-7	7.4	37	10	7.01	6	3.82	**1.37**	**OCP+HAP**	**1.32**	0.01	0.01
I-8	7.4	15	10	7.12	6	3.83	**1.33**	**OCP**	**1.29**	0.00	0.01
I-9	7.4	4	10	7.28	6	3.86	**1.27**	**DCPD+OCP**	**1.29**	0.02	0.01
I-10	3.6	37	10	8.35	6	4.32	**0.98**	**DCPD**	**1.01**	0.03	0.04
I-11	3.6	17	10	8.38	6	4.36	**0.99**	**DCPD**	**1.02**	0.01	0.00
I-12	3.6	4	10	8.44	6	4.44	**1.00**	**DCPD**	**0.98**	0.00	0.02
I-13	7.4	37	2	1.45	1.2	0.82	**1.43**	**OCP+HAP**	**1.45**	0.03	0.03
I-14	7.4	17	2	1.56	1.2	0.88	**1.38**	**OCP+HAP**	**1.36**	0.00	0.01
I-15	7.4	4	2	1.62	1.2	0.91	**1.31**	**OCP**	**1.28**	0.02	0.02
I-16	3.5	37	2	1.89	1.2	1.09	**1.00**	**DCPD**	**1.02**	0.00	0.01
I-17	3.5	17	2	1.90	1.2	1.10	**1.00**	**DCPD**	**0.97**	0.01	0.02
I-18	3.5	4	2	1.90	1.2	1.10	**0.99**	**DCPD**	**0.99**	0.01	0.00

- $[\Sigma Ca]_i$, $[\Sigma Ca]_f$, $[\Sigma P]_i$, $[\Sigma P]_f$: initial and final total calcium and phosphate contents calculated from *p*Ca and *p*H readings.
- Maximum error in WDS atomic ratios is ±2%.

readings, normalised on a per unit surface area basis. Table 3.2 summarises the results obtained from the various methods.

It is clear that different phases of calcium phosphate were formed under different experimental conditions. It is interesting to note that in spite of their abundance in the solutions, both K^+ and Cl^- ions were only present in the final products in trace amounts, fulfilling the purpose of KCl as an inert background electrolyte only for the stabilisation of ionic strength. Now, in a more acidic and more concentrated calcifying medium, the precipitate was predominantly DCPD; while the inclination to form OCP increased with decreases in acidity and/or calcium phosphate concentration. In the intermediate range, precipitates which contained both DCPD and OCP were obtained, with the formation of DCPD preceding that of OCP. When the acidity and the concentration dropped to very low levels, the Ca/P ratio of the precipitate sometimes surpassed considerably the value of 1.33 for pure OCP, suggesting the formation of HAP. However, pure HAP

was never obtained.

When we look at the supersaturations of the three phases, we notice that over the range of experimental conditions covered by this series of experiments, HAP was invariably the most supersaturated phase throughout. Thus, thermodynamically HAP had the greatest potential to be precipitated. So, why was HAP not readily formed? To explain this phenomenon, it is first necessary to understand the determining factors governing the precipitation process in a multi-phase system.

Whereas the precipitation reaction has to be energetically favourable, another major pre-requisite for the formation of a particular phase is that the activities of its constituent ions in the solution have to be high enough for the collision of these ions to be at least as likely as, if not likelier than, constituent ions of other phases. In general, in the cases of readily soluble electrolytes, the kinetic consideration is not of significance compared to the thermodynamic factors because all ions exist in abundance in the solution and thus appropriate ions for different phases should be able to come together with comparable ease. However, for sparingly soluble salts such as calcium phosphate, the formation of a certain phase is very much dictated by the collision probability of its constituents. Even though a phase may not be as supersaturated as another, its higher equilibrium solubility implies that its constituent ions exhibit higher stability in the solvated state. Hence the ionic equilibria will be shifted in such a way that favours higher concentrations of these ions and consequently the precipitation of more soluble but less supersaturated phases, despite giving rise to an energetically metastable system. In order to remedy this instability, precursor phases will subsequently remodel themselves and undergo phase transformation into more stable phases. These transformations are driven predominantly by thermodynamic potentials.

Ostwald (1879) observed the above characteristic about the precipitation of multi-phase sparingly soluble salts and summarised it as the Rule of Stages which states that: kinetic factors prompt the preferential formation of the most soluble (and thus the least supersaturated) phase prior to subsequent step-wise transformation to more stable phases as a result of thermodynamic driving forces. With this in mind, we can now verify whether the sequence of precipitated phases obtained in the experiments was consistent with Ostwald's Rule of Stages.

Looking back at the supersaturation surfaces (Figure 3.1d), the sequence of formation for the

various phases in each case should follow the reverse order of the supersaturation. Obviously, although kinetic factors may have favoured the nucleation of phases with a supersaturation value less than 1, any nuclei thus formed would immediately re-dissolve due to the undersaturation of that phase under those conditions. Hence only supersaturated phases were expected to precipitate. In all cases, at least one of DCPD and OCP was less supersaturated than HAP and the observed formation of precursor phase(s) was therefore in line with Ostwald's theory. The presence of pure DCPD was clearly detected at low levels of supersaturation, e.g. at low *p*H's or at very low calcium contents. The induction time for OCP formation decreased as the degrees of supersaturation increased. This suggests a link between the supersaturation and the rate of phase transformation of the precursor phase. However, the experimental instrumentation did not provide for firm control over the solution composition during the course of the experiments. In order to tackle this inadequacy, a more versatile set-up was therefore required to analyse the relationship between the supersaturation and the transformation behaviour of precursor phases. This shall be discussed later in Chapter 4.

3.3.3 Morphology of precipitate

Scanning electron micrographs (Figures 3.3 & 3.4) depict morphological characteristics of precipitates and their crystallographic relationships with the hydroxyapatite substrate.

Figure 3.3 shows the typical morphology of DCPD crystals on hydroxyapatite substrates. DCPD crystals grew as efflorescences with blade-like petals measuring ~ 50μm × ~ 10 μm × ~ 2 μm (Figure 3.3b). Efflorescences consisted mainly of two layers of petals, each petal tapering towards its end. The lower layer contained 6 to 8 petals, while the upper comprised 4 to 6 petals. The geometric characteristics of the efflorescences is diagrammatically represented in Figure 3.3c. One would expect two adjacent petals to intersect at the $\{1\bar{1}0\}$ plane, as this is a possible twin-plane in the monoclinic DCPD unit cell (Beevers 1958). With the aid of the lattice parameter of the crystal structure of DCPD (a = 5.812 Å, b = 15.180 Å, c = 6.239 Å, β = 116.42°), we found that:

$$180° - 2 \times \{ (001) \wedge (110) \} = 180° - 2 \times \{ (001) \wedge (1\bar{1}0) \} = 53.2° \qquad ...(3.13)$$

which is very close to the measured values of χ (55°), ∠AOB (51°) and ∠BOB′ (53°). Thus the characteristic appearance of the efflorescence was probably the consequence of intersecting $\{1\bar{1}0\}$

Figure 3.3 Morphology of DCPD crystals deposited on HAP substrates

(a) Low-magnification scanning electron micrograph

(b) High-magnification scanning electron micrograph depicting the characteristic geometry of an efflorescence of DCPD precipitate

(c) Schematic diagram of a typical DCPD efflorescence

Mean values of angles:

$\theta = 11.5°$
$\phi = 62.5°$
$\chi = 55.0°$
$\psi = 35.0°$

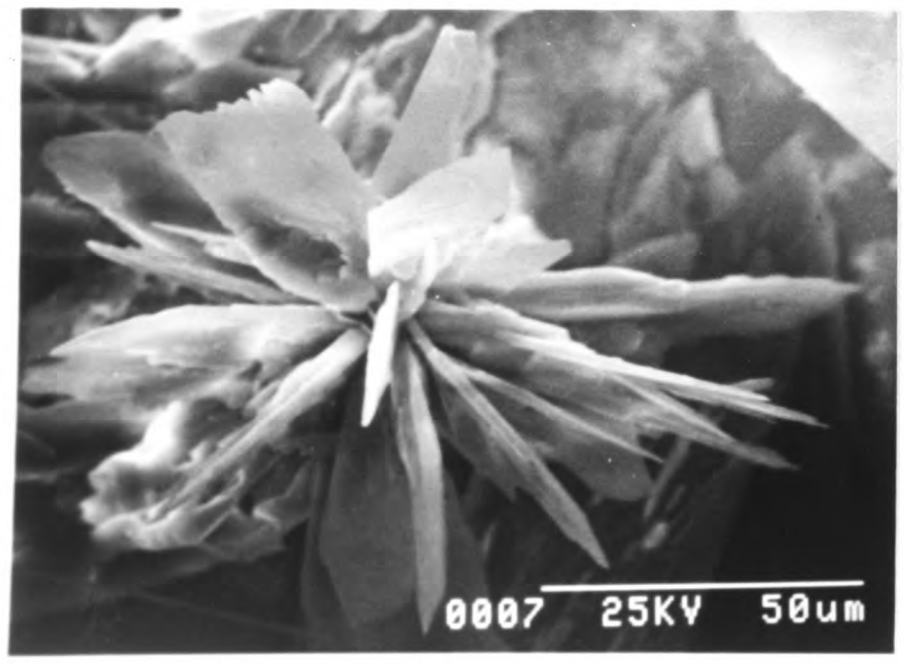

(b)

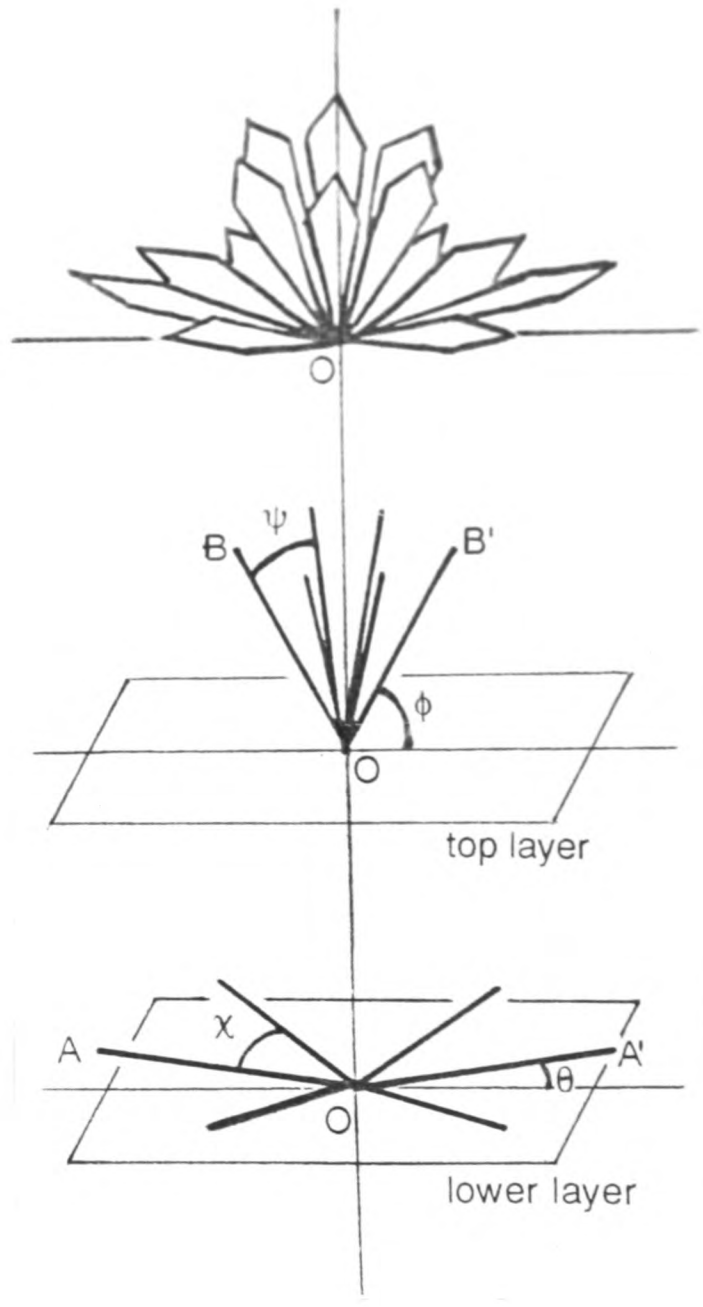

(c)

Figure 3.4 Morphology of OCP crystals deposited on HAP substrates

(a) Low-magnification scanning electron micrograph

(b) High-magnification scanning electon micrograph

(a)

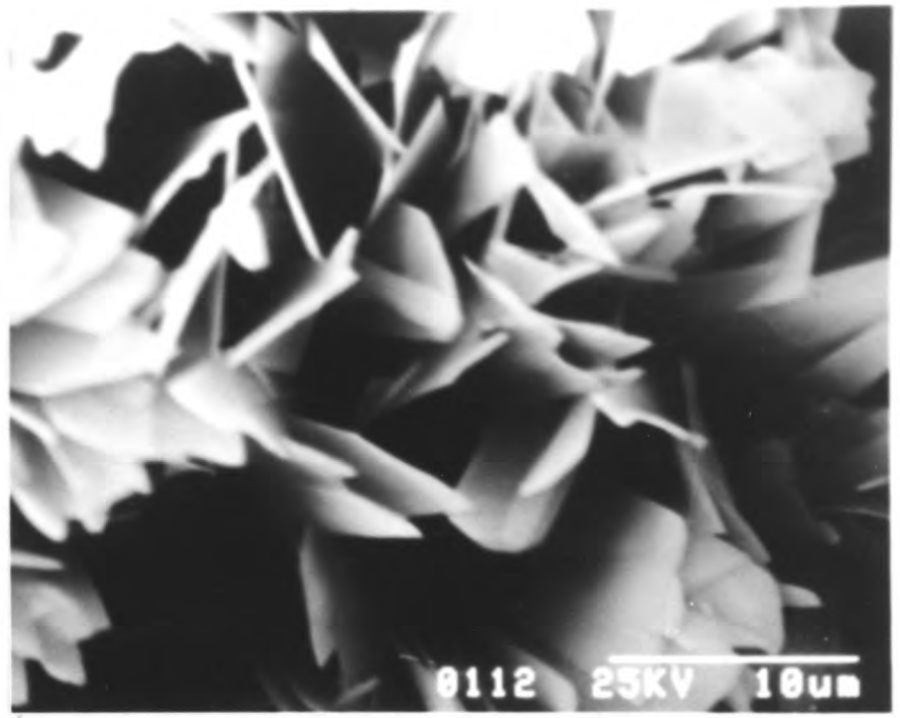

(b)

close-packed planes at the interfaces of adjacent DCPD crystals.

OCP crystals, on the other hand, were more randomly oriented and adopted a more plate-like appearance of dimensions ~ 10 μm × ~ 8 μm × ~ 1 μm (Figure 3.4b). OCP precipitate was also obtained more uniformly over the substrate surface than DCPD (Figures 3.3a & 3.4a). This is probably due to the high similarity between the lattice structures of OCP and HAP (see Section 2.4.1). Thus, crystallographic criteria for secondary nucleation on HAP substrates were less stringent for OCP than for DCPD. In other words, it was more likely for the crystal orientation of an HAP substrate to be suitable for the formation of an OCP-HAP interface than a DCPD-HAP epitaxial or near-epitaxial interface.

3.4 Conclusions

Although these constant-volume experiments only involved very simple instrumentation, they did provide us a lot of useful information about the precipitation behaviour of calcium phosphate in supersaturated aqueous solutions.

The precipitation rate was found to be affected by the concentration of calcium phosphate, the *p*H and the temperature of the system. An increased calcium phosphate content and an increased alkalinity accelerated the precipitation process due to an increase in supersaturation of the various phases, whereas a rise in temperature improved the kinetics of precipitation and thereby increased the rate of precipitate formation.

Having analysed the chemical compositions and the XRD patterns of the precipitates, it was established that although HAP had invariably been the most supersaturated phase in the calcifying solutions, its formation was preceded by the precipitation of less supersaturated precursor phases. The preferential formation of precursor phases has been explained by the fact that thermodynamic driving forces for precipitation were overtaken by kinetic potential, i.e. due to the higher probability of collision of constituent ions, phases of higher solubilities (and hence lower supersaturations) were first precipitated but they later transformed into more stable phases as a result of thermodynamic instability. The formation of precursor phases was in fact consistent with Ostwald's Rule of Stages for the precipitation of sparingly soluble salts.

DCPD and OCP precipitates had characteristic crystal morphologies. DCPD grew in efflorescences consisting of up to 16 blade-like petals. These efflorescences had unique geometric features which were likely to have resulted from common $\{1\bar{1}0\}$ planes at the intersection of adjacent petals. OCP crystals, on the other hand, were more plate-like and did not have geometric features as pronounced as for DCPD. However, the surface coverage of OCP crystals on HAP substrates was found to be more uniform than DCPD crystals. This may have been due to higher lattice compatibility at the OCP-HAP interface than at the DCPD-HAP interface.

In spite of having yielded valuable results, these experiments did reveal certain shortcomings of the constant-volume technique. As all chemical parameters were allowed to drift during the course of the experiments and the deviations depended on the individual conditions, it was difficult to standardise experimental data for rigorous quantitative analyses. Also, it was rather impossible to fully understand what had actually happened at the inception of precipitation since changes occurred at such a rapid rate that it was impossible to rule out the possibility of concomitant reactions. Furthermore, as the ultimate goal of this study is to benefit the understanding of physiological hard tissue mineralisation, we should be able to draw a reasonable analogy between the experimental conditions and the body environment. However, although it was possible to adjust the starting conditions to imitate physiological environment, the composition of body fluids very rarely undergoes changes as drastic as in the experiments. These inadequacies of the constant-volume method presented obstacles to a sound knowledge of the calcification phenomenon. In order to remedy the problems, a better technique needed to be adopted.

Chapter 4

CONSTANT-COMPOSITION PRECIPITATION EXPERIMENTS IN IONIC MEDIA

Since the precipitation behaviour of calcium phosphate is extremely sensitive to changes in the degrees of supersaturation with respect to the various phases, in order to facilitate prolonged and precise investigation, there must be a means to control the solution composition during the course of the experiments.

This problem was overcome with the development of the constant-composition method in which the chemical potentials of the solution species were maintained constant during the reactions. This technique was first developed by Tomson & Nancollas (1978) and has since been significantly modified and improved (Ebrahimpour *et al.* 1991). Further modifications have been necessary to examine a more complete reaction sequence (see Section 4.1.5). Basically, the composition of the solution is closely monitored and any deviation from the initial composition brought about by precipitation is compensated by the addition of appropriate reagents. By keeping the composition constant, it is then possible to look at the crystallisation phenomenon at specific points on the solubility diagram.

4.1 Theory

4.1.1 Basic principle of the constant-composition technique

A supersaturated solution of calcium phosphate acts as a reservoir of the following ions in free or complexed forms: Ca^{2+}, PO_4^{3-}, H^+, OH^-, K^+ and Cl^-. Any precipitation leads to a drop in [ΣCa], [ΣP] and *p*H, and thus appropriate amounts of calcium, phosphate and hydroxide ions which correspond to the stoichiometry of the precipitate need to be added to the solution in order to maintain the constancy of composition. Hence, we need to establish the relationship between the precipitated phase and the formulation of the required titrants.

4.1.2 Deviation in composition due to precipitation

The formation of any calcium phosphate phase can be represented by the following equation

(Winnand & Dallemagne 1962):

$$(5-\eta)\,Ca^{2+} + 3\,H_2PO_4^- + (7-2\eta)\,OH^- \rightarrow (Ca^{2+})_{5-\eta}(HPO_4^{2-})_{\eta}(PO_4^{3-})_{3-\eta}(OH^-)_{1-\eta} \qquad ...(4.1)$$

Here, the phase coefficient, η, acts as an indicator of the actual phase which is being precipitated. For HAP (Ca/P: 1.67), $\eta = 0$; for OCP (Ca/P: 1.33), $\eta = 1$; and for DCPD (Ca/P: 1.00), $\eta = 2$ (a negative OH^- being chemically equivalent to a positive H^+); but any intermediate value between 0 and 2 is also possible - either due to the formation of a mixed phase or as a result of non-stoichiometry. Hence, for a particular value of η, the amounts of the various ions required to maintain the constancy of the composition are in a fixed ratio.

4.1.3 Titrant compositions

The compensation for changes in solution composition is achieved through the addition of standard solutions containing Ca^{2+}, $H_2PO_4^-$ and OH^- ions. Owing to the low solubility of calcium phosphate, it is difficult for Ca^{2+} and $H_2PO_4^-$ to co-exist in a single titrant*. Thus these two ions need to be drawn from separate reservoirs. The auxiliary ions present in these titrants should be the same as in the neutral electrolyte used to stabilise the ionic strength of the solution, in order not to complicate the calculation of titrant compositions. The following calculation assumes that KCl is the electrolyte used and is based on a scheme previously devised by Heughebaert *et al.* (1990).

The addition of four components are necessary to maintain the composition and the ionic strength back at original value: $CaCl_2$, KH_2PO_4, KOH and KCl. These can be grouped into two titrant solutions: one containing $CaCl_2$ and KCl; the other KH_2PO_4 and KOH. If equal volumes of these titrants are added to the solution at the same time, their compositions can be expressed as:

Titrant 1

$$[CaCl_2]_t = (5-\eta)\,C_{eff} + 2\,[CaCl_2]_s\,;$$

$$[KCl]_t = (2\eta-10)\,C_{eff} + 2\,[KCl]_s\,;$$

* For example, at a *p*H value of 7.4, it is impossible to maintain the metastability of a solution with a $[\Sigma Ca] \times [\Sigma P]$ product exceeding a value of around 30 mM^2, as spontaneous precipitation is bound to take place in such a solution. However, to minimise the change in volume of the working solution, the concentration of the titrant needs to be considerably higher than this value.

Titrant 2

$$[KH_2PO_4]_t = 3\,C_{eff} + 2\,[KH_2PO_4]_s\,;$$
$$[KOH]_t = (7 - 2\eta)\,C_{eff} + 2\,[KOH]_s\,;$$

...(4.2)

$[j]_t$ and $[j]_s$ represent respectively the concentrations of j in the titrant and in the calcifying solution. The terms $2[j]_s$ allow for the concomitant dilution of the supersaturated solution as the overall volume of the system increases. Since it is necessary to know the values of $[j]_s$ for the correct formulation of the titrants, the preparation of the working solutions needs to follow a method different from the one used in the constant-volume experiments (see Section 4.2.2). The effective concentration, C_{eff}, denotes the number of moles of precipitate formed per unit volume of titrant addition. As $[KCl]_t$ cannot be less than zero, the maximum value of C_{eff} is $[KCl]_s / (5 - \eta)$. This value of C_{eff} decides the maximum concentrations of the various components in the titrants.

4.1.4 Calcium phosphate dissolution

We have already discussed the formation and the transformation of precursor phases in Chapter 3. The transformation to more stable phases involves solvent-mediated redissolution and recrystallisation. If this phenomenon is to be studied by the constant-composition technique, the dissolution reaction also needs to be compensated.

The dissolution of any calcium phosphate can be represented by the reverse of Equation 4.1, and if C_{eff} is defined as before, its corresponding value for dissolution should be negative, with a magnitude equal to the number of moles of solid dissolved per unit volume of titrant. The titrant compositions can be calculated similarly as above, the only difference being the replacement of KOH by HCl for the lowering of hydroxide level. Thus, for dissolution:

Titrant 1

$$[CaCl_2]_t = (5 - \eta)\,C_{eff} + 2\,[CaCl_2]_s\,;$$
$$[KCl]_t = (2\eta - 10)\,C_{eff} + 4\,[KOH]_s + 2\,[KCl]_s\,;$$

Titrant 2

$$[KH_2PO_4]_t = 3\,C_{eff} + 2\,[KH_2PO_4]_s\,;$$

$$[HCl]_t = (2\eta - 7)\,C_{eff} - 2\,[KOH]_s\,; \qquad ...(4.3)$$

Neither $[CaCl_2]_t$ nor $[KH_2PO_4]_t$ can be negative, hence the maximum value of $-C_{eff}$ is the smaller of $\{2\,[CaCl_2]_s / (5 - \eta)\}$ and $\{2\,[KH_2PO_4]_s / 3\}$.

4.1.5 Application and accuracy

The application of the constant-composition technique requires a means to detect chemical changes in the solution and to add appropriate amounts of titrants. This can be achieved by coupling ion selective electrodes to autoburettes.

For the precipitation of one single phase of a known value of η, the changes in the contents of various ions are always in a fixed ratio. Hence, the concentration of only one ionic species in the solution needs to be followed. The easiest way is to measure the *p*H of the solution and convert the potentiometric output to hydroxide concentration. Depending on the sensitivity of the *p*H meter, the addition of titrants is triggered by a response threshold in the potential difference of, say, $\Delta\delta_{th}$. This tolerance corresponds to a certain molar quantity of precipitation, Δn_{ppt}. Now the titrant concentrations are functions of C_{eff}, which in turn is determined by the volume of titrant to be added to compensate Δn_{ppt}. In general, small volumes are preferred especially in prolonged studies because the actual capacity of the reaction chamber also needs to be practical. Moreover, the injection of larger volumes inevitably lengthens the time delay for composition constancy to be retained. The volume of titrant ΔV should therefore be such that unit step error of the autoburette has negligible influence on the performance while the corresponding value of C_{eff} ($=\Delta n_{ppt} / \Delta V$) is still within the limits as discussed in the previous section.

The above forms the basis for the implementation of the constant-composition technique in systems involving one reaction. However, the precipitation of calcium phosphate very often involves either the simultaneous formation of more than one phase, or the concomitant dissolution and crystallisation of different phases. Thus, the method needs to be extended to respond to two simultaneous reactions.

This has been done by Ebrahimpour *et al.* (1991) by analysing the mutual interference between reactions involving common ions. In principle, two constant-composition devices incorporating two different sensors may be used to simultaneously control two processes. For simplicity, the various combinations of different reactions in the calcium phosphate system are discussed below using the following analogies: (i) growth of BA and BC crystals; and (ii) dissolution of BA and growth of BC crystals.

§ Growth of BA and BC crystals

We first consider the simultaneous growth of BA and BC crystals, utilising B and C electrodes to control BA and BC titrants respectively. As these two phases grow, the change in the concentration of B from the initial value $[B]_i$ to $[B]_x$ will register a potential difference,$\Delta\delta$, in the potentiometric output from B electrode, given by:

$$\Delta\delta = \frac{RT}{z\,F} ln \frac{[B]_x}{[B]_i} \qquad ...(4.4)$$

where z = charge carried by B ion;

R = gas constant;

T = absolute temperature; and

F = Faraday constant.

When the magnitude of $\Delta\delta$ exceeds the response threshold, $\Delta\delta_{th}$, the electrode will trigger the addition of BA titrants in order to compensate for the decline in the B concentration due to the concomitant growth of BA and BC. The relative concentration variation before the addition of BA titrants can be written as:

$$\theta = \frac{[B]_x - [B]_i}{[B]_i} = exp\left(\frac{z\,F\,\Delta\delta_{th}}{RT}\right) - 1 \qquad ...(4.5)$$

Thus, the value of θ depends on the valence of the controlled ion and the response threshold of the potential difference. Since we are only interested in the comparison between the estimated errors in

the single and the dual constant-composition techniques, for simplicity, we can assume θ to be the same for both B and C ions.

Now, if the volume of the working solution is V and the overall molar growth rates of BA and BC are respectively R_{BA} and R_{BC} (mol s^{-1}), the time elapsed before the addition of BA titrants is:

$$\Delta\tau_1 = \frac{\theta\,[B]_i\,V}{R_{BA} + R_{BC}} \qquad ...(4.6)$$

The volume of added BA titrants, ΔV_1, needed to restore [B] to the original value, is given by:

$$\Delta V_1 = \frac{\theta\,[B]_i\,V}{C_{eff}^{BA}} \qquad ...(4.7)$$

Although the concentration of B ions can be maintained constant through the addition of BA titrants, the concentration of C will decrease as the growth of BC proceeds. After a time interval, $\Delta\tau_2$, the change in [C] is sufficient to trigger the addition of BC titrants according to Equation 4.8:

$$\Delta\tau_2 = \frac{\theta\,[C]_i\,V}{R_{BC}} \qquad ...(4.8)$$

where $[C]_i$ is the starting concentration of C ions in the solution. It can be readily deduced that $\Delta\tau_2$ will be longer than $\Delta\tau_1$ if both electrodes have the same sensitivity. In the limiting case which would result in maximum concentration variations, no BC titrant addition would take place before the BA titrant addition of ΔV_1 has been completed. However, once the addition of BC titrant has commenced, it will continue until the C sensing electrode output retains the initial value. The volume of BC titrants added, ΔV_2, is given by:

$$\Delta V_2 = \frac{\theta\,[C]_i\,V}{C_{eff}^{BC}} \qquad ...(4.9)$$

Eventually a steady state will be reached, characterised by constant delay periods for the addition of either set of titrants. It is reasonable to assume that the minute variations in lattice ion concentrations will not change the growth rate or the activity coefficients of the ions. Since the change in [C] is produced by the growth of only the BC phase, BC titrant addition will be controlled by the C sensor as if only this phase were forming in the system. From Equations 4.8 and 4.9, the growth rate for the BC crystals can then be determined:

$$R_{BC} = C_{eff}^{BC} \frac{\Delta V_2}{\Delta \tau_2} \qquad ...(4.10)$$

In the time interval $\Delta\tau_2$, there would be $\Delta\tau_2/\Delta\tau_1$ pulses of BA titrant addition. However, the addition of ΔV_2 of BC titrants will reduce the amount of BA titrant required in the next time period of $\Delta\tau_2$. Therefore, at the steady state, the total amount of BA titrants required in the time period of $\Delta\tau_2$ will be given by:

$$\Delta V_{BA} = \Delta V_1 \frac{\Delta \tau_2}{\Delta \tau_1} - \Delta V_2 \frac{C_{eff}^{BC}}{C_{eff}^{BA}} \qquad ...(4.11)$$

Rearranging Equation 4.11 using Equations 4.6 and 4.7 gives:

$$C_{eff}^{BA} \frac{\Delta V_{BA}}{\Delta \tau_2} = C_{eff}^{BA} \frac{\Delta V_1}{\Delta \tau_1} - C_{eff}^{BC} \frac{\Delta V_2}{\Delta \tau_2} = R_{BA} + R_{BC} - R_{BC} = R_{BA} \qquad ...(4.12)$$

In Equation 4.12, $\Delta V_{BA} / \Delta \tau_2$ is the overall slope of the BA volume-time plot. Thus, the growth rates of BA and BC can be calculated from the corresponding recorded curves. Figure 4.1(a) shows the expected pattern of changes in the lattice ion concentrations. Tracing the changes in [C] after the initiation of precipitation, BC titrants will not be added until [C] decreases by a factor ofθ. This addition will cause a pulsed increase in [C] back to the initial value. This cycle should repeat throughout the experiment. For the common B ions, the concentration will fluctuate between$-\theta$ to $+\theta$. The upper limit will only be reached when the addition of both BA and BC titrants occur simultaneously. The changes in [A] likewise would be within $-\theta$ and $+\theta$.

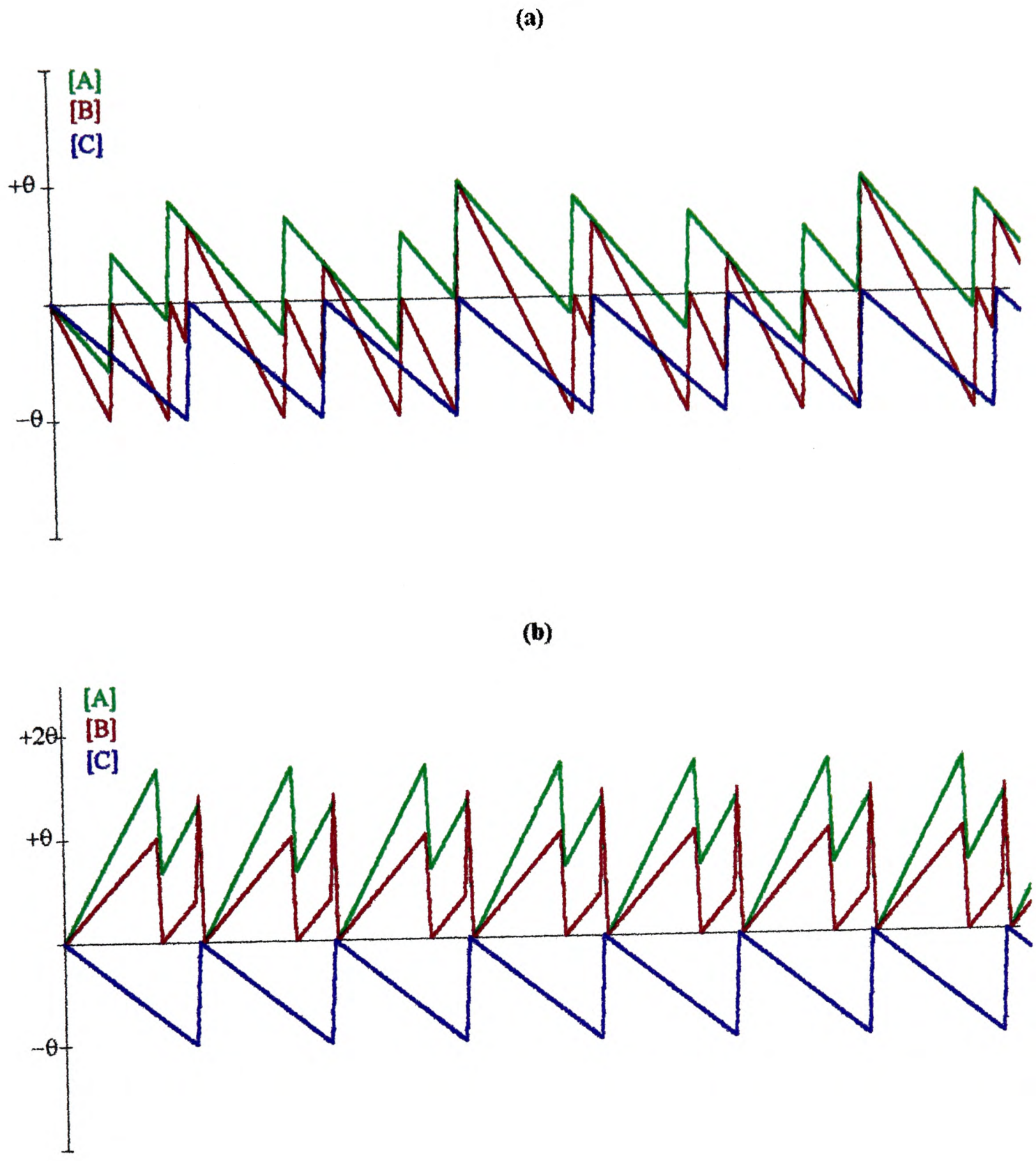

Figure 4.1 Variations in the relative concentrations of A, B and C ions during constant-composition experiments. (a) Simultaneous growth of BA and BC. (b) Simultaneous dissolution of BA and growth of BC. (Ebrahimpour *et al.* 1991)

§ Dissolution of BA and growth of BC crystals

Parallel logic can be applied to the simultaneous dissolution of BA and growth of BC crystals. The expected trends in concentration variations are summarised by Figure 4.1(b). [C] is still maintained between 0 and $-\theta$, while [A] and [B] can vary between 0 and 2θ since the increase in [B] due to BA dissolution is partly compensated by a decrease due to BC precipitation.

The above analysis indicates that the maximum possible concentration variations during a dual constant-composition experiment will be 2θ, double that for the constant-composition control of a single reaction. Provided that the electrodes are of high sensitivity, the thresholdθ should be small enough for relatively insignificant errors.

For the case of calcium phosphate, it is possible to use a Ca^{2+} selective electrode and a *p*H electrode to monitor two simultaneous reactions. As previously discussed, the long-term precipitation of calcium phosphate involves the formation and the subsequent transformation to more stable phases. With the aid of constant-volume experimental results, an expected sequence of formation and thus a scheme of serial reactions can be obtained. For the series of experiments to be discussed in later sections of this chapter, the dual constant-composition technique has been further modified for prolonged studies of phase transformation. The onset of a new reaction (i.e. redissolution of an existing phase or crystallisation of a new phase) would disturb the steady state in titrant addition, and with the aid of a computerised monitoring system, such perturbations would be detected by the monitoring programme and the appropriate action would be taken. For example, if DCPD is the first precursor, DCPD growth titrants are used at the very beginning. The growth rate of DCPD is then obtained from the steady state titration pattern. The formation of this DCPD precursor will proceed until the induction time for DCPD-OCP transformation is reached. At this point, DCPD begins to redissolve, hence lowering the net DCPD growth rate. This is indicated by a deceleration in the rate of DCPD titrant addition. The redissolution of DCPD also signifies the impending formation of OCP. Therefore, the OCP growth titrants should be activated in addition to the DCPD growth titrants. As the transformation proceeds, the net growth rate of DCPD continually decreases until the redissolution rate overtakes the residual growth. When this happens, the DCPD growth titrants will be replaced by the DCPD dissolution titrants. Both the DCPD dissolution and the OCP

growth will continue to speed up until a steady state is maintained. The net rate of the residual DCPD dissolution should become progressively slower because if thermodynamic equilibrium were allowed to be attained after an infinite amount of time, there should not be any net formation or dissolution of non-equilibrium phases. Therefore, at steady state, not only will the addition of OCP growth titrants be at a much faster rate than DCPD dissolution titrants, the actual remaining weight of solid DCPD will also be insignificant compared with OCP. This steady state should continue until OCP-HAP transformation takes place, at which point the DCPD dissolution titrants are replaced by HAP growth titrants; and similarly the OCP growth titrants will eventually be substituted by OCP dissolution titrants.

From the above, it can be seen that the original constant-composition technique has been considerably improved and applied to the prolonged studies of experiments which involve sequential occurrence of reactions. Detailed analysis of the error associated with this theory will be discussed later in this chapter.

4.2 Materials and method

4.2.1 Instrumentation

The experimental set-up comprised two ion analysers and two autoburettes connected to a computer for automatic monitoring. Basically, the potentiometric outputs from the ion meters were sent to the computer which responded to any changes in the solution composition beyond the response threshold by triggering the addition of the appropriate titrants through the automatic burettes. The experimental supervision was performed by a computer programme which was also capable to detect variations in the pattern of titrant addition which signified the onset of new reactions. Appropriate changes in the titrants would then be carried out accordingly. Potentiometric outputs and titration data were registered for future analysis of the variation profiles.

High precision meters and burettes were required to minimise the intrinsic response threshold of the system. A Radiometer PHM85 precision *p*H meter and a Radiometer ION85 ion analyser were used. These meters ran on equivalent circuitries and were chosen for their identical sensitivities. The *p*H meter was used in connection with Radiometer GK2401 combined glass*p*H electrodes while Ca^{2+} activity was measured by Radiometer F2002 Ca^{2+} selective electrodes coupled with calomel

reference electrodes (Radiometer K4040). At least two sets of electrodes needed to be standardised and calibrated at the same time for each experiment because their reliability decreased with the time of usage. Therefore at the recommended three-day intervals, instead of recalibrating the electrodes which would undoubtedly disrupt the flow of the experiments, they were replaced to a new set of pre-standardised electrodes for continuous monitoring. The electrodes were calibrated using standard solutions and buffers as described previously (see Section 3.1.3). Temperature sensors (Radiometer T801) were again attached to the meters for corrections in the outputs. After careful calibration and necessary corrections, the maximum inaccuracy in the potentiometric outputs of*p*H and *p*Ca would not exceed 0.002. Thus a response threshold of 0.005 in the *p*H and *p*Ca outputs was chosen. Depending on the initial values of *p*H and *p*Ca, the corresponding values of Δn_{ppt} for the two reactions in question could be calculated.

Next, two Radiometer ABU91 autoburettes were incorporated into the set-up. Essentially, they were high-precision dispensers which worked on a syringe-type mechanism. The resolution (smallest step size) was 1 $\mu\ell$ with an accuracy of ±0.2% of the injected volume per injection. The smallest possible values of ΔV, the injected volume, were calculated using Δn_{ppt} and the maximum values of C_{eff} for different reactions. These minimum values of ΔV were often used in order to minimise the increase in the total volume of the working solutions.

Both the meters and the burettes were then connected to an IBM-compatible 80386 computer using RS232C serial interface. Two additional dual-channel serial communication boards (Amplicon Liveline PC47AT) were installed in the computer to provide the required communication ports. The boot sector of the operating system was then edited and the ports were configured using the PC42 software (Amplicon Liveline) to match the specifications of the ion meters and the burettes. Since the port configurations of the meters and the burettes were different from the standard arrangement for serial interfacing, special communication cables were tailor-made. The final set-up was then tested using simple test-programmes written to verify the correct interfacing among the different pieces of equipment.

The reception of potentiometric outputs and the transmission of titration commands were handled by a dedicated programme written in C. This programme continuously registered the*p*H and *p*Ca signals, compared these values to the initial composition and sent out signals to the

autoburettes whenever the response threshold was exceeded. The burettes then automatically selected the appropriate titrant and the amount to be injected. The time delays in both burettes were also recorded, and any perturbation from the steady-state would lead to a change in the reservoirs from which titrants were drawn. Finally, the profiles of*p*H, *p*Ca, titrant addition, etc. were recorded in a datafile for subsequent quantitative analysis.

4.2.2 Stock solutions

From the discussion in Section 4.1.3, it is clear that in order to calculate the correct compositions of the titrants, the equivalent concentrations of the titrant components in the working solution need to be known. The method of solution preparation as used in the constant-volume experiments would therefore render difficulties in this respect. The most straightforward way to solve this problem was to prepare stock solutions using the actual titrant components.

Hence, instead of synthetic hydroxyapatite powder, AnalaR grade $CaCl_2$ (Fisons) and KH_2PO_4 (BDH) were used to make up the supersaturated solutions in a manner similar to that of Nancollas and Koutsoukos (1980). Pure solutions of $CaCl_2$ and KH_2PO_4 at the desired concentrations were mixed and the *p*H of the resultant mixture was brought to the required value by the careful addition of KOH. A calculated amount of KCl was then added to maintain a stabilised ionic strength. All these quantities were carefully recorded and were used to calculate the corresponding titrant compositions.

4.2.3 Titrants

Various titrants were prepared for the following reactions: the growth of DCPD, OCP and HAP; plus the dissolution of DCPD and OCP. Their respective concentrations were calculated using Equations 4.2 and 4.3, with the aid of the correct values of η, the chosen values of C_{eff} and the composition of the stock solutions.

4.2.4 Experimental procedure

This series of experiments were performed at the physiological temperature of 37°C which was maintained by means of a water bath. The compositions of the calcifying solutions are summarised in Table 4.1. The calcium content was fixed at 2 mM because firstly this value was very

Table 4.1 Details of constant-composition experiments

Experiment number	[ΣCa] (mM)	[ΣP] (mM)	*p*H	[KCl] (M)	Temp. (°C)	*log* β_{DCPD}	*log* β_{OCP}	*log* β_{HAP}
II-1	2.0	1.2	5.6	0.1	37	0.03	–0.02	4.39
II-2			6.0			0.04	0.07	4.68
II-3			6.4			0.05	0.27	5.15
II-4			6.7			0.06	0.60	5.70
II-5			7.0			0.08	1.10	6.48
II-6			7.4			0.11	1.72	7.32
II-7			7.8			0.16	2.56	8.35

close to the calcium content in body fluid; and secondly, for higher concentrations, it would be extremely difficult to prepare supersaturated solutions over such a broad *p*H range which would remain metastable for durations as long as one week. In spite of the lack of variation in the total calcium content, the supersaturations with respect to the different phases were still nevertheless varied over a very wide range through changes in *p*H. Thus, the fixing of the calcium content did not in any way impair the thoroughness of this study.

In each experiment, an initial volume of 200 $\mu\ell$ was used into which electrodes and burette dispensers were dipped. Moisture-saturated nitrogen gas was bubbled through the solution to eliminate any dissolved CO_2 and the stirring was further enhanced by a magnetic stirrer. As soon as hydroxyapatite substrates were introduced into the solution, the monitoring programme was started and the adjustment of solution composition was then performed automatically. Solid samples were removed from the reaction chamber at regular intervals and the electrodes were changed every 72 hours and recalibrated if necessary. Experiments were allowed to proceed for 7 days. The precipitate was then characterised using methods as described in Section 3.1.4.

4.3 Results and discussion

4.3.1 Rate of precipitation

The overall rate of precipitation was reflected by the rate of titrant addition. Figure 4.2 shows the respective uptake rates of calcium ions for different experiments. It is obvious that precipitation took place at a much faster rate at higher *p*H values. This trend can be explained in terms of supersaturation.

If we take a cross-section of the three-dimensional supersaturation profiles for 37°C (Figure 3.1) at a $[\Sigma Ca] \times [\Sigma P]$ value of 2.4 mM^2, the supersaturation isotherms for the three phases as in Figure 4.3 are obtained. It is clear that as the alkalinity of the solution increases, the various degrees of supersaturation increase accordingly. Thus solutions which were kept at high *p*H values would undoubtedly impart a great differential in free energies between the metastable and the equilibrium states which consequently provided a more remarkable driving force for precipitation.

4.3.2 Precursors and phase transformation

The chemical composition of the precipitate was analysed and once again, the formation of less supersaturated phases was observed. The Ca/P atomic ratios as determined by WDS are listed in Table 4.2 and the corresponding scanning electron micrographs and XRD patterns are also included (Figures 4.4-4.17).

These analyses have provided evidence that at low *p*H values (below 6.7), DCPD was predominantly present in the precipitate for a long period of time. This was particularly true for *p*H values below 6.1 in which cases the solution is undersaturated in OCP, eliminating the possibility of OCP as a precursor. As the *p*H increased, the presence of OCP became progressively apparent. The induction time for OCP formation correspondingly decreased with increasing alkalinity. Indeed, at *p*H 7.4, the presence of DCPD was hardly detected at all, and OCP was found to be the sole precursor phase for almost 100 hours. The presence of HAP was detected in samples obtained towards the end of the experiments at *p*H values higher than 6.7.

From Figure 4.3, the supersaturations with respect to the three phases of calcium phosphate under the current experimental conditions can be obtained. According to Ostwald's Rule of Stages, the emerging phases should follow the sequence of increasing supersaturation with time. Precursors

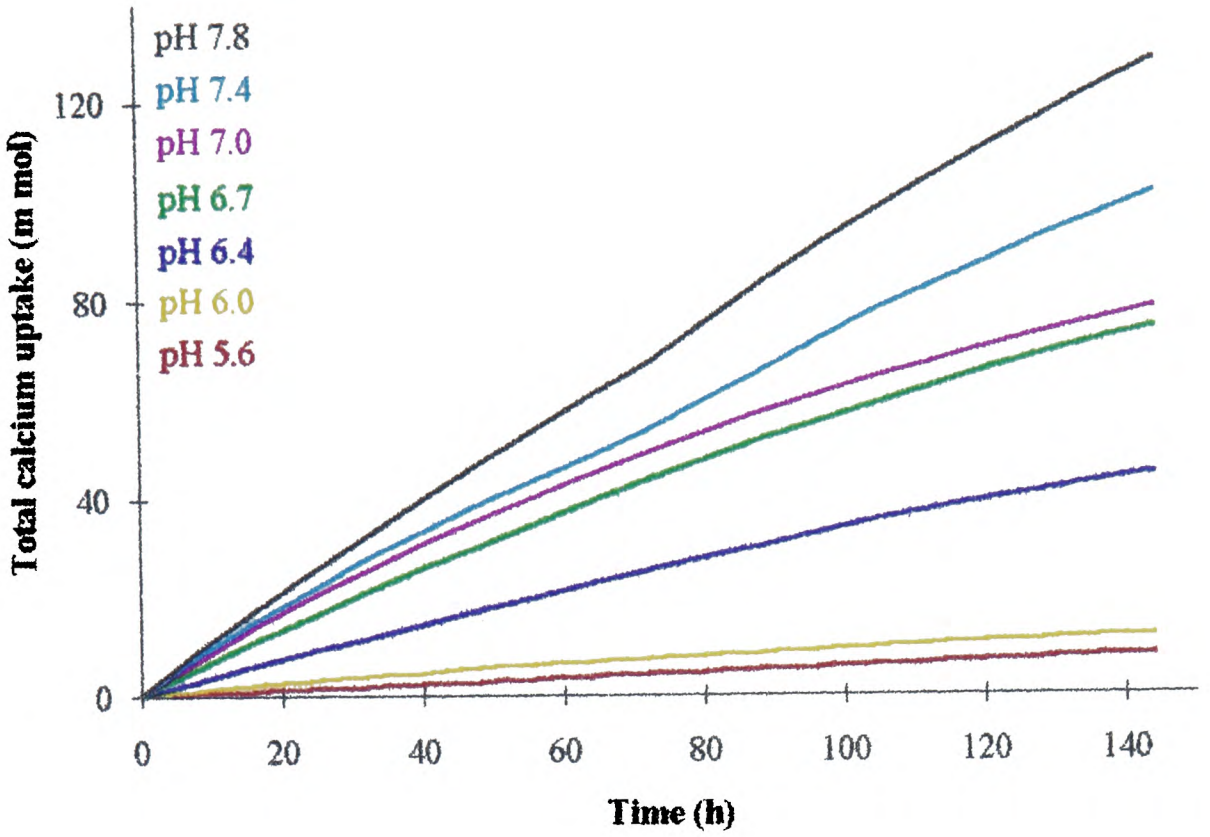

Figure 4.2 The graphs of total calcium uptake against time

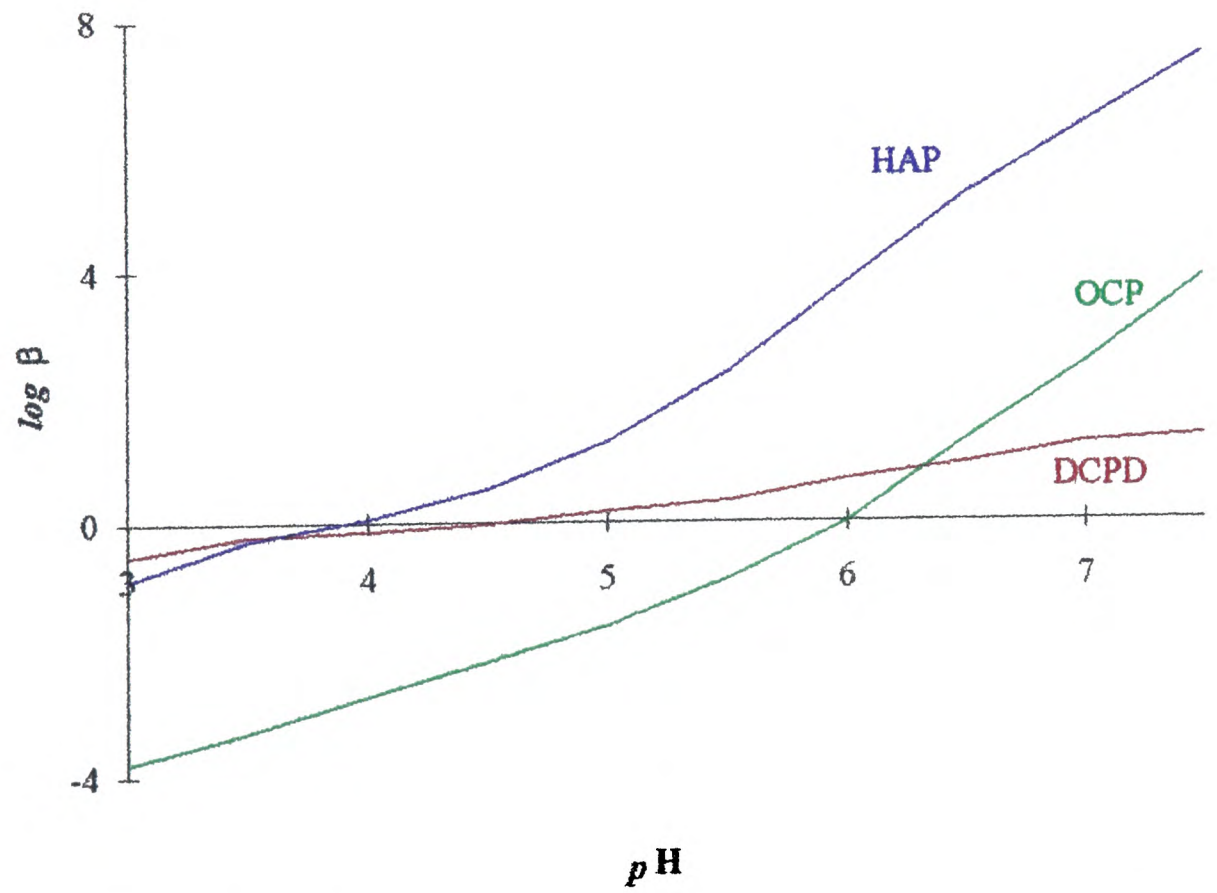

Figure 4.3 Supersaturation isotherms ($[\Sigma Ca] \times [\Sigma P] = 2.4\ mM^2$, 37 °C)

Figure 4.4 Scanning electron micrographs of the precipitate obtained at *p*H 5.6 after 144 hours

(a) Low-magnification micrograph showing the small extent of precipitation and the sparse surface coverage

(b) High-magnification micrograph of the precipitate which has a morphology characteristic of DCPD crystals

Figure 4.5 Scanning electron micrographs of the precipitate obtained at *p*H 6.0 after 144 hours

(a) Low-magnification micrograph showing a much higher degree of precipitation than at *p*H 5.6

(b) High-magnification micrograph which again shows the typical DCPD morphology

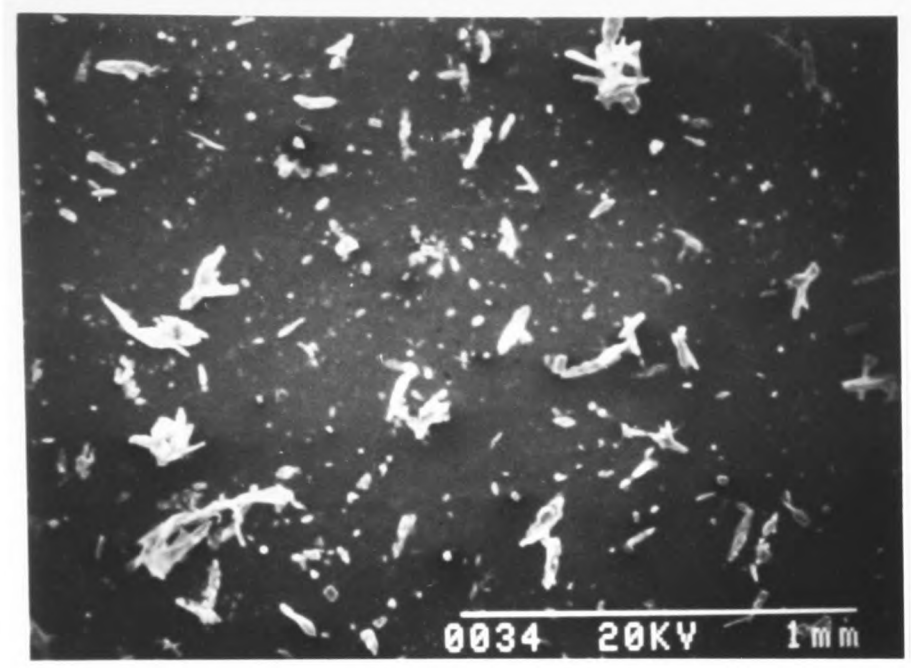

(a)

(b)

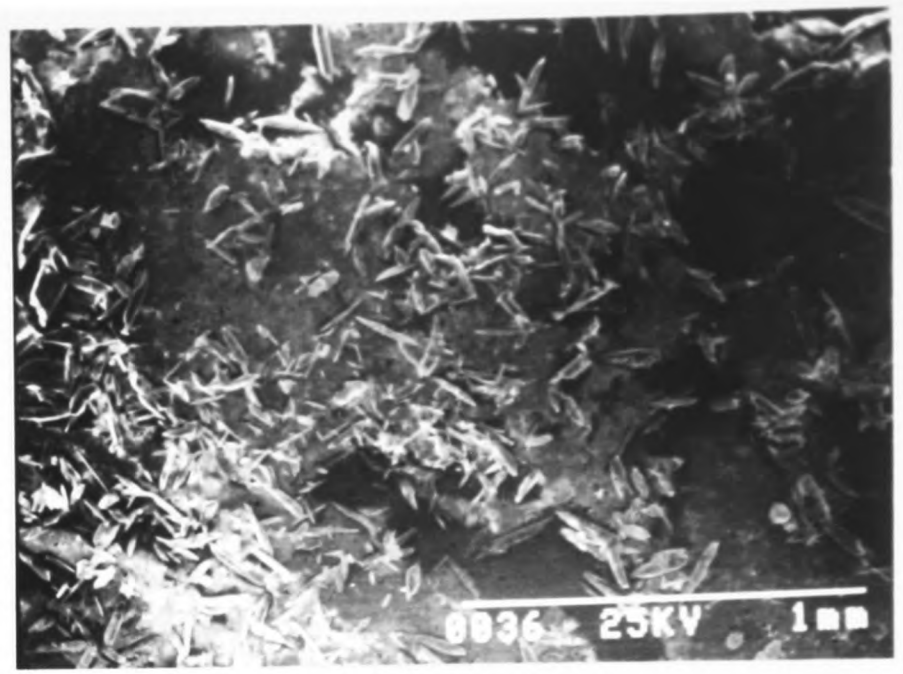

(a)

(b)

Figure 4.6 Scanning electron micrograph of effloresccnces of thick plate-like DCPD crystals obtained at *p*H 6.4 after 144 hours

Figure 4.7 Scanning electron micrographs of the precipitate obtained at *p*H 6.7

(a) DCPD plates, 36 hours

(b) OCP, 72 hours

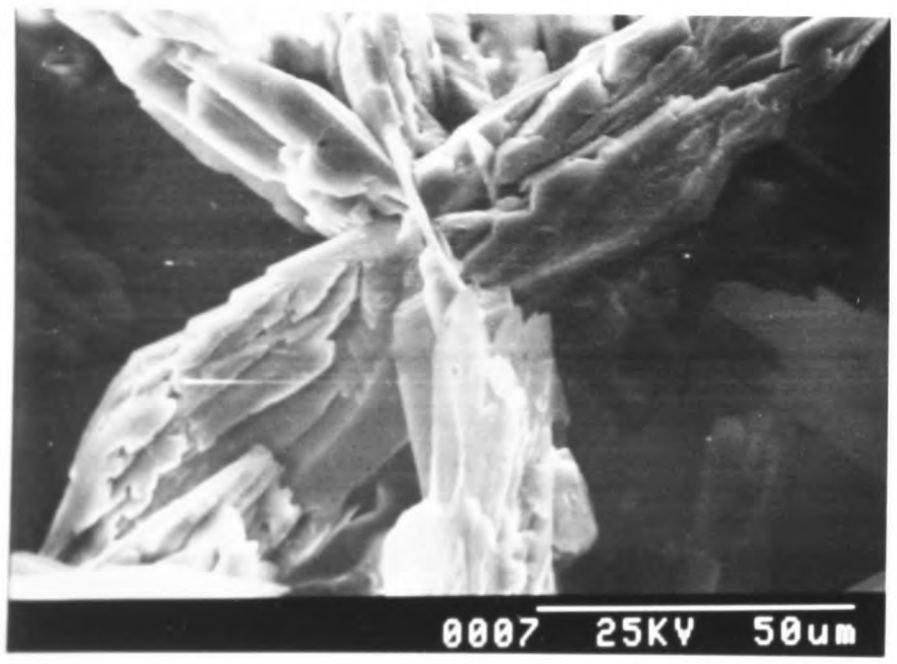

(a)

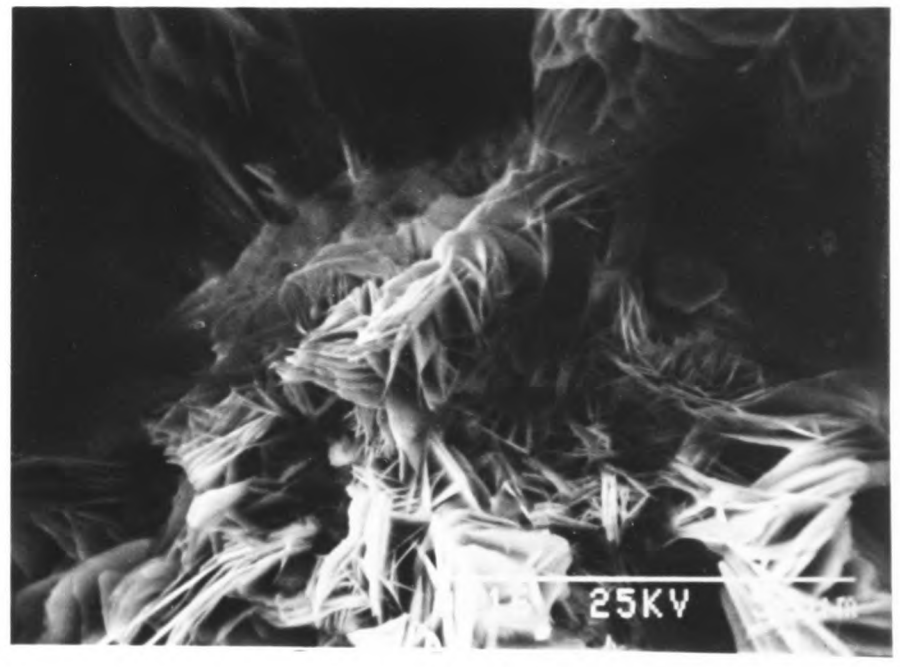

(b)

Figure 4.8 Scanning electron micrographs of the precipitate obtained at *p*H 7.0

(a) OCP plates, 54 hours

(b) (i) OCP with partial transformation to HAP, 140 hours

(b) (ii) High-magnification picture of HAP globule

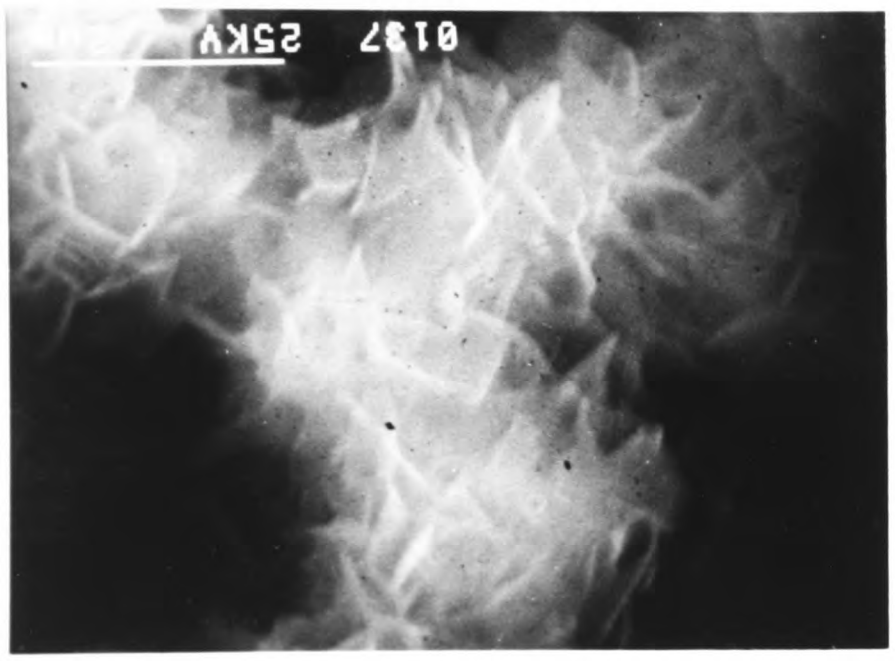

(b) (ii)

(b) (i)

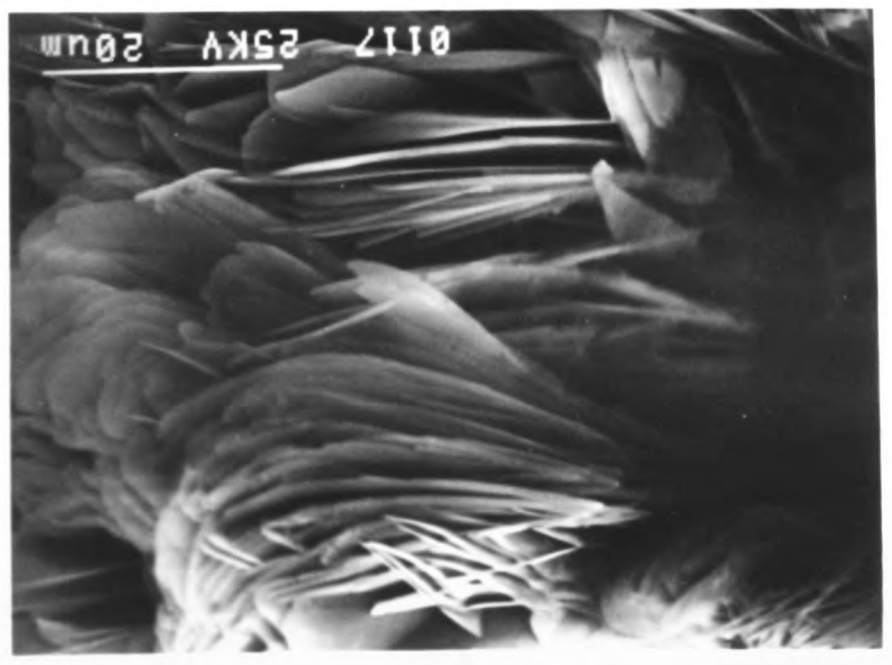

(a)

Figure 4.9 Scanning electron micrographs of the precipitate obtained at *p*H 7.4

(a) OCP plates, 48 hours

(i) Low-magnification micrograph

(ii) High-magnification micrograph

(b) OCP with partial transformation to HAP, 84 hours

(c) HAP platelets, 144 hours

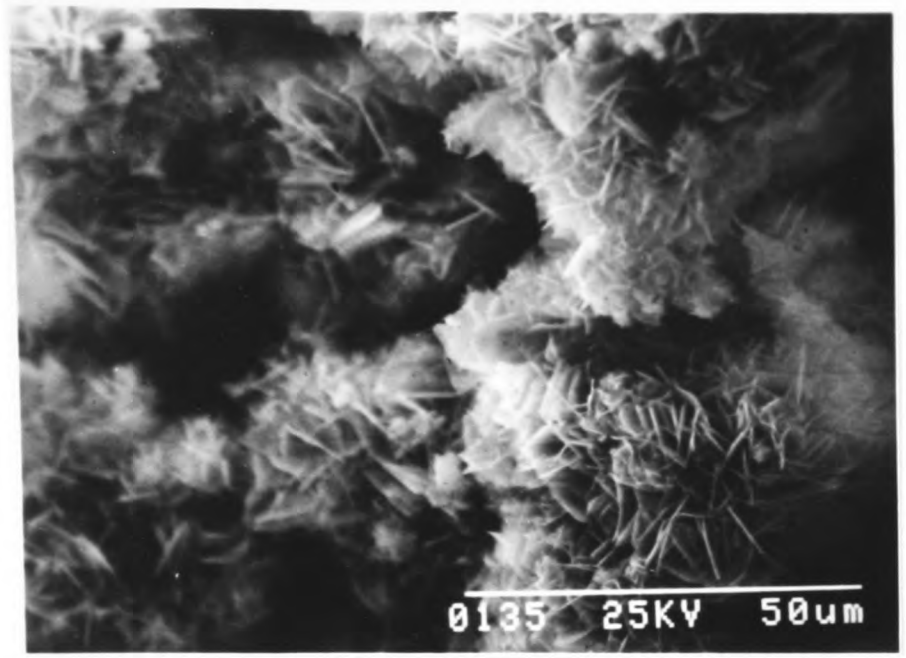

(a) (i)

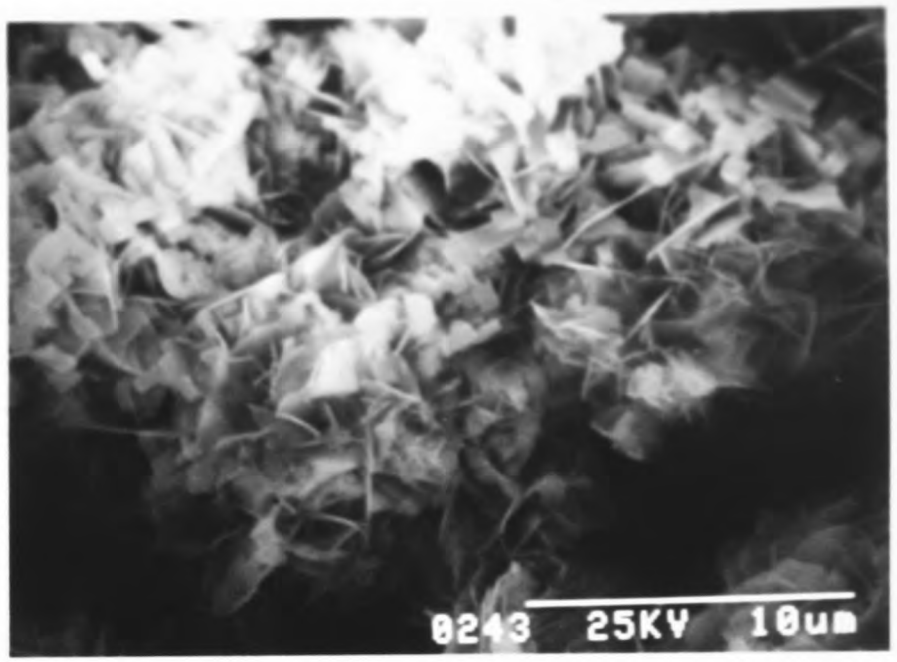

(b)

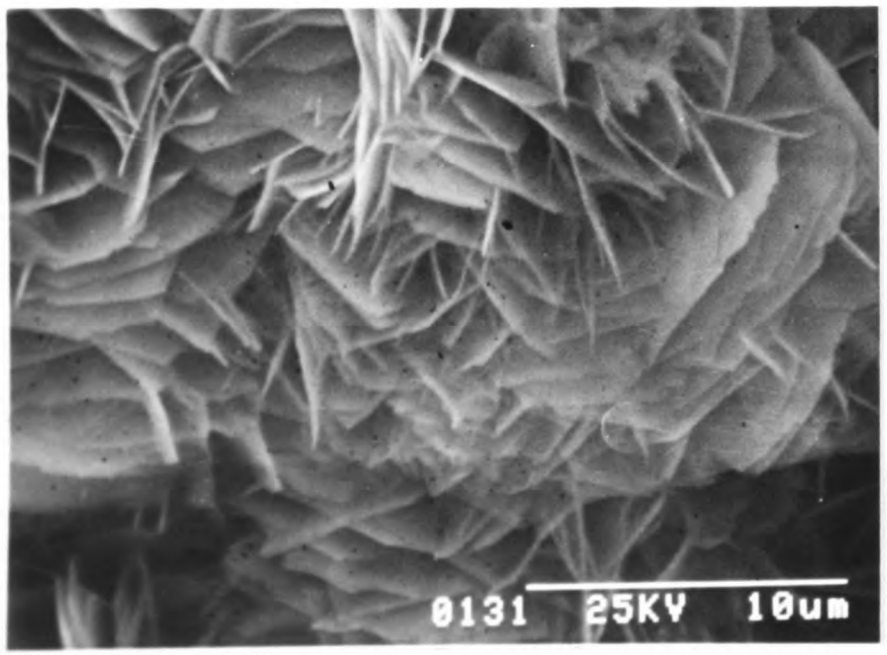

(a) (ii)

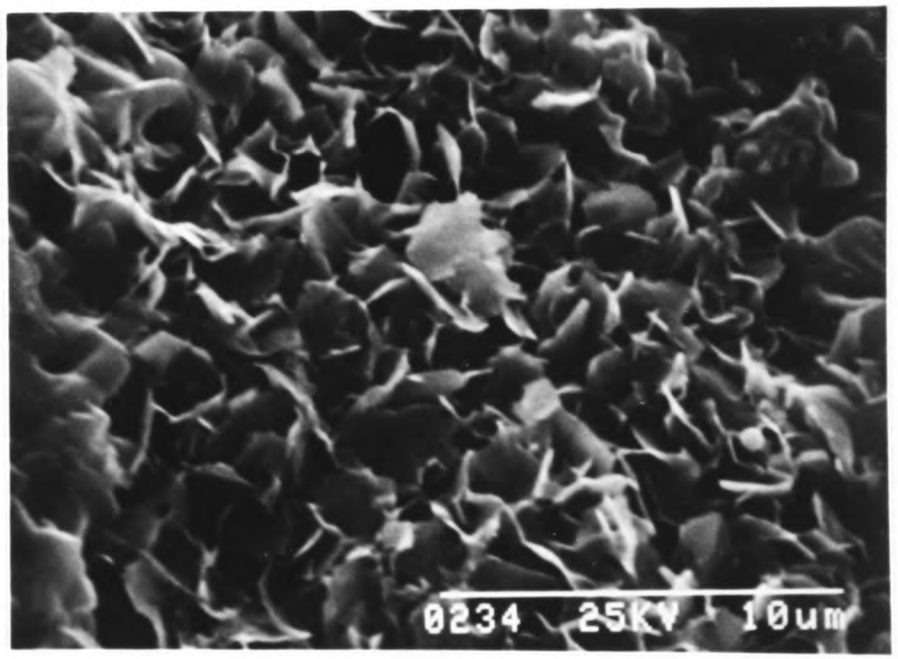

(c)

Figure 4.10 Scanning electron micrographs of the precipitate obtained at *p*H 7.8

(a) OCP, 24 hours

(b) Transformation to HAP, 48 hours

(c) HAP, 84 hours

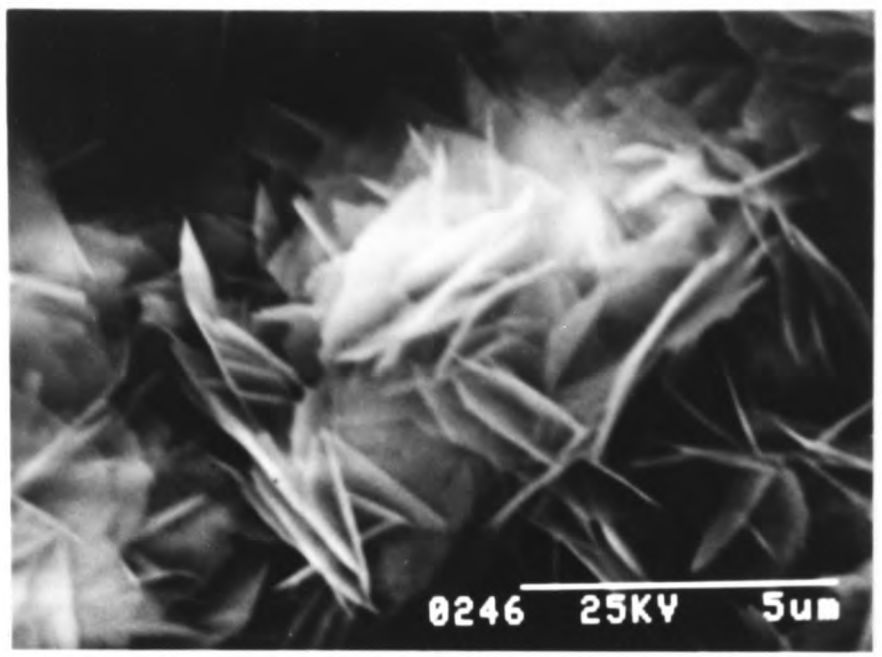

(a)

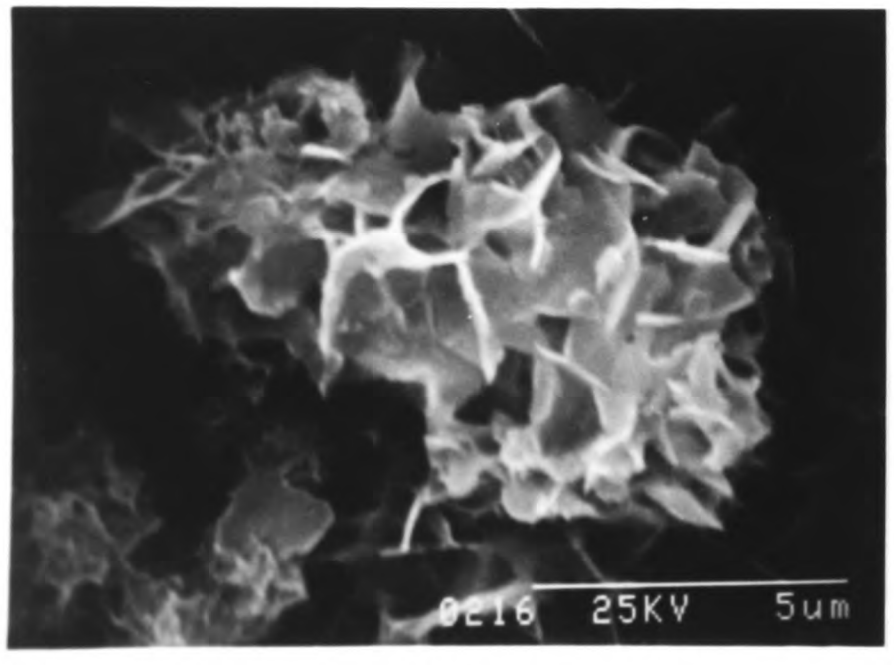

(b)

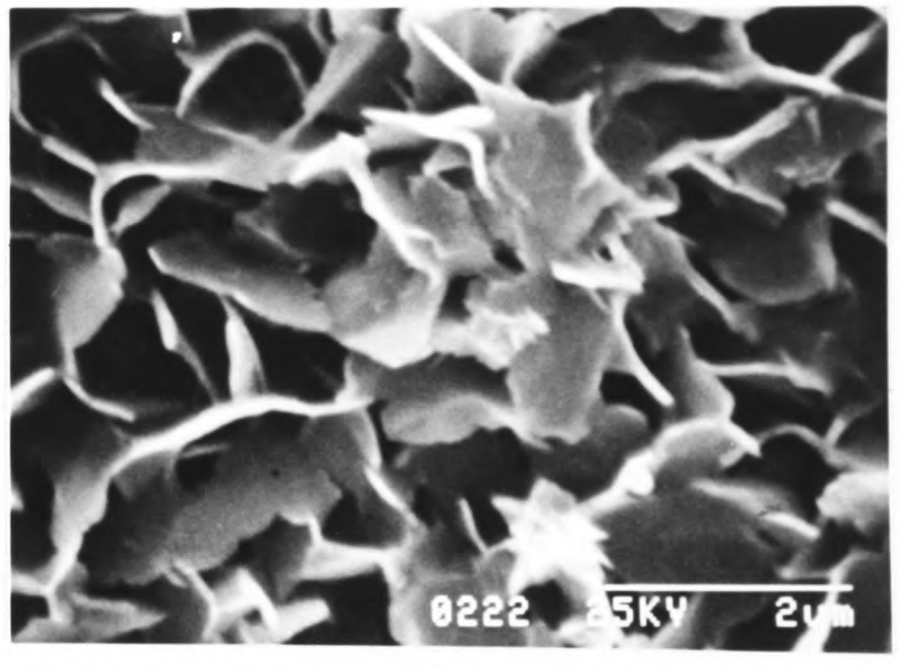

(c)

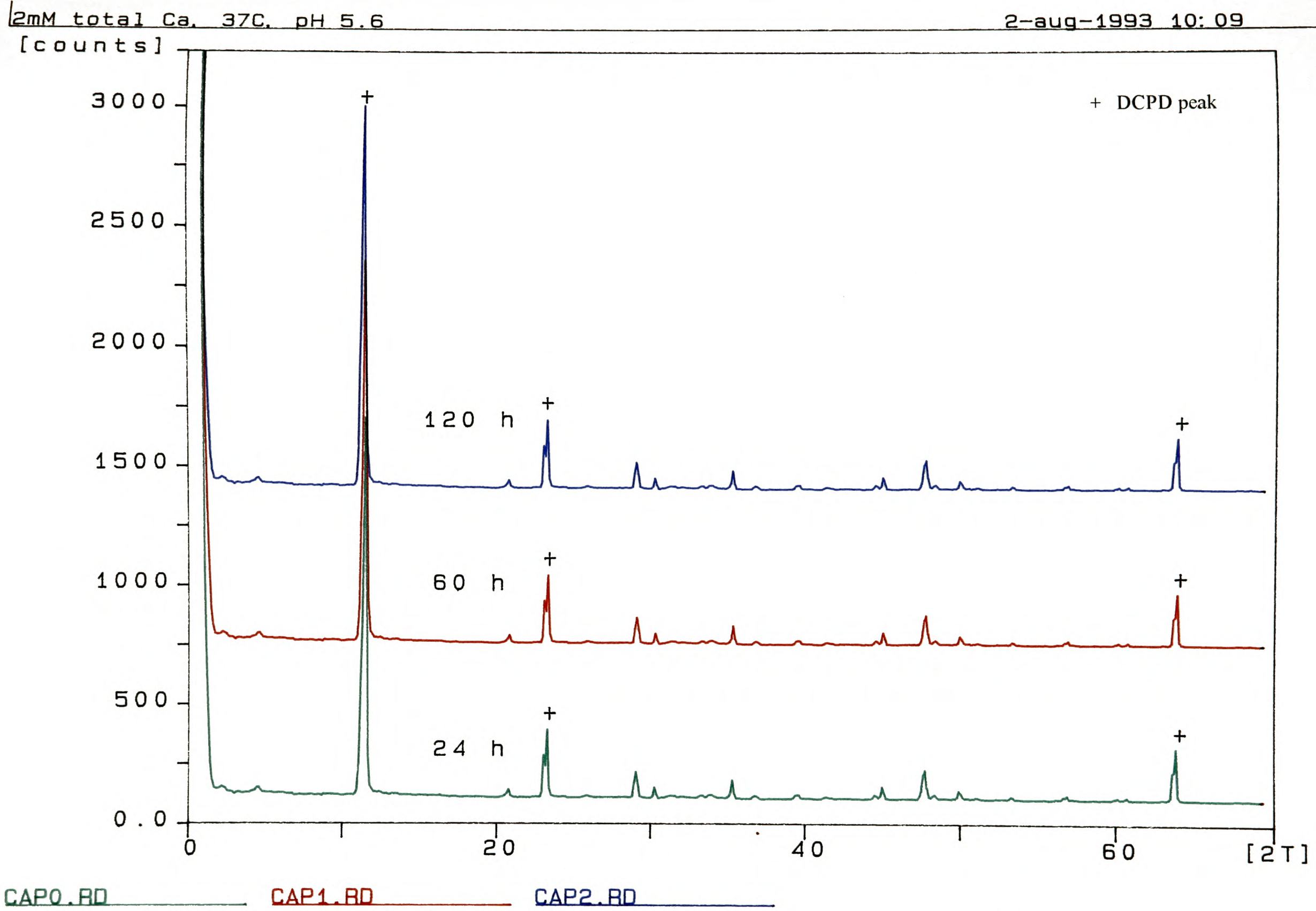

Figure 4.11 Powder X-ray diffraction patterns of solid precipitate obtained at *p*H 5.6

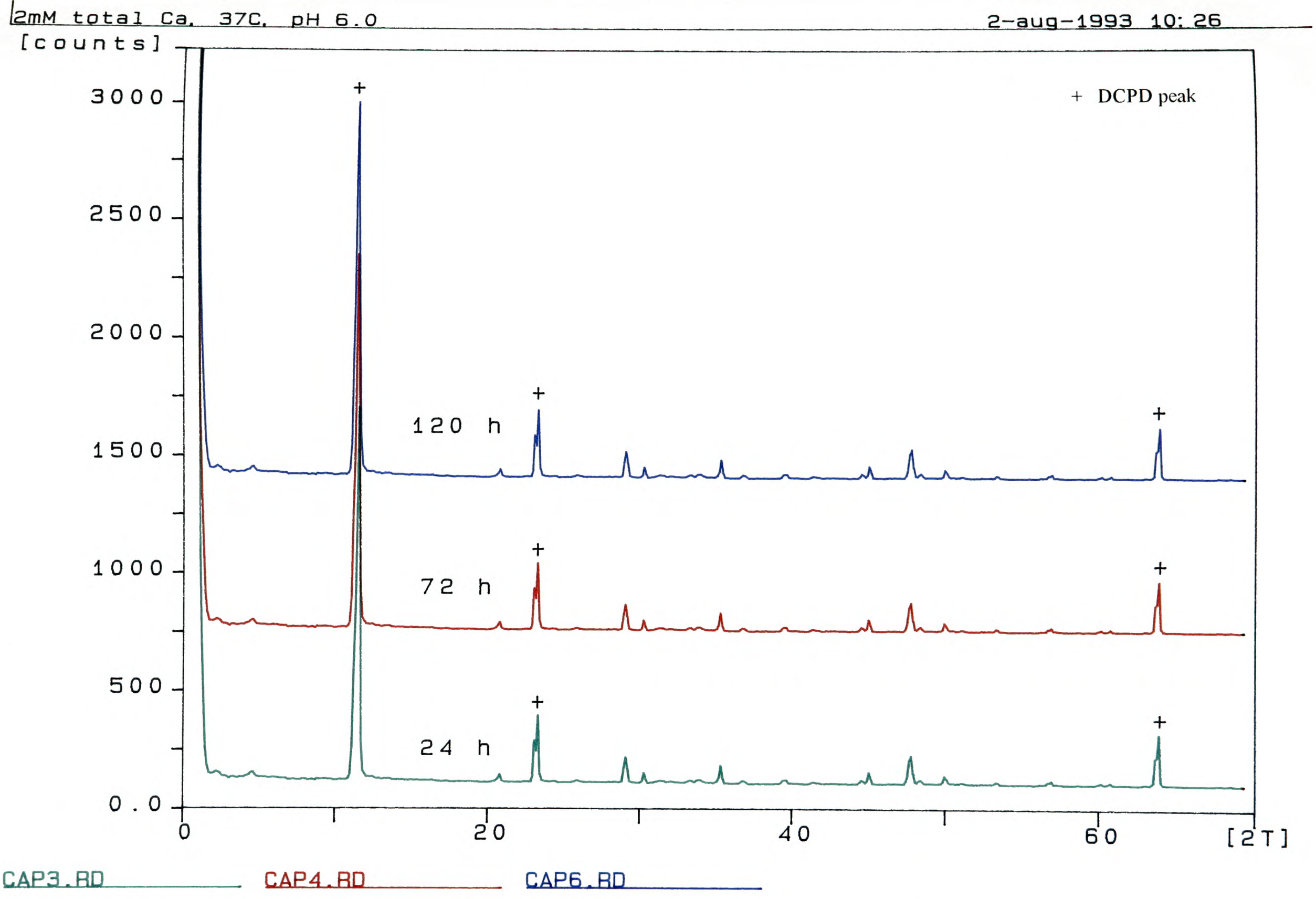

Figure 4.12 Powder X-ray diffraction patterns of solid precipitate obtained at *p*H 6.0

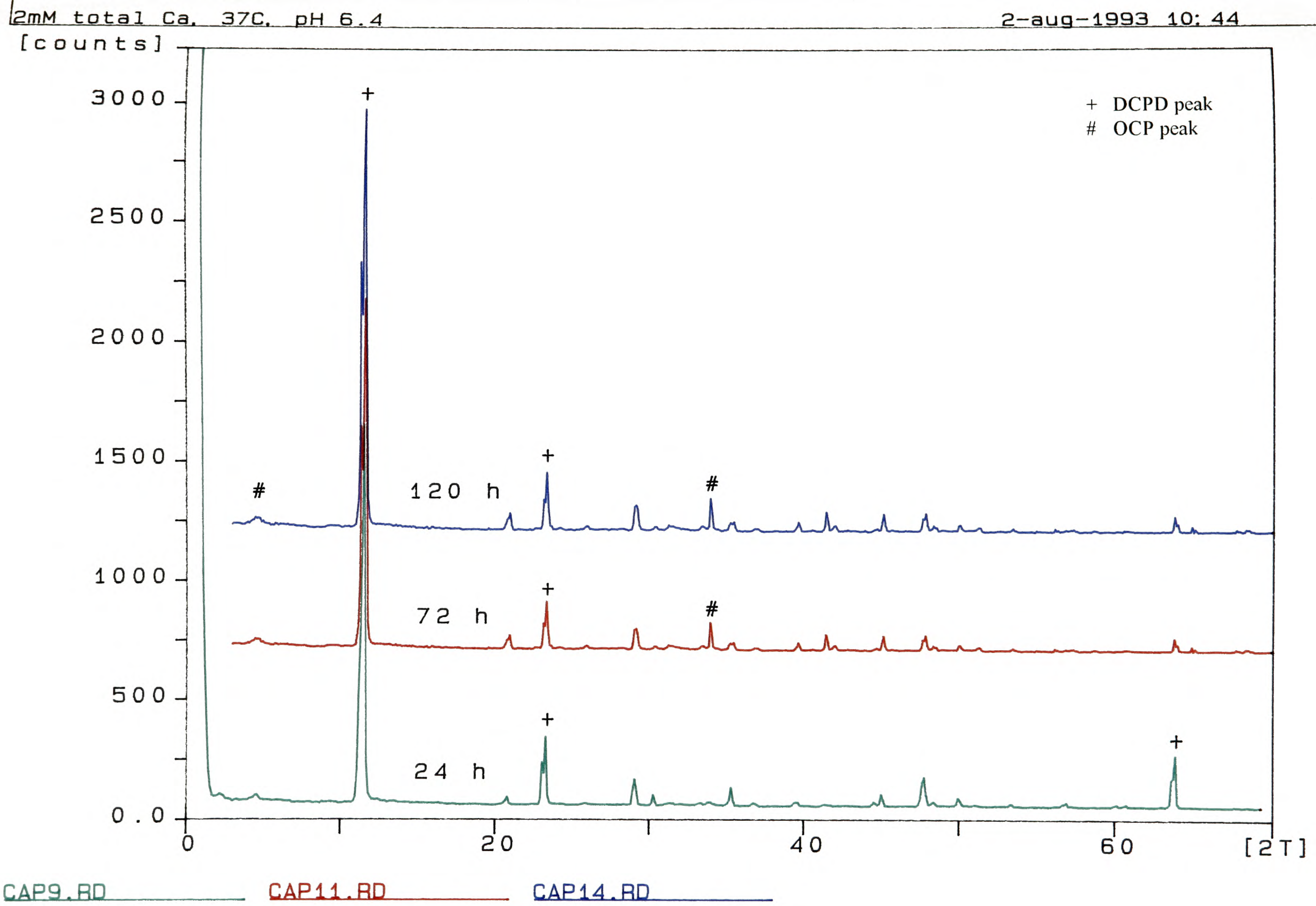

Figure 4.13 Powder X-ray diffraction patterns of solid precipitate obtained at *p*H 6.4

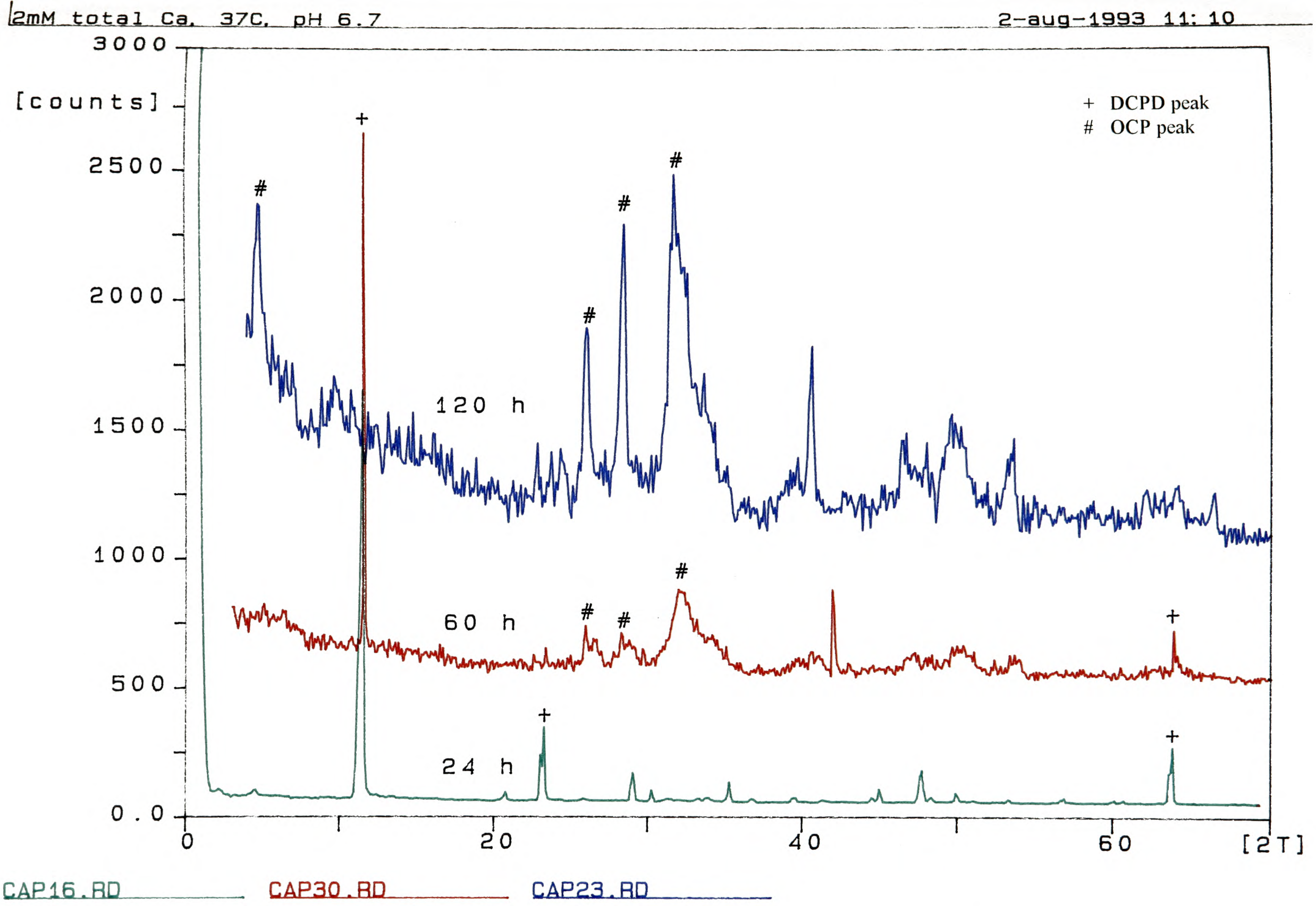

Figure 4.14 Powder X-ray diffraction patterns of solid precipitate obtained at *p*H 6.7

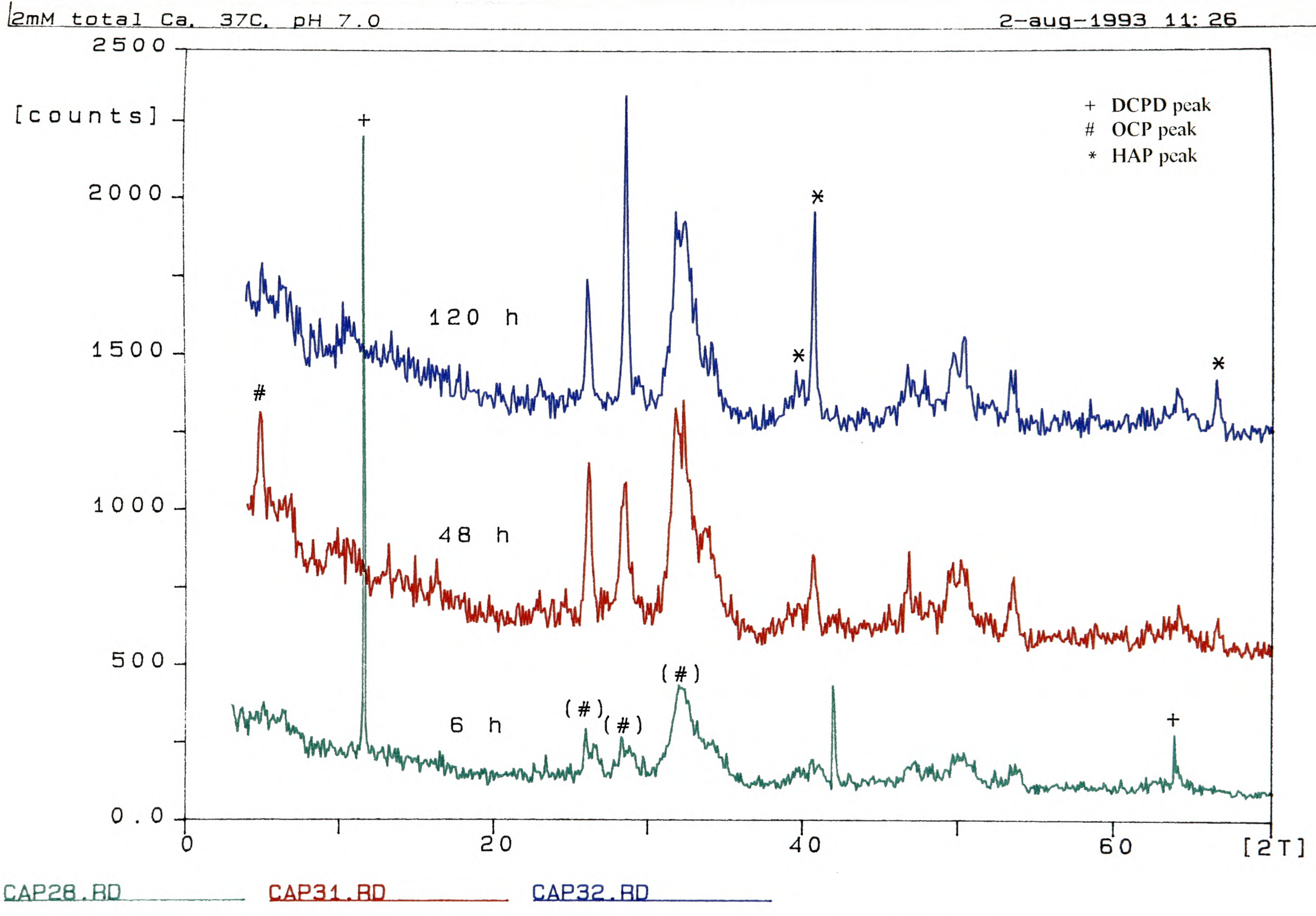

Figure 4.15 Powder X-ray diffraction patterns of solid precipitate obtained at *p*H 7.0

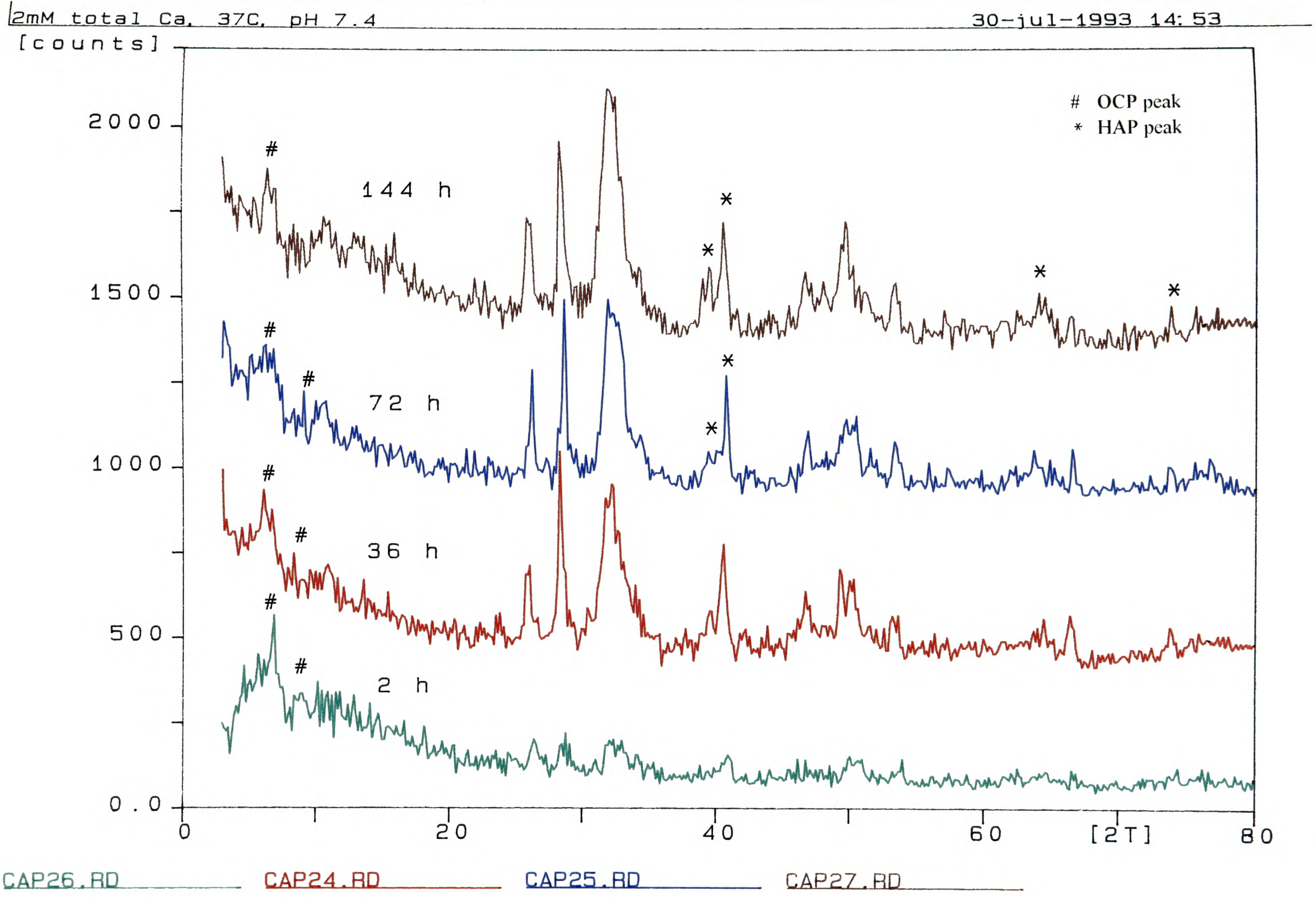

Figure 4.16 Powder X-ray diffraction patterns of solid precipitate obtained at *p*H 7.4

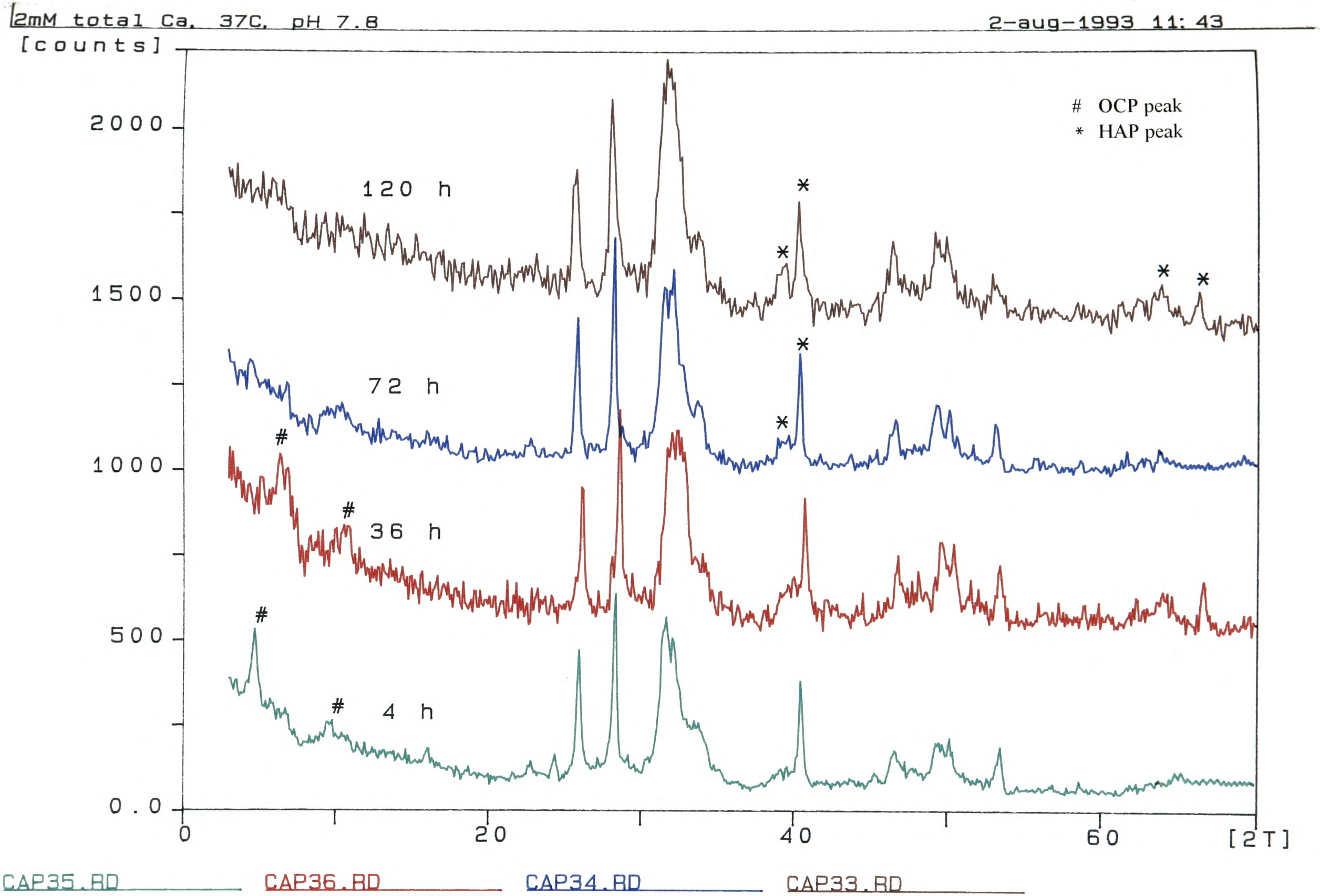

Figure 4.17 Powder X-ray diffraction patterns of solid precipitate obtained at *p*H 7.8

Table 4.2 Ca/P atomic ratio of precipitates from WDS analyses

Expt. no.	*p*H	Elapsed time (h)	WDS Ca/P atomic ratio (±2%)			
			1st reading	2nd reading	3rd reading	Mean
II-1	5.6	24	0.96	0.96	1.00	**0.973**
		60	0.99	0.98	0.99	**0.987**
		120	0.96	1.02	0.98	**0.980**
II-2	6.0	24	0.97	0.98	0.97	**0.973**
		72	0.96	1.00	1.01	**0.990**
		120	1.04	1.06	1.07	**1.057**
II-3	6.4	24	0.96	0.98	0.99	**0.977**
		72	0.95	1.00	1.02	**0.990**
		120	1.08	1.07	1.07	**1.073**
II-4	6.7	24	0.97	0.99	1.01	**0.990**
		60	1.14	1.18	1.15	**1.157**
		120	1.29	1.27	1.30	**1.287**
II-5	7.0	6	1.17	1.20	1.15	**1.173**
		48	1.30	1.28	1.32	**1.300**
		120	1.39	1.41	1.42	**1.407**
II-6	7.4	2	1.28	1.26	1.29	**1.277**
		36	1.29	1.32	1.32	**1.310**
		72	1.39	1.42	I.39	**1.400**
		144	1.58	1.59	1.57	**1.580**
II-7	7.8	4	1.31	1.27	1.30	**1.293**
		36	1.31	1.34	1.35	**1.333**
		72	1.59	1.59	1.61	**1.597**
		144	1.60	1.64	1.63	**1.623**

would then transform in a stage-wise manner eventually to HAP. This trend was generally observed in this series of experiments, and it is also clear that a change in *p*H had significant effects on the growth and transformation rates of the precursor phases. The difference in transformation rates and induction periods is best illustrated by plotting the molar uptake ratio of Ca/P against time (Figure 4.18). The induction times for DCPD-OCP and OCP-HAP transformations decreased quite significantly with increased *p*H. Again, the one major determining factor here is supersaturation. For the same [ΣCa] and [ΣP], an increase in *p*H would increase the supersaturation of all three

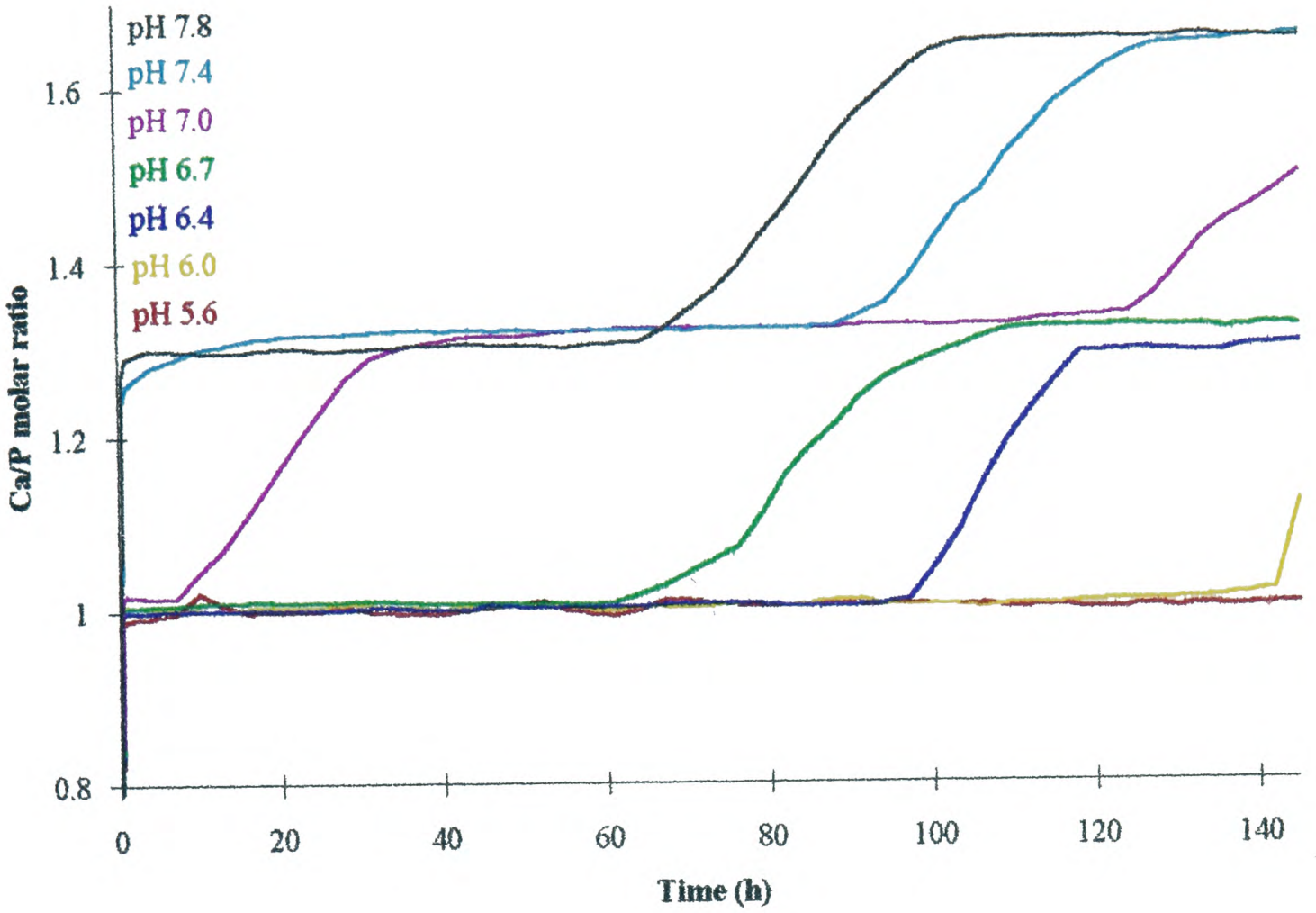

Figure 4.18 The graphs of Ca/P molar uptake ratio against time

phases. However, referring to Figure 4.3, it can be seen that the sensitivity of supersaturation on *p*H variations is not identical for all three phases. DCPD supersaturation does not respond dramatically to *p*H variations, while the supersaturations of OCP and HAP are extremely susceptible to even minor changes in acidity. Now, the transformation to OCP and HAP involved not only the redissolution of precursor but also the formation and growth of nuclei of these new phases, higher OCP and HAP supersaturations indeed improved the probability of nucleation as well as the driving force for the growth of nuclei. Evidence for the difference in nucleation and growth rates was captured by the scanning electron micrographs. The nucleation rate is reflected by the number of crystals per unit surface area or, equivalently, the percentage surface coverage. The growth rate, on the other hand, is closely related to the actual size and dimensions of the crystals. It is quite clear that both these attributes increased when the supersaturations were raised. In short, supersaturation played an important rôle in influencing both the kinetics and the thermodynamics of the transformation process.

4.3.3 Error due to interference between reactions

The accuracy of the dual constant-composition technique may be dependent on the nature of the reactions. It is absolutely essential to make sure that the computer responds to changes in *p*H and *p*Ca values in the correct manner. For the case of simultaneous dissolution and crystallisation reactions, which concurrently exert opposite effects on the overall solution composition, there may be a remote chance that the wrong set of titrants would be added during the period before the system reaches a steady state, yet any maladjustment in solution content would easily be detected and the correct titrants would then be added. However, for the case of parallel precipitation of two different phases, either of the reactions is accompanied by a decrease in the *p*H and the *p*Ca outputs. Since these signals independently trigger the addition of different sets of titrants, there may be a possibility for the wrong set of titrants to be selected. It is therefore necessary to investigate the consequence this may bring about.

Let us consider the case of the simultaneous precipitation of DCPD and OCP, controlled respectively by the Ca^{2+} and the *p*H electrodes. Although the addition of only OCP titrants could maintain constant *p*H, the calcium and phosphate concentrations would not be maintained for any

extended period as a result of the co-existence with the DCPD precipitation reaction. In the initial part of these reactions, upon the precipitation of DCPD, a corresponding volume of DCPD titrants, Ω, should be required. However, if a volume Φ of OCP titrants was instead added in error, the following concentrations would be obtained by considering the material balance:

$$[\Sigma Ca]_x = \frac{2\,V_{x-1}\,[\Sigma Ca]_{x-1} - \Omega\,C_{eff}^{DCPD} + 4\,\Phi\,C_{eff}^{OCP} + 2\,\Phi\,[CaCl_2]_s}{2\,(V_{x-1} + \Phi)} \quad ...(4.13)$$

$$[\Sigma P]_x = \frac{2\,V_{x-1}\,[\Sigma P]_{x-1} - \Omega\,C_{eff}^{DCPD} + 3\,\Phi\,C_{eff}^{OCP} + 2\,\Phi\,[KH_2PO_4]_s}{2\,(V_{x-1} + \Phi)} \quad ...(4.14)$$

$$[KOH]_x = \frac{2\,V_{x-1}\,[KOH]_{x-1} - \Omega\,C_{eff}^{DCPD} + 5\,\Phi\,C_{eff}^{OCP} + 2\,\Phi\,[KOH]_s}{2\,(V_{x-1} + \Phi)} \quad ...(4.15)$$

where subscripts x–1 and x denote the state of the working solution before and after the addition of OCP titrants of volume Φ. On the right hand side of Equations 4.13-4.15, the second terms describe the decrease in the solution concentrations of calcium phosphate and base due to the precipitation of DCPD crystals; and the third and fourth terms represent the increase in the solution concentrations of these species caused by the addition of OCP titrants. The factors of 2 in these expressions account for the concomitant dilution due to an increase in reaction volume. Now, since the $[KOH]_t/[CaCl_2]_t$ and $[KOH]_t/[KH_2PO_4]_t$ molar ratios in the OCP titrants were greater than those for the DCPD growth titrants, the former set of titrants would not provide sufficient calcium and phosphate while still maintaining a constant *p*H value. Thus, the response threshold for the addition of DCPD titrants would eventually be exceeded and the addition of the correct titrants would commence. At this point, the material balance of the system would yield the following expressions similarly as before:

$$[\Sigma Ca]_y = \frac{2\,V_{y-1}\,[\Sigma Ca]_{y-1} - \Omega\,C_{eff}^{DCPD} + 3\,\Theta\,C_{eff}^{DCPD} + 2\,\Theta\,[CaCl_2]_s}{2\,(V_{y-1} + \Theta)} \quad ...(4.16)$$

$$[\Sigma P]_y = \frac{2\,V_{y-1}\,[\Sigma P]_{y-1} - \Omega\,C_{eff}^{DCPD} + 3\,\Theta\,C_{eff}^{DCPD} + 2\,\Theta\,[KH_2PO_4]_s}{2\,(V_{y-1} + \Theta)} \quad ...(4.17)$$

$$[KOH]_y = \frac{2\,V_{y-1}\,[KOH]_{y-1} - \Omega\,C_{eff}^{DCPD} + 3\,\Theta\,C_{eff}^{DCPD} + 2\,\Theta\,[KOH]_s}{2\,(V_{y-1} + \Theta)} \quad ...(4.18)$$

where subscripts $y-1$ and y denote the state of the working solution before and after the addition of DCPD titrants of volume Θ.

The potentiostatically controlled titrant additions were made in pulses with a response threshold of 0.005 in *p*H and *p*Ca. For an initial calcium content of 2 mM, the corresponding change in [ΣCa], θ, required to trigger DCPD titrant addition was about 0.3%. If the volume added per injection, ΔV, was 0.05 mℓ, simulated calculations (Ebrahimpour *et al.* 1991) would furnish the variations in [ΣCa], [ΣP] and *p*H resulting from the maladjustment of solution composition by the addition of OCP titrants as in Figure 4.19. The time interval for OCP titrant addition was only about 0.6 s as estimated from the rate of DCPD growth. Although in reality the time interval could easily exceed this by the slow response of a potentiostat, the calculations show that the period for the delivery of the incorrect titrant would be extremely short. Hence any error thus generated was negligible.

4.3.4 Inadequacy of the dual constant-composition technique

Although the original constant-composition technique has been considerably refined to monitor two simultaneous reactions, there is still room for improvement. The present version has been designed in such a way that any disturbance to the steady state would be recognised as the onset of a new reaction and, since the set-up can only accommodate two reactions, one of the original reactions has to be assumed to have reached completion at that instant. Hence the possibility of having three or more concomitant reactions is ruled out. However, such possibilities do exist - for example, OCP may begin its transformation to HAP before the completion of DCPD-OCP transformation. In this case, the *p*H change brought about by the residual dissolution of DCPD would be compensated by OCP-dissolution titrants. A situation like this would cast uncertainty onto the constancy of composition.

Fortunately in the calcium phosphate systems studied under the present experimental conditions, residual reactions did not present any serious problems. The difference in the induction times for the formation of the different phases was so great (up to 100 hours) that the chances of having three reactions proceeding at comparable rates at the same time were insignificant (see Section 4.3.2). Also, once OCP growth had started, its reaction rate was a lot faster than that for the

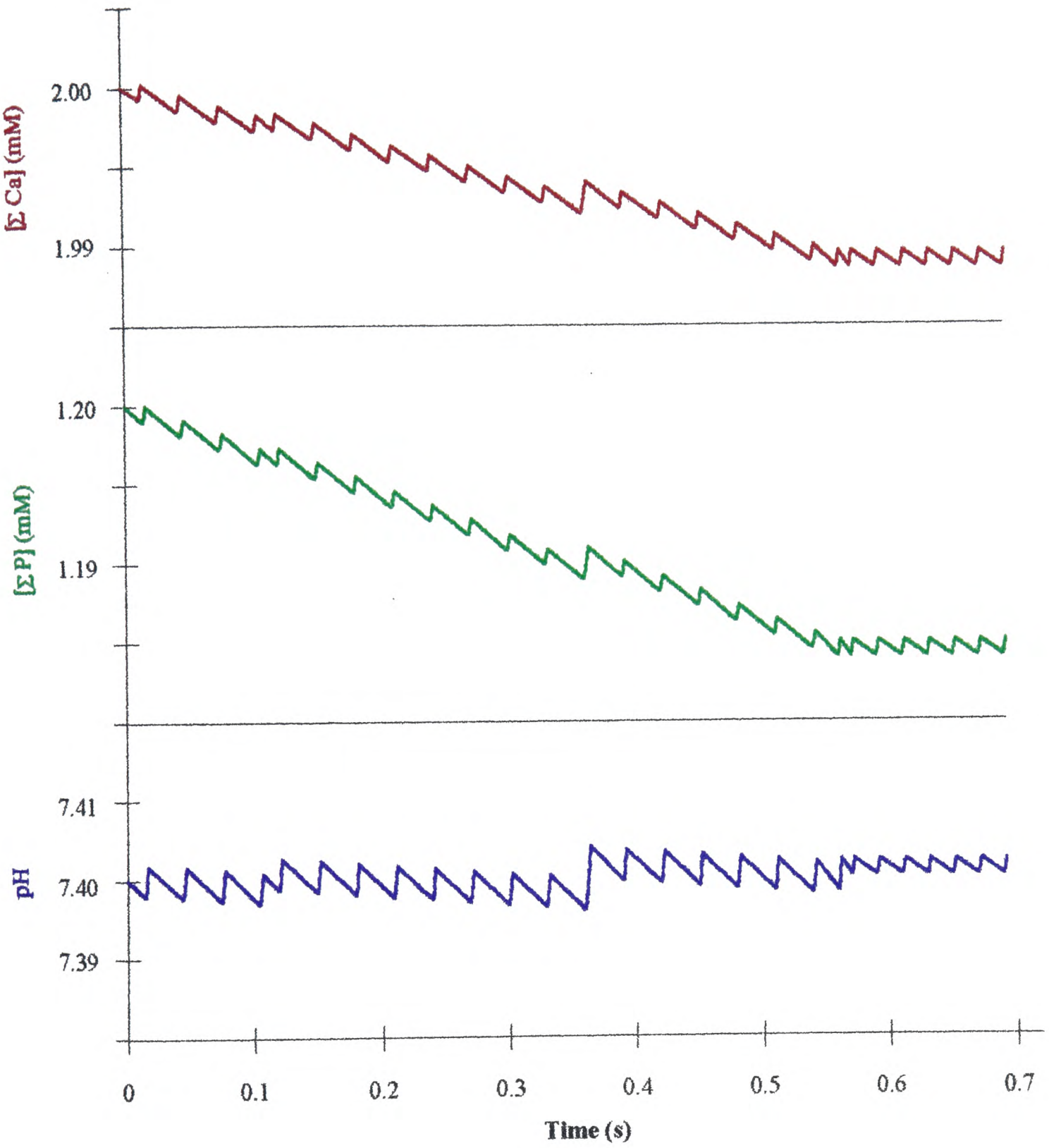

Figure 4.19 Discrepancies in *p*H, [ΣCa] and [ΣP] due to the addition of incorrect titrants, calculated for simultaneous growth of DCPD and OCP (Ebrahimpour *et al.* 1991)

dissolution of DCPD, firstly because it was driven by a much greater supersaturation potential and secondly because the observed dissolution of DCPD was the net result of two conflicting reactions, both of which were a lot slower than OCP growth. At the steady state, the actual DCPD dissolution rate was extremely slow as reflected by the titration profiles. The absence of any major irregularity in the *p*H and *p*Ca profiles around the disruption points of the steady states validated that the assumption that the residual DCPD dissolution had almost no net effect on the overall system. The current method, therefore, still provided an opportunity to study the long-term precipitation behaviour of calcium phosphate with unprecedented accuracy.

Nevertheless, the aforementioned uncertainty may become more prevalent under conditions not covered by these experiments and so there is still a genuine necessity for the further improvement of the technique. However, in order to apply the same principle, the activity of a third (or even a fourth) ionic species needs to be measured. Now, among all the active reactants within the system, Ca^{2+} and H^{+} ions are the ions whose activities can be accurately measured by special selective electrodes. Unless and until we can secure an accurate means to assess continuously the activity of another ion, this problem will remain and it would be difficult to evaluate the ensuing inaccuracy.

4.4 Conclusions

A dual constant-composition equipment was constructed and prolonged studies on the precipitation behaviour of calcium phosphate have been performed. Upon the detailed analysis of any system uncertainties, it was concluded that the present technique has presented a method for the investigation of long-term calcification with unprecedented accuracy.

It was found that the rôle played by supersaturation in the various sub-processes of precipitation is of paramount importance. A high supersaturation not only provided a thermodynamic driving force for crystal growth, the high concentration of dissolved lattice ions also increased the probability for nucleation to occur. Hence, both nucleation and growth, the two processes in crystallisation, depended very much on the degrees of supersaturation. Chemically, supersaturation determined the preferred precipitation of the precursor phase, its chemical composition and its stability; whereas physically, the number of crystals per unit area, the dimensions

and morphology of the crystals and the overall surface coverage were also functions of supersaturation.

However, despite having been the subject of extensive research, the precipitation behaviour can still not be quantitatively explained in terms of the physical and chemical parameters of the system. One reason for this is the extreme complexity of the phase and solution chemistries of calcium phosphate and the lack of understanding of the various determining factors. In the next chapter, an attempt will be made to develop a new precipitation model for calcium phosphate by modifying existing phenomenological relationships and adapting them to this particular system.

Chapter 5

MODELLING OF THE PRECIPITATION BEHAVIOUR OF CALCIUM PHOSPHATE

The precipitation behaviour of calcium phosphate often involves the preferential formation of precursor phases and their subsequent transformation to thermodynamically more stable phases. Although this phenomenon has been extensively studied, there are still no existing models which successfully correlate the determining factors to the transformation process in a quantitative manner. In this chapter, an expression will be derived to describe the overall precipitation behaviour by modifying the Avrami-Johnson-Mehl formula to adapt to aqueous ionic systems. The accuracy of this expression and, in particular, its relevance to *ex vivo* precipitation under physiological conditions will be discussed.

5.1 Derivation of precipitation model

5.1.1 Overview of the precipitation processes

The formation of solid precipitate in a supersaturated solution invariably involves two major processes: nucleation and growth. The ease of these processes determine which particular phases are formed in a supersaturated solution. Although the precipitation of certain phases may not be thermodynamically preferred, their kinetic advantage may still lead to their formation, giving rise to a metastable system. The thermodynamic potential in this metastable system subsequently induces the transformation to equilibrium phases. The detailed mechanism for this phase transformation is still not fully understood, but it has generally been agreed that it is most likely to be a solvent-mediated redissolution and recrystallisation process (Zhang & Nancollas 1990). The following derivation will focus on the various factors which affect the different aspects of precipitation.

5.1.2 Necessary conditions for nucleation and growth

For a particular phase of calcium phosphate to precipitate, the following criteria must first be satisfied:

- Precipitation must be thermodynamically feasible and favourable. This can be true only when the solution is supersaturated with respect to that particular phase, i.e. $\beta > 1$.
- Nucleation must be energetically and probabilistically possible. Appropriate lattice ions and radicals need to collide and the bond energies thus dissipated have to be able to overcome the increase in surface energy associated with a nucleus of critical size.
- Stable nuclei have to be able to grow. This requires thermodynamic driving forces - supersaturation and favourable potential in Gibbs' free energy.

5.1.3 Avrami-Johnson-Mehl expression

Avrami (1939, 1940, 1941) and Johnson & Mehl (1939) proposed that, for a three-dimensional nucleation and growth process involving randomly distributed nuclei, the fractional formation of any particular phase is given by:

$$\phi = 1 - exp\left(- \frac{\pi}{3} N^{n/4} \Gamma^{3n/4} t^{n} \right) \qquad ...(5.1)$$

where ϕ = fractional formation (by volume);

N = nucleation rate (number of nuclei m^{-3} s^{-1});

Γ = growth rate or interface velocity (m s^{-1});

t = time (s); and

n depends on the nucleation and growth mechanism.

Equation 5.1 assumes that nucleation is random in the sense that if we divide the assembly into small equal volume elements, the probability of forming a nucleus in unit time is the same for all these elements. This assumption is as close to reality as possible in the case of dilute and homogeneous solutions. With a random but uniform nucleation probability, the expression for fractional formation of a new phase then builds on the idea that a thermodynamically more favourable phase will crystallise provided that there are pre-existing "germ nuclei" of this new phase in the old phase. Thus N and Γ in Equation 5.1 are respectively the formation and growth rates of such "germ nuclei". This assumption has been generally adopted and Equation 5.1 has indeed been widely used in predicting phase transformation in complex systems such as: (i) Guinier-Preston (GP) zone$\rightarrow \theta'' \rightarrow \theta' \rightarrow \theta$ transformation in aluminium-copper alloys; and (ii) austenite $\rightarrow$ pearlite / bainite

transformations in steels. Although Equation 5.1 has found its widest application in solid-state phase transformation, the original Avrami expression made no assumptions on the type of reaction mechanism, and should therefore be equally applicable to describe transformations of solid phases in contact with solutions. However, it is then necessary to look into the geometry of the actual precipitation process.

For heterogeneous precipitation involving particulate seed substrates in a well-agitated solution, the assumption about the random three-dimensional distribution of "germ nuclei" is close to reality. Unfortunately, for large planar substrates as used in the experiments described in this thesis, the overall precipitation phenomenon actually involves a two-dimensional nucleation process followed by three-dimensional growth. Since the value of n in Equation 5.1 has different indications in two-dimensional and three-dimensional cases, it is important to interpret the significance of any empirically determined value of n. The two-dimensional nature of the nucleation process is in a sense analogous to grain boundary nucleation in solid-state phase transformation. Various models on grain boundary nucleation have been developed (Christian 1975). The value of n is dictated by whether saturation of nucleation site occurs, in which case n takes on a value of 1. This takes place when there are no longer any available nucleation zones on the substrate surface for the heterogeneous formation of stable nuclei. This is true only when the surface coverage of precipitate on the substrate is 100%.

Looking back at Figures 4.4 to 4.10, it can be seen that complete surface coverage was never obtained during precipitation experiments. Consequently, provided that site saturation does not occur, and considering the high degree of approximation and simplification made during the derivation of the original Avrami expression, we will continue to use Equation 5.1 as the starting point for the development of a precipitation model of calcium phosphate in solution. It is, however, important to note that the nucleation rate term used henceforth is in fact modified from the true value.

Now, let us look at the parameters in Equation 5.1 individually.

5.1.4 Nucleation rate, N

The classical equation for the homogeneous nucleation rate in supersaturated solutions is (Boistelle & Lopez-Valero 1990):

$$N = \xi \, exp\left(-\frac{\Delta G_c^{homo}}{k\,T}\right) \qquad ...(5.2)$$

where ξ = kinetic (frequency) factor (number $m^{-3}\ s^{-1}$);

k = Boltzmann constant = 1.3806×10^{-23} J K^{-1};

T = absolute temperature (K);

ΔG_c^{homo} = change in free energy due to homogeneous nucleation.

ΔG_c^{homo} is the summation of the reduction in Gibbs' free energy of the system and the increase in surface energy at the solid-liquid interface. Numerically (Boistelle & Lopez-Valero 1990):

$$\Delta G_c^{homo} = \frac{f\,v^2\,\gamma_{SL}^3}{(kT)^2\,(ln\,\beta)^2} \qquad ...(5.3)$$

where f = shape factor of nucleus, $16\pi/3 \le f \le 32$;

v = volume per molecule in unit cell (m^3); and

γ_{SL} = solid-liquid interfacial free energy of nucleus (J m^{-2}).

The values of v for the different phases can be calculated using the lattice parameters, thus:

for DCPD, monoclinic system;

lattice parameters: a = 5.812 Å, b = 15.180 Å, c = 6.239 Å, β = 116.42°;

unit cell volume = a b c *sin* β = 494.03 $Å^3$;

number of molecules per unit cell = 4;

hence, v = 494.03 $Å^3$ / 4 = 123.51 $Å^3$.

for OCP, triclinic system;

lattice parameters: a = 19.715 Å, b = 9.534 Å, c = 6.839 Å,

α = 90.14°, β = 92.52°, γ = 108.67°;

unit cell volume = $a\,b\,c\sqrt{1 - cos^2\alpha - cos^2\beta - cos^2\gamma + 2\,cos\,\alpha\,cos\,\beta\,cos\,\gamma}$

= 1220.57 $Å^3$;

number of molecules per unit cell = 4;

hence, v = 1220.57 $Å^3$ / 4 = 305.14 $Å^3$.

for HAP, hexagonal system;

lattice parameters: a = 9.432 Å, c = 6.881 Å,

unit cell volume $= \sqrt{3}\ a^2\ c\ /\ 2$

$= 528.80\ Å^3$;

number of molecules per unit cell = 2;

hence, v $= 528.80\ Å^3\ /\ 2 = 264.40\ Å^3$.

γ_{SL}, on the other hand, has been found to vary with *p*H for certain calcium phosphate phases. Using experimental results furnished by Boistelle & Lopez-Valero (1990), these variations in dilute solutions have been approximated to the following linear functions for a *p*H range of 5 to 11:

for DCPD, $\gamma_{SL} = 0.0350\ J\ m^{-2}$ (independent of *p*H);

for OCP, $\gamma_{SL} = (0.0109\ pH - 0.0195)\ J\ m^{-2}$;

for DCPD, $\gamma_{SL} = (0.0283\ pH - 0.1017)\ J\ m^{-2}$.

The kinetic factor, ξ, in Equation 5.2 is a function of the configurational entropy of the system. In the case of crystallisation in dilute solutions, ξ can be approximated to be proportional to the probability (Π) that the appropriate constituent ions collide to form a nucleus. It is assumed that:

- only the appropriate lattice ions of each phase are involved in the processes - dissociation kinetics of other entities in the solution are not taken into account;
- the probability for the lattice ions to meet simultaneously is equal to the probability of drawing them from an infinite reservoir of the given composition of the solution - intrinsic differences in ion mobilities are neglected;
- the collision of the growth unit ions results in a molecule which has the composition of the crystal.

Hence,

$$\xi = K_i\ \Pi \qquad ...(5.4)$$

where K_i is a constant (number $m^{-3}\ s^{-1}$).

Let us consider an infinite reservoir containing n_1 Ca^{2+} ions, n_2 HPO_4^{2-} ions, n_3 PO_4^{3-} ions, n_4 OH^- ions and n_5 H^+ ions. For the formation of a DCPD nucleus, it is necessary for one Ca^{2+} and one HPO_4^{2-} ion to collide. Such a probability is given by (Boistelle & Valero-Lopez 1990):

$$\Pi^{DCPD} = \frac{\binom{n_1}{1}\binom{n_2}{1}}{\binom{n_1+n_2}{2}} \qquad ...(5.5)$$

In a solution of molarity m_j in each growth unit of type j, the corresponding n_j per unit volume is equal to $N_A\, m_j$, where N_A is the Avogadro's number. Hence Equation 5.5 can be rewritten as:

$$\Pi^{DCPD} = \frac{2!\, N_A\, m_1 \times N_A\, m_2}{(N_A\, m_1 + N_A\, m_2)!\,/\,(N_A\, m_1 + N_A\, m_2 - 2)!} \qquad ...(5.6)$$

Since the number of growth units are large, the denominator of Equation 5.6can be simplified in the following way:

$$\frac{(N_A\, m_1 + N_A\, m_2)!}{(N_A\, m_1 + N_A\, m_2 - 2)!} \approx (N_A\, m_1 + N_A\, m_2)^2 \qquad ...(5.7)$$

Accordingly, Equation 5.6 can be approximated to:

$$\Pi^{DCPD} = \frac{2!\, N_A\, m_1 \times N_A\, m_2}{(N_A\, m_1 + N_A\, m_2)^2} = \frac{2!\, m_1\, m_2}{(m_1 + m_2)^2} \qquad ...(5.8)$$

By similar reasoning, Π for all calcium phosphate phases can be derived, viz.:

$$\Pi^{DCPD} = \frac{2!\,[Ca^{2+}]\,[HPO_4^{2-}]}{([Ca^{2+}] + [HPO_4^{2-}])^2}$$

$$\Pi^{OCP} = \frac{7!\,[Ca^{2+}]^4\,[HPO_4^{2-}]\,[PO_4^{3-}]^2}{4!\,2!\,([Ca^{2+}] + [HPO_4^{2-}] + [PO_4^{3-}])^7}$$

$$\Pi^{HAP} = \frac{9!\,[Ca^{2+}]^5\,[PO_4^{3-}]^3\,[OH^-]}{5!\,3!\,([Ca^{2+}] + [PO_4^{3-}] + [OH^-])^9} \qquad ...(5.9)$$

However, since typical crystallisation processes involve heterogeneous nucleation on existing seeds rather than spontaneous homogeneous nucleation, certain alterations must be made in Equation 5.2 to account for the creation of solid-solid interfaces. The following expression relates homogeneous and heterogeneous nucleation rates (Christian 1975):

$$\frac{N^{hetero}}{N^{homo}} = \lambda = \frac{\delta}{L} \exp\left(\frac{\Delta G_c^{homo} - \Delta G_c^{hetero} - \Delta g^{strain}}{k\,T}\right) \qquad ...(5.10)$$

where δ = boundary layer thickness;

L = substrate crystal grain size; and

Δg^{strain} = strain energy due to lattice mismatch between precipitate and substrate.

Provided that precipitation takes place in a well-stirred working solution and that the substrate seeds are of uniform grain size, δ and L in Equation 5.10 can be assumed constant. ΔG_c^{hetero} is a function of free energies of both the substrate and the precipitating phases as well as the solid-solid interfacial energy, γ_{xy}. The term Δg^{strain} comes into effect whenever the substrate is a different phase from the precipitate. Owing to the high similarity of their respective crystal structures along certain directions, Δg^{strain} is minimal at an OCP-HAP interface. However, Δg^{strain} may be more prominent in the cases of DCPD-OCP and DCPD-HAP interfaces as a result of significant lattice distortions at the solid interface (See section 2.4.1). The dimensionless variable λ in Equation 5.10, therefore, accounts for the combined effect of the heterogeneity of nucleation and the strain arising from lattice mismatch.

Combining Equations 5.2-5.10, the rate of heterogeneous nucleation is in the form of:

$$N^{hetero} = K_{ii}\,\lambda\,\Pi \exp\left[-\frac{f\,v^2\,\gamma_{SL}^3}{(kT)^3\,(ln\,\beta)^2}\right] \qquad ...(5.11)$$

where K_{ii} is a constant (number $m^{-3}\,s^{-1}$).

5.1.5 Growth rate, Γ

An interface is created during the nucleation stage and then propagates during the growth stage. While the nucleation stage determines many features of the crystallisation and transformation, most of the crystallisation product is formed during the growth stage by the transfer of ions across the moving precipitate-solution interface.

Growth of existing nuclei is controlled either by bulk diffusion or by interface reactions (Porter & Easterling 1981). The value of n in Equation 5.1 depends on the nucleation and growth mechanisms (Christian 1975). Provided that there is no change in the nucleation and growth mechanisms, n is independent of temperature. As there is little hindrance to diffusion in dilute aqueous solutions (i.e. the interfacial composition of the solution can be approximated to be the same as the bulk composition), crystal growth under these circumstances is very likely to be interface-controlled. This is true particularly at smooth solid-liquid interfaces. If a single molecule leaves the liquid and attaches itself to the flat solid surface, a number of bonds on the solid surface near the growth site will need to be broken to accommodate the new molecule, therefore increasing the interfacial energy. This is likely to be the rate-determining step during crystal growth, implying that movement of smooth solid-liquid interfaces should be interface-controlled (Porter & Easterling 1981). For two-dimensional nucleation, n is greater [less] than 2 if growth is interface- [diffusion-] controlled. Correspondingly for three-dimensional nucleation, the value of n which differentiates between interface- and diffusion- controlled growth is 3.

The rate of crystal growth in a dilute solution is given by (Porter & Easterling 1981):

$$\Gamma = K_{iii}\, k\, T\, ln \frac{IP^{1/\nu}}{K_{sp}^{1/\nu}} = \frac{K_{iv}\, T}{\nu} ln\, \beta \qquad ...(5.12)$$

where K_{iii} (m s^{-1} J^{-1}) and K_{iv} (m s^{-1} K^{-1}) are interfacial mobility constants, whileν represents the number of ions or radicals per molecule. The values ofν for DCPD, OCP and HAP are respectively 2, 8 and 9.

5.1.6 Modified Avrami equation

Substituting Equations 5.11 and 5.12 in Equation 5.1, the original Avrami equation becomes:-

$$\phi = 1 - exp\,[-(\kappa\lambda)^{n/4}\ \zeta^{n/4}\ t^{n}] \qquad ...(5.13)$$

where $\kappa\lambda$ = transformation coefficient ($K^{-3}\ s^{-4}$); and

$$\zeta = \left(\frac{T\ ln\ \beta}{\nu}\right)^{3}\ \Pi\ exp\left[-\frac{f\ v^{2}\ \gamma_{SL}^{3}}{(kT)^{3}\ (ln\ \beta)^{2}}\right]\ (K^{3}) \qquad ...(5.14)$$

Although ζ appears to be a rather complicated function, its value can in fact be determined for particular experimental conditions. Supersaturation (β) and collision probability (Π) are both functions of the respective concentrations of individual ions, which in turn can be calculated by considering the various complexation equilibria, solubility constants, activity coefficients, the ionic strength and the *p*H of the calcifying solution. Now, it is very difficult to precisely evaluate the shape factor (f) for new nuclei, but as long as their morphology remains uniform, it is reasonable to assume an intermediate value of 25. On the other hand, values of v and γ_{SL} have been measured for the various phases. Thus the value of ζ should be calculable.

The only unknowns left in Equation 5.13 are the transformation coefficient ($\kappa\lambda$) and n. In the transformation coefficient, κ is a constant term whereas λ, as previously explained, is the variable which accounts for the heterogeneous nature of the nucleation process. In order to use Equations 5.13 and 5.14 for prediction of the actual event, the values of these parameters need to be found out.

5.1.7 Evaluation of transformation parameters

It is possible to work out the values of the transformation parameters with the aid of published experimental data (Perez *et al.* 1989, Ebrahimpour *et al.* 1991, Zhang & Nancollas 1992) in conjunction with results of constant-composition experiments presented in Chapter 4 of this thesis.

§ Time exponent, n

Equation 5.13 can be rewritten as follows:

$$\phi = 1 - exp\,[-(\kappa\lambda)^{n/4}\ \zeta^{n/4}\ t^{n}\,]$$

$$ln\left[ln\left(\frac{1}{1-\phi}\right)\right] = n\ ln\ t + \frac{n}{4}[(ln\ (\kappa\lambda) + ln\ \zeta] \qquad ...(5.15)$$

Thus, by plotting $ln\ \{\ ln\ [\ 1\ /\ (1-\phi)\ ]\ \}$ against ln t, the value of n can be determined. This is shown in Figure 5.1 and Table 5.1, from which it is apparent that over quite a wide range of solution composition, the values of n, given by the slopes of the plots, are all within the limits of 3.36 ± 0.24, at a confidence level of 88% (χ^2 test). These values of n imply that saturation of nucleation sites did not occur during the experiments and that growth was interface-controlled. The relative constancy in the value of n justifies the approximation in the model geometry and suggests that the current analysis is useful within its appropriate limits.

Figure 5.1 The graphs of $ln\ \{\ ln\ [\ 1\ /\ (1-\phi)\ ]\ \}$ against ln t for different values of *p*H

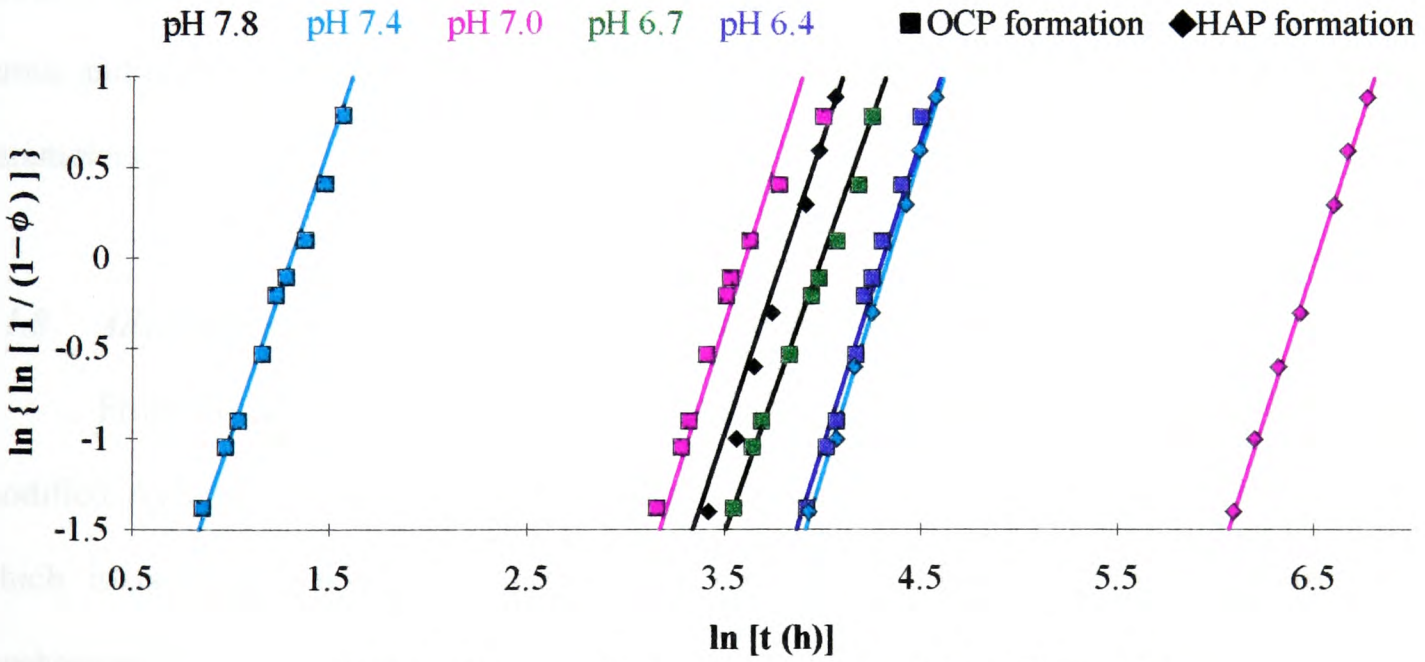

Table 5.1 Values of n obtained from Figure 5.1

*p*H		6.4	6.7	7.0	7.4	7.8
n	OCP formation	3.44	3.12	3.46	3.24	-
	HAP formation	-	-	3.39	3.52	3.55
	mean	**3.44**	**3.12**	**3.43**	**3.38**	**3.55**

§ Transformation coefficient, $\kappa\lambda$

Having found the value of n, it is then possible to estimate the transformation coefficient. As $\kappa\lambda$ is a combination of various system parameters, this is achieved by iterating for values which, when substituted in Equation 5.13, give the best fit to experimental data under different conditions. Figure 5.2 shows the relationship between time and the fractional formation of different phases in solution with a total calcium content of 2 mM at various *p*H values. It is obvious that the trend described by the modified Avrami expression is in close agreement with the actual event; and can be well-fitted to experimental results by adjusting the transformation coefficient alone. Surprisingly, although the λ term is dependent on the physical conditions inside the reaction medium, the overall coefficient $\kappa\lambda$ varies only slightly within the limits of $10^{-10.63\pm0.35}$ K^{-3} s^{-4} (χ^2 confidence level 86.7%) over a *p*H range from 6.0 to 7.5. This relative constancy reflects that despite being a variable term, λ is comparatively insusceptible to variations in *p*H and β, i.e. changes in the chemical composition of the calcifying media do not bear any strong influence on the heterogeneity of nucleation and the lattice strain energy of the resulting precipitate. In fact, it isζ in Equation 5.14 which is most sensitive to changes in physical and chemical conditions as a result of prevailingβ terms, and is not uncommon to deviate in orders of magnitude up to 10 upon slight changes in system parameters.

5.1.8 Advantages and limitations of the precipitation model

From the above derivation and development of the precipitation model, it is clear that the modified Avrami expression is able to furnish description of the overall crystallisation behaviour which is consistent with experimental findings without in-depth analysis of the microscopic mechanisms for nucleation, growth and dissolution. It provides a straightforward and convenient method to predict the macroscopic precipitation pattern expected under particular experimental conditions. It actually predicts the preferential formation of precursor phases and their subsequent phase transformations. The induction periods for the formation of each phase and the extents of transformation can be compared along the logarithmic time scale.

However, this model does present some limitations. First of all, as discussed previously, it is based on a very simple form of the Avrami model and it therefore necessitates great care when

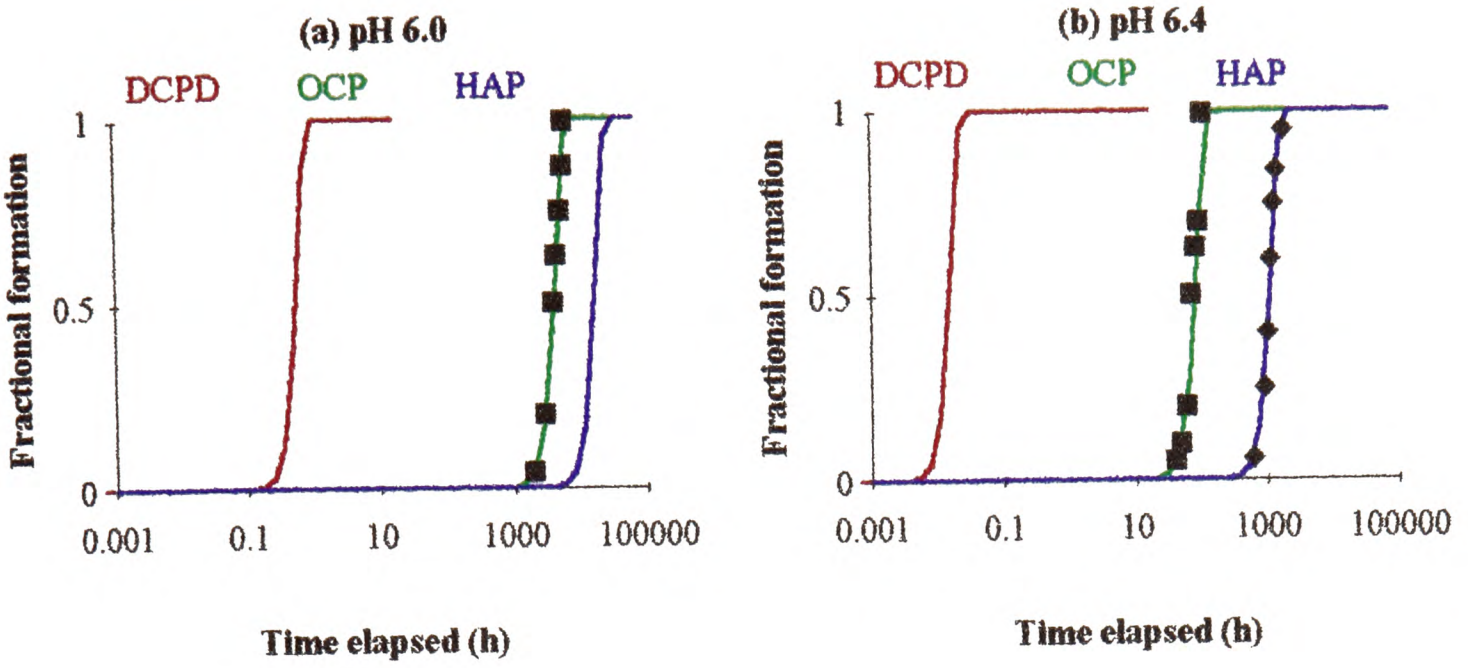

Values of *log* [$\kappa\lambda$ (K^{-3} s^{-4})]:

(a) – 10.324
(b) – 10.699
(c) – 10.805
(d) – 10.427
(e) – 10.602

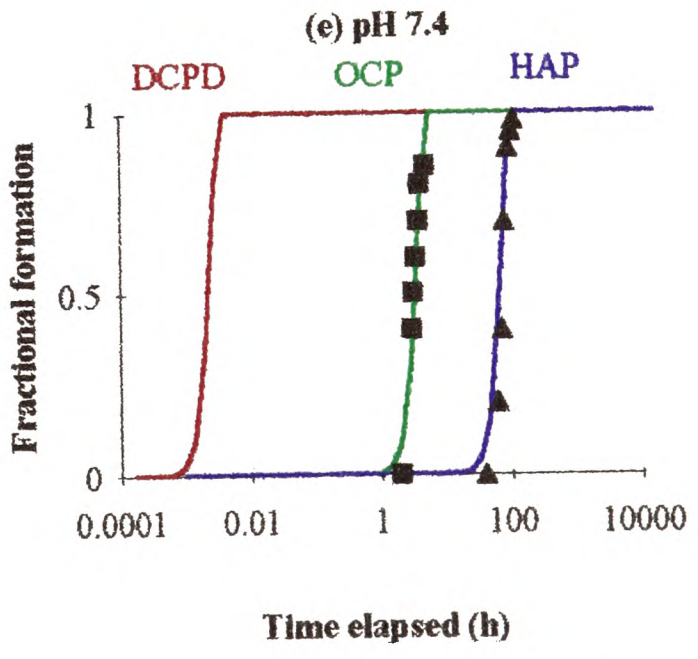

Figure 5.2 Fractional formation of different phases of calcium phosphate calculated from experimental data fitted to profiles obtained from Equations 5.12 and 5.13 by adjusting the value of $\kappa\lambda$

interpreting empirical values of n and $\kappa\lambda$. The ensuing transformation curves are also of an approximate nature. Also, owing to its non-mechanistic approach, it may not be versatile enough to be adapted to systems in which there are additional prevailing factors, e.g. the presence of precipitation promoters and inhibitors. Also, the reliability of this model is now verified using experimental data from only a limited range of experimental conditions, and thus its accuracy under more extreme conditions cannot at this stage be guaranteed. For instance, for calcification experiments performed with a solution of calcium content of 2 mM, there has never been any reported detection of the formation of HAP at *p*H's below 6.0 or the formation of DCPD at *p*H's above 7.5 although Ostwald's rule of stages does suggest the possibility of both of these events. From Figure 5.2(a), it can be seen that at low *p*H values, the formation of HAP is not likely to commence until at least 2000 hours; whereas from Figure 5.2(e), the formation of DCPD at high*p*H values is brought to completion in a matter of seconds. Neither of these time scales is practical in experimental studies. It is believed that these reactions do take place, but unless and until the necessary improvement in experimental techniques is achieved for the detailed studies in time scales as extreme as these, it is impossible to verify how accurately the present model predicts the actual event under these exceptional circumstances. Nevertheless, provided that one is aware of these limitations, the present model still present a useful means for the prediction of the overall precipitation behaviour of calcium phosphate in aqueous media.

5.2 Application of precipitation model to describe physiological calcification

Let us now look at the precipitation of calcium phosphate under physiological condition, which is by far the most important for the understanding of natural mineralisation. Figure 5.2(e) shows the precipitation pattern at *p*H 7.4 and a $[\Sigma Ca] \times [\Sigma P]$ value of 2.4 mM^2 as described by Equations 5.12 and 5.13. It predicts the presence of OCP as the major precursor for at least 90% of the induction period for HAP formation. This is consistent with results of*ex vivo* calcium phosphate precipitation experiments in purely ionic media.

However, care needs to be taken if this model is to be applied to describe physiological calcification. The body environment differs significantly from experimental conditions in a good number of ways. In contrast to pure inorganic solutions used in the experiments, the physiological

process involves a highly complex body fluid which contains, apart from calcium phosphate, a whole collection of inorganic and organic bio-chemicals. Depending on their nature, individual chemicals can exert significant influence on the calcification process by promoting or retarding the nucleation and growth processes. According to the present model, these compounds effectively shift the transformation curves and alter various determining parameters: interfacial free energy (γ_{SL}), change in system free energy (ΔG_c^{hetero}), interfacial strain energy (Δg^{strain}), solution composition and supersaturation (β), transformation coefficient ($\kappa\lambda$) and ζ. It is therefore necessary to study the effects of different bio-chemicals on the precipitation process before any modification on the present model can be made to describe the *in vivo* process.

5.3 Conclusions

A new model has been developed to describe the preferential formation of precursor phases and their subsequent step-wise transformation to thermodynamically more stable phases during the precipitation of calcium phosphate in a supersaturated solution. This model made use of the original Avrami-Johnson-Mehl expression, but it modifies the nucleation rate terms which are dictated by the system geometry. Using correct expressions for the rates of nucleation and growth and a few assumptions about the otherwise indeterminate system, the resulting model is numerically expressed by Equations 5.13 and 5.14. Certain unknown parameters in the model were found by fitting the predictions given by the model to existing experimental results. These predictions, in fact, described several aspects of the actual event very satisfactorily - the sequence of phase formation, the induction time for transformation and the extent of transformation as a function of time. Predictions using this model also suggested that the transformation reactions follows an interface-controlled growth mechanism without the occurrence of saturation of nucleation sites, and that the solution composition has little effect on the heterogeneity of the precipitation process. Indeed, the most influential factor which governs the transformation behaviour is supersaturation - a factor which dictates both kinetic and thermodynamic potentials. Thus, in spite of simplicity of this model, it has proved to be useful within its appropriate limits.

Although this model has been found to describe quite successfully the process of *ex vivo* calcium phosphate precipitation in purely ionic media, it still needs a fair amount of modification

before any attempt to use it for *in vivo* mineralisation may prove fruitful. The main difference between the two phenomena is that body fluids contain, apart from calcium phosphate, a variety of bio-chemicals which may exert significant influence on the precipitation process. Although the underlying principles of the present model should still be valid, it will be extremely difficult to apply it directly to biological systems without the knowledge of the rôles played by these chemicals. Therefore, in the following chapters, the effects of certain compounds on calcium phosphate precipitation will be discussed.

Chapter 6
PRECIPITATION OF CALCIUM PHOSPHATE IN THE PRESENCE OF NON-COLLAGENOUS BONE-SPECIFIC BIO-CHEMICALS

It is known that various non-collagenous matrix bio-chemicals including proteins and lipids participate in the *in vivo* mineralisation process (see Section 2.6). Although many of these chemicals have been identified and their influence on calcification have been extensively studied *in vitro*, a general agreement on the rôles played by these compounds is still to be reached. In light of this, the effects of certain non-collagenous organic compounds on the precipitation of calcium phosphate have been carefully examined and the experimental results will be discussed in this chapter.

6.1 Non-collagenous bone-specific bio-chemicals

Although there is a wide range of bone-specific bio-chemicals, they can be categorised into several classes according to their functional groups (Boskey 1989).

6.1.1 Phosphoproteins

Phosphoproteins, e.g. phosphophoryn (Fujisawa *et al.* 1987), osteonectin (Termine *et al.* 1981b), osteopontin (Oldberg *et al.* 1986) and casein (van Kemenade & de Bruyn 1989), are significantly present in bone and teeth, and both inhibitory and promotional effects on mineralisation have been reported (Termine *et al.* 1980, 1981a, Veis 1988, Blumenthal 1989). The main distinctive feature of phosphoproteins is the presence of the residues of phosphorylated amino acid ester units, particularly those of phosphoserine (SerP) and phosphothreonine (ThrP) which together account for almost all of the total organic phosphorus content (Cohen-Solal *et al.* 1978). It has been shown that these phosphorylated amino acid residues have high tendencies to bind to free calcium ions (Aoba & Moreno 1985). However, the ability of a phosphoprotein to strongly bind to a large number of calcium ions can be both advantageous and detrimental to the calcification process. The potential ability to bind to calcium ions is, of course, one of the requirements necessary for a component to participate in the nucleation of calcium phosphate crystals from solution, but the calcium ions may be

be bound either electrochemically or stereochemically in such a way that they may be rendered unreactive and unavailable for further interaction with other ions. The need to find out exactly how such an interaction affects the calcification process has thus led to extensive precipitation studies under the influence of phosphoproteins as well as the elementary phosphorylated amino acids.

6.1.2 Phospholipids

Acidic phospholipids (e.g. phosphatidylserine) appear mainly in matrix vesicles which are believed to be the site of initial calcification in many tissues (Boskey & Posner 1977). Again, they contain calcium-binding phosphoryl end-groups, but these end-groups are believed to be more rigid when bound to free calcium ions (Boskey & Dick 1991). Thus, although they are thought to be active at the initiation of calcification, they have shown signs of inhibition towards crystal growth.

6.1.3 Other organics

Other organic compounds are also present in natural hard tissue matrix. Glycoproteins and proteoglycans such as alkaline phosphatase (Beertsen & van den Bos 1992), serum proteins such as albumin (Mura-Galelli *et al.* 1991), and other bulk molecules including polyphosphates, phosphonates and poly(carboxylic acids) (Amjad 1987) have all been reported to exert an influence on crystal growth of calcium phosphate. Obviously there is no single mechanism which can fully explain the effects of different classes of organic compounds.

6.1.4 Inorganic ions

Magnesium (Abbona *et al.* 1986, 1988, Abbona & Franchini-Angela 1990) and aluminium ions (Blumenthal & Posner 1984) have been found to be inhibitors of calcification. Mg^{2+} ions readily substitute for Ca^{2+} in the calcium phosphate lattice, thereby distorting the structure of newly-formed nuclei, encouraging redissolution and preventing further growth. Smaller, trivalent Al^{3+} ions, on the other hand, coordinate oxygen atoms in a different manner from Ca^{2+}, thus blocking active growth sites on the surface of existing crystals.

Clearly, it is impossible to study every single compound which may play a part in the*in vivo* mineralisation process. Among the different classes of bio-chemicals, only the reaction mechanism of inorganic ions has been quite well-understood. In this series of experiments, the effects of typical compounds from the three organic categories on the precipitation behaviour of calcium phosphate crystals were investigated.

6.2 Experimental

6.2.1 Choice and sources of organic additives

The chemicals chosen for this study are listed in Table 6.1. The first four compounds are all present in natural hard tissues. Although phosphoserine does not exist on its own in hard tissues, it does account for almost all the phosphorus content in phosphoproteins and phospholipids. The direct introduction of phosphoserine into calcifying media should yield a fair indication of the true effect of its residues in phospho-organic compounds. Therefore it was included in the list of additives to be studied.

O-phospho-L-serine (SerP), L-α-phosphatidyl-L-serine (PS) and bovine serum albumin (BSA) were purchased from Sigma Chemicals. Bone protein extract (BPE) and osteonectin (ONec) were derived from bovine bone in methods described below.

Table 6.1 Non-collagenous bio-chemicals used in the precipitation studies

Chemical	Category	Symbol
Bone protein extract (from bovine femurs and fibulæ)	Bone-specific matrix proteins	BPE
Osteonectin	Phosphoproteins	ONec
Bovine serum albumin	Serum proteins	BSA
L-α-phosphatidyl-L-serine	Phospholipids	PS
O-phospho-L-serine	Phosphorylated amino acids	SerP

BPE was purified to homogeneity from guanidine-HCl extracts of bovine bone following the procedure of Termine *et al.* (1981a). Fœtal bovine bone slices were prepared from femurs and fibulæ taken from fœti 4 to 6 months *in utero*. Iced bovine limbs were dissected within 3 to 5 hours after sacrifice. Upon mechanical removal of epiphyses, soft tissue and periosterm, longitudinal surface slices with a thickness of 1 to 2 mm were taken from the subperiosteal bone collars of the fœtal bone shafts. The bone slices were washed extensively in a cold (4 °C) physiological salt solution containing several protease inhibitors and stored at −75 °C. The slices were then extracted (1 g / 200 mℓ) at 4 °C under dissociative conditions using 4 M guanidine-HCl in the presence of protease inhibitors. This BPE contained a variety of bone-specific proteins and was free from collagen and cartilage or marrow contamination.

ONec was further derived from the guanidine-HCl extract. Another extraction was performed (1 g of original bone slices / 200 mℓ) at 4 °C under dissociative conditions using a mixture of 4 M guanidine-HCl and 0.5 M EDTA in the presence of protease inhibitors. The extraction product was predominantly osteonectin. Both the first extraction product and the osteonectin were concentrated at 4 °C by ultrafiltration and stored at −75 °C*.

6.2.2 Experimental procedure

Apart from SerP and PS, all the additives were biological bulk polymers with no fixed chemical formulæ or molecular weights. Also, it was not clear whether these compounds worked by a catalytic mechanism or whether they were actually present in the final products. Therefore, it would be extremely difficult to devise constant-composition experiments since an attempt to establish the chemical equilibria among the free inorganic ions and the organic additives would not have been conclusive. Hence, constant-volume experiments were performed. Clearly, the primary aim of these experiments was to compare the various effects these compounds had on the different aspects of the precipitation process, but the results would also be used to determine the active rôles of these chemicals in the precipitation reactions.

The experimental set-up has been previously described in Section 3.1.3. Table 6.2

* BPE and ONec extractions were performed by Mrs. Barbara Dowling in the Medical Research Council Bone Research Laboratory at Nuffield Orthopædic Centre, Oxford.

Table 6.2 Compositions of calcifying solutions

Expt. no.	Initial [ΣCa] (mM)	Initial [ΣP] (mM)	Initial *p*H	[KCl] (M)	Temp. (°C)	Added bio-chemical	Amount added (mg)
III-1	2	1.2	7.4	0.1	37	no addition	(control)
III-2						BPE	2
III-3						ONec	2
III-4						BSA	5
III-5						PS	5
III-6						SerP	5

summarises the composition and the quantity of any organic addition in each of the calcifying solutions. Precipitation was allowed to proceed for 72 hours at which time hydroxyapatite substrates were removed from the solution and dried in a desiccator. Solid samples were then characterised using SEM, XRD and WDS.

6.3 Results

6.3.1 Overall rate of precipitation

The rates of total calcium phosphate per unit surface area of substrate, calculated from the *p*Ca and *p*H outputs, are plotted against time in Figure 6.1. By comparing with the result of the control experiment, the effects of the various additives on the overall precipitation rate, i.e. the combined calcium consumption due to both nucleation and growth, can be deduced. It is clear that SerP had the highest efficacy in promoting mineral deposition onto the substrate, whereas BPE, PS and ONec appreciably hindered precipitate formation, with almost no precipitation occurring after 10 hours. The overall effect of BSA was, however, not obvious from this plot.

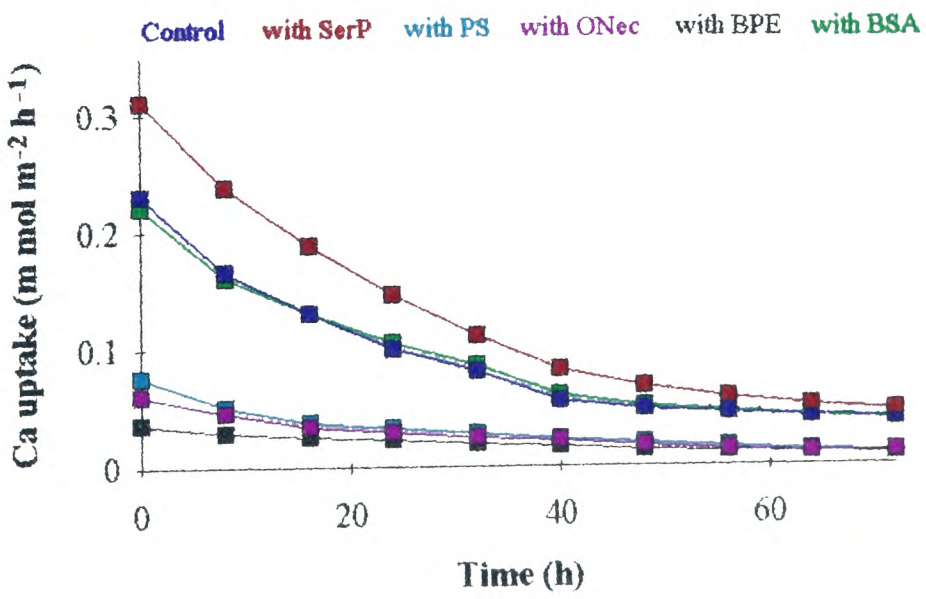

Figure 6.1
The graphs of molar rate of calcium uptake against time for the precipitation under the influence of various organic bio-chemicals

6.3.2 Precipitate morphology and crystal dimensions

Figures 6.2-6.7 show respectively low and high magnification scanning electron micrographs of samples removed from the calcifying media after 72 hours of precipitation. Without any organic addition, a large number of thin, plate-like crystals measuring ~ 15 μm × ~ 7 μm × ~ 0.5 μm were obtained (Figures 6.2), with a morphology similar to the OCP precipitate shown in Figure 3.6. (The chemical compositions of the precipitates will be discussed in the next section.)

In the presence of the organic compounds, the physical appearance of the crystals differed drastically. Figure 6.3 shows the precipitate obtained under the influence of SerP. It is clear from Figure 6.3a that SerP promoted the formation of numerous tiny plate-like crystals. Comparing Figures 6.2b and 6.3b, it becomes apparent that the crystal dimensions were almost halved (longest dimension ~ 8 μm with the addition of SerP) while the number of crystals per unit surface area was at least doubled in the presence of SerP. However, the actual shape of the crystals was still quite similar to that in the control experiment.

With the introduction of PS, the precipitation was very much impeded. Figure 6.4a clearly depicts the small extent of crystallisation. At a higher magnification, some interesting physical features of the crystals are portrayed. The rather poorly defined nuclei grew and aggregated to form crystals of a unique morphology. These crystals assumed a slightly askew cubic structure with almost uniform dimensions of ~ 10 μm (Figure 6.4b), in contrast to the blade- and plate-like appearance usually taken up by calcium phosphate crystals.

ONec had similar effects on the precipitate morphology as PS. The quasi-cubic appearance was again taken up by the precipitate. The dimensions were slightly smaller (~ 7 μm, Figure 6.5b), but the number of crystals per unit substrate surface area was greater (Figure 6.5a).

The addition of BPE led to the formation of a very small amount of large plate-like crystals (Figure 6.6). These plates measured ~ 25 μm × ~ 5 μm × ~ 2 μm.

BSA induced the formation of a characteristic, "furry" coverage of precipitate clusters consisting of thin wavy sheets of irregular dimensions (Figure 6.7). These sheets were packed very closed together in good order with around 5 of these sheets per μm thickness of each precipitate cluster.

Figure 6.2 Scanning electron micrographs of the precipitate obtained in the control experiment

(a) Low-magnification picture showing even coverage of OCP plates

(b) High-magnification picture of OCP crystals

Figure 6.3 Scanning electrnon micrographs of the precipitate obtained in the presence of SerP

(a) Low-magnification picture showing the higher number of crystals per unit surface area of substrate, i.e. enhanced nucleation

(b) High-magnification picture of OCP crystals illustrating the decrease in crystal size compared to the control experiment

(a)

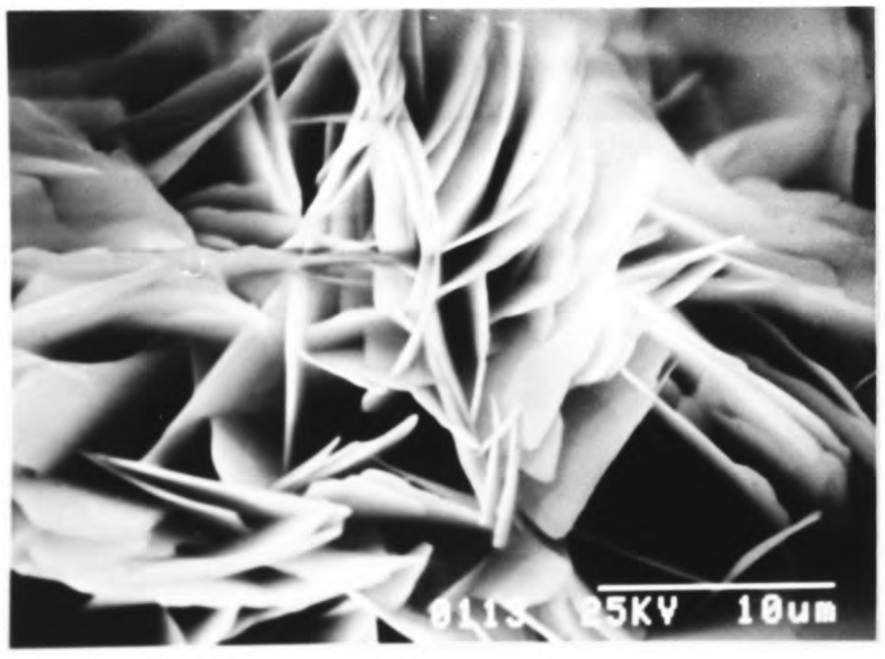

(b)

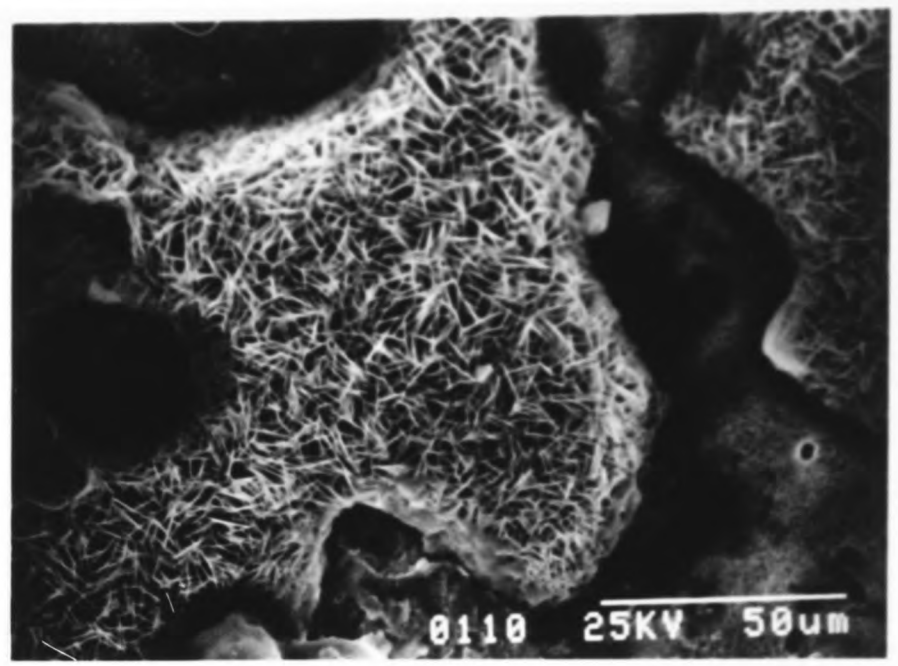

(a)

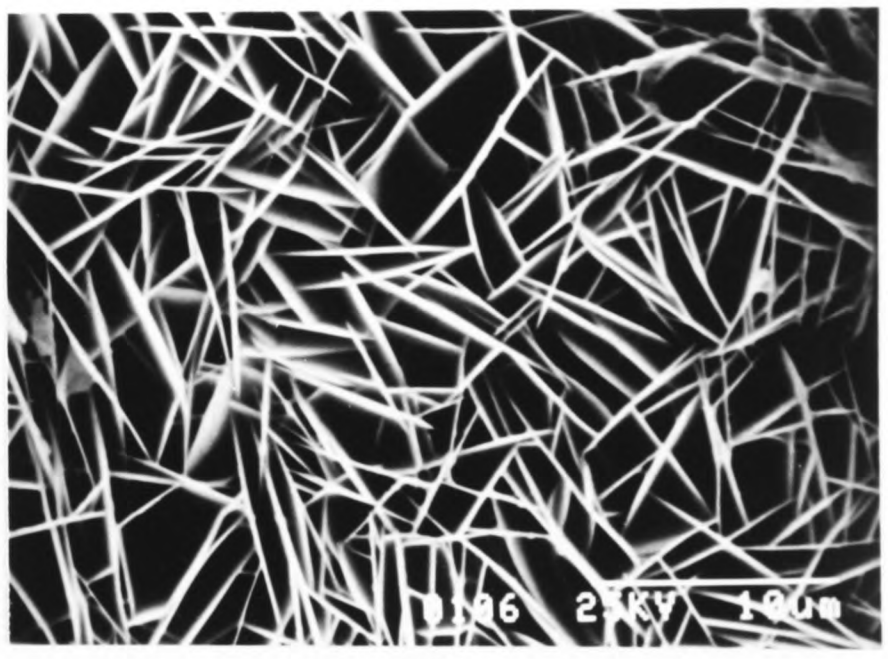

(b)

Figure 6.4 Scanning electron micrographs of the precipitate obtained in the presence of PS

(a) Low-magnification picture showing the small extent of precipitation

(b) High-magnification picture of a quasi-cubic OCP crystal

Figure 6.5 Scanning electron micrographs of the precipitate obtained in the presence of ONec

(a) Low-magnification picture showing the low surface coverage of precipitate

(b) High-magnification picture of a quasi-cubic OCP crystal similar to, but smaller than, the ones obtained with the addition of PS

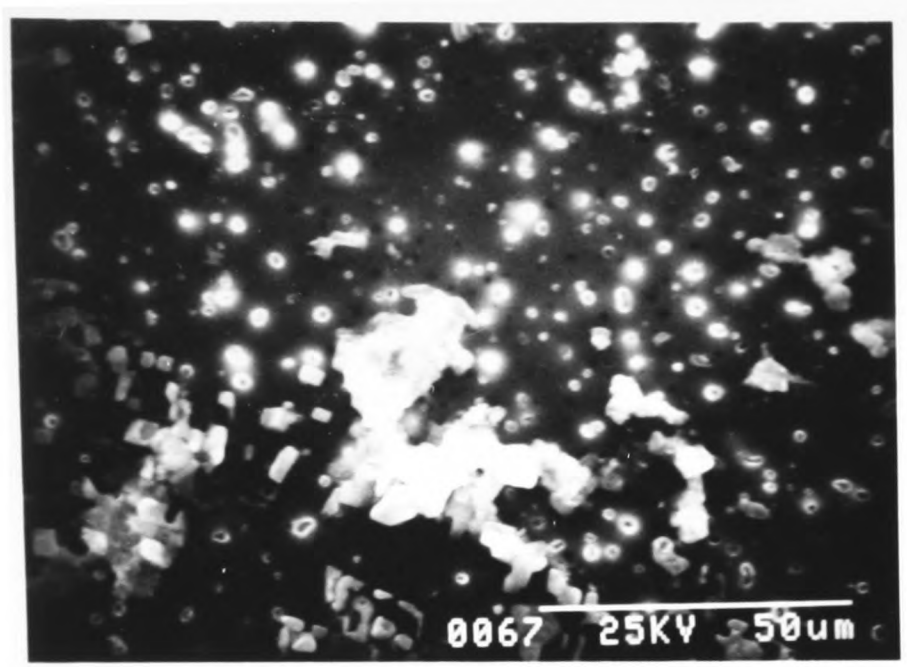

(a)

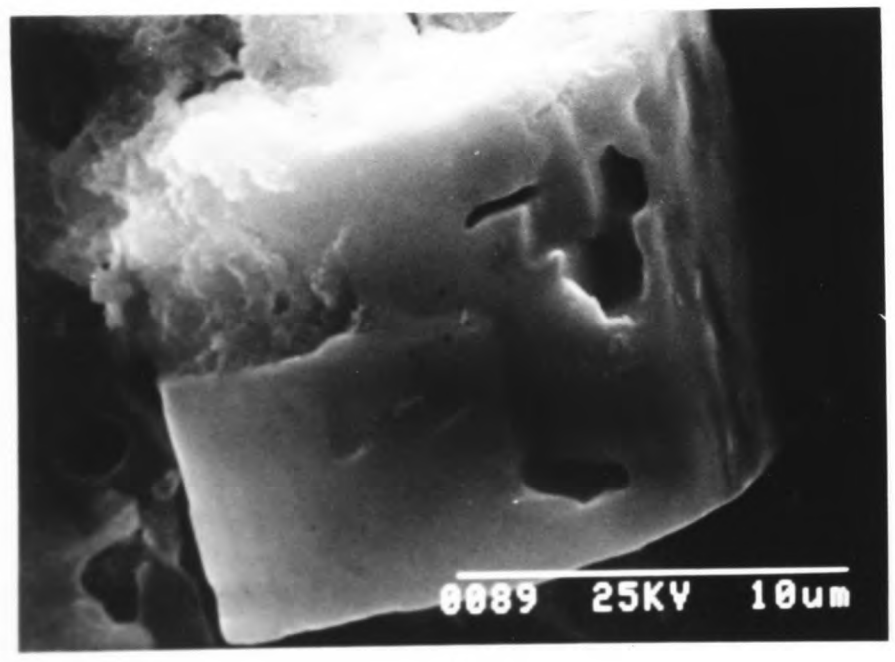

(b)

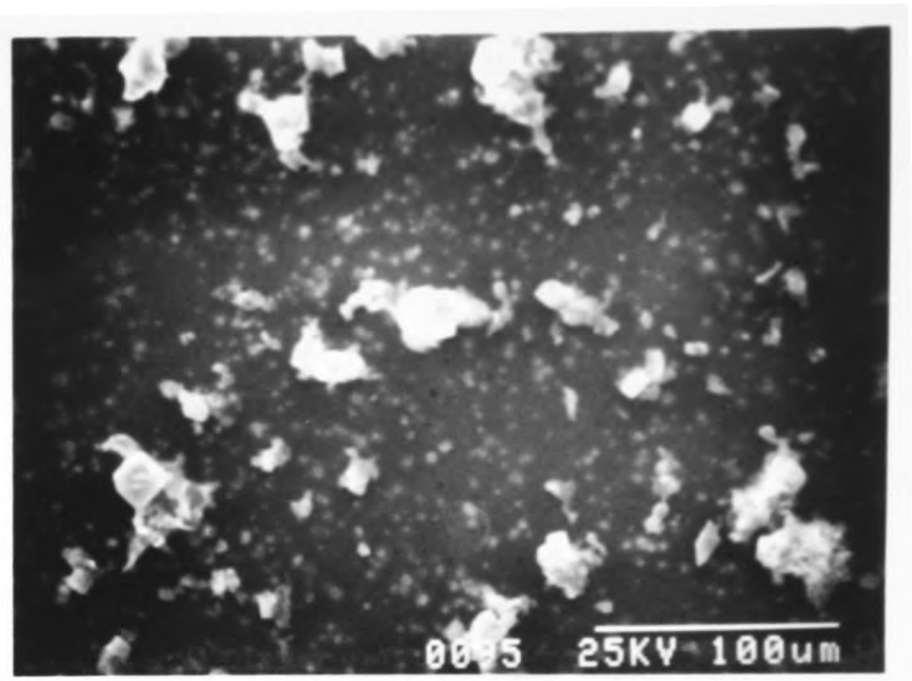

(a)

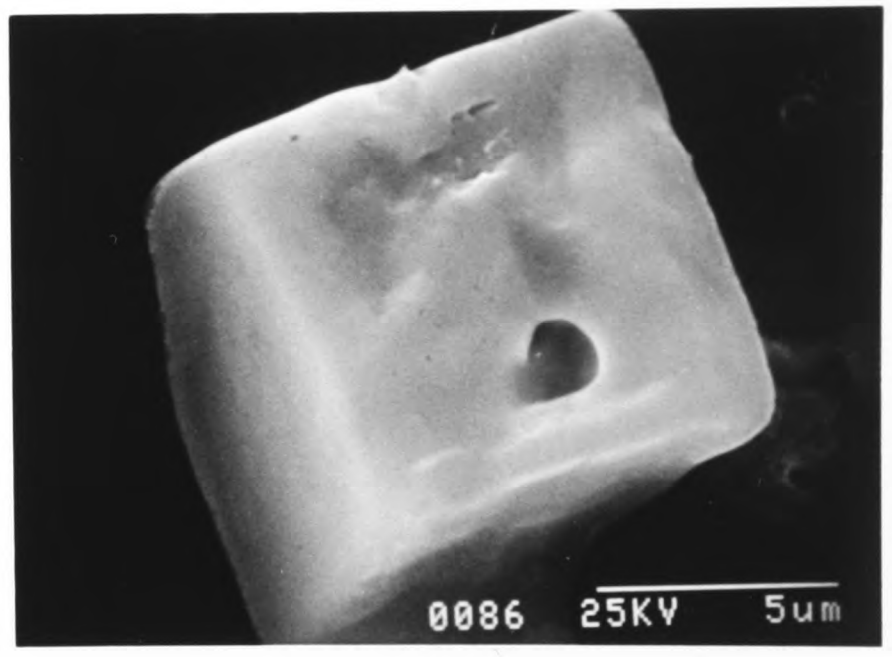

(b)

Figure 6.6 Scanning electron micrograph of large OCP plates obtained in the presence of BPE

Figure 6.7 Scanning electron micrographs of the precipitate obtained in the presence of BSA

(a) Uneven distribution of clusters of OCP precipitate

(b) High-magnification picture showing the "wavy" sheets which constitute these OCP clusters

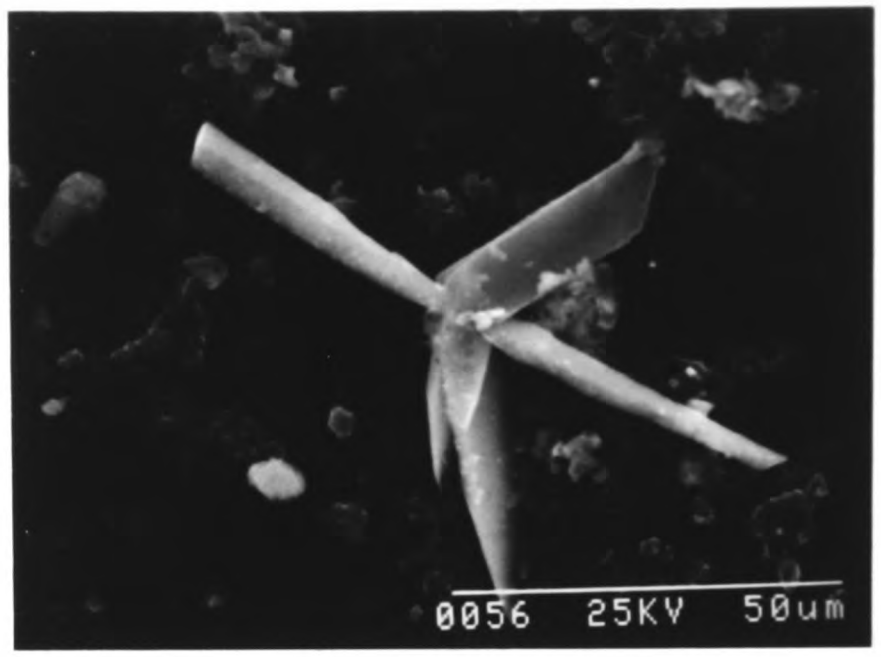

(a)

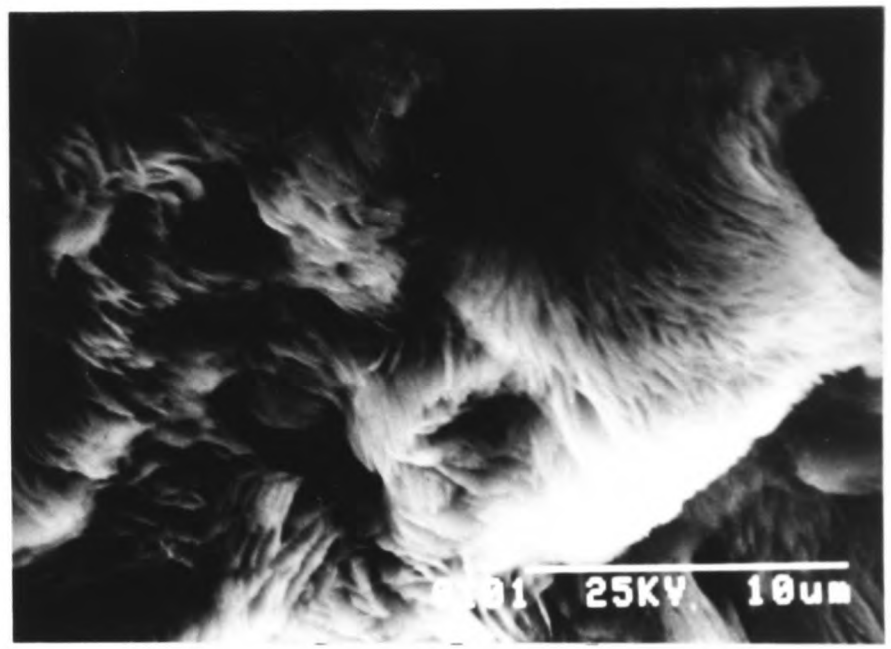

(b)

6.3.3 Chemical composition and stoichiometry of precipitate

XRD and WDS respectively provided crystallographic and stoichiometric information on the composition of the precipitate. XRD spectra of all the precipitate matched quite closely the theoretical peaks for OCP (Figure 6.8), which has previously been shown to be the most probable precursor phase under the present experimental conditions after 72 hours of precipitation. Hence, if stoichiometric OCP was obtained, the corresponding Ca/P atomic ratios of the precipitate should be close to 1.33.

WDS results are summarised in Table 6.3. Looking at the mean Ca/P values, it is clear that in all cases (except for the precipitate obtained with the addition of BSA), the atomic ratios agreed quite closely to the OCP composition, although all the precipitate samples were slightly deficient in calcium. However, despite the resemblance of its XRD spectra to the standard OCP pattern, the crystals obtained under the influence of BSA had an unexpectedly low Ca/P atomic ratio of 0.52. The possibility of experimental error during WDS was ruled out, as a second round of analysis performed after re-calibrating the equipment still yielded the same result. This implies that the precipitate obtained in the presence of BSA was a highly calcium-deficient or phosphate-rich form of OCP.

Table 6.3 Ca/P atomic ratio from WDS analyses

Expt. no.	**Organic additive**	**WDS Ca/P atomic ratio (±2%)**			
		1st reading	**2nd reading**	**3rd reading**	**Mean**
III-1	(control)	1.26	1.27	1.30	**1.277**
III-2	BPE	1.29	1.29	1.27	**1.283**
III-3	ONec	1.29	1.31	1.28	**1.293**
III-4	BSA	0.54	0.51	0.51	**0.520**
III-5	PS	1.32	1.28	1.30	**1.300**
III-6	SerP	1.26	1.29	1.27	**1.273**

Figure 6.8 High-resolution X-ray diffraction patterns of solid precipitates

(a) Control experiment

(b) with BPE

(c) with ONec

(d) with BSA

(e) with PS

(f) with SerP

all showing characteristic OCP peaks

STOE Powder Diffraction System

31-JUL-92

CONTROL

Intensity (Abs)

1000
750
500
250
0

OCTACALCIUM PHOSPHATE - JCPDS powder diffraction file 26 1056

Intensity (Rel)

75
50
25
0

10.0
20.0
30.0
40.0
50.0

2Theta

STOE Powder Diffraction System 2-AUG-93

With BONE PROTEIN EXTRACT

Intensity (Abs)

1000
750
500
250
0

OCTACALCIUM PHOSPHATE - JCPDS powder diffraction file 26 1056

Intensity (Rel)

75
50
25
0

10.0 20.0 30.0 40.0 50.0

2Theta

Powder Diffraction System

2-AUG-93

With OSTEONECTIN

Intensity (Abs)

1500

1000

500

0

OCTACALCIUM PHOSPHATE - JCPDS powder diffraction file 26 1056

Intensity (Rel)

75

50

25

0

10.0

20.0

30.0

40.0

50.0

2Theta

STOE Powder Diffraction System 31-JUL-92

With BOVINE SERUM ALBUMIN

Intensity (Abs)

1000

500

0

OCTACALCIUM PHOSPHATE - JCPDS powder diffraction file 26 1056

Intensity (Rel)

75

50

25

0

10.0 20.0 30.0 40.0 50.0

2Theta

With O-PHOSPHO-L-SERINE

Intensity (Abs)

1500
1000
500
0

OCTACALCIUM PHOSPHATE - JCPDS powder diffraction file 26 1056

Intensity (Rel)

75
50
25
0

10.0
20.0
30.0
40.0
50.0

2Theta

STOE Powder Diffraction System 2-AUG-93

With PHOSPHATIDYLSERINE

Intensity (Abs)

1000
750
500
250
0

OCTACALCIUM PHOSPHATE - JCPDS powder diffraction file 26 1056

Intensity (Rel)

75
50
25
0

10.0 20.0 30.0 40.0 50.0

2Theta

Powder Diffraction System

31-JUL-92

With O-PHOSPHO-L-SERINE

Intensity (Abs)

1500

1000

500

0

OCTACALCIUM PHOSPHATE - JCPDS powder diffraction file 26 1056

Intensity (Rel)

75

50

25

0

10.0

20.0

30.0

40.0

50.0

2Theta

6.4 Discussion

It is clear that different classes of organic compounds have rather different effects on the precipitation of calcium phosphate, even if they may possess the same functional group. In this section, the effects of the individual organic additives will be discussed and compared.

6.4.1 Nucleation and growth

The differences in nucleation and growth rates as a result of the presence of different additives are reflected by the surface coverage and the crystal size of the precipitate. Among the various organic compounds, SerP showed the best signs of promoting heterogeneous nucleation on existing HAP substrates. Also, the smaller size of the plate-like crystals signified the slightly reduced growth rate. The formation of large numbers of tiny crystals is of particular interest to biomaterials research because it is one of the pre-requisites for the effective strengthening of natural hard tissues. The uniformity of surface coverage also suggests that the promotional effect of SerP on nucleation is not heavily dependent on the relative lattice orientation at the interface.

Next, let us look at BSA. Although a high number of crystal units were present in each of the clusters of precipitate, the overall surface coverage of the precipitate was not as uniform as in the control or the SerP experiment. This implies that although BSA may have positive effects on heterogeneous nucleation, these would be strongly dependent on the lattice relationship at the solid-solid interface. This is not surprising if we consider the difference between the molecular structures of SerP and albumin molecules. Regardless of the mechanism through which each of these compounds work, they must need to react with the calcium and phosphate ions in solution and on the substrate surface. Now, BSA has an average molecular mass of ~ 60000, more than 300 times bigger than that of SerP. The actual groups on BSA which are instrumental in promoting nucleation are bonded to an intrinsically bulky and geometrically complicated carbon-chain, compared to the much simpler structure of SerP. Hence, as a result of its more accessible functional group, SerP has a better chance of reacting with substrates with different lattice orientations even if that may require the accommodation of a certain amount of steric strain; whereas for BSA, its geometric constraints over the approach of free ions to the active groups present a more stringent directional requirement on the lattice compatibility at the interface. In other words, when there is an orientational mismatch at the

interface, the steric strain imparted on a SerP molecule is a lot smaller than on BSA. This results in the localisation of promotional effects of BSA at sites of specific lattice orientations of the substrate which are compatible with the three-dimensional molecular structure of the protein. The non-uniform coverage of clusters with high density of crystals is in line with this theory.

The inhibitory effects of PS and ONec on both nucleation and growth have been briefly discussed during the comparison of overall precipitation rates. In addition, the quasi-cubic appearance of the crystals was characteristic of the precipitate obtained in the presence of these two compounds. Referring back to the lattice parameters of the OCP unit cell (Table 2.2), it can be seen that, despite being triclinic, the actual deviation of the unit cell from a cubic structure is quite small (the three inter-axial angles being 90.14°, 92.52° and 108.67°). Now, the main difference between the formation of plate-like and quasi-cubic crystals is that in the former case, the growth rates along the three main principal axes are very different - growth is either suppressed along certain directions or significantly speeded up along others. In contrast, the formation of quasi-cubic precipitate means that there is no directional preference for growth in any of the three principal directions - in this case, the growth along all three axes seemed to have been hindered by the presence of PS or ONec to roughly the same extent. Conversely, the formation of plate-like crystals, such as in the case of SerP addition, implies that the organic additives were bound specifically to particular ions within the unit cell in certain preferred orientations, bringing about the alteration in the growth rate along those directions.

The inhibitory effects of ONec on calcium phosphate precipitation presented some interesting insight into its actual rôle in physiological mineralisation. It has been reported that ONec is an excellent promoter of binding between collagen and existing apatite particles (Termine*et al.* 1981b). Experimental results proved that ONec attached itself first to Type I collagen, the resultant complex was then bound to synthetic apatite crystals and free calcium ions, but not to phosphate ions. In the same paper, the ONec-collagen complex was also reported to promote mineral nucleation. However, it has been shown that ONec itself did not induce*de novo* formation of apatite (Doi *et al.* 1989); and it also delayed the transformation of precursor phases. The present results show further still that ONec hindered the crystallisation of calcium phosphate on HAP substrates, i.e. it retarded the growth of calcium phosphate crystals in supersaturated solutions. Thus, although

ONec may promote and strengthen the collagen-mineral interfacial bonding between collagen and existing calcium phosphate crystals, there is no evidence that it actually enhances either the nucleation or the growth of new mineral crystals in the absence of collagen.

From the rates of calcium uptake, it can be seen that BPE decelerated the precipitation to the greatest extent among the different organic additives. The effects of BPE on nucleation and growth can be deduced from Figure 6.6. The extremely limited extent of surface coverage clearly implies the negative effect of BPE on nucleation. The actual size of the crystals was not, however, very much affected by BPE. Now, BPE contains a mixture of bone-specific proteins, among which is a small proportion of ONec. Since precipitation proceeded at an even lower speed in the presence of BPE than with ONec, it is clear that the other components of BPE had a greater inhibitory effect than ONec itself.

6.4.2 Precipitate stoichiometry

WDS and XRD analyses yielded interesting information about the composition and the stoichiometry of the precipitated solid specimens. Although the XRD spectra of all the collected precipitate matched the theoretical OCP pattern closely, the actual Ca/P atomic ratios did show some variation, particularly in the case of BSA addition.

Results from XRD directly reflect the lattice structure of the solid sample being examined. As the diffraction spectra of precipitates from the various experiments all match the theoretical OCP pattern, their respective atomic packings and lattice structures must be highly similar to that of a perfect OCP crystal. This means that the preferential formation of precursor phases was not strongly influenced by the addition of bio-chemicals. In other words, irrespective of the added organic compound, the overall $[\Sigma Ca] \times [\Sigma P]$ product and thus the supersaturation during the experiments were still the determining factors and they had maintained a high potential for the formation of the OCP as the predominant precursor phase under the present conditions, in agreement with the discussion in Sections 3.3.2 and 4.3.2. Indeed, for most of the samples, the Ca/P ratio was found to be very close to the 1.33 mark of OCP, confirming this hypothesis. The slightly lower values denote a minor calcium deficiency - a phenomenon observed at very similar levels in the various samples, and in particular, even in the absence of any organic additives in the control experiment. Similar

degrees of calcium deficiency have been previously reported for the precipitation of various calcium phosphate phases (Heughebaert *et al.* 1990, Zawacki *et al.* 1990), and were likely to result from lattice vacancies at the sites of the calcium ions in the unit cell. These vacancies were created in order to remedy the charge imbalance arising from the small but significant extent of substitution by acidic phosphates (i.e. HPO_4^{2-} and $H_2PO_4^-$) at the PO_4^{3-} sites. Substitution of cations and anions respectively by the background K^+ and Cl^- was minimal, as WDS results have shown.

However, compositional analysis of BSA-induced precipitate gave a Ca/P ratio of 0.52, remarkably lower than 1.33, in spite of the close resemblance between its diffraction spectrum and the OCP peak pattern. Such a high degree of non-stoichiometry cannot possibly be explained by the creation of vacancies at the Ca^{2+} sites to counter the effects of acidic phosphate inclusion, as the lattice would have been distorted in such a drastic manner that the XRD could not have been as close to the theoretical OCP pattern. A similar extent of lattice distortion would also have been brought about had the low Ca/P been due to the interstitial inclusion of phosphate ions in the unit cell. However, in order to accommodate more than twice the number of phosphate ions interstitially than in the thermodynamically stable configuration, the unit cell would have needed to expand by such an enormous amount that the Bragg angles would have to be altered. Furthermore, although BSA does contain some phosphorylated end groups, the big difference in molecular sizes between itself and OCP obviously rules out the possibility of the inclusion of BSA inside the OCP unit cell. Thus, it was impossible for the low Ca/P to be consequent purely of internal alterations inside the OCP unit cells.

Since there could not have been any major intrinsic distortion in the lattice structure, the only other possible mechanism which brought about the low Ca/P ratio must have involved reactions at the surface of the precipitate. As the presence of BSA was the only difference between this calcifying solution and the one used in the control experiment, the surface reaction must have involved BSA. In the previous section, it has been pointed out that the promotional effects of BSA on nucleation and growth depends strongly on its directional relationship with the solid phase. It is therefore very likely that if BSA approached and formed a bond with the solid phase in a orientation which did not facilitate the subsequent access of ions in solution, it would simply adhere on the surface and effectively block that particular site from further growth. This reaction would not alter

the intrinsic lattice structure of the existing crystal, yet at the same time the phosphorus content of the bulk molecule itself and, perhaps, the ability of the remaining part of the BSA molecule to attract phosphate ions would lead to a localised increase in phosphorus content on the crystal surface. This hypothesis is supported by the analytical results as well as the morphology of the precipitate. Firstly, the overall resemblance between the diffraction spectra of the precipitate and the OCP perfect crystal confirms the lack of intrinsic lattice distortion. However, upon closer inspection of the XRD patterns of BSA-induced precipitate and the samples obtained in the control experiment, and even that of the SerP-induced precipitate (Figure 6.9), it becomes apparent that, although the various spectra seemed generally similar, BSA-induced precipitate showed broadening of certain diffraction peaks, most notably the broadening and merging of the following pairs of distinct peaks into single widened peaks: (260) and $(2\bar{4}1)$; (070) and $(1\bar{6}1)$. This indicates that there was a specific irregularity in the crystal structure in the BSA-induced sample along these particular planes, confirming the directional influence on the precipitate. Furthermore, the "waviness" in the crystal morphology of BSA-induced precipitate (Figure 6.7), in contrast to straight blade- and plate-like crystals obtained otherwise, again suggests a change in the preference in growth direction during the course of precipitation under the influence of BSA addition. This is because the attachment of a bulky BSA molecule on a growing crystal would undoubtedly dictate the directional accessibility of that particular growth site. Also, since WDS was performed on small areas of the crystal surface, the low Ca/P ratio does not contradict the present conjecture on the mechanism through which BSA locally raised the phosphorus content at the surface growth sites. However, although this proposed mechanism is consistent with the experimental findings, systematic verification is still necessary. Infra-red spectroscopy and solid-state nuclear magnetic resonance analysis are two methods which may be able to produce conclusive information, but unfortunately neither was available during the course of this project.

6.4.3 Catalyticity of additives in the precipitation process

The choice of performing constant-volume experiments was made mainly because it was not clear whether the organic additives would be irreversibly consumed or they would simply take on a

Figure 6.9 Magnified HRXRD patterns showing the broadening of the following pairs of peaks in the presence of BSA:

(260) & ($2\bar{4}1$);

and

(070) & ($1\bar{6}1$)

STOE Powder Diffraction System

29-JUL-93

With BOVINE SERUM ALBUMIN

Intensity (Abs)

400
300
200
100

With O-PHOSPHO-L-SERINE

Intensity (Abs)

300
200
100

260
2$\bar{1}$1
070
1$\bar{3}$1

CONTROL

Intensity (Abs)

200
150

260
2$\bar{1}$1
070
1$\bar{3}$1

30.0 31.0 32.0 33.0 34.0 35.0

2Theta

catalytic rôle during the crystallisation process. With the results from constant-volume studies, it can now be possible to speculate on the catalyticity of the various bio-chemicals in the reaction.

If a compound is consumed during a precipitation reaction, it must either transform into other aqueously soluble but chemically different species or enter into the resulting solid phase. In our particular case, it is very unlikely for organic compounds and, especially, bulky macropolymers to break down completely in an aqueous solution into purely ionic entities. Thus if any bio-chemical was depleted during the calcification experiments, it should be possible to trace its inclusion in the final product. Now, as the presence of any alien moieties in a crystalline precipitate is bound to lead to variations in chemical composition, stoichiometry and lattice structure, the catalyticity of the various organics can be inferred from analytical results.

An inhibitor [promoter] of precipitation can work in a few ways - (i) by lowering [raising] the activities of the lattice ions, probably through the formation of relatively inert [reactive] complexes; (ii) by promoting [suppressing] the redissolution of any newly formed nuclei, through its capability to attract lattice ions from [to] the solid phase; (iii) by increasing [reducing] the surface free energy of the solid phase, thus increasing [lowering] the energy barrier for the heterogeneous formation of stable nuclei; or (iv) by deactivating [activating] growth sites. The first two modes involve reversible reactions of complex formation, whereas the latter two require the permanent attachment of the inhibitor [promoter] to specific growth sites on the precipitate surface. Thus the first two modes are classified here as "catalytic" (i.e. non-depletive) while the latter two are categorised as "exhaustive" (i.e. depletive).

We have seen previously that neither SerP, PS, ONec nor BPE induced any significant changes in the chemical composition or the microscopic lattice structure of the OCP precipitate. Thus they are most likely to exert their influence on precipitation via one of the catalytic mechanisms. (The catalyticity of SerP will be substantiated in the next chapter.) On the other hand, the presence of BSA led to changes in the surface composition and the atomic packing on specific planes, which leads us to the conclusion that BSA is likely to be irreversibly adsorbed on the solid precipitate during the course of precipitation.

To verify this deduction about BSA, the microscopic changes within the crystal lattice need to be further investigated. Since the inclusion of the organic additives would result in a distortion in

the lattice packing, the fracture paths would also be affected. Thus examining the fracture behaviour of the precipitated crystals should provide information about the catalyticity of the different organic compounds. As the precipitate was scraped off one of the substrates for XRD in each experiment, this substrate provided a good source of fracture surfaces for examination. Therefore, the substrates, from which crystals were removed, were subsequently sputter-coated and examined by SEM for the study of the fracture behaviour.

It is only meaningful to compare the fracture surfaces of crystals with similar morphologies. In this case, the plate-like crystals obtained in the control experiment and in the presence of BSA are compared. Figure 6.10 shows the micrographs of the fracture surfaces. For the control experiment, the fracture paths within the plate-like crystals were virtually straight lines; whereas in BSA-induced crystals, the crystals fractured along a stepped route. This is a very convincing sign for a change in preferred fracture plane within the crystal structure, most probably due to the adhesion of BSA onto the OCP lattice. A stepped route effectively lengthens the fracture path. In other words, BSA would be expected to increase the effective fracture toughness of the OCP crystals.

The non-catalytic rôle of BSA can be further verified by performing another precipitation experiment with a different concentration of BSA in the calcifying solution. Such an experiment was performed, using a supersaturated solution identical to that of Experiment IV-4 except for the amount of BSA addition which was now doubled. Figure 6.11 compares the coverage and the morphology of the resulting precipitate to that obtained in Experiment IV-4. It is clear that although the "waviness" of the crystals was still preserved, there was definitely less precipitation and lower surface coverage when the BSA content was doubled. The appearance of the crystal clusters was also different from the previous case. Now, had BSA been a catalytic agent in the precipitation of calcium phosphate, doubling its concentration would only have led to a change in the overall precipitation rate, without affecting the general appearance and the coverage pattern of the resulting crystals. Also, WDS (Ca/P = 0.59) and XRD results of the second batch of precipitate are very similar to those of the first experiment, again indicating a high calcium-deficiency and lattice distortions at the same high-indexed planes. Thus, from these pieces of information, the active consumption of BSA can be deduced. Moreover, as doubling the concentration of BSA actually reduced the extent of precipitation, its potential to deactivate nucleation and growth sites should be more prominent than

Figure 6.10 Fracture surfaces of precipitated crystals

(a) Control experiment
- straight fracture paths

(b) BSA-induced crystals
- stepped fracture paths

Figure 6.11 Scanning electron micrographs of the precipitate obtained in the presence of different amounts of BSA

(a) 5 mg, as in Figure 6.7(b)

(b) 10 mg - extent of precipitation reduced

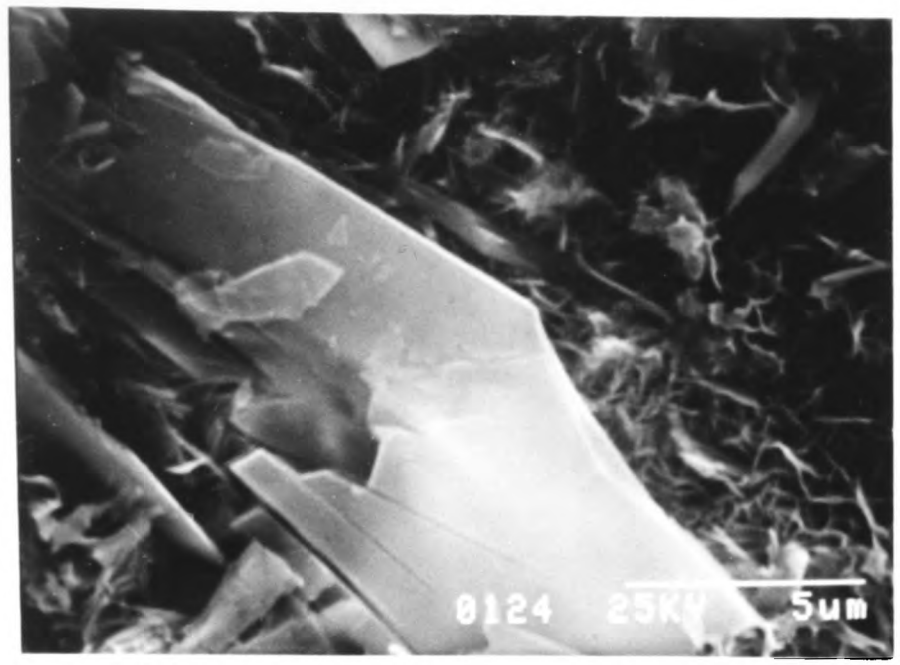

(a)

(b)

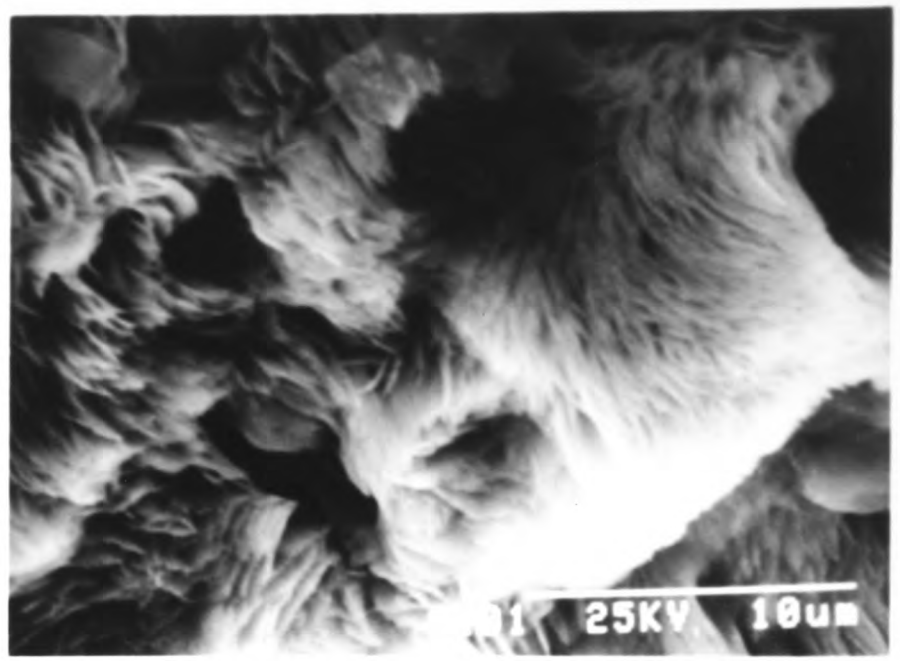

(a)

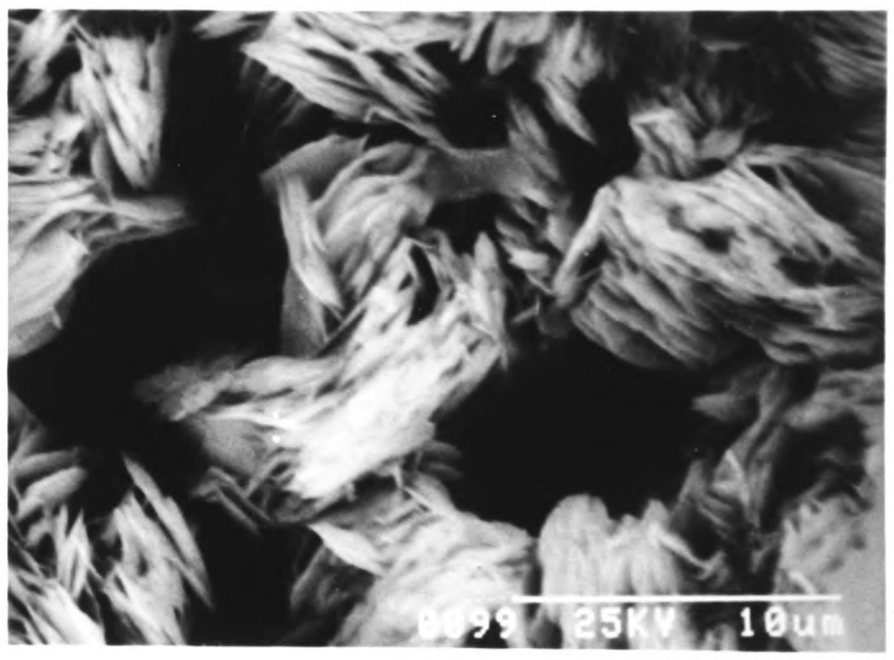

(b)

its ability to promote crystallisation, i.e. it is less probable for BSA molecules to bond to calcium sites in such an orientation that facilitates the formation of calcium phosphate precipitate.

One further point of interest which can be seen in Figure 6.10a is that, underneath the large plates of OCP crystal, there is an undergrowth of small crystals with morphology very similar to that of SerP-induced precipitate (Figure 6.3a). This shows that SerP not only promoted heterogeneous nucleation and the formation of small plate-like crystals, it also prevented the growth and evolution of these tiny crystals into large plates. This property is of particular interest in biological mineralisation studies because, as discussed in Section 2.4.2, optimum strengthening of collagen requires the deposition of small calcium phosphate crystal in specific locations regularly located along the collagen chains.

6.4.4 SerP vs. PS: how the aliphatic side-groups affect the performance of bio-chemicals

It is very difficult to make any comparison among bulk protein macromolecules based on their chemical compositions due to the uncertainty in defining the exact sequences of amino acid residues and the actual sizes of these biopolymers. However, among the various bio-chemicals used in this series of studies, SerP and PS are relatively simple molecules of known chemical compositions. It is therefore possible to compare the two compounds from a chemical point of view.

The structures of SerP and PS are shown in Figure 6.12. The main difference between them is in the aliphatic side-chain which is attached to the phosphorylated serine functional unit. It has been found that the two compounds exerted very different effects on calcium phosphate precipitation, and there must therefore be a relationship between the side-chains on the phosphoryl group and the overall effects on nucleation and growth.

Figure 6.12 Molecular structures of (a) phosphoserine, and (b) phosphatidylserine

(a)

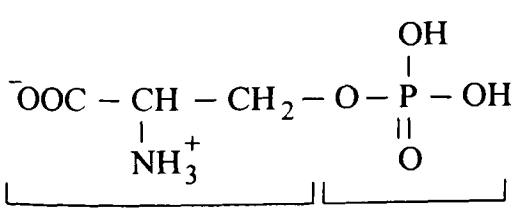

(b)

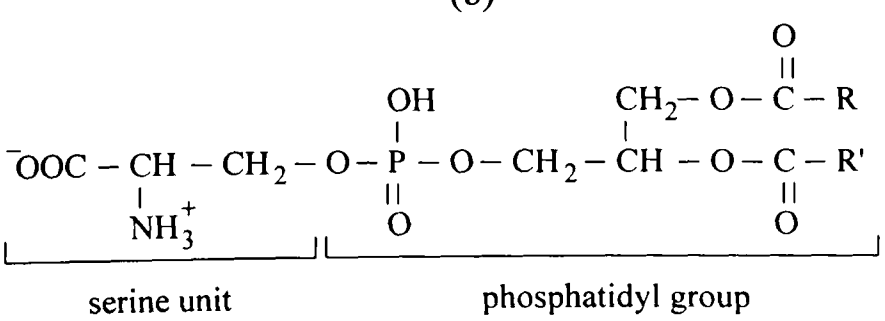

Phosphorylated organic compounds participate in calcification due to the high affinity of the phosphoryl group for Ca^{2+} ions (Figure 6.13). However, the ease with which free Ca^{2+} ions can approach a phospho-organic compound depends on two main factors: (i) the electrostatic attraction between the free cation and the electronegative phosphoryl group; and (ii) the geometry of the organic compound, i.e. the orientational limitation for easy Ca^{2+} approach. Both of these factors are dependent on the nature of the side-chains.

Let us first compare the electrostatics of the PS and SerP. Owing to the bigger difference in electronegativity between O and H than between O and C, the substitution of the hydrogen in the phosphorus-bonded –OH group with an aliphatic chain makes the bond less polarised. Consequently, the whole phosphoryl group in PS is thereby rendered less electronegative for the attraction of Ca^{2+} ions, reducing the chemical reactivity of the PS.

Next, we consider the geometrical difference between the two compounds. Clearly PS is a much less accessible molecule as its phosphoryl group is attached to an extra bulky carbon chain in addition to the serine end-group. As a result, PS presents much a more stringent spatial restriction for the successful approach of free Ca^{2+} ions to the active phosphoryl site. Also, since it is likely that neither of these compounds is actually present in the final product, the formation of calcium phosphate precipitate must therefore entail the release of these organocomplexed Ca^{2+} ions by the formation of ionic bonds with the appropriate forms of phosphate ions in the solution. This again requires the fulfilment of specific geometric criteria. In other words, both the formation of organocalcium complexes and the subsequent release of these complexed Ca^{2+} ions by phosphate ions are more difficult in the case of PS. This reinforces the deactivating effect on the phosphoryl group in PS. It is therefore not surprising to find that, despite having the main skeleton of SerP, PS actually inhibited the formation of calcium phosphate precipitate during the experiments.

Figure 6.13 Electrostatic attraction between a free Ca^{2+} ion and a phosphorylated amino acid

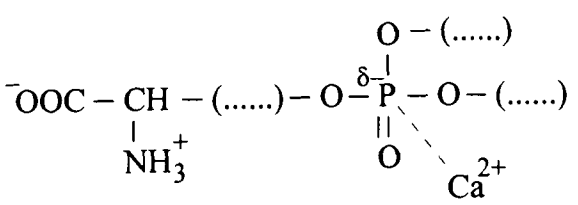

6.5 Conclusions

In this chapter, the effects of various organic bio-chemicals on the precipitation of calcium phosphate have been discussed based on experimental results. First of all, the precipitate obtained in each experiment gave an XRD spectrum resembling closely the theoretical peak pattern of OCP, which is the expected phase predominantly present in the precursor under physiological conditions after 72 days of precipitation. Therefore, the sequence of phase emergence was not affected by the inclusion of small amounts of organic compounds in the calcifying media. Indeed, the supersaturations with respect to the various calcium phosphate phases were still the crucial determining factor for the preferential formation of thermodynamically unfavourable phases.

However, organic compounds did exert considerable influence on various aspects of the precipitation phenomenon. It was found that SerP accelerated the overall rate of calcium phosphate formation while PS, ONec and BPE significantly slowed down the process. When the substrate surfaces were examined, information about the changes in nucleation and growth rates was deduced. SerP initiated the formation of numerous tiny plate-like crystals and, by observing the undergrowth of crystallites underneath the big crystals in the control experiment, SerP was also found to curb the small crystals from growing into large plates. The uniform surface coverage suggested that its promotional effect is not likely to be strongly dependent on the crystallographic relationship at the substrate-precipitate interface. BSA was found to induce the localised formation of clusters of precipitate with a wavy sheet-like morphology. This supports the hypothesis that the interaction between BSA and the solid phase is affected by the interfacial steric relationship. PS and ONec both caused the resulting precipitate to assume a quasi-cubic appearance with inter-planar angles not far from those in the triclinic OCP unit cell. The growth of the precipitate with dimensions closely resembling the unit cell geometry instead of a blade- or plate-like appearance indicated that growth was not selectively accelerated or suppressed along any of the principal directions, i.e. there was no directional preference for growth. BPE exhibited the strongest inhibitory effect on calcium phosphate precipitation, hindering both nucleation and growth.

Compositional analyses of the precipitate confirmed that the phases obtained in the control experiment and in the presence of SerP, PS, ONec and BPE were all OCP with a very low degree of calcium deficiency. However, under the influence of BSA, the Ca/P ratio of the precipitate plunged

dramatically to 0.52 despite having an XRD spectrum close to the OCP pattern. This has been explained by the adsorption of BSA on the crystal surface and the consequent blockage of growth sites.

Not only did BSA differ from the other organics used in these experiment in the above manner, it was also likely to be the only organic chemical which was actively consumed during the reaction. Changes in the XRD pattern along planes of high Miller indices and in the fracture behaviour denote an intrinsic alteration in the crystal lattice structure in BSA-induced precipitate. The lack of evidence indicating the depletion of the other compounds suggests that they affected the crystallisation process through a non-exhaustive, or catalytic, mechanism.

Since SerP and PS both consist of an identical backbone with different aliphatic side-chains, their effects on calcification were compared in detail. It has been found that despite having the same phosphoserine functional unit, their influence on the reaction was very different. Detailed analysis of their molecular structures and the mechanism through which calcium and phosphate ions were successively attracted to the electronegative phosphoryl group led to the conclusion that the efficiency to react with the ions in solution is a function of the electropositivity and the three-dimensional geometry of these side-chains. A sound understanding of the effects of differences in molecular structure of different phospho-organic compounds is useful in establishing the actual parts played by phosphorus-rich organic macromolecules in the heterogeneous precipitation of calcium phosphate. The present discussion has provided a brief introduction to the impact different organic side-chains can make on the phosphoryl group in an organic molecule, but obviously there is a need for a systematic approach of studying these effects. In Chapter 7, the effects of different phosphorylated amino acids on the precipitation of calcium phosphate will be discussed in detail.

Chapter 7

EFFECTS OF PHOSPHORYLATED AMINO ACIDS ON THE PRECIPITATION OF CALCIUM PHOSPHATE UNDER PHYSIOLOGICAL CONDITIONS

In the last chapter, the effects of various bone-specific non-collagenous bio-chemicals on the precipitation behaviour of calcium phosphate have been discussed. One common characteristic of most bone-specific macromolecules is that they all contain a high proportion of phosphorylated amino acid residues. These phosphoryl end groups are specifically involved in the mineralisation process due to their electronegativity and consequently their potential to bond to positive calcium ions. However, it has been shown that different phospho-organic compounds exert very different effects on the precipitation process. Phosphoserine (SerP) has been found to promote secondary nucleation of tiny plate-like crystals whereas, for the same weight fraction, phosphatidylserine (PS) has an overall inhibitory effect on calcification. As both these compounds have a basic phosphoserine backbone, the difference in their effects on the precipitation behaviour implies a possible link between the side-chain and the calcium-binding affinity of the phosphoryl group of the amino acid (Figure 6.13). Any direct relationship between them is likely to have important implications in the physiological mineralisation process, as phosphoserine residues account for a big proportion of the phosphorus content in bone-specific phosphoproteins, which are known to be heavily involved in the calcification phenomenon.

Apart from the nature of the side-chains, another aspect of the presence of phospho-organic compounds may also affect the manner in which the precipitation process is influenced. Since these phosphorylated amino acids interfere in the calcification reaction by complexing with free calcium ions in the solution, it is extremely likely that altering the concentration of these organic additives within the solutions would lead to a change in the overall precipitation rate (Thudichum 1901, Koch & Pike 1910, Koch & Todd 1911, Abramson *et al.* 1964, Papahadjopoulos & Hanahan 1964). In this chapter, results from precipitation experiments performed with the addition of different phospho-amino acids will be discussed, putting special emphasis on the two main issues of side-chains and concentration.

7.1 Materials and method

7.1.1 Phosphorylated amino acids

The residues of phosphorylated amino acids account for the high phosphorus contents in phosphoproteins. In this series of experiments, four phospho-amino acids (Table 7.1), obtained from Sigma Chemicals, were introduced to the calcifying media. These amino acids were chosen firstly because they cover a rather wide range of molecular mass, but more importantly because they impart different degrees of steric constraint for the successful approach of ions in solution for complexation to occur. Among the four, SerP is the smallest and has the most accessible phosphoryl group. ThrP is sterically slightly more demanding than SerP due to the presence of a branched side-chain. Both TyrP and ArgP are much bigger molecules than SerP, but their bulkiness is enhanced through different mechanisms - TyrP contains a rigid aromatic ring along its side-chain, whereas ArgP has a longer aliphatic chain and also contains a strongly basic imino (–NH–) group.

7.1.2 Experimental procedure

Two sets of experiments were performed - one for the investigation of the effects of different phospho-amino acids on the calcification process; and the other for the verification of the relationship between the reaction rate and the concentration of the additive. Now, considering that SerP and PS showed evidence in support of a non-depletive catalytic mechanism, the amino acids chosen for the

Table 7.1 List of phosphorylated amino acids added in the calcifying solutions

Chemical	Symbol	Formula
O-phospho-L-serine	SerP	$^{-}OOC-\underset{\underset{NH_3^+}{|}}{CH}-CH_2-O-PO_3^{2-}$
O-phospho-L-threonine	ThrP	$^{-}OOC-\underset{\underset{NH_3^+}{|}}{CH}-\underset{\underset{CH_3}{|}}{CH}-O-PO_3^{2-}$
O-phospho-L-tyrosine	TyrP	$^{-}OOC-\underset{\underset{NH_3^+}{|}}{CH}-CH_2-C_6H_4-O-PO_3^{2-}$
Phospho-L-arginine	ArgP	$^{-}OOC-\underset{\underset{NH_3^+}{|}}{CH}-(CH_2)_3-NH-\underset{\underset{NH}{||}}{C}-NH-PO_3^{2-}$

7.1 Materials and method

7.1.1 Phosphorylated amino acids

The residues of phosphorylated amino acids account for the high phosphorus contents in phosphoproteins. In this series of experiments, four phospho-amino acids (Table 7.1), obtained from Sigma Chemicals, were introduced to the calcifying media. These amino acids were chosen firstly because they cover a rather wide range of molecular mass, but more importantly because they impart different degrees of steric constraint for the successful approach of ions in solution for complexation to occur. Among the four, SerP is the smallest and has the most accessible phosphoryl group. ThrP is sterically slightly more demanding than SerP due to the presence of a branched side-chain. Both TyrP and ArgP are much bigger molecules than SerP, but their bulkiness is enhanced through different mechanisms - TyrP contains a rigid aromatic ring along its side-chain, whereas ArgP has a longer aliphatic chain and also contains a strongly basic imino (–NH–) group.

7.1.2 Experimental procedure

Two sets of experiments were performed - one for the investigation of the effects of different phospho-amino acids on the calcification process; and the other for the verification of the relationship between the reaction rate and the concentration of the additive. Now, considering that SerP and PS showed evidence in support of a non-depletive catalytic mechanism, the amino acids chosen for the

Table 7.1 List of phosphorylated amino acids added in the calcifying solutions

Chemical	Symbol	Formula
O-phospho-L-serine	SerP	$^{-}OOC-\underset{\underset{NH_3^+}{|}}{CH}-CH_2-O-PO_3^{2-}$
O-phospho-L-threonine	ThrP	$^{-}OOC-\underset{\underset{NH_3^+}{|}}{CH}-\underset{\underset{CH_3}{|}}{CH}-O-PO_3^{2-}$
O-phospho-L-tyrosine	TyrP	$^{-}OOC-\underset{\underset{NH_3^+}{|}}{CH}-CH_2-C_6H_4-O-PO_3^{2-}$
Phospho-L-arginine	ArgP	$^{-}OOC-\underset{\underset{NH_3^+}{|}}{CH}-(CH_2)_3-NH-\underset{\underset{NH}{||}}{C}-NH-PO_3^{2-}$

new experiments should also follow a similar route, especially since they all comprise the same phosphoryl functional group. Having made the assumption that none of the added chemicals would be irreversibly consumed during precipitation, and since their exact chemical formulæ were known, it should then be possible to devise experiments using the constant-composition technique, the basic principles of which has already been discussed in Chapter 4. Thus, by performing a constant-composition experiment with the inclusion of these phosphorylated amino acid and tracing the phosphate content throughout the experiment, the catalytic property of these compounds could be verified. The difficulty for the continuous regulation of phosphate ions (or, in fact, any ions apart from calcium and hydrogen ions) has been pointed out in Section 4.3.4, but during these test runs, the concentration of phosphate was qualitatively determined at regular intervals adopting the colorimetric technique developed by Fogg and Wilkinson (1958). Basically a measured amount of ammonium molybdate tetrahydrate [$(NH_4)_6Mo_7O_{24} \cdot 4H_2O$] was added to the solution, creating molybdophosphate complexes. These complexes were then reduced by the addition of ascorbic acid (Vitamin C), and the resulting characteristic molybdenum blue colour was indicative of the phosphate content of the starting solution. There was no detectable change in the phosphate content throughout these preliminary constant-composition experiments, and the catalyticity of these phospho-amino acids was thus established.

With the confirmation of the catalytic behaviour of these phospho-amino acids, detailed constant-composition precipitation experiments were performed. Table 7.2 summarises the different composition of the solutions. In each case, precipitation was allowed to proceed for up to 7 days. Precipitate characterisation was performed using SEM, XRD and WDS as before.

7.2 Results and discussion

In both sets of experiments, although the compositions of the calcifying solutions were different, the $[\Sigma Ca] \times [\Sigma P]$ product was kept constant throughout, a situation which is similar to the actual physiological conditions - even though the concentrations of different bio-chemicals may differ at different parts of the anatomy, the total calcium and phosphate contents in the body fluid are maintained almost constant at all bone-growth sites (Vaughan 1981). The effects of the side-chains and the relative concentration of the organics are discussed below.

Table 7.2 Compositions of calcifying solutions

[ΣCa] = 2 mM; [ΣP] = 1.2 mM; [KCl] = 0.1 M; *p*H = 7.4; 37 °C

Expt. no.	Added amino acid	Amount added		Expt. no.	Added amino acid	Amount added	
		(mM)	(mol / mol [ΣCa])			(mM)	(mol / mol [ΣCa])
IV-1[a]	no addition	(control)	0%	V-1[a]	no addition	(control)	0%
IV-2[b]	SerP	0.2	10%	V-2	SerP	0.02	1%
IV-3	ThrP			V-3		0.1	5%
IV-4	TyrP			V-4[b]		0.2	10%
IV-5	ArgP			V-5		0.5	25%
				V-6		1.0	50%
				V-7		2.0	100%

[a] Instead of repeating identical experiments, Experiments IV-1 and V-1 have been replaced by Experiment II-6 (see Chapter 4).

[b] Again owing to the identical experimental conditions, results from Experiment IV-2 have been used for Experiment V-4.

7.2.1 Effects of the side-chains of phosphorylated amino acids

In the first set of experiments, equal quantities (mol/mol) of organics were present in different batches of working solution in order to evaluate the relationship between the side-chains and the overall effect of the phosphorylated amino acids on calcium phosphate precipitation.

§ Overall precipitation rate

Figure 7.1 shows the total calcium uptake rates as functions of time. It is obvious that, compared to the results from the control experiment, the whole precipitation rate was most significantly accelerated by SerP, the smallest and most accessible amongst the organic compounds. This promotional effect tailed off with increasing bulkiness of the additive and, indeed, in the presence of TyrP and ArgP, the overall crystallisation rate was slowed down.

This trend confirms the prediction made previously in Section 6.4.4, based upon the reduced electronegativity of the phosphoryl group and the more restricted ionic approach due to the presence of longer side-chains attached to the phosphoryl end. Furthermore, it is now possible to deduce the relative prominence of these two factors from the results of experiments incorporating TyrP and

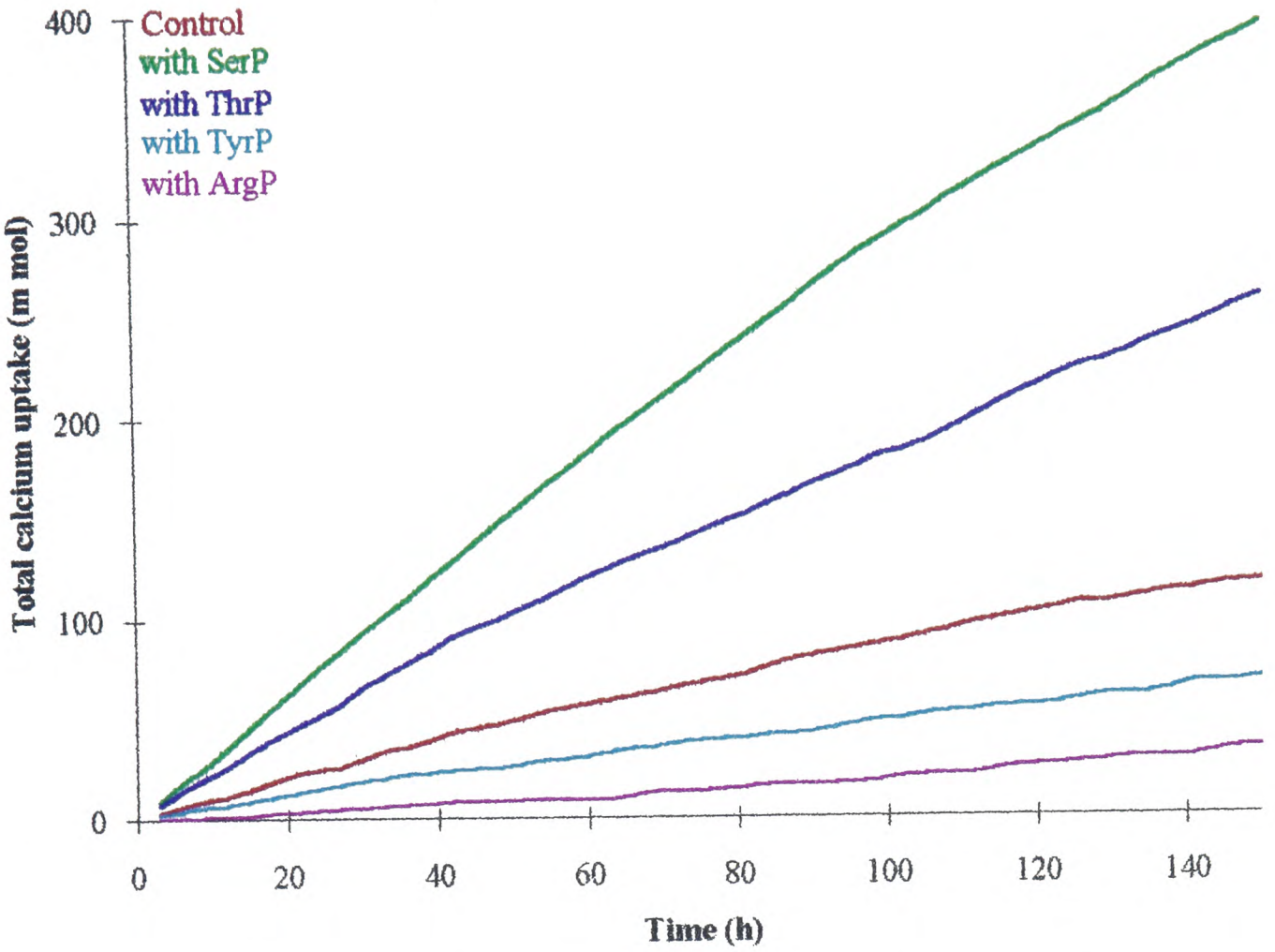

Figure 7.1 The graphs of total calcium uptake against time

Figure 7.2 The graphs of Ca/P molar uptake ratio against time

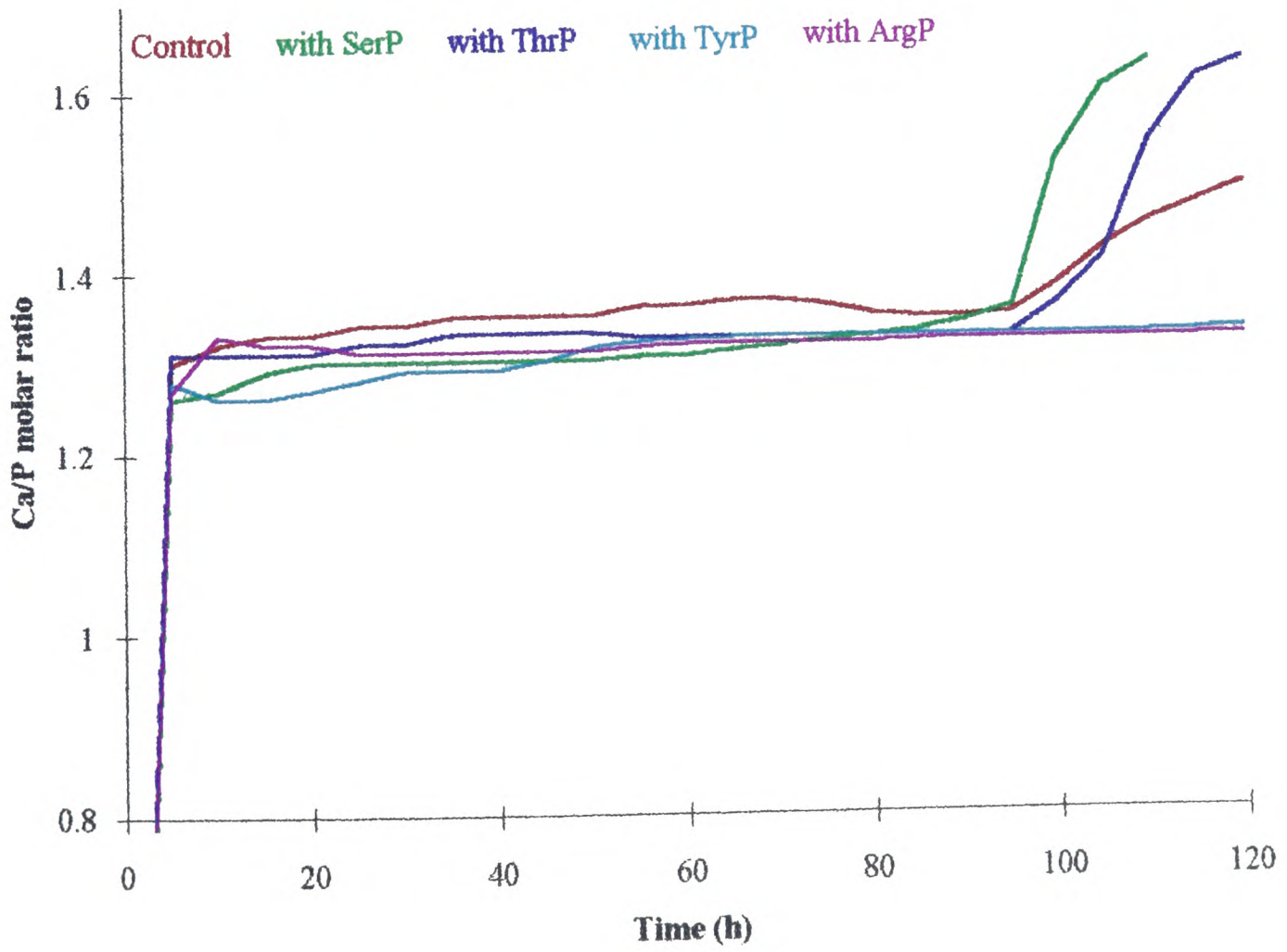

ArgP. Although the polarisation of the R–(O)–PO_3^{2-} bonds (R denoting an alkyl side-chain) is somewhat reduced by the presence of a long side-chain, the phosphoryl group still retains certain amount of its electronegativity and is therefore still potentially capable to increase the reactivity of the Ca^{2+} ions in solution. However, both of these compounds showed an overall inhibitory effect on calcification. Thus it becomes apparent that the steric restriction exerted a comparatively heavier effect in determining the promotional or inhibitory nature of a phospho-amino acid.

§ Precursors and phase transformation

Figure 7.2 displays the ratio of uptake rates of calcium against phosphate for the different experiments. It can be seen that, in every case, the initial Ca/P ratio was close to 1.3 which corresponds to the stoichiometry of octacalcium phosphate (Ca/P ratio 1.33). Thus, although the systems were under the influence of different bio-chemicals, the precursor phase to hydroxyapatite formation was still predominantly determined by the ionic product of total calcium and total phosphate. However, these organics did affect the subsequent phase transformation to thermodynamically stable hydroxyapatite (HAP, Ca/P ratio 1.67). With reference to the Ca/P uptake ratios (Figure 7.2), the XRD patterns (Figures 7.3-7.7) and the WDS Ca/P atomic ratios (Table 7.3), it is clear that again, SerP induced the earliest transformation of OCP to HAP; and with increasing bulkiness of the individual amino acids, the transformation rate was accordingly retarded. Scanning electron micrographs of solid specimens (Figures 7.8-7.12) clearly depict that after 48-54 hours of precipitation, only in the case of SerP addition can the growth of a secondary phase over a primary crystal coverage be observed (Figure 7.9). The identities of the precipitated phases were confirmed by XRD (Figure 7.4) and WDS (Table 7.3). Only OCP was obtained in all experiments after such a period of time, with the exception of SerP-induced reaction, where a primary OCP and a secondary HAP phase were present in the resulting precipitate. Comparable degrees of OCP-HAP phase transformation as above were achieved in the control experiment and in the case of ThrP only after considerably longer periods (around 90 hours, Figures 7.3, 7.5, 7.8, 7.10). After 144-160 hours, transformation to hydroxyapatite was complete in the control as well as with SerP and ThrP. However, no visible transformation was observed in the case of TyrP (Figure 7.11), while for ArgP, the nucleation rate was so slow that only large plates of OCP were obtained (Figure 7.12).

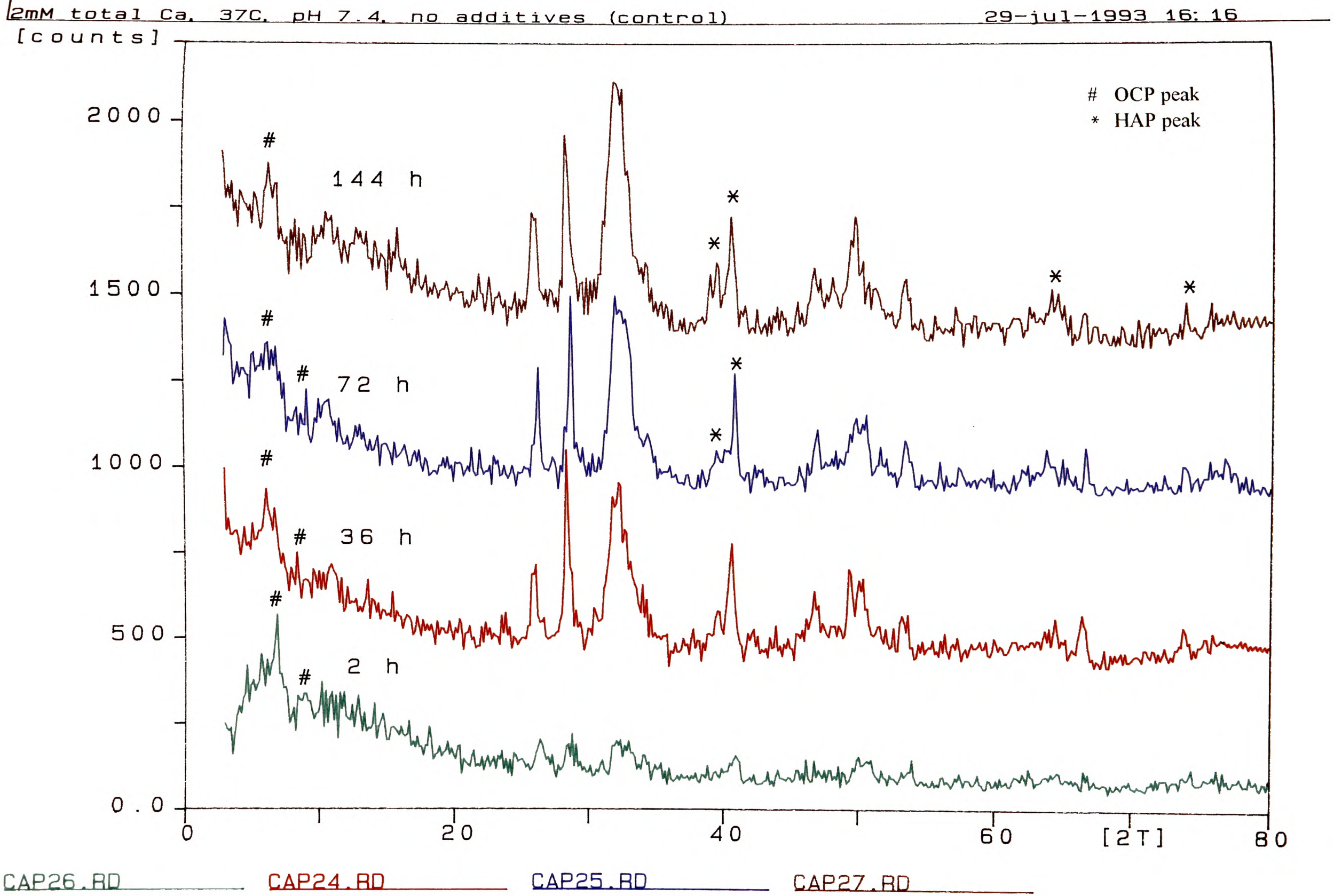

Figure 7.3 Powder X-ray diffraction patterns of solid precipitate obtained in the control experiment

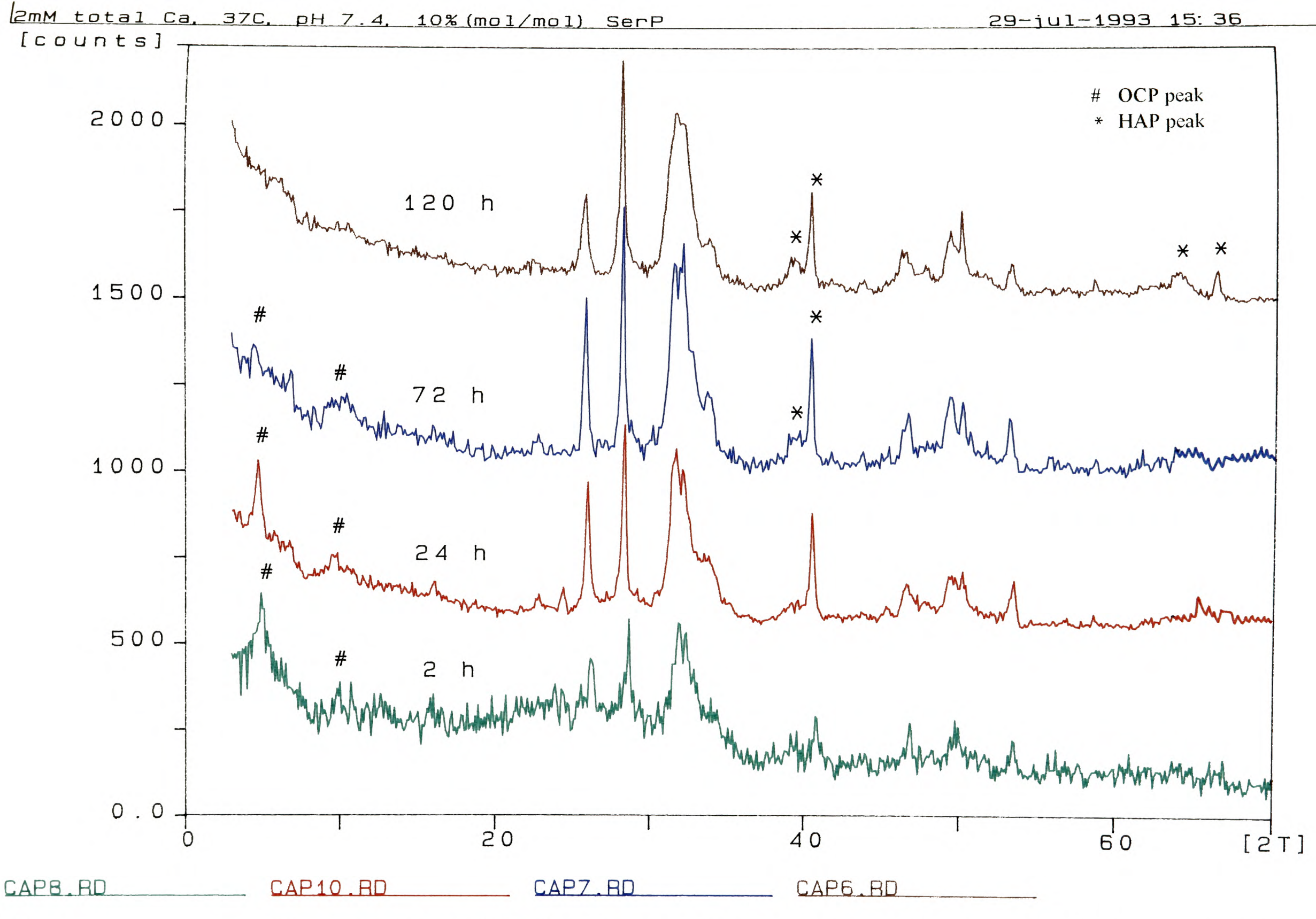

Figure 7.4 Powder X-ray diffraction patterns of solid precipitate obtained in the presence of 10% (mol/mol) SerP

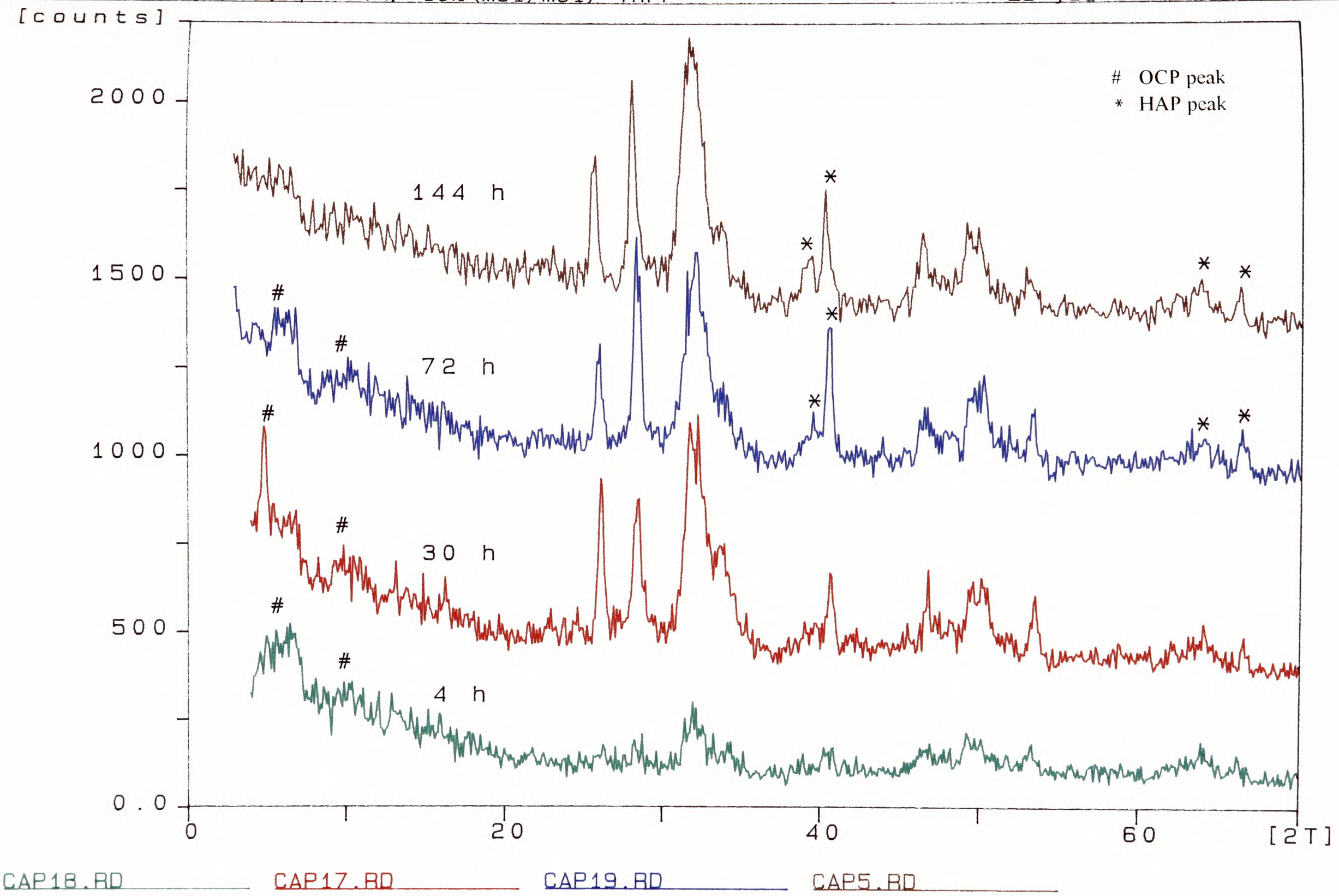

Figure 7.5 Powder X-ray diffraction patterns of solid precipitate obtained in the presence of 10% (mol/mol) ThrP

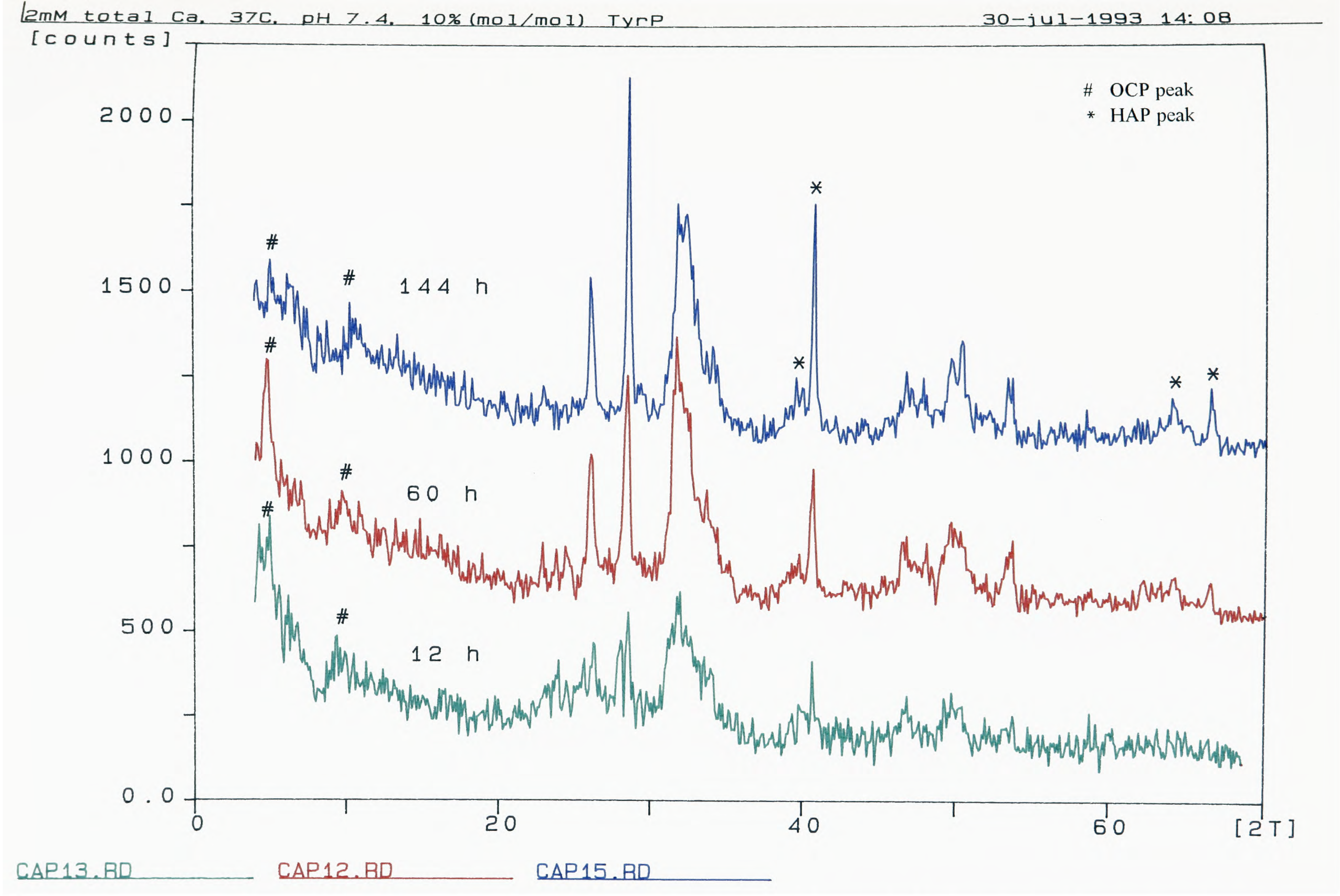

Figure 7.6 Powder X-ray diffraction patterns of solid precipitate obtained in the presence of 10% (mol/mol) TyrP

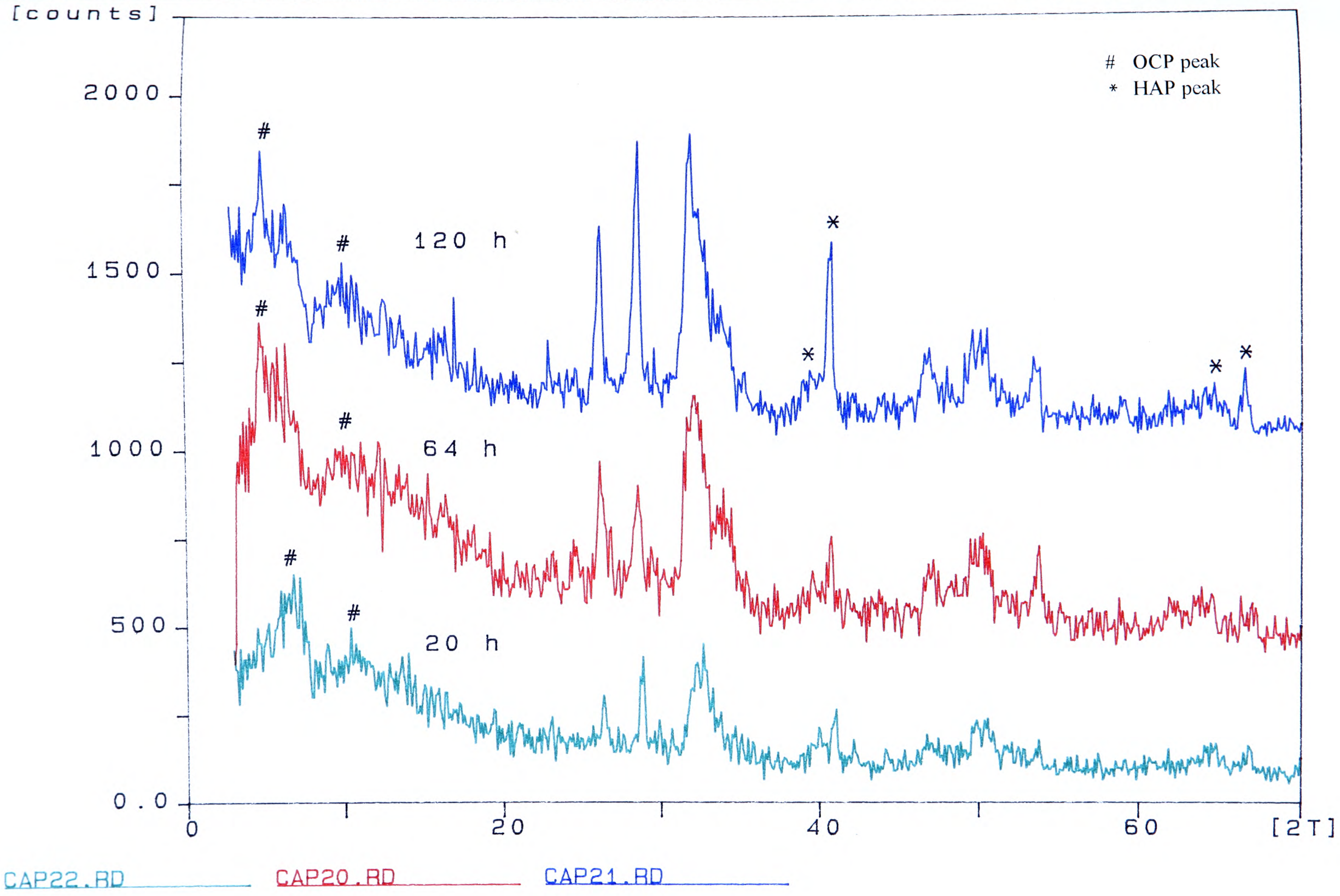

Figure 7.7 Powder X-ray diffraction patterns of solid precipitate obtained in the presence of 10% (mol/mol) ArgP

Figure 7.8 Scanning electron micrographs of the precipitate obtained in the control experiment

(a) OCP crystals, 48 hours

(b) Transformation to HAP, 84 hours

(c) HAP platelets, 144 hours

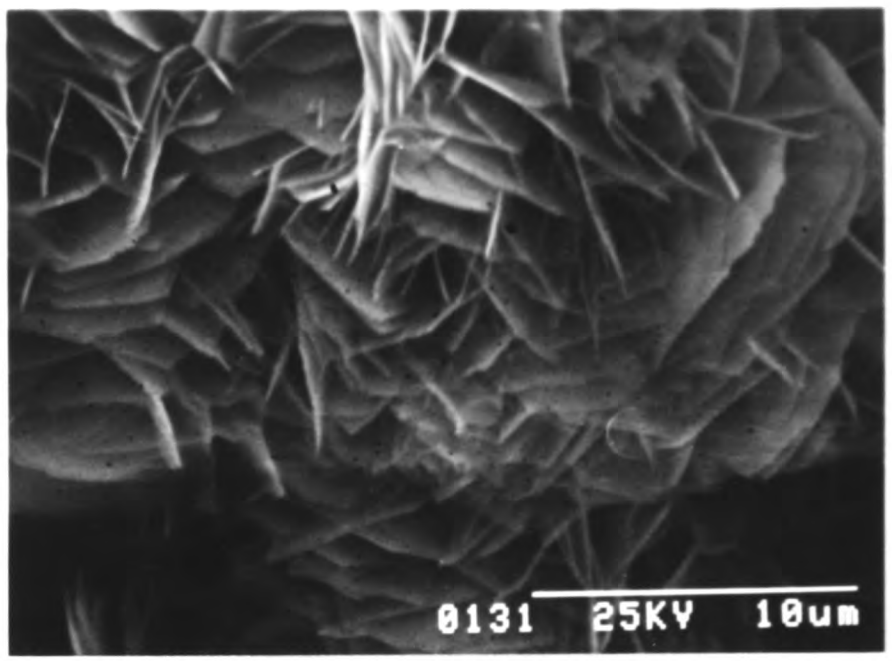

(a)

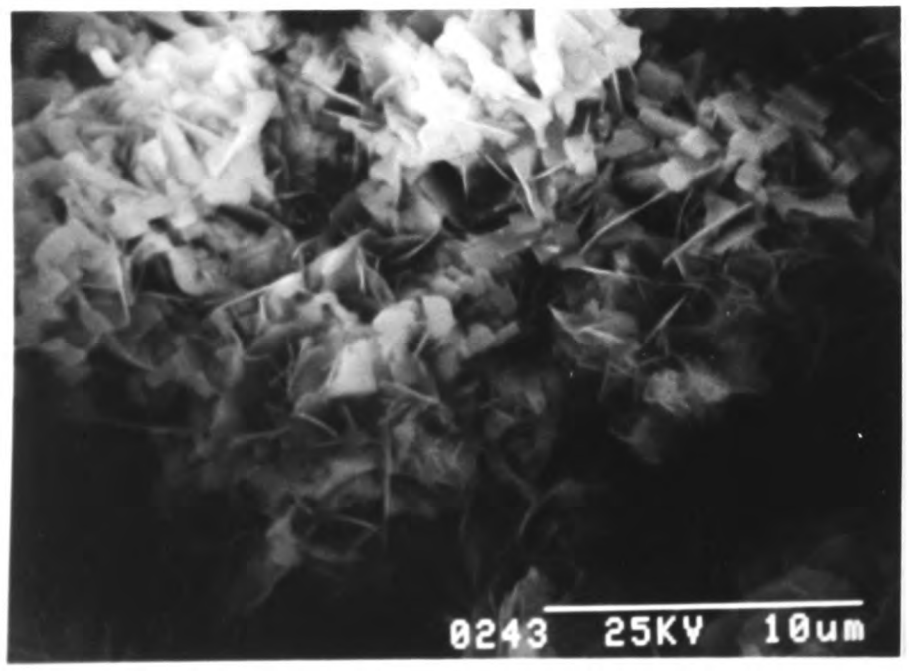

(b)

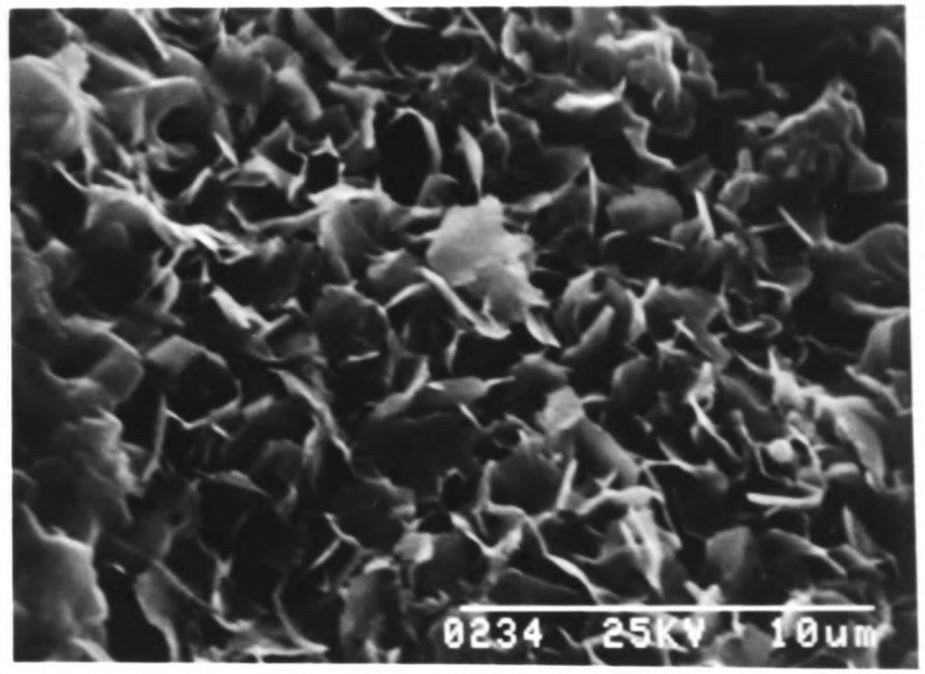

(c)

Figure 7.9 Scanning electron micrographs of the precipitate obtained in the presence of 10% (mol/mol) SerP

(a) OCP crystals and the commencement of transformation to HAP
32 hours

(b) Further transformation to HAP,
54 hours

(c) Transformation almost complete.
96 hours

(d) HAP plates,
144 hours

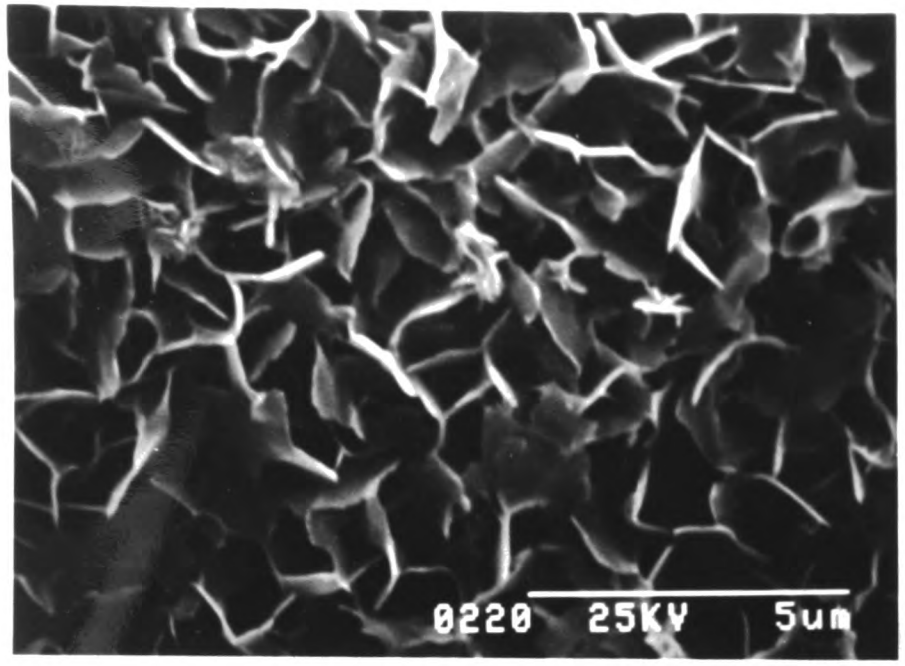

(a)

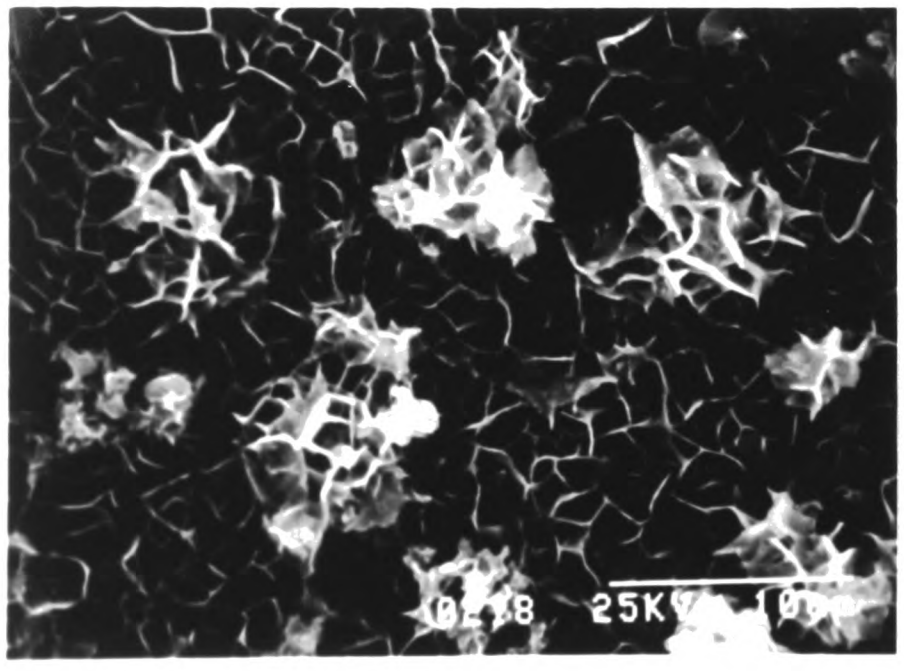

(b)

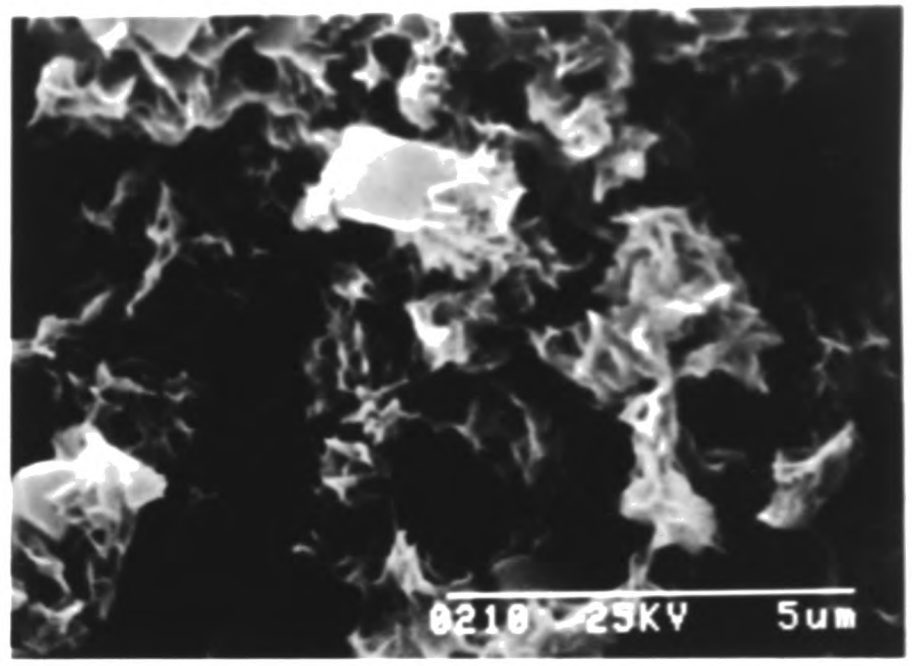

(c)

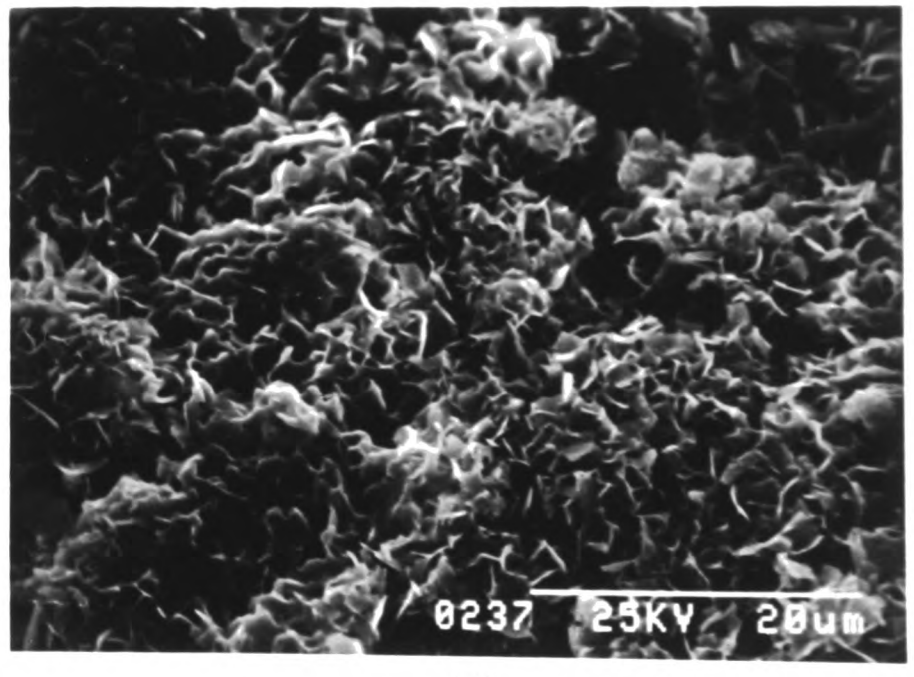

(d)

Figure 7.10 Scanning electron micrographs of the precipitate obtained in the presence of 10% (mol/mol) ThrP

(a) Small OCP crystals, 16 hours

(b) OCP plates, 48 hours

(c) Transformation to HAP, 96 hours

(d) Small HAP crystals, 160 hours

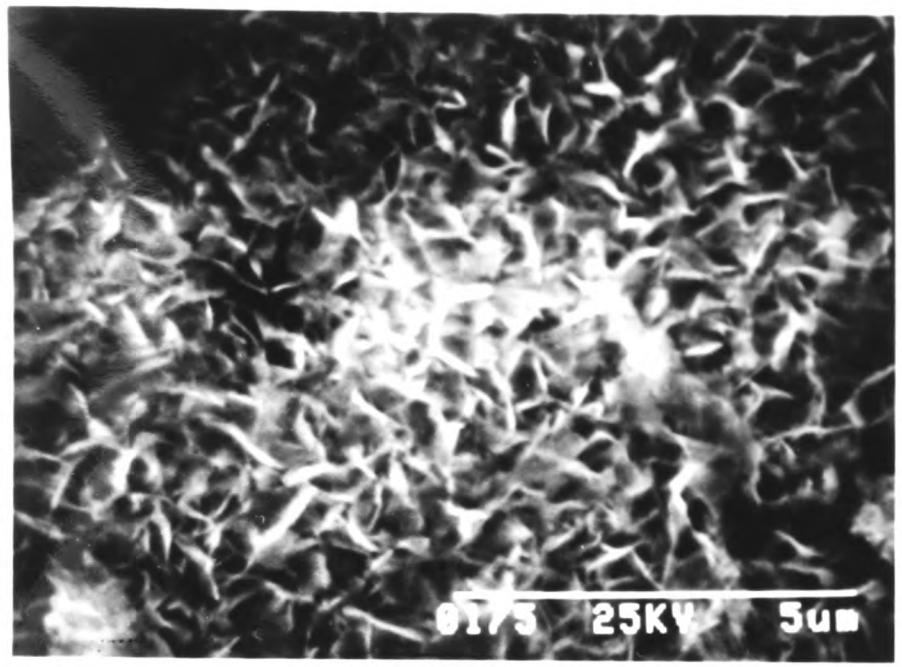

(a)

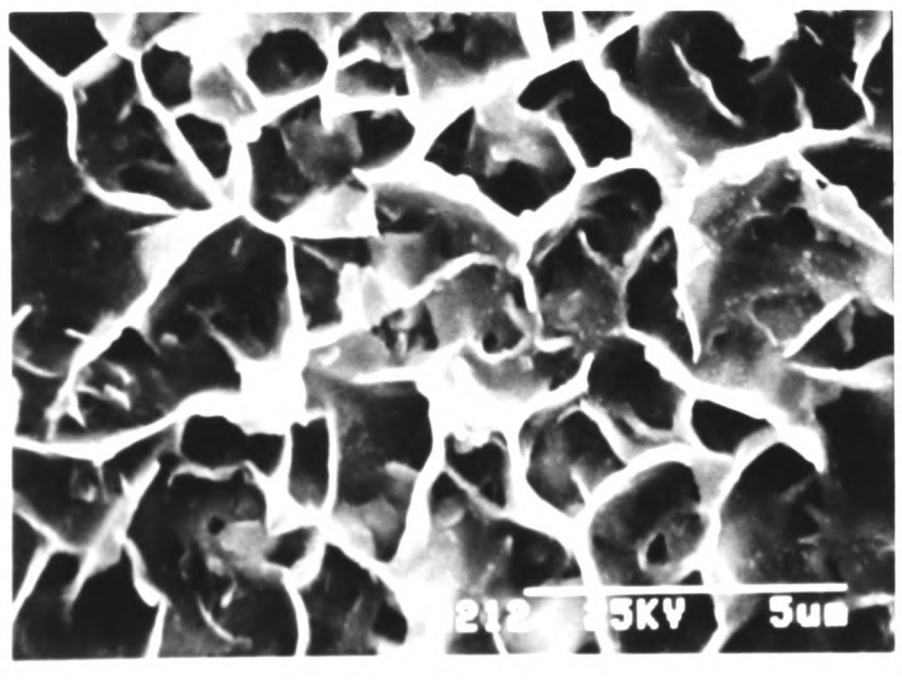

(b)

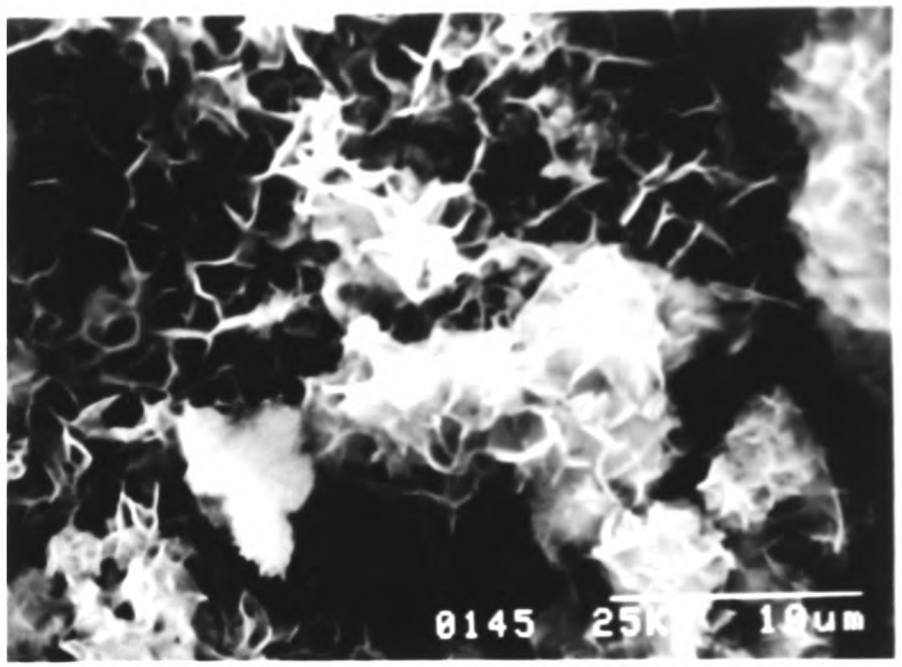

(c)

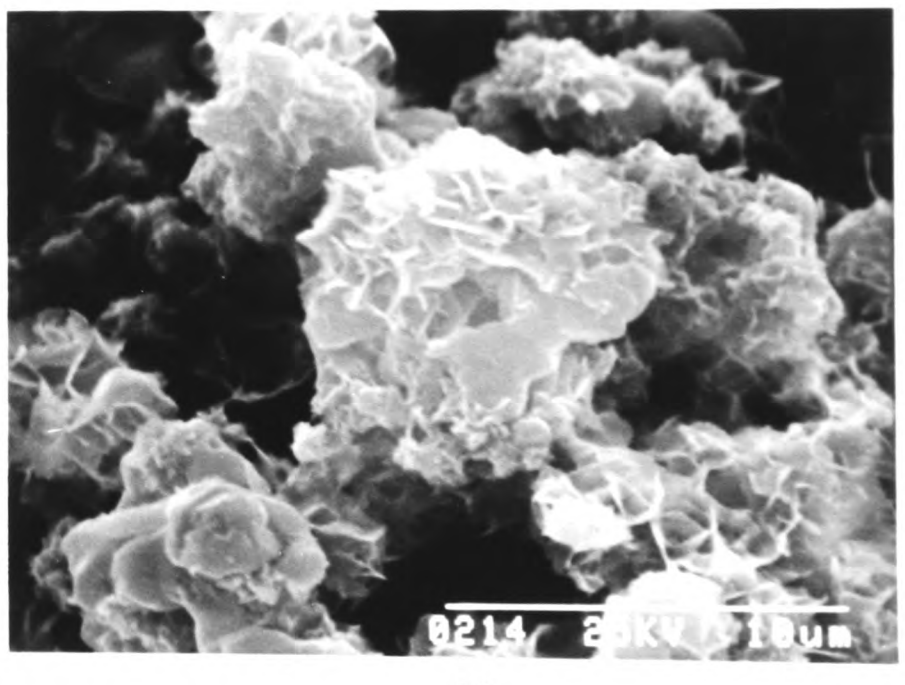

(d)

Figure 7.11 Scanning electron micrographs of the precipitate obtained in the presence of 10% (mol/mol) TyrP

(a) Small OCP crystals, 48 hours

(b) OCP plates, 144 hours

Figure 7.12 Scanning electron micrographs of the precipitate obtained in the presence of 10% (mol/mol) ArgP

(a) Slow nucleation led to the formation of a small quantity of relatively large OCP crystals, 60 hours

(b) Large OCP plates, 160 hours

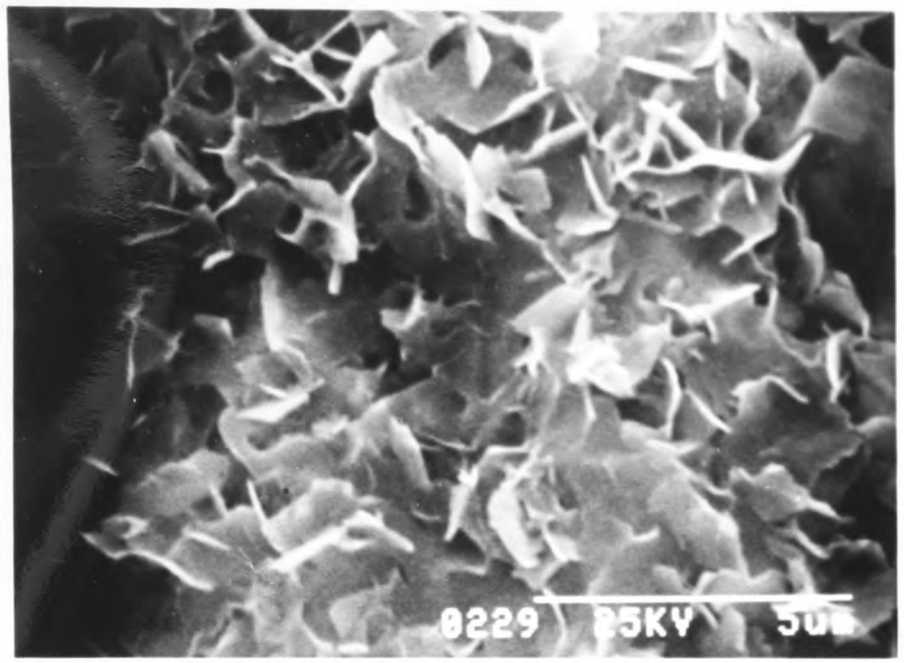

(a)

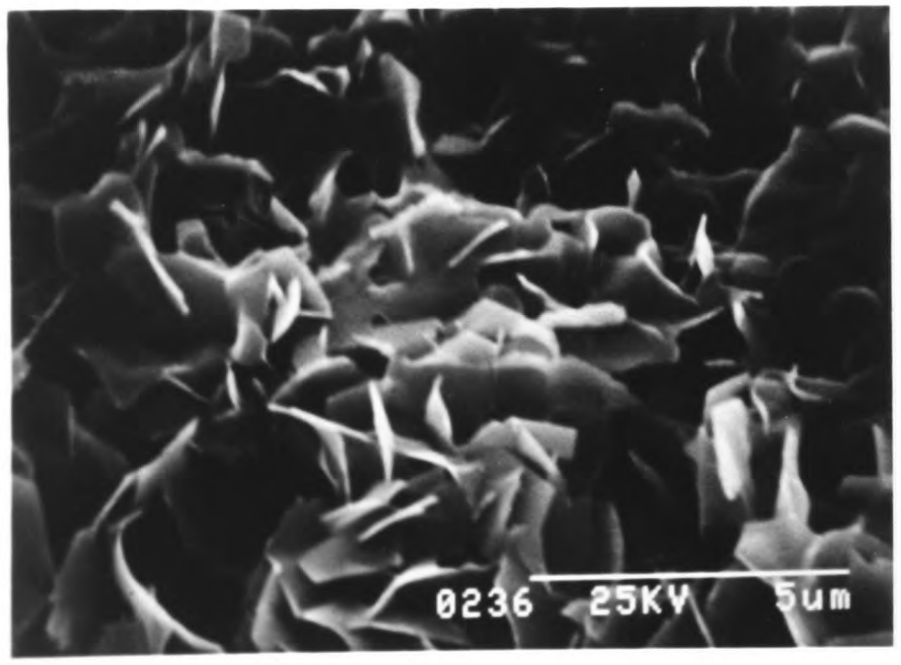

(b)

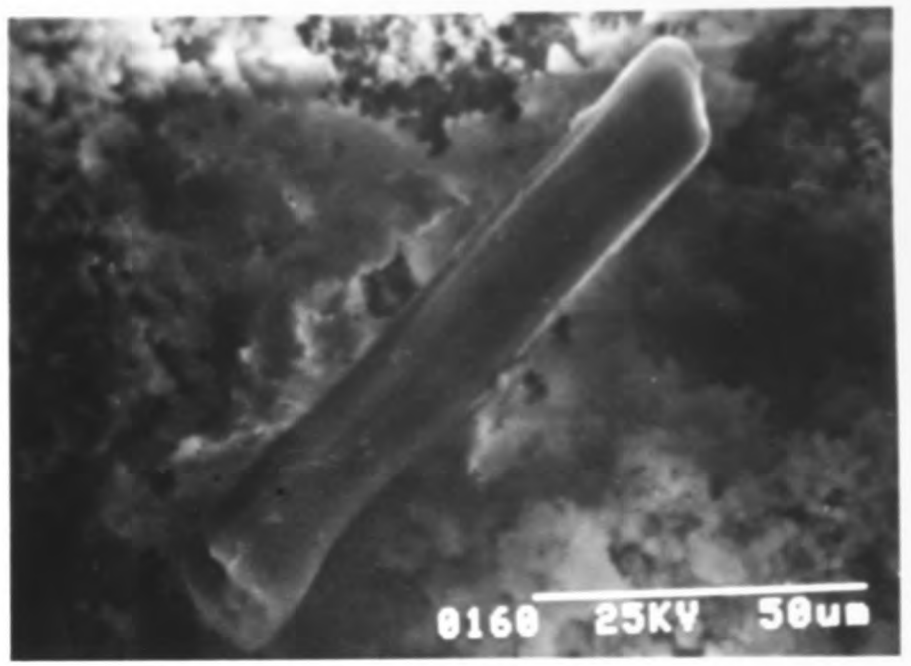

(a)

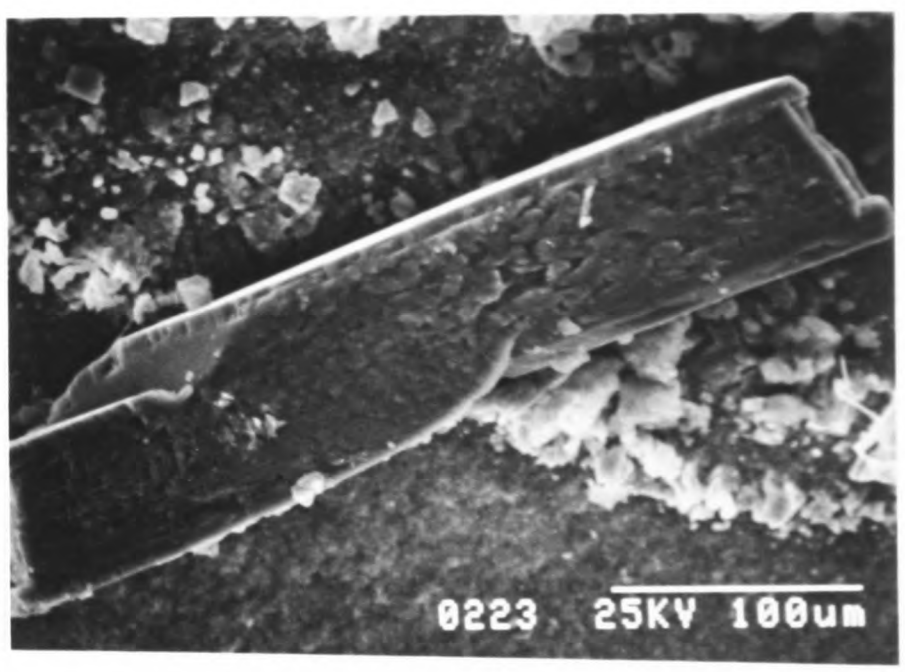

(b)

Table 7.3 Ca/P atomic ratio of precipitates from WDS analyses

Expt. no.	Added amino acid	Elapsed time (h)	WDS Ca/P atomic ratio (±2%)			
			1st reading	2nd reading	3rd reading	Mean
IV-1 (from II-6)	no addition (control)	2	1.28	1.26	1.29	**1.277**
		36	1.29	1.32	1.32	**1.310**
		72	1.39	1.42	1.39	**1.400**
		144	1.58	1.59	1.57	**1.580**
IV-2	SerP	2	1.31	1.29	1.29	**1.297**
		24	1.31	1.32	1.34	**1.323**
		72	1.52	1.52	1.50	**1.513**
		120	1.64	1.61	1.63	**1.627**
IV-3	ThrP	4	1.27	1.29	1.28	**1.280**
		30	1.33	1.30	1.32	**1.317**
		72	1.46	1.45	1.46	**1.457**
		144	1.59	1.62	1.59	**1.600**
IV-4	TyrP	12	1.27	1.27	1.26	**1.267**
		60	1.30	1.30	1.31	**1.303**
		144	1.39	1.36	1.38	**1.377**
IV-5	ArgP	20	1.28	1.28	1.28	**1.280**
		64	1.30	1.28	1.30	**1.293**
		120	1.34	1.35	1.32	**1.337**

The differences in transformation rates again imply a direct dependence on the nature of the organic additives. This relationship, in fact, provides information about the actual mechanism of the transformation process. It has always been assumed that the process is a solvent-mediated redissolution and recrystallisation reaction (Christoffersen*et al.* 1989) instead of a purely solid-state transformation reaction from one crystal structure to the other, as in metals and alloys. Now, had the latter case been the prevailing mode for OCP-HAP transformation, the reaction would have been initiated in the solid state throughout the OCP crystal lattice and would not have been significantly affected by the presence of organic additives in the external supersaturated solution. Instead, the dependence of the transformation rate on the presence of different organic bio-chemicals supports the premise that it involves a surface reaction on the OCP crystal. This therefore ties in well with the assumption about the solution-mediated mechanism of the transformation reaction.

7.2.2 Effects of percentage concentration of additives

In addition to their chemical compositions, there is also a possible link between the relative concentration of organic additives and their effects on the precipitation phenomenon. The second set of experiments were performed in order to verify whether such a correlation exists.

§ Precipitation and transformation rates

The total calcium uptake rates are shown in Figure 7.13. With small amounts (<10%) of addition of SerP, the overall precipitation rate increased with increasing concentration. However, between 10% and 25% SerP, there appeared to be an optimum concentration beyond which additional SerP only imparted a decelerating effect. A parallel trend was observed for the transformation rates when the time-profiles of the Ca/P molar uptake ratio are compared (Figure 7.14). From the graph, it can be seen that the promotional effect on the transformation rate from OCP (precursor phase again unaffected by inclusion of SerP) to HAP again reached a peak between a concentration of 10% and 25%. The identities of the precipitated phases were confirmed to be predominantly OCP and HAP by XRD (Figures 7.15-7.21) and WDS (Table 7.4).

The variations in the extents of nucleation, growth and transformation with time can also be collated by examining the electron micrographs of the precipitates (Figures 7.22-7.28). The first precipitated phase in all the experiments showed a plate-like morphology typical of OCP crystals. The formation of a secondary phase was first captured in micrographs in the sample removed after 32 hours of precipitation in the presence of 10% mol/mol SerP (Figure 7.25b). After 120-144 hours, maturation of HAP in solutions with SerP concentration up to 25% mol/mol has all progressed to an appreciable extent, while in the presence of 50% mol/mol SerP, OCP-HAP transformation has hardly commenced. With 100% mol/mol SerP addition, not only was there little precipitation, there was no sign of the formation of a secondary phase in the same time either. Also, through the comparison between the amounts of precipitate obtained after different time intervals, effects of SerP concentration on the nucleation and growth rates can be easily observed. Again, the result supports the idea of an optimum SerP concentration at which maximum enhancement is imparted on precipitation and phase transformation in a solution with a constant $[\Sigma Ca] \times [\Sigma P]$ value under the present experimental conditions.

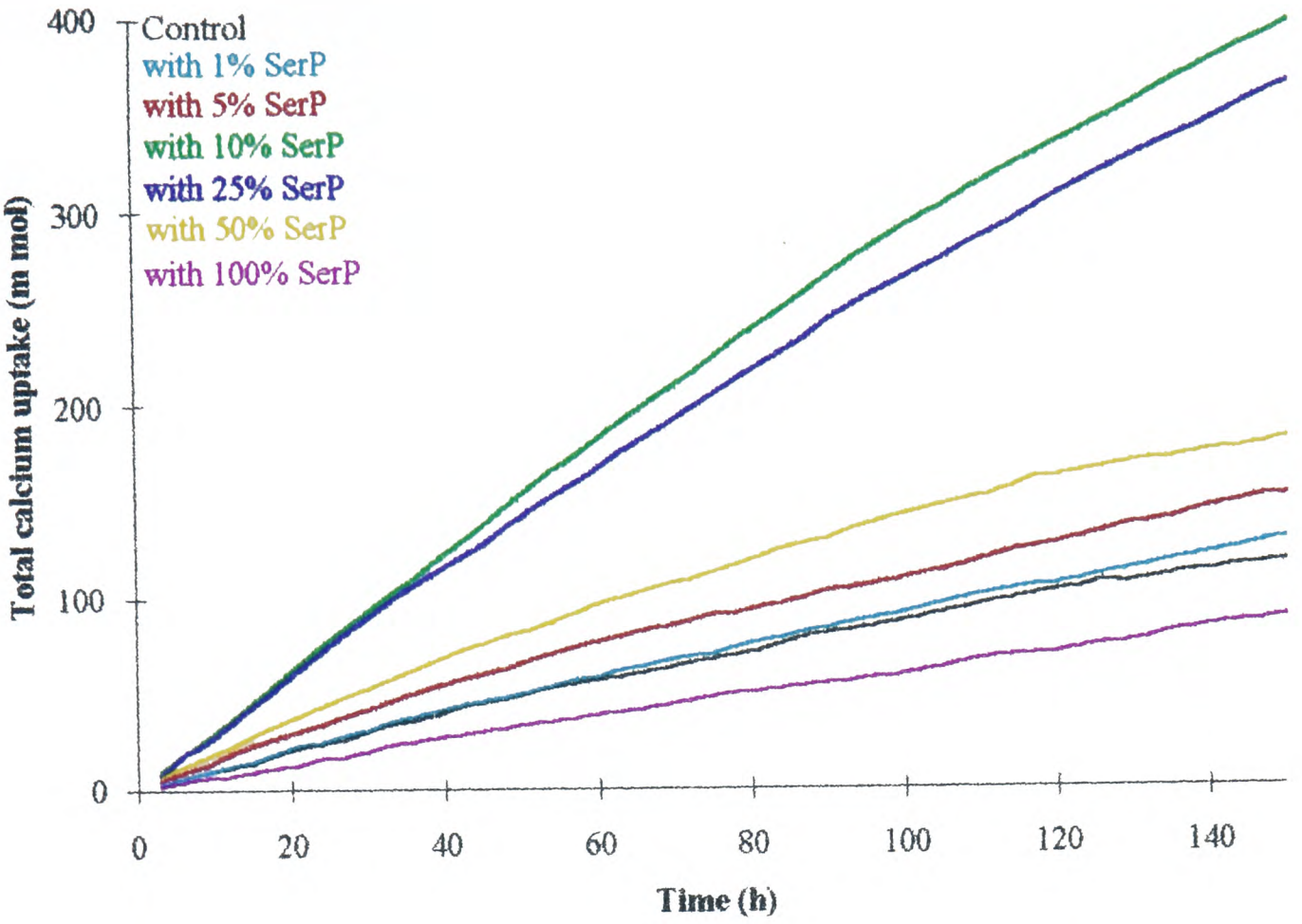

Figure 7.13 The graphs of total calcium uptake against time

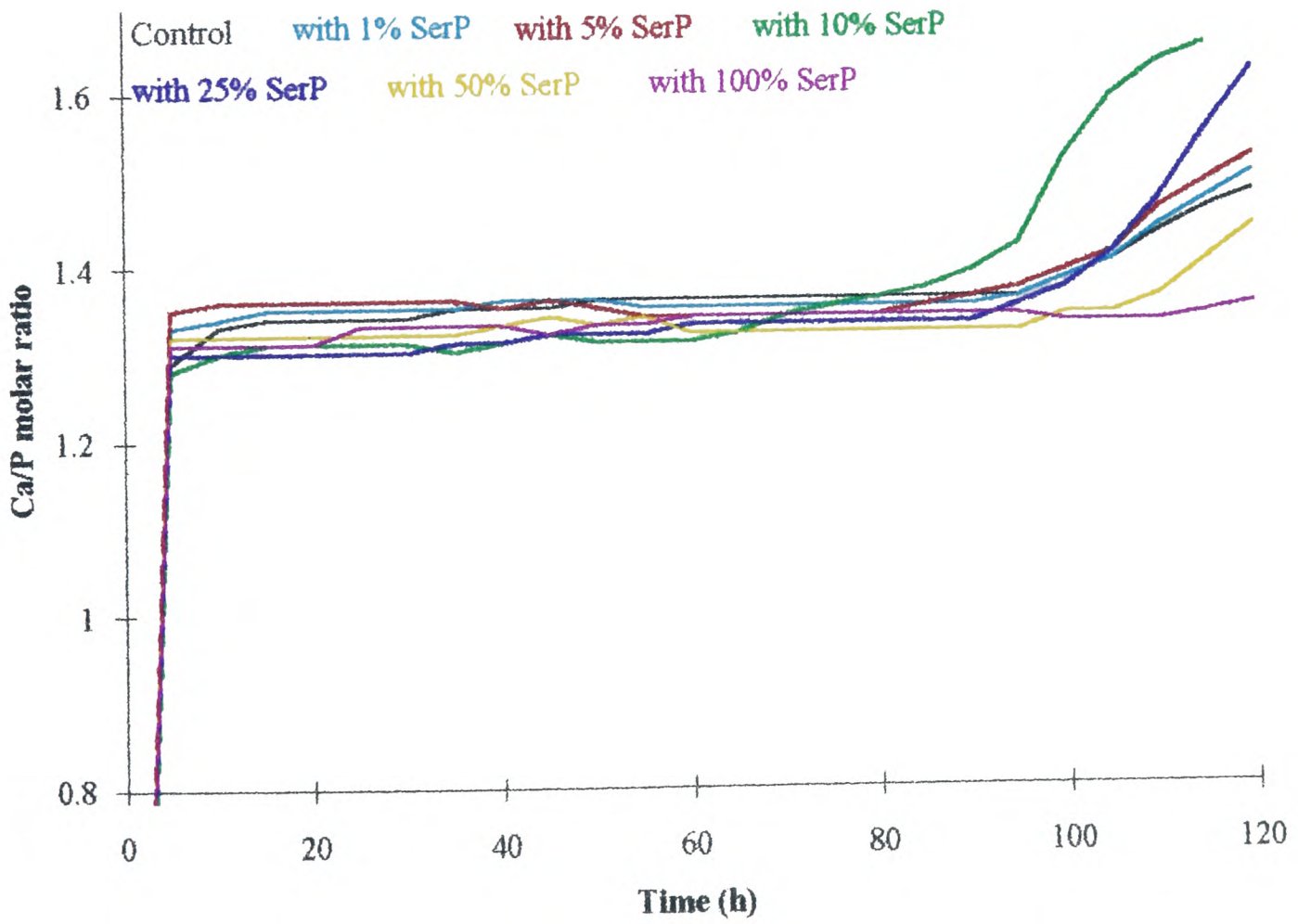

Figure 7.14 The graphs of Ca/P molar uptake ratio against time

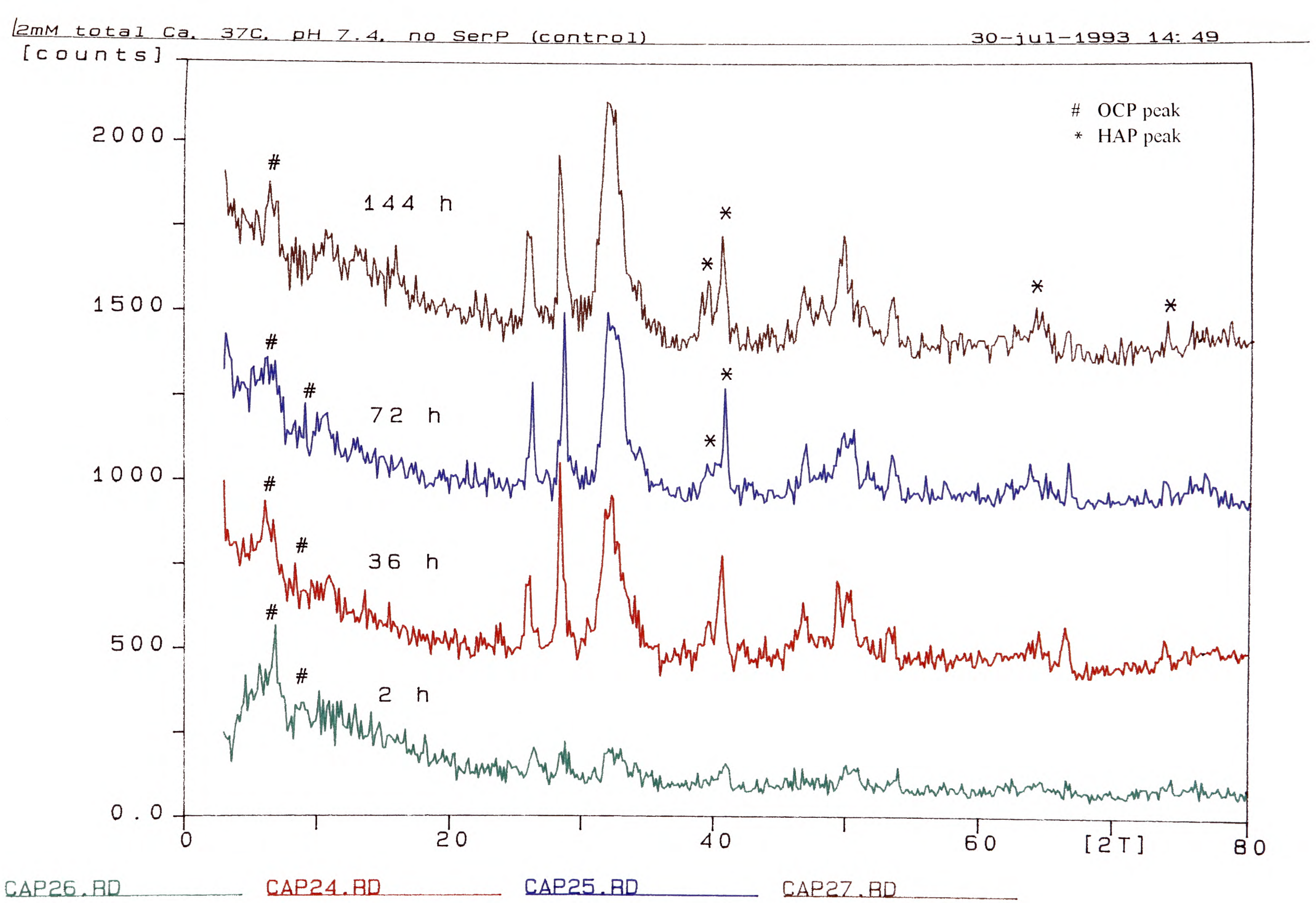

Figure 7.15 Powder X-ray diffraction patterns of solid precipitate obtained in the presence of 0% (mol/mol) SerP

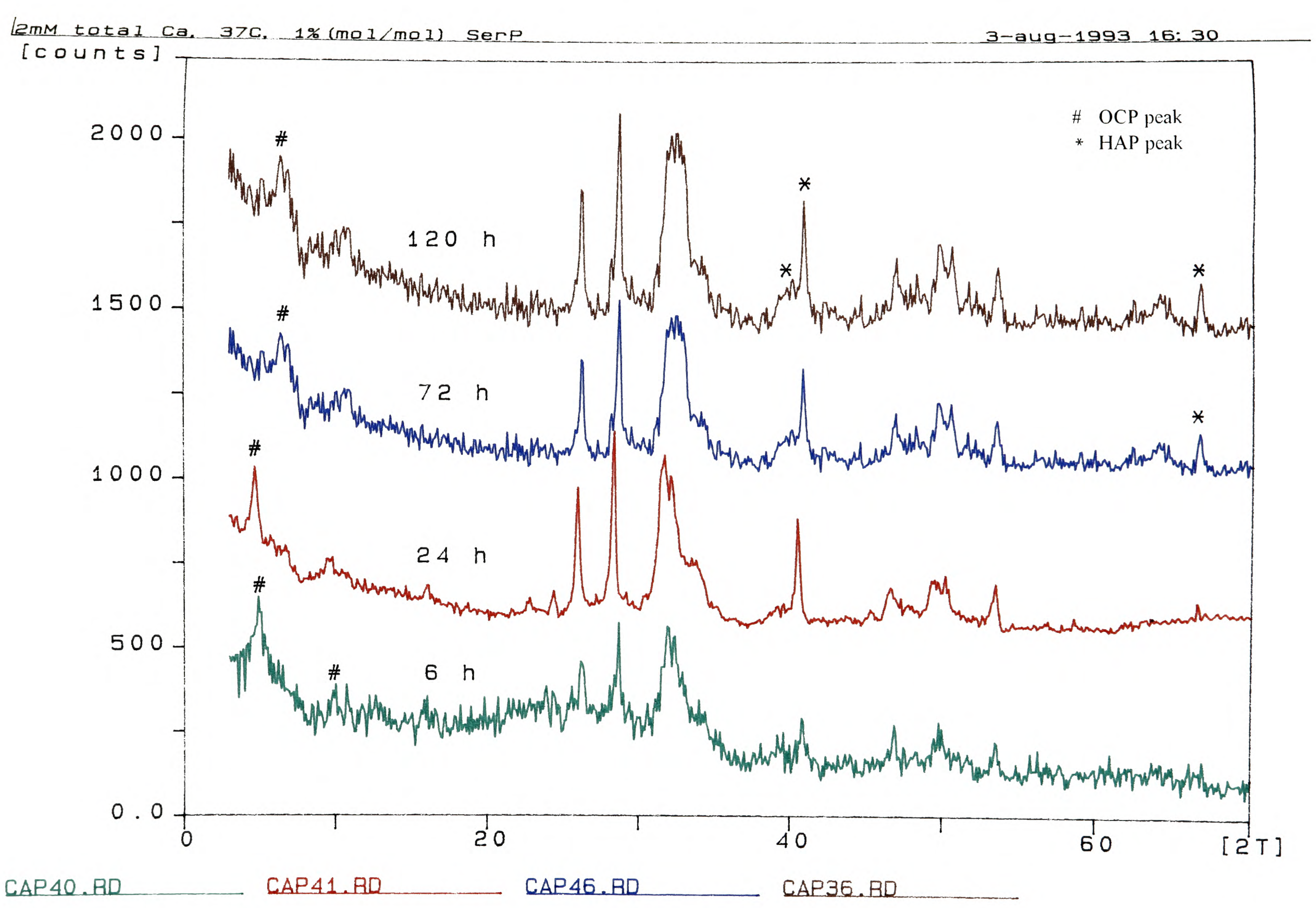

Figure 7.16 Powder X-ray diffraction patterns of solid precipitate obtained in the presence of 1% (mol/mol) SerP

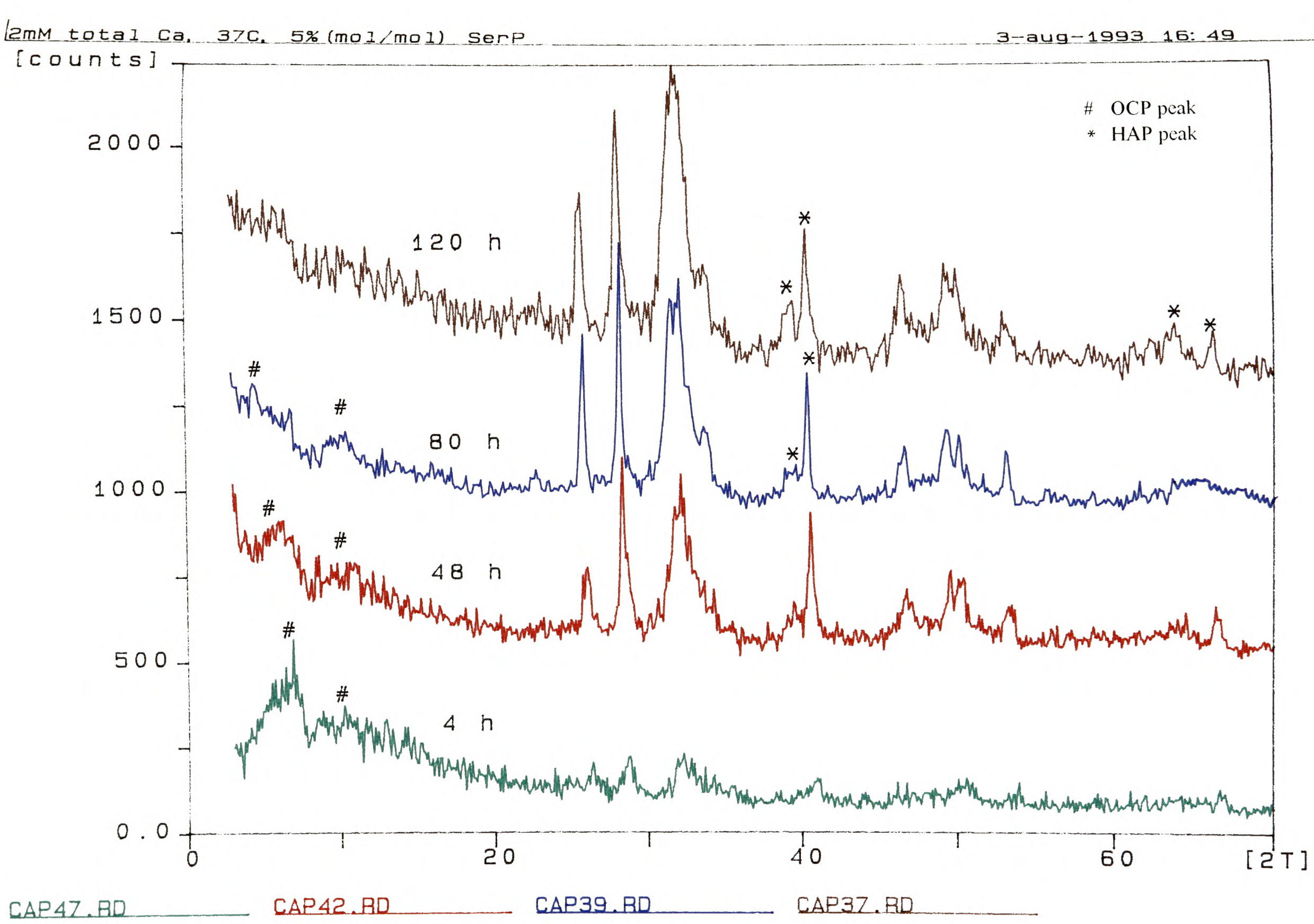

Figure 7.17 Powder X-ray diffraction patterns of solid precipitate obtained in the presence of 5% (mol/mol) SerP

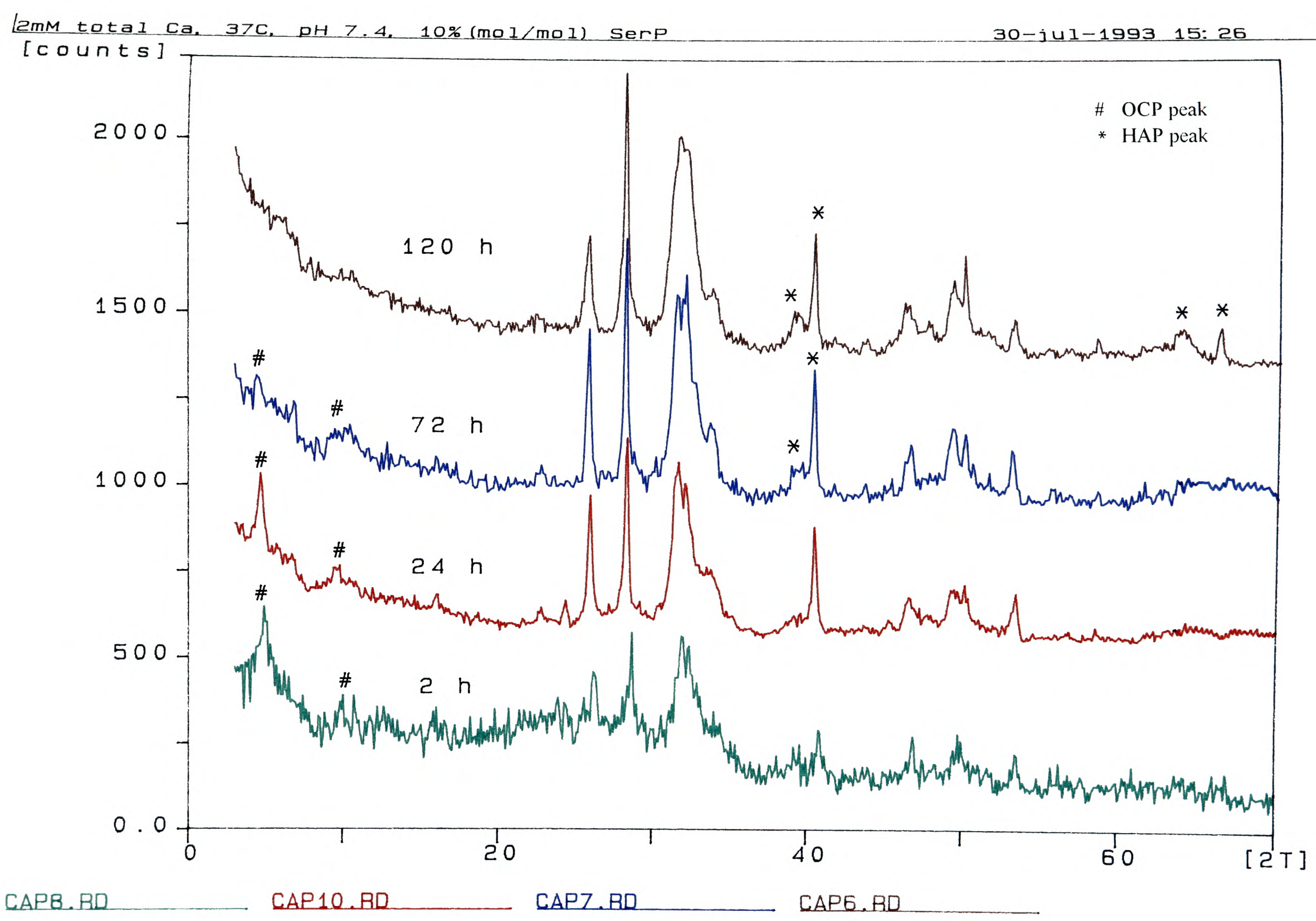

Figure 7.18 Powder X-ray diffraction patterns of solid precipitate obtained in the presence of 10% (mol/mol) SerP

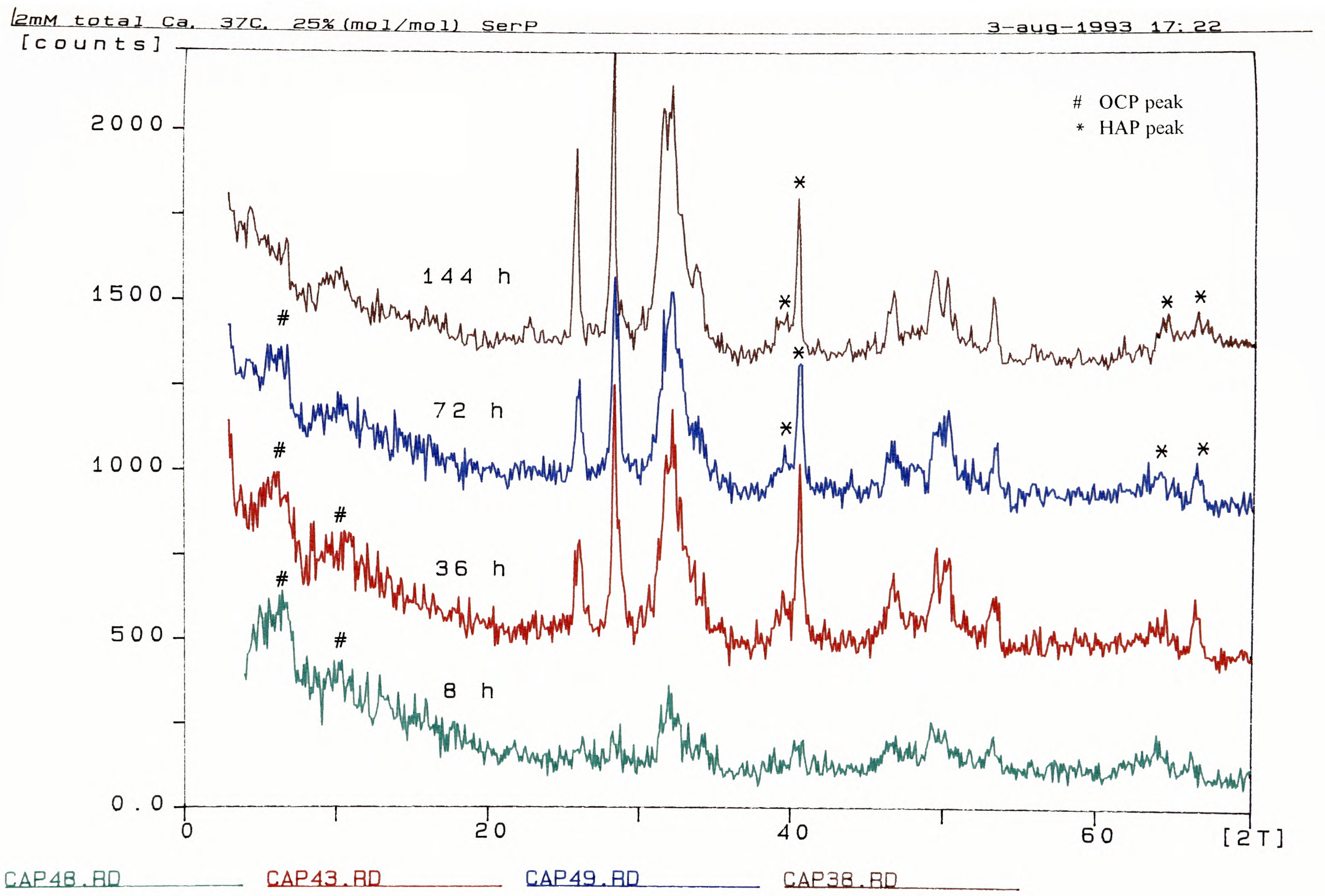

Figure 7.19 Powder X-ray diffraction patterns of solid precipitate obtained in the presence of 25% (mol/mol) SerP

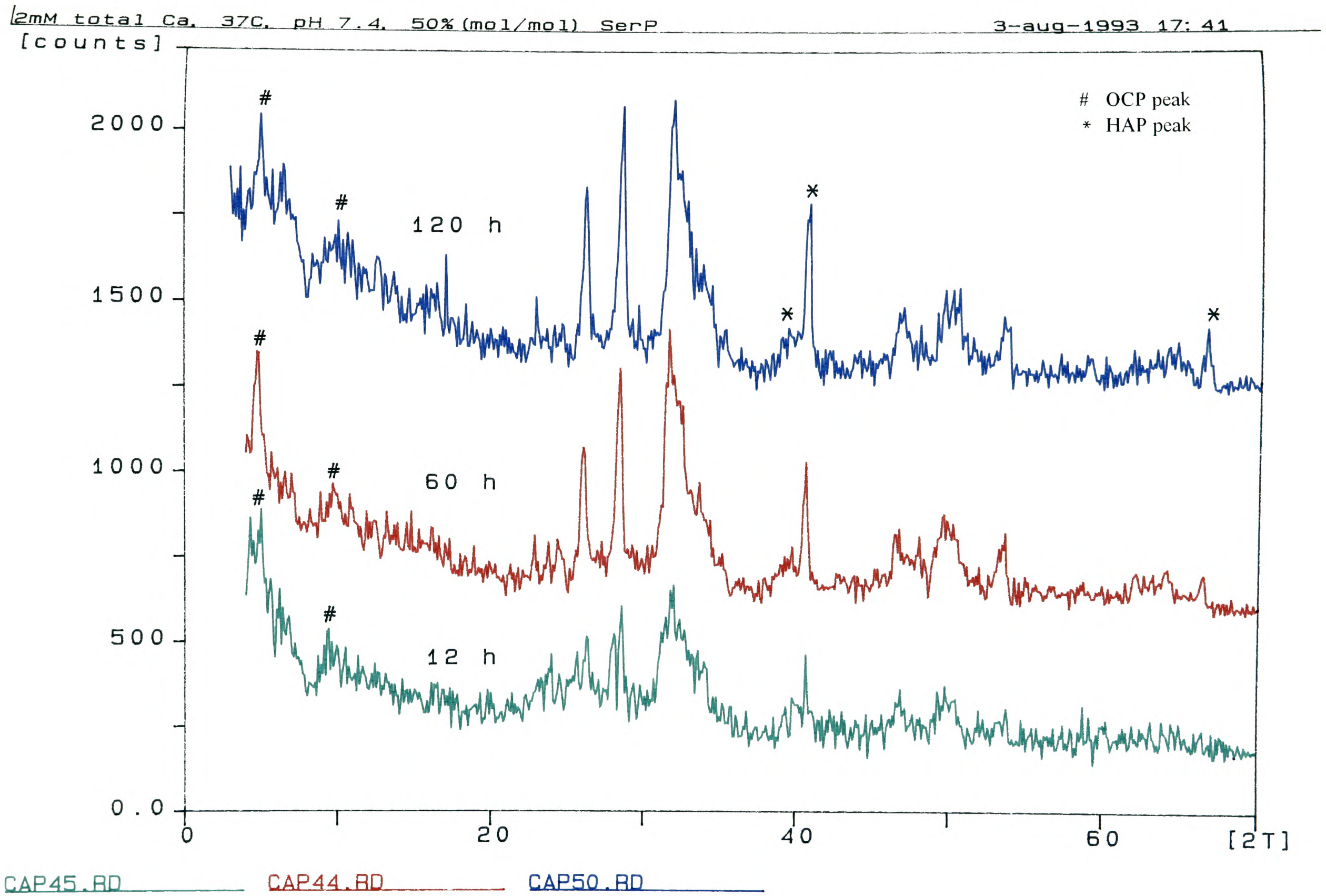

Figure 7.20 Powder X-ray diffraction patterns of solid precipitate obtained in the presence of 50% (mol/mol) SerP

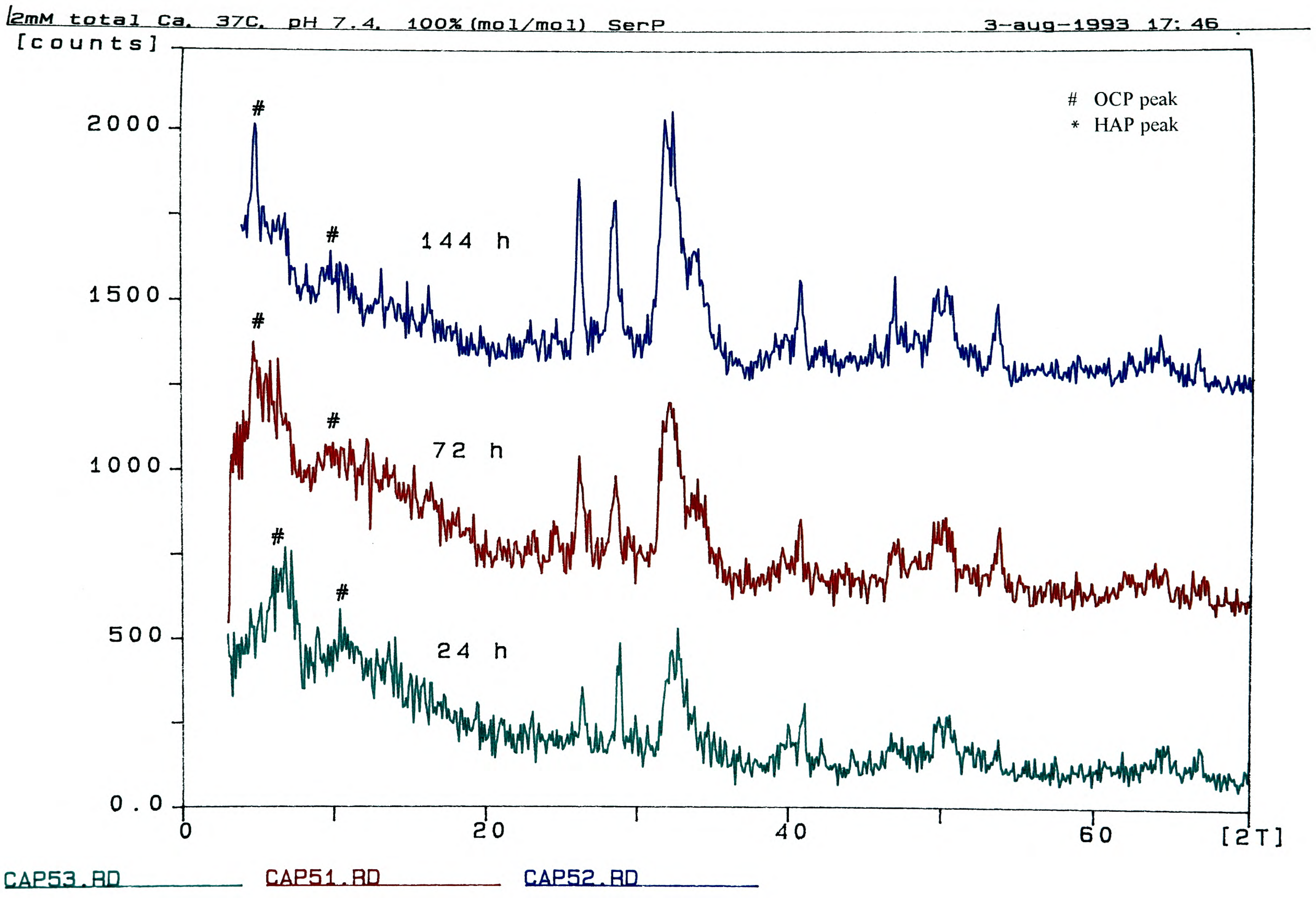

Figure 7.21 Powder X-ray diffraction patterns of solid precipitate obtained in the presence of 100% (mol/mol) SerP

Figure 7.22 Scanning electron micrographs of the precipitate obtained in the absence of SerP

(a) OCP crystals, 48 hours

(b) Transformation to HAP, 84 hours

(c) HAP platelets, 144 hours

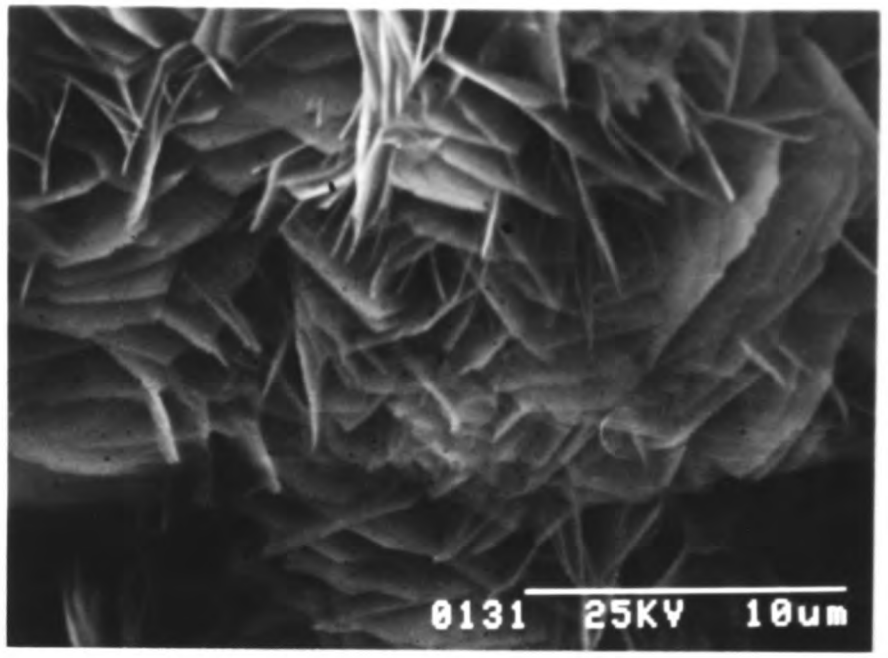

(a)

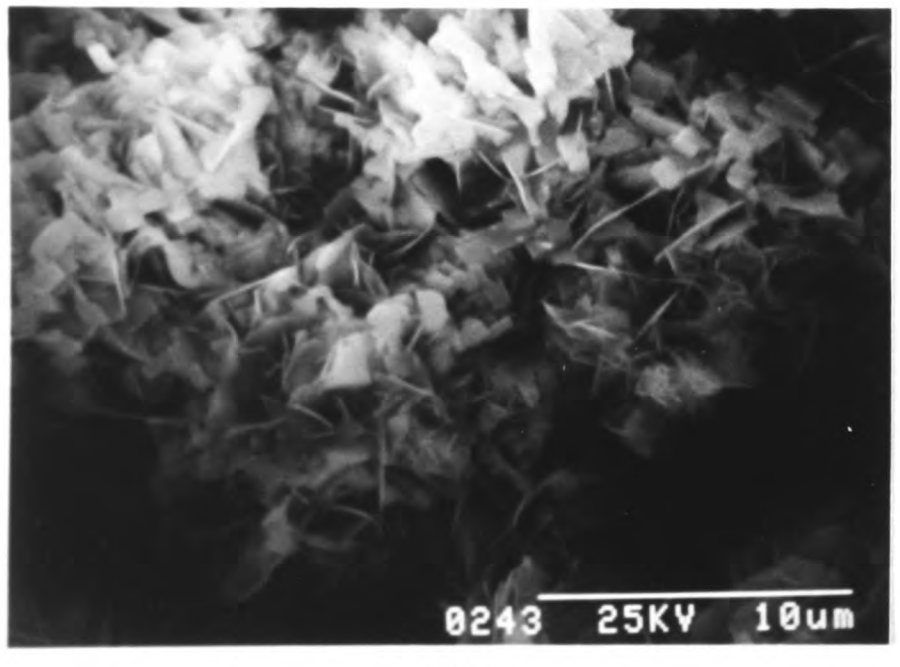

(b)

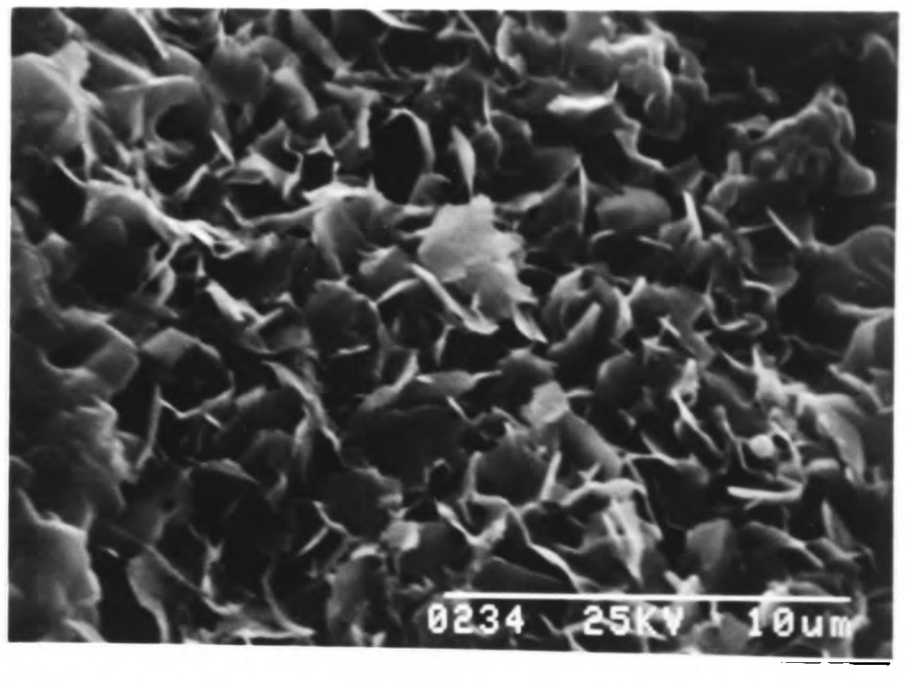

(c)

Figure 7.23 Scanning electron micrographs of the precipitate obtained in the presence of 1% (mol/mol) SerP

(a) OCP crystals, 48 hours

(b) HAP plates, 100 hours

(c) HAP plates, 144 hours

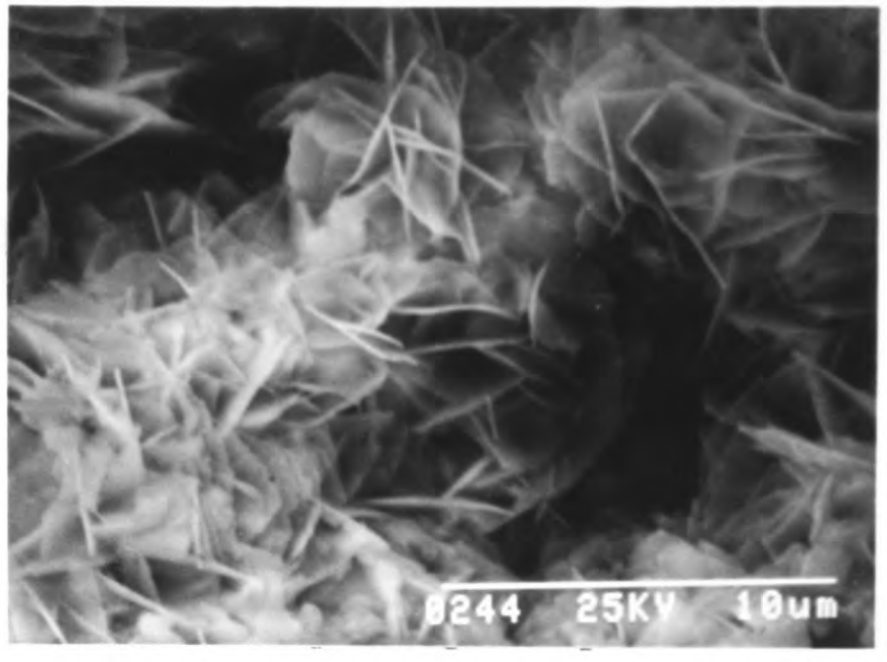

(a)

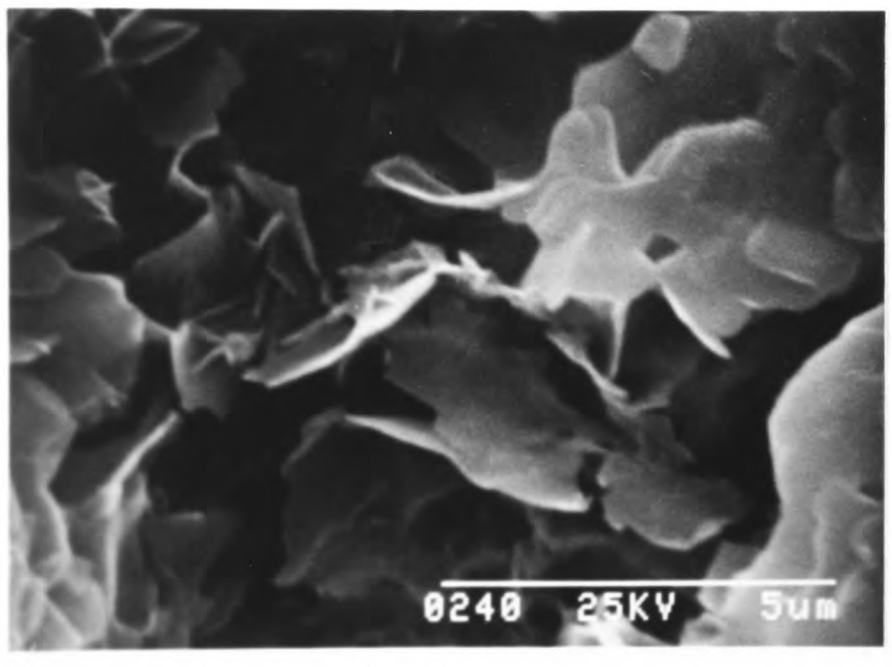

(b)

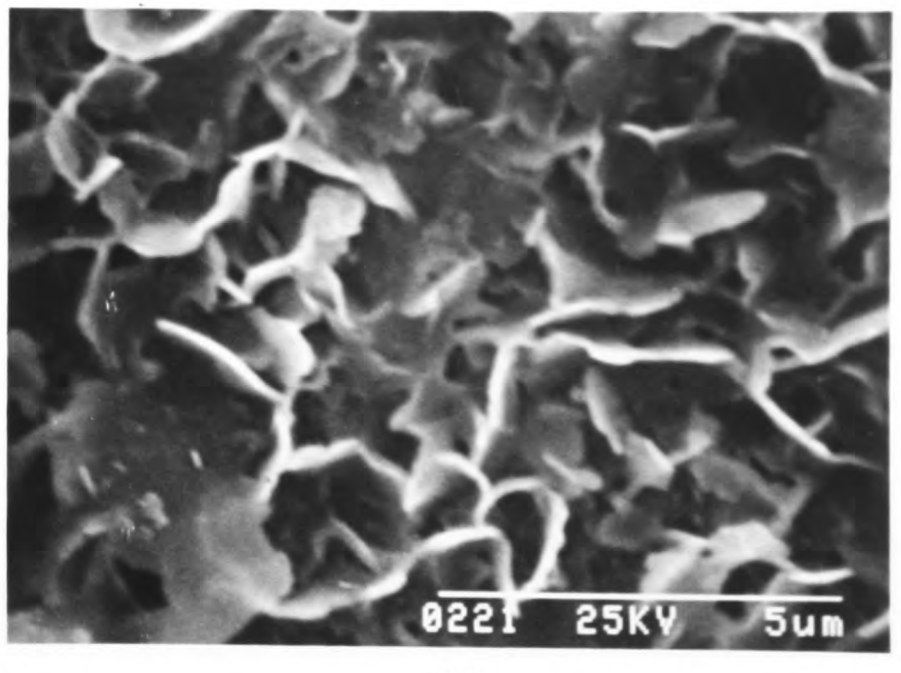

(c)

Figure 7.24 Scanning electron micrographs of the precipitate obtained in the presence of 5% (mol/mol) SerP

(a) OCP plates, 36 hours

(b) Transformation to HAP, 54 hours

(c) HAP crystals, I44 hours

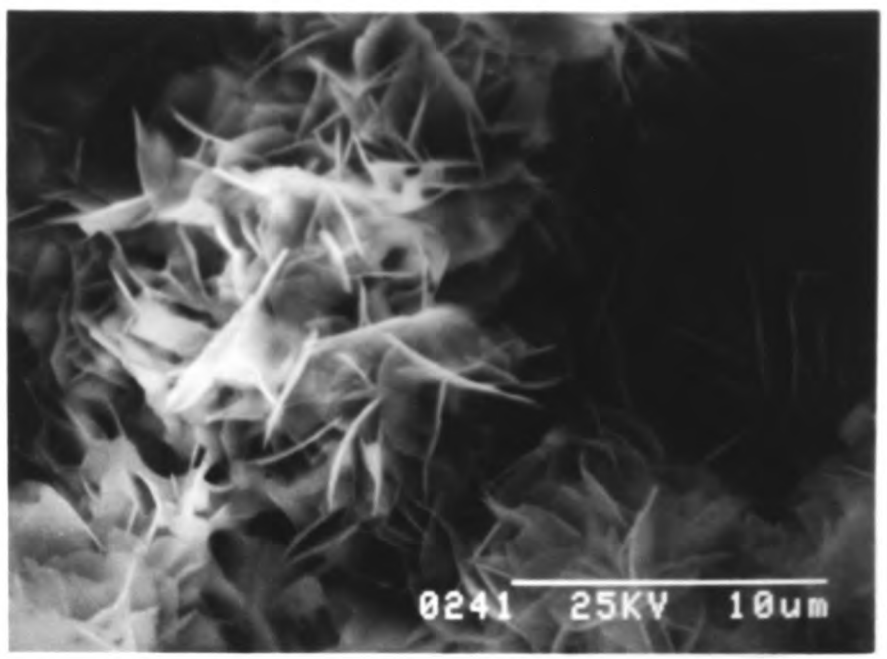

(a)

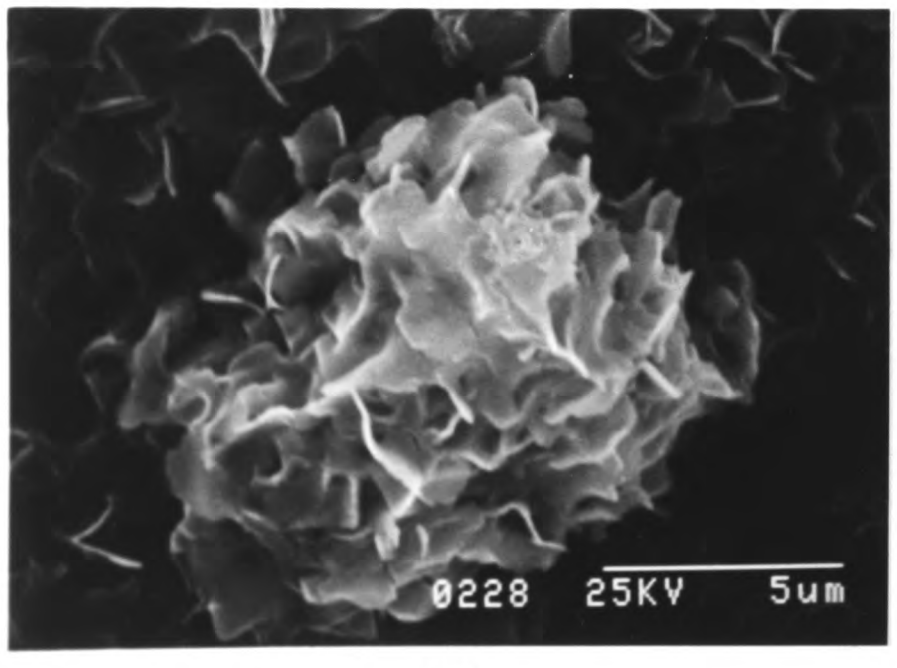

(b)

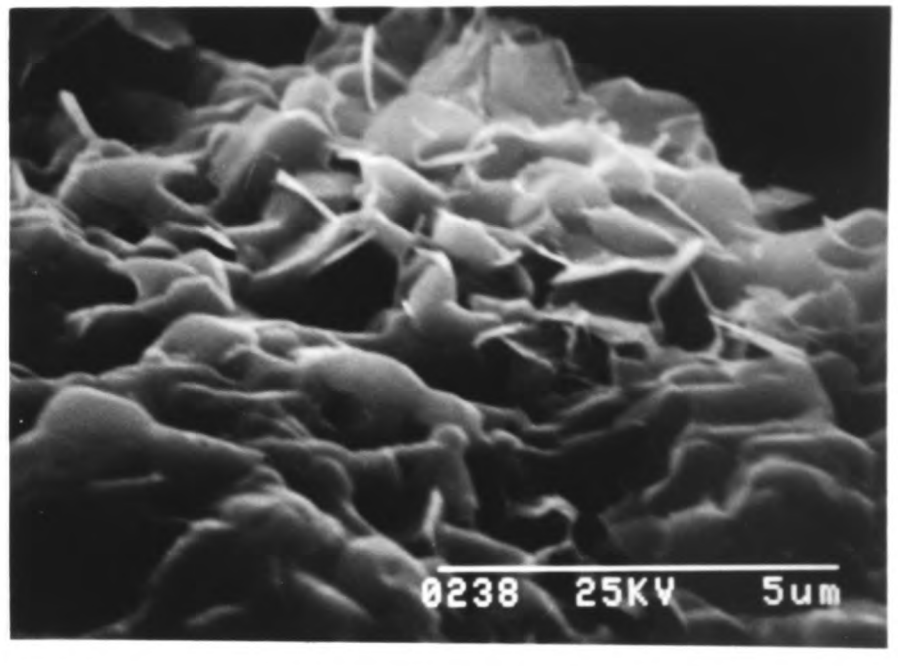

(c)

Figure 7.25 Scanning electron micrographs of the precipitate obtained in the presence of 10% (mol/mol) SerP

(a) OCP crystals and the commencement of transformation to HAP, 32 hours

(b) Further transformation to HAP, 54 hours

(c) Transformation almost complete, 96 hours

(d) HAP plates, 144 hours

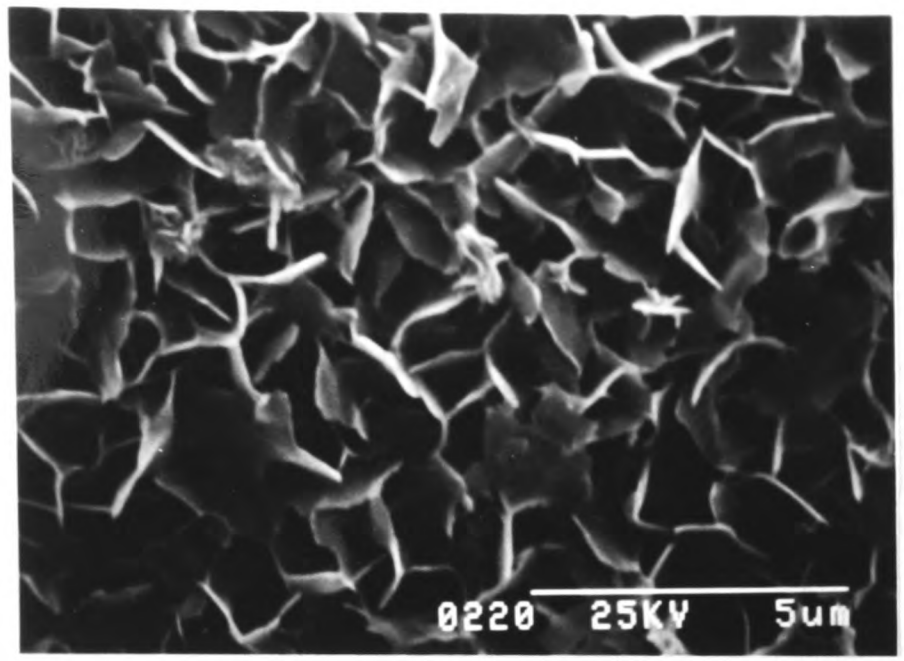

(a)

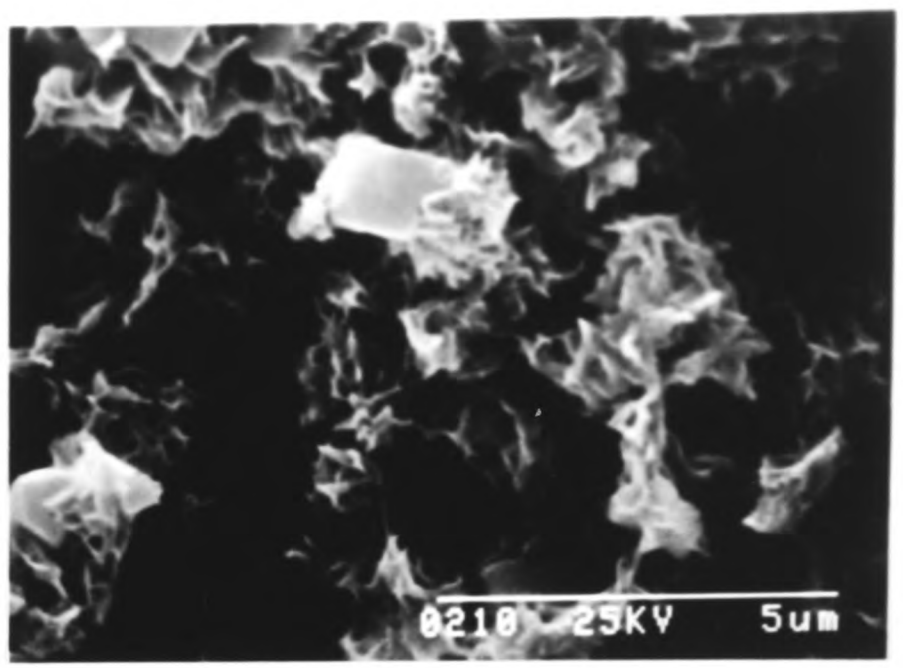

(c)

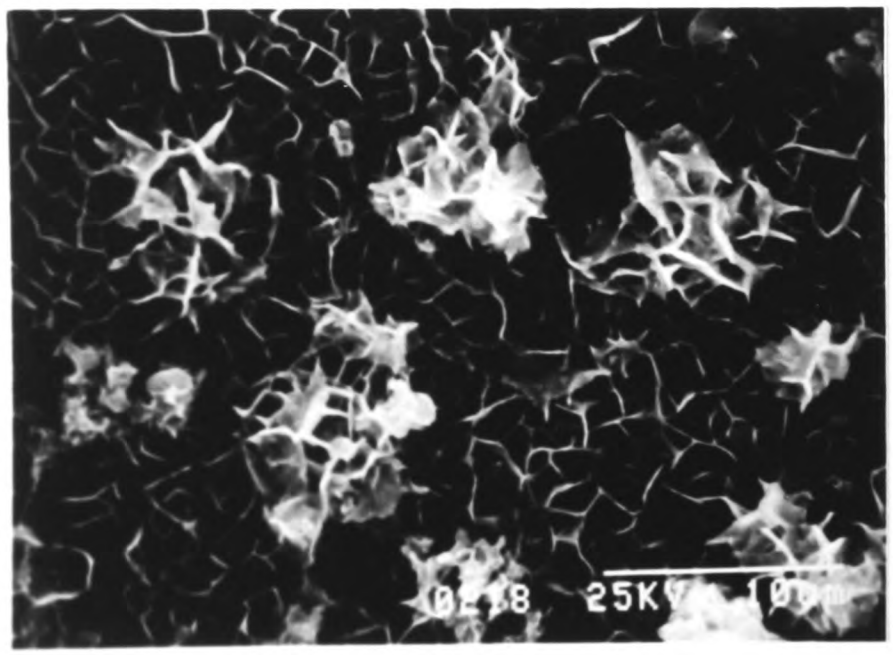

(b)

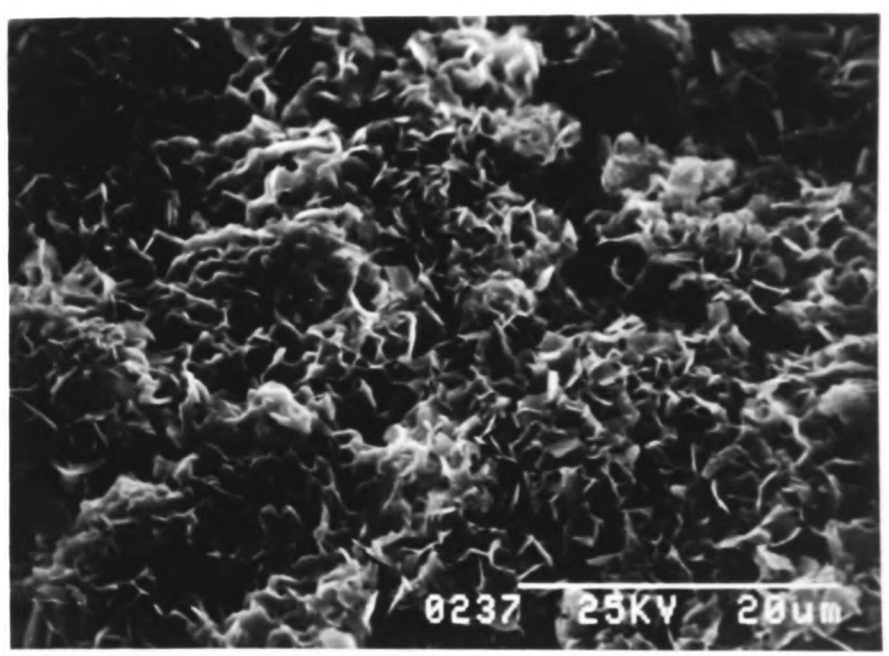

(d)

Figure 7.26 Scanning electron micrographs of the precipitate obtained in the presence of 25% (mol/mol) SerP

(a) OCP, 48 hours

(b) Transformation to HAP, 72 hours

(c) HAP, 120 hours

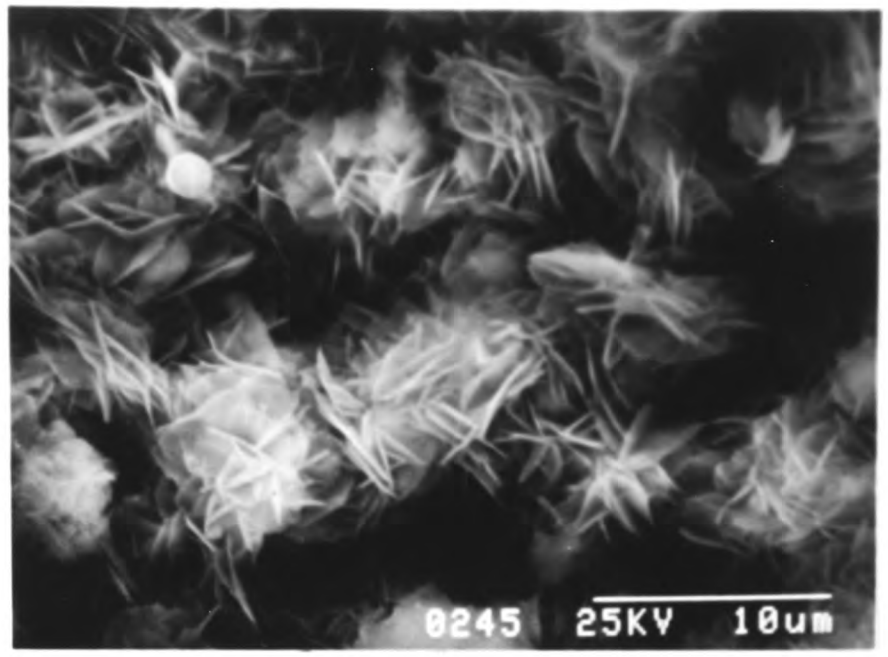

(a)

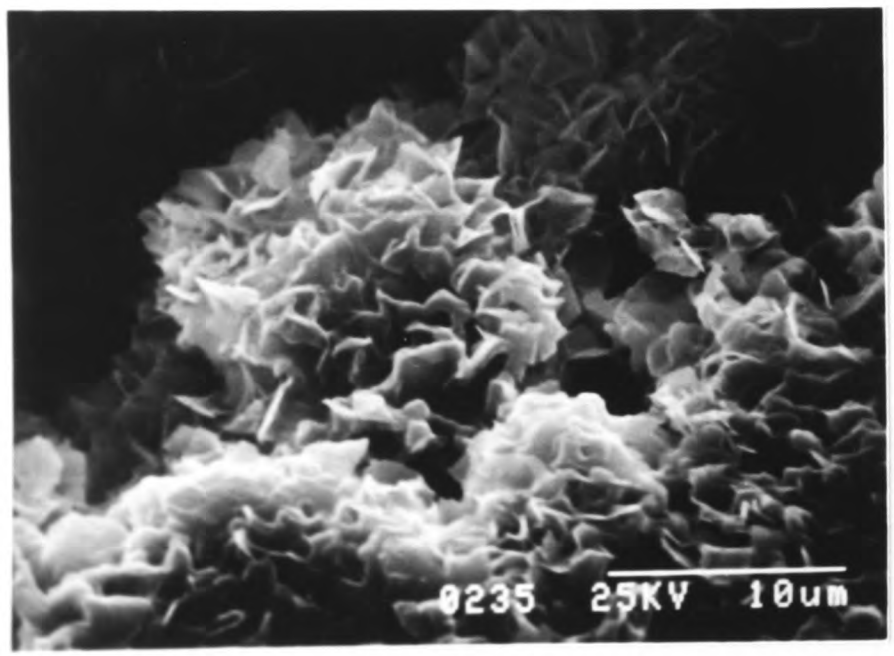

(b)

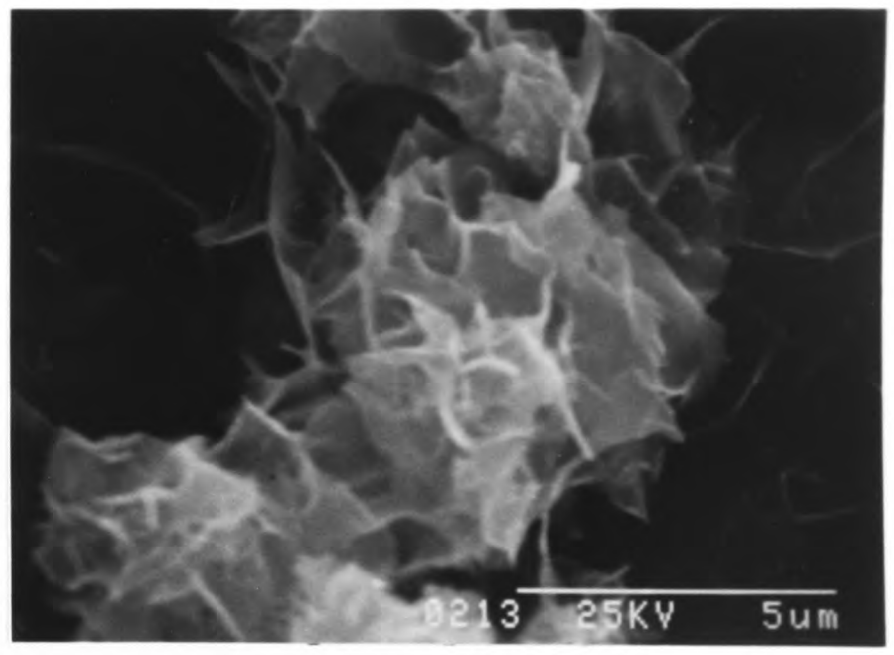

(c)

Figure 7.27 Scanning electron micrographs of the precipitate obtained in the presence of 50 % (mol/mol) SerP

(a) OCP, 48 hours

(b) Transformation to HAP, 120 hours

Figure 7.28 Scanning electron micrographs of the precipitate obtained in the presence of 100% (mol/mol) SerP

(a) OCP, 48 hours

(b) OCP, 144 hours

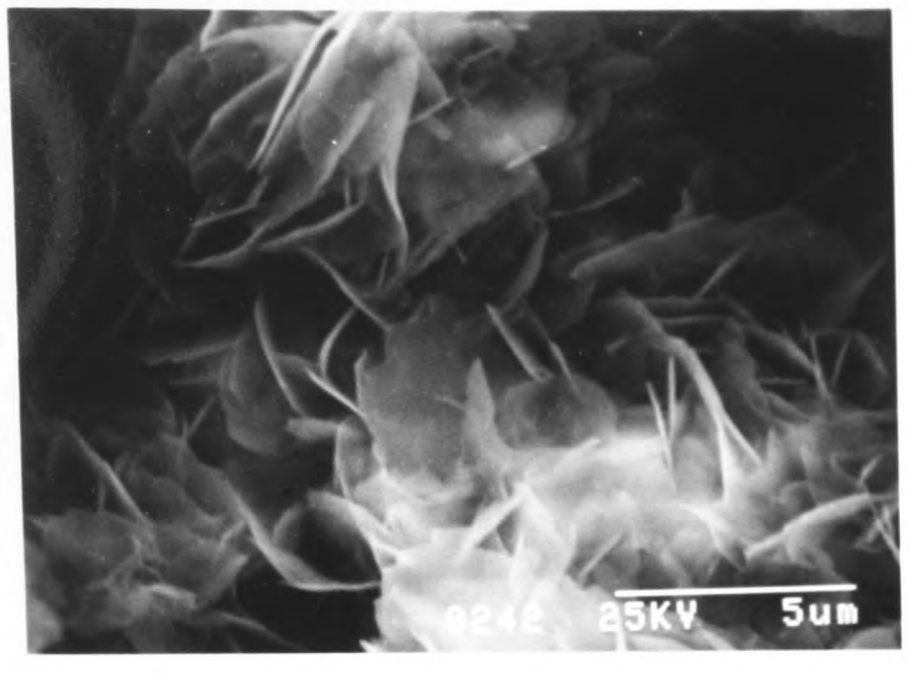

(a)

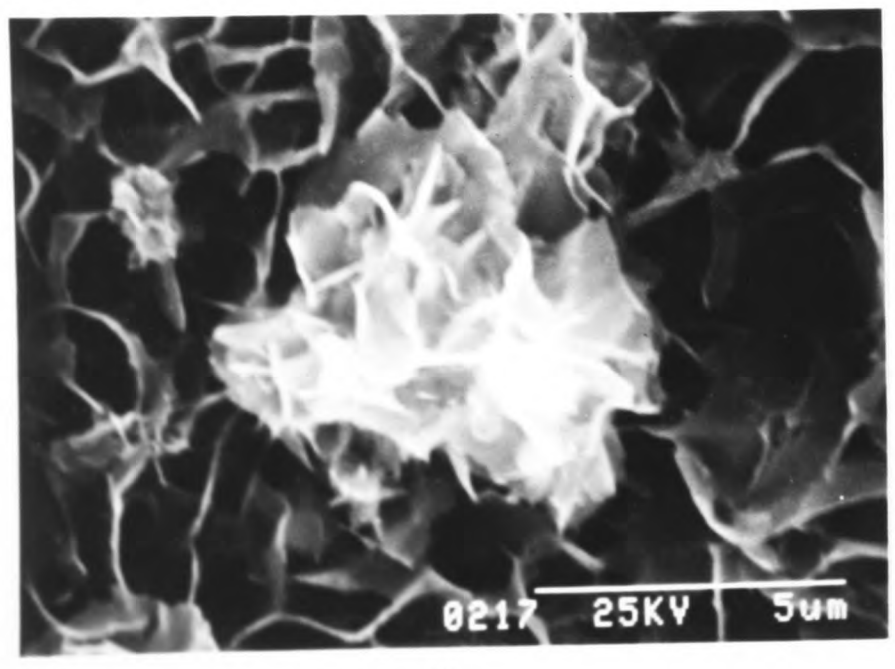

(b)

(a)

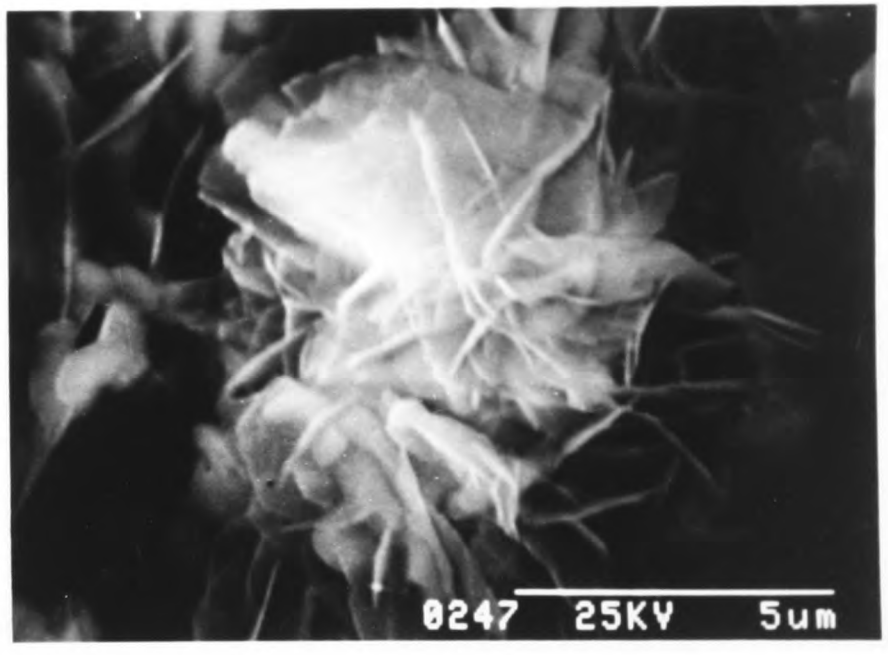

(b)

Table 7.4 Ca/P atomic ratio of precipitates from WDS analyses

Expt. no.	Molar % of SerP	Elapsed time (h)	WDS Ca/P atomic ratio (±2%)			
			1st reading	2nd reading	3rd reading	Mean
V-1 (from II-6)	no addition (control)	2	1.28	1.26	1.29	**1.277**
		36	1.29	1.32	1.32	**1.310**
		72	1.39	1.42	1.39	**1.400**
		144	1.58	1.59	1.57	**1.580**
V-2	1%	6	1.28	1.29	1.28	**1.283**
		24	1.33	1.31	1.30	**1.313**
		72	1.43	1.45	1.42	**1.433**
		120	1.58	1.60	1.61	**1.597**
V-3	5%	4	1.29	1.29	1.29	**1.290**
		48	1.33	1.31	1.32	**1.320**
		80	1.47	1.50	1.48	**1.483**
		120	1.59	1.62	1.59	**1.600**
V-4 (from IV-2)	10%	2	1.31	1.29	1.29	**1.297**
		24	1.31	1.32	1.34	**1.323**
		72	1.52	1.52	1.50	**1.513**
		120	1.64	1.61	1.63	**1.627**
V-5	25%	8	1.30	1.30	1.29	**1.297**
		36	1.33	1.30	1.33	**1.320**
		72	1.48	1.52	1.50	**1.500**
		144	1.63	1.59	1.61	**1.610**
V-6	50%	12	1.26	1.26	1.25	**1.257**
		60	1.33	1.30	1.32	**1.317**
		120	1.35	1.34	1.35	**1.347**
V-7	100%	24	1.23	1.26	1.26	**1.250**
		72	1.26	1.27	1.28	**1.270**
		144	1.30	1.28	1.28	**1.287**

In order to account for the apparent existence of an optimum SerP concentration, it is first necessary to look back at the reaction between the organic molecule and the lattice ions of OCP and HAP. It is now known that the phosphoryl end group in these phospho-amino acids is mainly responsible for any influence, be it promotional or inhibitory, on the precipitation process. This phenomenon involves the change in activation energy through the formation of complexes between these organics and free Ca^{2+} ions and the subsequent release of these organocomplexed Ca^{2+} ions by

negative phosphate ions (acidic or otherwise). In the previous section, it has been concluded that less bulky and hence sterically more accessible phospho-amino acids tend to promote the formation of these intermediates, thus accelerating the precipitation process. However, we now find that this promotional effect is not directly proportional to the concentration of phospho-amino acids in solution. This can be explained if we consider the balance between free and organocomplexed Ca^{2+} ions inside the calcifying medium. Although SerP has a high tendency to complex with Ca^{2+} ions to form intermediates crucial for accelerating the precipitation process, at the same time it essentially diminishes the supply of available free Ca^{2+} ions. Thus with increasing SerP contents, in spite of the enhanced reactivity due to the formation of these essential complexes, the reduced availability of the free Ca^{2+} source actually lowered the chance for the formation and growth of critical nuclei during the experiments. The apparent optimum SerP concentration therefore reflects the condition at which these two conflicting factors were best compromised. As the same complexing mechanism should apply to other phospho-amino acids, parallel trends should also be exhibited. However, at the same molar concentrations, a phosphorylated amino acid with a smaller molecular mass and a more electronegative phosphoryl group should still induce a higher precipitation and transformation rate, even though the corresponding optimum concentrations of the various phospho-amino acids may differ.

7.3 Effects of the presence of phosphorylated amino acids on the modified Avrami model

The precipitation and transformation model derived in Chapter 5 has been applied to purely ionic systems. It has been pointed out that, in order to adapt this model to the physiological system, the effects of certain bio-chemicals on the process must be evaluated. Here, an attempt will be made to assess the influence exerted on the model by the different phospho-amino acids and by changes in the concentration of organic addition.

7.3.1 Changes in system parameters due to the inclusion of phospho-amino acids

As explained in Section 5.2, the introduction of an organic additive would lead to variations in a number of system parameters, including degrees of supersaturation (β), interfacial free energy (γ_{SL}), and interfacial strain energy (Δg^{strain}). In order to study the effect these organics have on the

precipitation and transformation behaviour of calcium phosphate, it is first necessary to understand the influence they exert on these physical and chemical parameters.

§ Supersaturation (β)

The degrees of supersaturation with respect to the different phases of calcium phosphate in a solution are different before and after the addition of phosphorylated amino acids as a result of the establishment of even more chemical equilibria. For a precise evaluation of the supersaturation levels, it is important that the balance among all the ionic and complexed species can be quantitatively assessed. Unfortunately, there is, until now, little published material which focusses on the chemical equilibria in systems containing calcium phosphate and this particular class of organic compounds, since the vast number of uncertain secondary and tertiary equilibria involving primary reaction products have made the system indeterminate*. In order to reduce the degree of uncertainty so that approximated values of concentration to be obtained, the following assumptions have been made in this study:

- *Upon dissolution in aqueous media, the phosphoryl end-group completely releases the two protons from its –OH groups.*

In other words, we assume the occurrence of the following reaction when a phosphorylated amino acid dissolves in an aqueous medium:

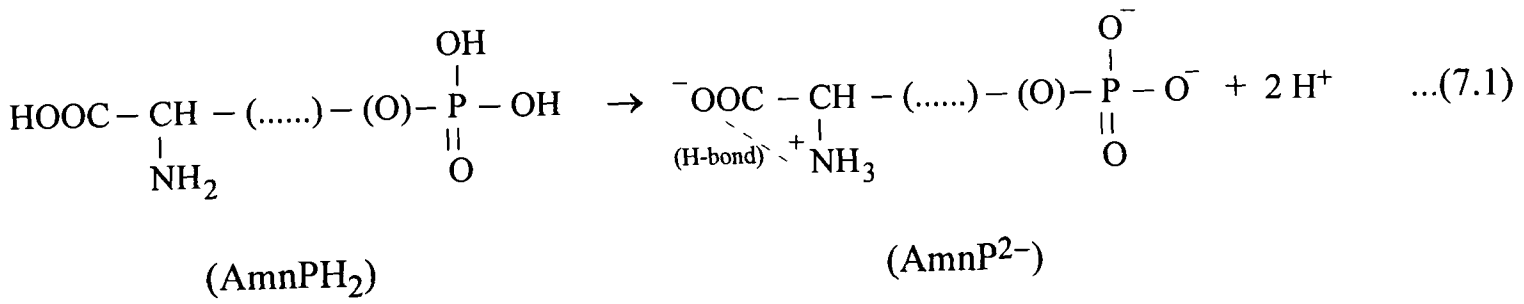

In reality, the release of both protons from the phosphoryl group should indeed proceed almost to full extent due to the high tendency of the highly polarised –P–O←H bonds to dissociate and

* The limited number of available papers all focus on the Ca-SerP complexation reaction (Hendrickson & Fullington 1965, Sillén & Martell 1971, Aoba & Moreno 1985). However, the values of the equilibrium constants provided by these studies differ by as much as two orders of magnitude, and are therefore not totally reliable.

form an organic phosphate radical in solution. This is especially true under alkaline conditions, where the deprotonation reaction is favoured - in fact this is the case for phospho-amino acids under the slightly basic physiological conditions (Stryer 1981). The deprotonation of phospho-amino acids is analogous to the different stages of dissociation of phosphoric acid (H_3PO_4). Referring back to the equilibrium constants listed in Equation 3.6, it can be seen that the second dissociation, i.e. the formation of HPO_4^{2-}, is much more favoured than any of the other states. For phosphorylated amino acids, the only structural difference from phosphoric acid is the substitution of one of the hydrogen atoms by an alkyl group. Hence, the dissociation mechanism should still be similar, and it is therefore reasonable to assume that the reaction stated in Equation 7.1 is complete. This assumption also rules out the possibility of a second Ca^{2+}-binding site through the release of a third proton from the molecule at the carboxylic acid group (–COOH) in the main amino acid skeleton. In fact, such a deprotonation reaction does occur when amino acids are dissolved aqueously, but the dissociated proton immediately forms a dative covalent bond with the lone pair of electrons on the nitrogen atom in the amine group. Upon the protonation of the amine group, a hydrogen bond is established between the acidic amine group and the carboxyl end, as shown in Equation 7.1. This hydrogen bond stabilises the two otherwise extremely reactive groups and renders them rather inert towards the formation of complexes. Conversely, the phosphate- and hydroxide-binding potential of the electropositive–NH_3^+ group (evolved from the basic amine group) is similarly disregarded*.

This particular assumption about the dissolution of phosphorylated amino acids is important in reducing the uncertainty of the aqueous systems in several aspects. First of all, it simplifies the systems by eliminating the presence of the undissociated amino acid ($AmnPH_2$) and of the singly charged $AmnPH^-$ radical from any subsequent calculations. Not only are the dissociation constants of these two species not known, they would also exhibit different affinities for the formation of complexes with Ca^{2+} ions due to the different degrees of concentration of the negative charge on the phosphoryl group. As a result, it would be impossible to estimate the

* Indeed, the only reaction in which these amino acid groups are likely take part, is the formation of a peptide (or amide) bond by the condensation reaction between the carboxyl group of one amino acid and the amino group of another, thereby forming a dipeptide (dimer). However, the equilibrium of this reaction lies far on the side of hydrolysis (i.e. decomposition of the dimer) rather than synthesis, as the formation of a peptide bond requires an input of free energy, whereas the hydrolysis is thermodynamically downhill (Stryer 1981).

extent of complexation for each amino acid. In addition, the condition for electroneutrality (Equation 3.7) would become indeterminate if this assumption was not made, since amino acids at different stages of deprotonation carry different units of charge. Also, only the basic phosphoryl group is now left to be considered for any complexation reactions, considerably reducing the intricacy of the system.

- *The electronegative phosphoryl group only attracts free Ca^{2+} ions for the formation of complexes.*

We assume that the deprotonated $AmnP^{2-}$ radicals are only involved in the following complexation reaction:

$$AmnP^{2-} + Ca^{2+} \Leftrightarrow AmnPCa^{\circ} \qquad ...(7.2)$$

Although $AmnP^{2-}$ are potentially capable of attracting any positive ions in the solution, the approach of only reasonably small cations is feasible again due to the orientational limitations the bulky organic radicals present. Hence, the probability for $CaOH^{+}$ or $CaH_2PO_4^{+}$ to successfully advance towards the phosphoryl group and form a stable complex is relatively small compared to the much smaller and more charge-concentrated Ca^{2+} ion. In the solution, there are also H^{+} and K^{+} ions which should be attracted to the $AmnP^{2-}$ radicals. However, as a corollary of our first assumption, the attachment of a hydrogen ion will be instantaneously reversed. K^{+} ions, on the other hand, have a considerably lower charge density than Ca^{2+} ions, due to a lower number of charge units and a bigger volume. In addition, K^{+} ions have already been shown to be rather inert towards forming complexes with simple and acidic phosphate ions. Owing to the chemical similarities between inorganic phosphates and the basic phosphoryl group, it is therefore reasonable to ignore the formation of $AmnPK^{-}$ or $AmnPK_2^{\circ}$ complexes in comparison to $AmnPCa^{\circ}$ formation.

Such an assumption again simplifies the system by eliminating the effects of low concentration species in subsequent calculations for the equilibrium constant, supersaturation, ionic strength and electroneutrality.

- *The electrically neutral organocalcium complexes are not involved in any further complexation reactions.*

This effectively means that the bond with the phosphoryl group would not be strong enough to withstand the electrostatic attraction on the calcium ion should a phosphate ion in the solution approach the organocalcium complex in the correct orientation. This is obviously a plausible assumption as $AmnP^{2-}$ exhibits a much lower ionic character than any of the inorganic phosphate ions, firstly due to the presence of a long and non-polar side-chain, and secondly due to the much lower volumetric charge density. This means that the reverse of Equation 7.2 is brought about only through the release of the Ca^{2+} ion by an inorganic phosphate ion in solution - $AmnPCa^{\circ}$ is not itself involved in any other reactions in the system.

These three assumptions essentially imply that the introduction of a phosphorylated amino acid to a supersaturated calcium phosphate solution would only lead to the establishment of one main chemical equilibrium, namely the formation of the electrically neutral organocalcium complex, $AmnPCa^{\circ}$ (Equation 7.2). Thus, with a known quantity of added amino acid, the additional equilibrium constant can be evaluated by comparing the *p*Ca reading to that in the control experiment. For example, if $[Ca^{2+}]_{control}$ and $[Ca^{2+}]_{AmnP}$ are the respective concentrations of free Ca^{2+} ions in the control and in the solution with the phospho-amino acid at a concentration of $[AmnP]_{added}$, the equilibrium constant for the complexation reaction is:

$$AmnPCa^{\circ} \Leftrightarrow AmnP^{2-} + Ca^{2+};$$

$$K_{AmnP} = \frac{[AmnP^{2-}]\,[Ca^{2+}]}{[AmnPCa^{\circ}]} = \frac{\{[AmnP]_{added} - ([Ca^{2+}]_{control} - [Ca^{2+}]_{AmnP})\}\;[Ca^{2+}]_{AmnP}}{[Ca^{2+}]_{control} - [Ca^{2+}]_{AmnP}} \quad ...(7.3)$$

Although Equation 7.3 is obtained only after making a few assumptions, it still provides a standard means to compare the complexing potential of the different phospho-amino acids. Indeed, as equilibrium constants are thermodynamic properties and are only dependent on temperature, the validity of the various assumptions can be verified by comparing the values of K_{AmnP} at different concentrations of organic addition. This will be discussed in more details in Section 7.3.3. Make a

note of the definition of K_{AmnP} in Equation 7.3 - it has a unit of M and a smaller value corresponds to a higher tendency to form the organocalcium complex. This constant has been defined in such a way that it is in a parallel form to the other equilibrium constants of the inorganic ions as shown in Equation 3.6.

Having established the additional chemical equilibrium, it is then possible to calculate the concentrations of the individual ions and complexes in the solution using the *p*H and *p*Ca values, in a similar manner to Section 3.2. The correct evaluation of these concentrations is necessary for the subsequent calculation of supersaturations and collision probabilities. Supersaturation (β), the thermodynamic driving force, should have the same definition as in Equations 3.2-3.4. However, for the collision probability (Π), all the $[Ca^{2+}]$ terms for the collision probability (Equation 5.8) should be replaced by ($[Ca^{2+}]$ + [AmnPCa°]), since the end result is identical no matter whether the anions collide with free Ca^{2+} or an organocomplexed AmnPCa°. Thus,

$$\Pi^{DCPD} = \frac{2!\,([Ca^{2+}] + [AmnPCa^{\circ}])\,[HPO_4^{2-}]}{([Ca^{2+}] + [AmnPCa^{\circ}] + [HPO_4^{2-}])^2}$$

$$\Pi^{OCP} = \frac{7!\,([Ca^{2+}] + [AmnPCa^{\circ}])^4\,[HPO_4^{2-}]\,[PO_4^{3-}]^2}{4!\,2!\,([Ca^{2+}] + [AmnPCa^{\circ}] + [HPO_4^{2-}] + [PO_4^{3-}])^7}$$

$$\Pi^{HAP} = \frac{9!\,([Ca^{2+}] + [AmnPCa^{\circ}])^5\,[PO_4^{3-}]^3\,[OH^-]}{5!\,3!\,([Ca^{2+}] + [AmnPCa^{\circ}] + [PO_4^{3-}] + [OH^-])^9} \qquad ...(7.4)$$

§ Interfacial free and strain energies (γ_{SL} & Δg^{strain})

γ_{SL} and Δg^{strain} denote respectively the free energies at the solid-liquid and the solid-solid interfaces. Since any added phosphorylated acid is capable of reacting with ions both in solution and on the solid surfaces, it is not surprising that both of these factors should be affected. In order to apply the modified Avrami transformation model, it is therefore necessary to assess the changes in these energy terms. However, it is very difficult to explicitly and precisely evaluate the absolute changes in the surface energies, but it is possible to approximate these variations by making certain suppositions based on the reaction mechanism.

- *The change in solid-solid interfacial strain energy (Δg^{strain}), arising from the interference from the organic additives, is negligible.*

  Δg^{strain} was introduced in Equation 5.9 to account for the strain energy which results from the lattice mismatch between the precipitate and the substrate. It has previously been pointed out that the organic additives assume a catalytic rôle in the precipitation process (Section 6.4.3). Hence, although these bio-chemicals may react with both the substrate and the precipitate individually, none of these molecules should be present within the lattice of either of the solid phases. In other words, the formation of a substrate-precipitate interface should automatically entail the concurrent elimination of any complexed amino acid molecules attached to the adjoining calcium phosphate unit cells at the interface. Therefore, Δg^{strain} should still be a result of the lattice mismatch between the two purely inorganic calcium phosphate at the solid-solid interface, in spite of any influence the organic compound may exert on either of the phases before and after the formation of the interface.

- *The change in the specific solid-liquid interfacial free energy (γ_{SL}) is directly proportional to the concentration and complexation potential of organic molecules.*

  The acceleration or deceleration of precipitation brought about by the presence of phospho-amino acids is a result of a modified surface reaction at the solid-liquid interface. This interference, although mainly chemical in nature, can also partly manifest itself through the modification of the solid-liquid surface free energy. The change in surface energy should be proportional to the surface density of bonded phospho-amino acid molecules at the interface. There are two ways these organic molecules can act as bridges between the solid and liquid phases. Firstly, organic molecules which are not already bound to Ca^{2+} ions in solution can attach themselves to lattice Ca^{2+} ions on the solid surface. Now, when we discussed the complexation reaction of the amino acid, it has been pointed out that each anionic phosphoryl group has the highest tendency to form a complex with only one calcium ion. In other words, it is unlikely for a calcium site on the solid surface to be simultaneously attached to more than one phosphorylated amino acid. Apart from the binding of phosphorylated amino acid molecules to calcium sites, another mode of surface reaction involves the attraction of an organocalcium

complex in the solution to a phosphate site on the solid surface. If we assume the tendency for each of these surface reactions to be the same, the effect of a particular phospho-amino acid on the interfacial free energy should be proportional to its complexation potential with aqueous calcium ions. Also, as γ_{SL} is the energy needed to create a unit area of solid-liquid interface, the change in γ_{SL} arising from the presence of a particular phospho-amino acid should logically be directly proportional to the number of calcium-phosphoryl bonds formed per unit surface area, itself a linear function of concentration. Hence, the new solid-liquid interfacial free energy γ'_{SL} can be expressed algebraically as:

$$\frac{\gamma_{SL} - \gamma'_{SL}}{\gamma_{SL}} = \frac{K_s\ [AmnP]_{added}}{K_{AmnP}} \qquad ...(7.5)$$

where K_s is a dimensionless proportionality constant which takes on a positive [negative] value if the solid-liquid interfacial free energy is reduced [increased]. Equation 7.5 predicts a zero net change in the interfacial energy if no amino acid is added, which is consistent with reality. Once again, note that K_{AmnP} is the equilibrium constant for the reverse of the complexation reaction.

§ Alterations in the modified Avrami transformation model

Since various system parameters are altered as a result of the presence of phosphorylated amino acids, corresponding changes need to be made in the transformation model (Equations 5.13 & 5.14). Considering the alteration in various parameters, the model needs to be rewritten as follows:

(5.13) $\Rightarrow$
$$\phi = 1 - exp\,[-(\kappa\lambda)^{n/4}\ \zeta^{n/4}\ t^n] \qquad ...(7.6)$$

(5.14) $\Rightarrow$
$$\zeta = \left(\frac{T\ ln\ \beta}{\nu}\right)^3\ \Pi\ exp\left[-\frac{f\ v^2\ \psi\ \gamma_{SL}^3}{(kT)^3\ (ln\ \beta)^2}\right] \qquad ...(7.7)$$

where
$$\psi = \left(\frac{K_{AmnP} - K_s\ [AmnP]_{added}}{K_{AmnP}}\right)^3 \qquad ...(7.8)$$

ψ accounts for the change in solid-liquid interfacial free energy as a result of the substrate-organic reaction. If the interfacial free energy is reduced by an amino acid, $K_S > 0$, and hence $\psi < 1$, leading to an increased ζ and consequently an increased ϕ. Conversely, if the interfacial free energy is increased by an amino acid, $K_S < 0$, and hence $\psi > 1$, leading to a decreased ζ and consequently a decreased ϕ. Thus, according to this model, a reduced surface energy barrier results in the acceleration of the transformation process, and vice versa. This prediction is in line with experimental evidence (Section 7.3). In Equation 7.6, since Δg^{strain} is assumed to be independent of the presence of any organic catalyst, the value of $\kappa\lambda$ should accordingly be unchanged.

By fitting this modified model (Equations 7.6-7.8) to describe the transformation behaviour of calcium phosphate under the influence of different organic bio-chemicals, the effects of side-chains and concentration can be deduced from the values of n and ψ. The value of n can be found using a similar method as before (Section 5.1.6). Having found n for the control experiment, the value of $\kappa\lambda$ in the absence of any organic addition (i.e. $\psi = 1$) can then be iterated to give the best fit to the experimental result. With this value of $\kappa\lambda$, which is supposed to be independent of any organic additives, the value of ψ can then be approximated by fitting the prediction yielded by Equations 7.6-7.8 to the actual experimental precipitation patterns.

7.3.2 Effects of different phosphorylated amino acids

Values of $ln \{ ln [1 / (1-\phi)] \}$ for experiments IV-1 to IV-5 are plotted against ln t in Figure 7.29, and the best fits given by the modified model are shown in Figure 7.30. The values of n, $\kappa\lambda$, ψ (obtained using $\kappa\lambda$ value of the control experiment), K_{AmnP} (calculated from *p*Ca and *p*H values) and K_S (from K_{AmnP} and ψ) are summarised in Table 7.5, together with the supersaturations and collision probabilities of the three calcium phosphate phases.

The calculated values of K_{AmnP} follow the trend $K_{SerP} < K_{ThrP} < K_{TyrP} < K_{ArgP}$. Correspondingly, SerP has the highest complexing tendency while ArgP has the lowest, supporting the hypothesis made in Section 7.2.1 that sterically accessible phospho-amino acid molecules exhibit higher degrees of complexation with free Ca^{2+} ions. However, the complexation reaction inevitably leads to a decrease in supersaturation, the thermodynamic driving force. Yet, it is interesting to find that despite a decrease in the degrees of supersaturation, the overall precipitation and transformation

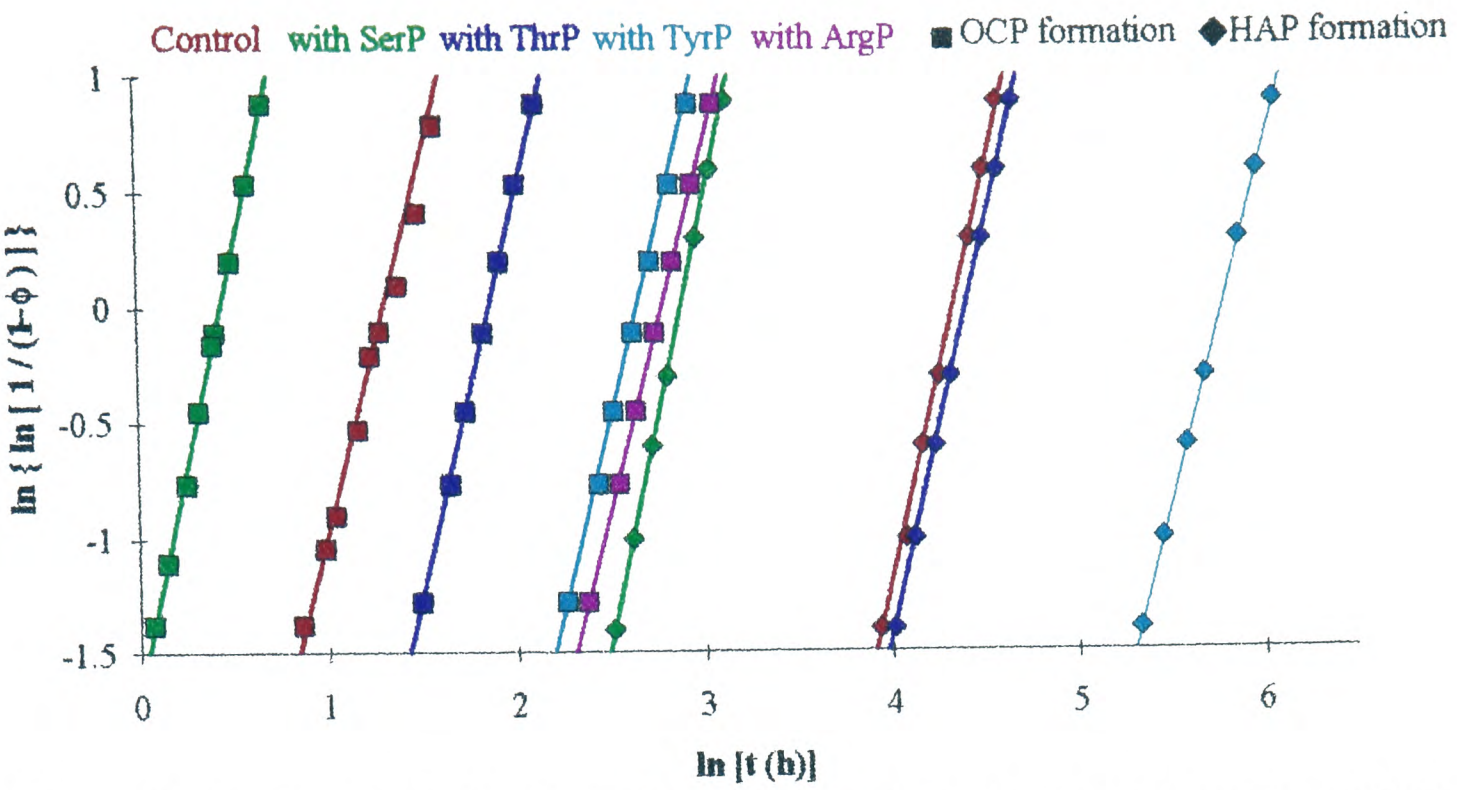

Figure 7.29 The plots of *ln* { *ln* [1 / (1−ϕ)] } against *ln* t for Experiments IV-1 to IV-5

Figure 7.30
Fractional formation of different phases of calcium phosphate from experimental data fitted to profiles obtained from Equations 7.6 to 7.8

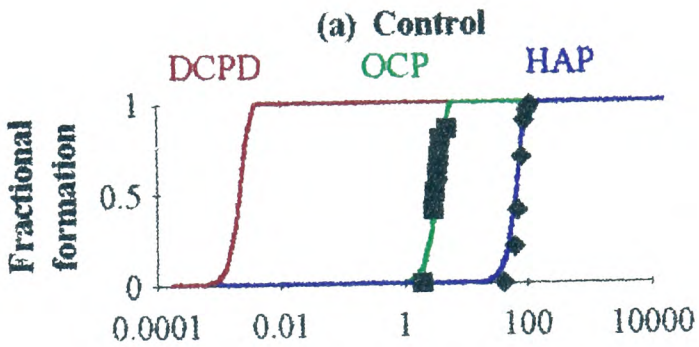

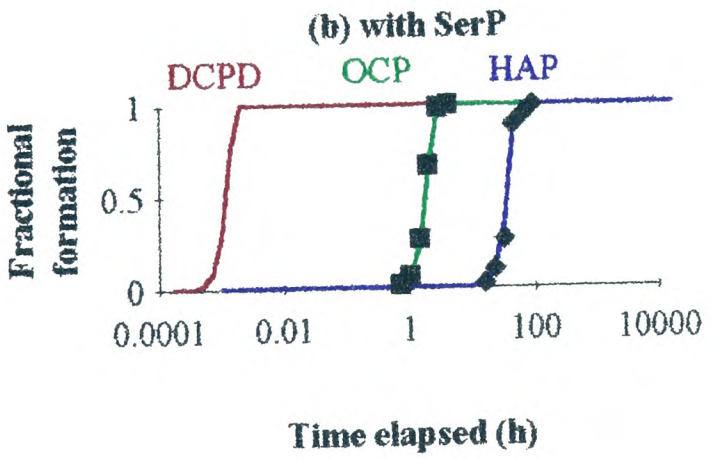

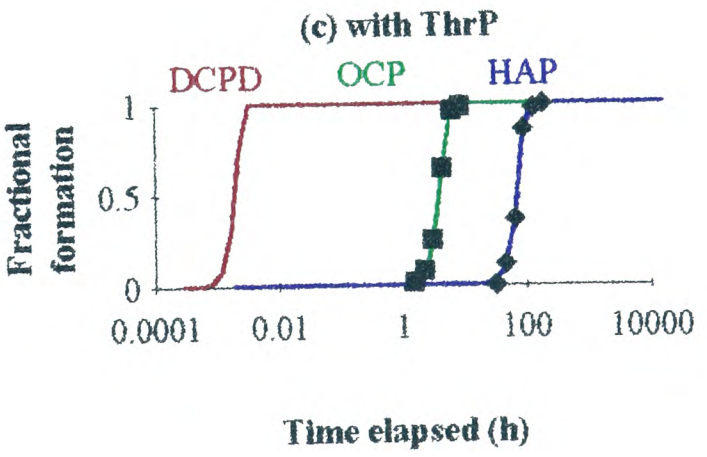

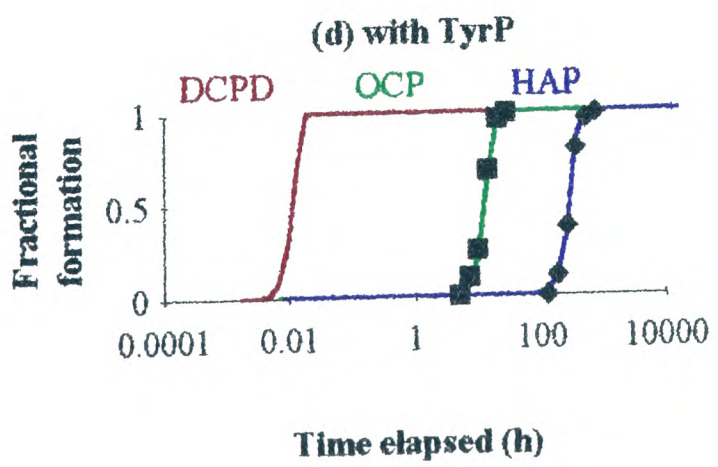

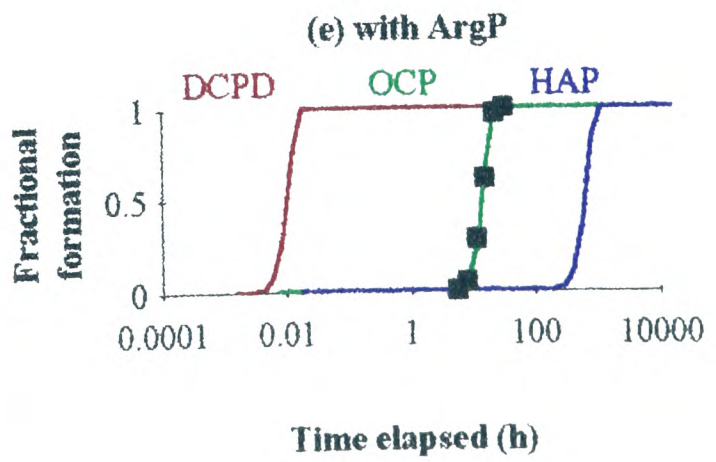

Table 7.5 System properties of solutions with different phosphorylated amino acids

Phospho-amino acid		(control)	SerP	ThrP	TyrP	ArgP
n	**OCP formation**	3.24	3.81	3.47	3.26	3.17
	HAP formation	3.52	3.83	3.54	3.22	–
	mean	3.38	3.82	3.51	3.24	3.17
$\kappa\lambda$ (K^{-3} s^{-4})		$10^{-10.60}$	($10^{-10.60}$)			
ψ		(1)	0.911	0.980	1.015	1.018
K_{AmnP} (M)		–	0.0382	0.0985	0.2485	0.3271
K_s		(0)	5.810	3.305	–6.351	–9.883
ln β	**DCPD**	0.253	0.251	0.253	0.253	0.253
	OCP	3.962	3.875	3.919	3.941	3.947
	HAP	16.903	16.222	16.667	16.903	16.903
log Π	**DCPD**	–0.304	–0.306	–0.305	–0.304	–0.304
	OCP	–7.626	–7.773	–7.739	–7.687	–7.642
	HAP	–13.210	–14.660	–13.933	–13.592	–13.354

rates during the calcification experiments still traced a parallel trend to the complexation tendencies. Thus, the decrease in supersaturation was not apparently the most predominant factor in controlling the reaction rates. It is necessary to examine the changes in other variables.

Looking at the collision probabilities of the various phases, it is clear that the high complexing capability of SerP and ThrP considerably improved the chances for successful collision to take place during precipitation, while the chance is reduced for TyrP and ArgP. As pointed out previously (Section 5.1.4), this kinetic factor is usually more important in the preferential nucleation of precursor phases during the precipitation of a multi-phase sparingly soluble inorganic salt. Thus, the first-order influence of Π in the expression for heterogeneous nucleation (Equation 5.10) partly counteracts the effect due to changes in supersaturation.

The crucial factor in the modified model is ψ, the term pertaining to the change in interfacial free energy. From Table 7.5, it can be seen that the value of ψ increases with the molecular mass of the amino acids, meaning that small and accessible molecules like SerP and ThrP show a high effectiveness in lowering the energy barrier when creating new solid-liquid interface. The linear dependence of the exponential term in Equation 7.7 on ψ overrides the effect of $(1 / ln\ \beta)^2$ at the present level of 10% mol/mol addition. It can be observed from the values of K_s the wide range of change in the surface free energy due to the presence of different phosphorylated amino acids.

More about the changes in nucleation and growth can be inferred by comparing the different values of the time exponent, n. The significance of the value of n has been explained in Chapter 5. Now, the various values of n still fall within the range of 3 to 4, which corresponds to an interface-controlled growth mechanism without site saturation. However, with increasing molecular mass of the organic molecule, the value of n decreases. This suggests that the relative reactivity of the potential nucleation sites is reduced by the presence of bulkier organic compounds, equivalently increasing the probability of site saturation. The growth patterns as captured by the electron micrographs (Figures 7.8-7.12) provide further physical evidence in support of the variation in nucleation and growth rates.

7.3.3 Effects of concentration of organic addition

Similar analyses are performed on the results of experiments V-1 to V-7. Figure 7.31 shows the graphs of $ln\ \{\ ln\ [\ 1 / (1-\phi)\ ]\ \}$ against ln t, and the predictions based on the modified model are displayed in Figure 7.32. The values of n, $\kappa\lambda$, ψ, K_{SerP}, K_s, β and Π are again tabulated in Table 7.6.

During the derivation of the modified model, certain assumptions were made, leading to the declaration that the complexation equilibrium constant as defined in Equation 7.3 is characteristic of each phosphorylated amino acid at a particular temperature, and is independent of its concentration. The validity of these assumptions can at this point be verified by comparing the different values of K_{SerP}. From Table 7.6, K_{SerP} covers the range of (0.0375 ± 0.0037) M, at a χ^2 confidence level of 92%, i.e. the statistical error from the expected value is less than 10%, a relatively insignificant error in comparison to the wide range of K_{AmnP} exhibited by different amino acids. Moreover, this value

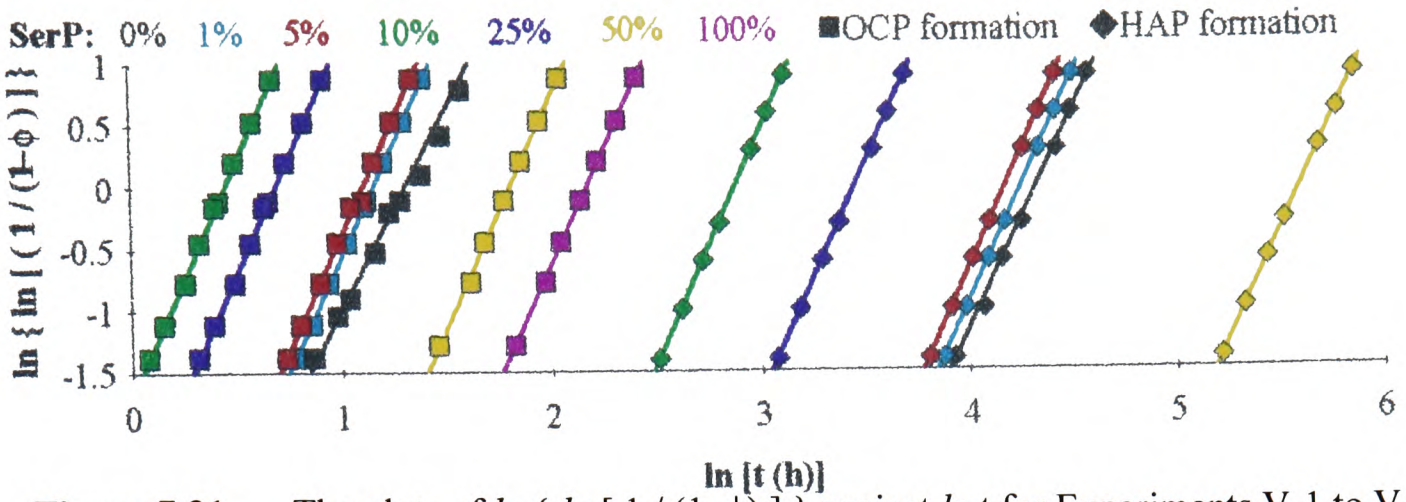

Figure 7.31 The plots of *ln* { *ln* [1 / (1–ϕ)] } against *ln* t for Experiments V-1 to V-7

Figure 7.32
Fractional formation of different phases of calcium phosphate calculated from experimental data fitted to profiles obtained from Equations 7.6 to 7.8

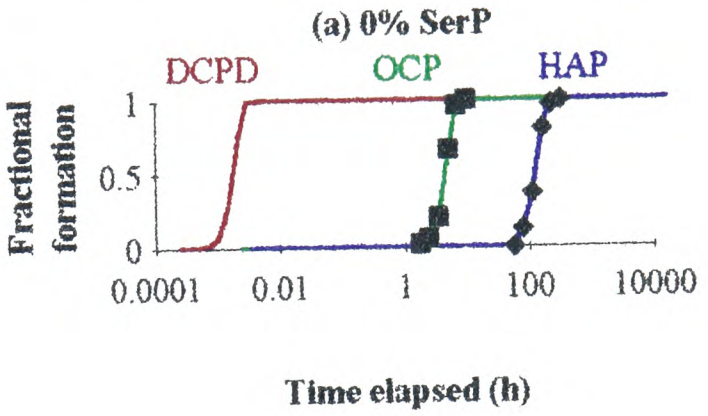

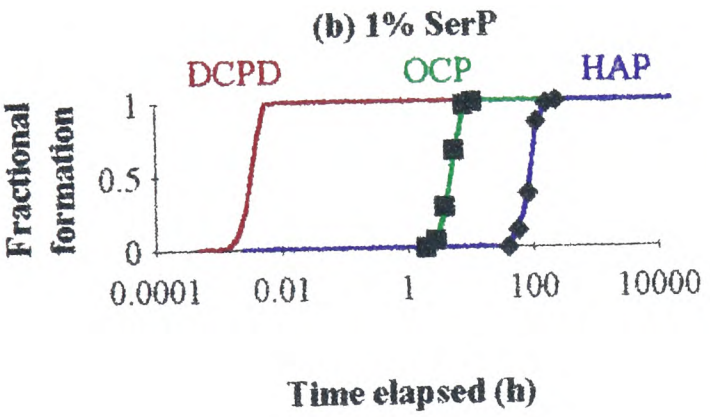

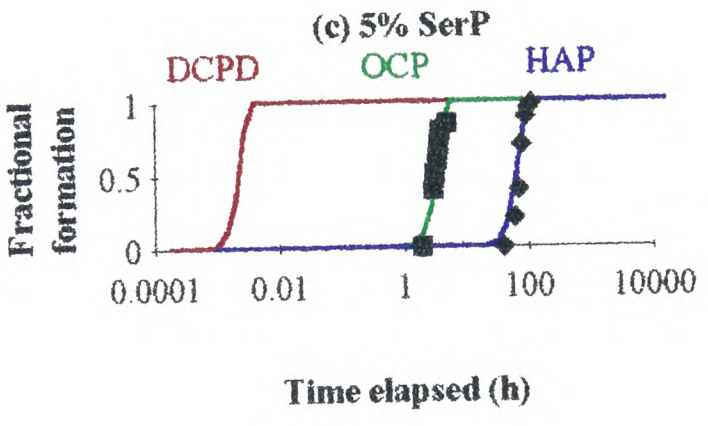

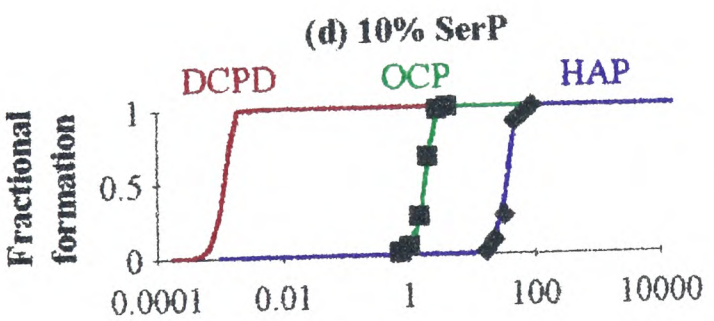

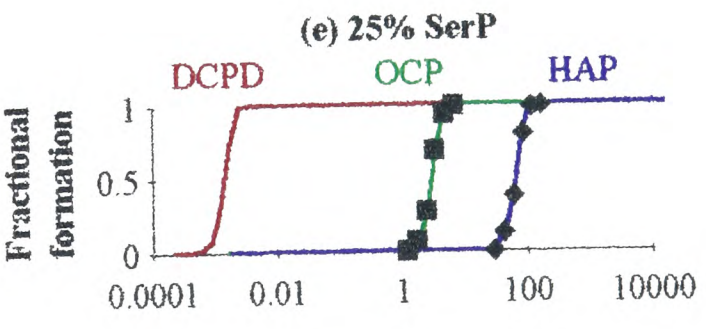

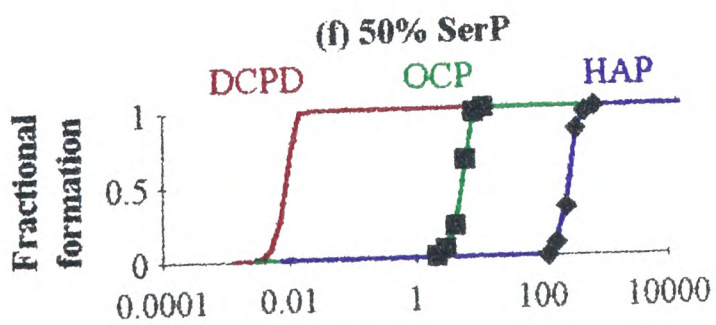

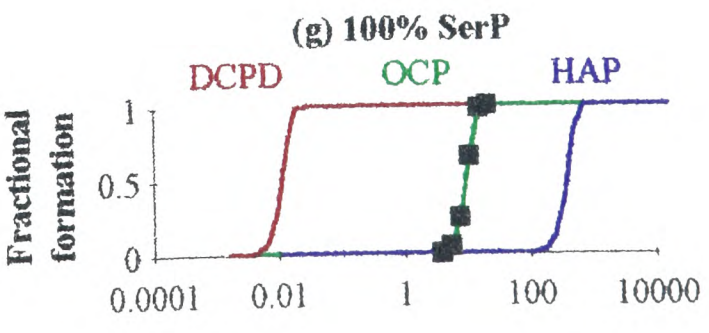

Table 7.6 System properties of solutions with different amounts of added SerP

$[SerP]_{added}$ / [ΣCa]		0%	1%	5%	10%	25%	50%	100%
n	**OCP formation**	3.24	3.68	3.75	3.81	3.78	3.73	3.66
	HAP formation	3.52	3.72	3.77	3.83	3.75	3.67	–
	mean	3.38	3.82	3.7	3.82	3.77	3.70	3.66
$\kappa\lambda$ (K^{-3} s^{-4})		$10^{-10.60}$	($10^{-10.60}$)					
ψ		(1)	0.990	0.955	0.911	0.800	0.627	0.372
K_{SerP} (M)		–	0.0350	0.0384	0.0382	0.0399	0.0401	0.0392
K_s		(0)	5.923	5.872	5.810	5.821	5.787	5.779
ln β	**DCPD**	0.253	0.253	0.253	0.252	0.251	0.249	0.247
	OCP	3.962	3.937	3.910	3.875	3.661	3.290	2.761
	HAP	16.903	16.713	16.552	16.013	12.700	9.258	7.255
log Π	**DCPD**	–0.304	–0.304	–0.305	–0.306	–0.308	–0.310	–0.313
	OCP	–7.626	–7.651	–7.687	–7.773	–7.899	–8.018	–8.293
	HAP	–13.210	–13.488	–13.962	–14.660	–15.567	–17.033	–19.888

of K_{SerP} is extremely close to the empirical value of 0.0372 reported by Sillén & Martell (1971)*. Also, K_s, the proportionality constant regarding the change in the interfacial free energy, is almost completely independent of the concentration of SerP. Thus the aforementioned assumptions have not led to a major deviation from reality.

Unlike the previous series of experiments, the effects of reduced supersaturation are no longer completely overridden by the reduction in interfacial free energy. When the SerP concentration was as high as 50% or 100% mol/mol, the drop in supersaturation, as shown in Table 7.6, began to play a rôle as important as, if not more important than, the changes in ψ and Π. In fact, both nucleation and growth would be restricted due to the considerable decrease in the supply of free

* In this reference, the complexation reaction and the equilibrium constant were defined as follows:
$SerP^{2-} + Ca^{2+} \Leftrightarrow SerPCa^{\circ}$; $K = [SerPCa^{\circ}] / ([SerP^{2-}]\,[Ca^{2+}])$ (unit: M^{-1}).
The value of *log* K was given to be 1.43. Equivalently, $K_{SerP} = 1/K = 10^{-1.43} = 0.0372$ (M).

Ca^{2+} ions in solution.

From Equation 7.6, it can be seen that, provided that $[SerP]_{added}$ is the only variable, the percentage formation of each particular phase is dependent on ζ. Now, if we define a variable Z such that:

$$Z = \left[ln\left(\frac{1}{1-\phi}\right)\right]^{4/n} \qquad ...(7.9)$$

then at a particular time, the degrees of formation, and thus the corresponding values of Z, in two solutions with SerP addition at the concentrations $[SerP]_i$ and $[SerP]_{ii}$, can be represented by:

$$\frac{Z_{ii}}{Z_i} = \frac{\zeta_{ii}}{\zeta_i} = \left(\frac{N_{ii}}{N_i}\right)\left(\frac{\Gamma_{ii}}{\Gamma_i}\right)^3 \qquad ...(7.10)$$

where $$\frac{N_{ii}}{N_i} = \frac{\Pi_{ii}}{\Pi_i} exp\left\{ -\frac{f\, v^2\, \gamma_{SL}^3}{(kT)^3}\left[\frac{\psi_{ii}}{(ln\ \beta_{ii})^2} - \frac{\psi_i}{(ln\ \beta_i)^2}\right]\right\} \qquad ...(7.11)$$

and $$\frac{\Gamma_{ii}}{\Gamma_i} = \frac{ln\ \beta_{ii}}{ln\ \beta_i} \qquad ...(7.12)$$

Equation 7.10 is derived from Equation 7.7. Now, by definition (Equation 7.9), Z increases with increasing ϕ. In Equation 7.11, Π, β and ψ are all highly complicated but determinate functions of $[SerP]_{added}$. Therefore, using zero-addition as a reference point,

$$\frac{\phi}{\phi^\circ} = f_1\left(\frac{Z}{Z^\circ}\right) = f_1\left[\left(\frac{N}{N^\circ}\right)\times\left(\frac{\Gamma}{\Gamma^\circ}\right)^3\right] = f_1\left\{ f_2\left(\frac{[SerP]_{added}}{[\Sigma Ca]}\right)\times f_3\left(\frac{[SerP]_{added}}{[\Sigma Ca]}\right)\right\} \qquad ...(7.13)$$

A computer programme was written to analyse the functions f_2 and f_3, and thus Z/Z°, (all in terms of $[SerP]_{added}/[\Sigma Ca]$) for the various calcium phosphate phases. These trends are graphically represented in Figure 7.33. It can be seen that although f_2 (nucleation) is an increasing function with increasing SerP addition, its does tend towards a plateau value as the increase inΠ is counteracted by decreases in ψ and β (see Equation 7.11). This predicted trend in the nucleation rate is supported by

Figure 7.33

The plots of f_2 [nucleation], f_3 [growth] and Z/Z° (= $f_2 \times f_3$) [fractional formation] as defined in Equations 7.9, 7.10 and 7.13 against $[SerP]_{added}$ / [ΣCa] for:

(a) DCPD;
(b) OCP; and
(c) HAP.

For DCPD, none of these functions is sensitive to changes in the x-variable. The degrees of variation range only between 0.9 and 1.3.

For OCP and HAP, nucleation is accelerated by an increased concentration of SerP, but the effect tends towards an upper limit; whereas the growth rate is decreased in a more uniform manner in both cases. The combined effect results in an optimum [SerP] value at which the formation of each of the phases is most effectively speeded up.

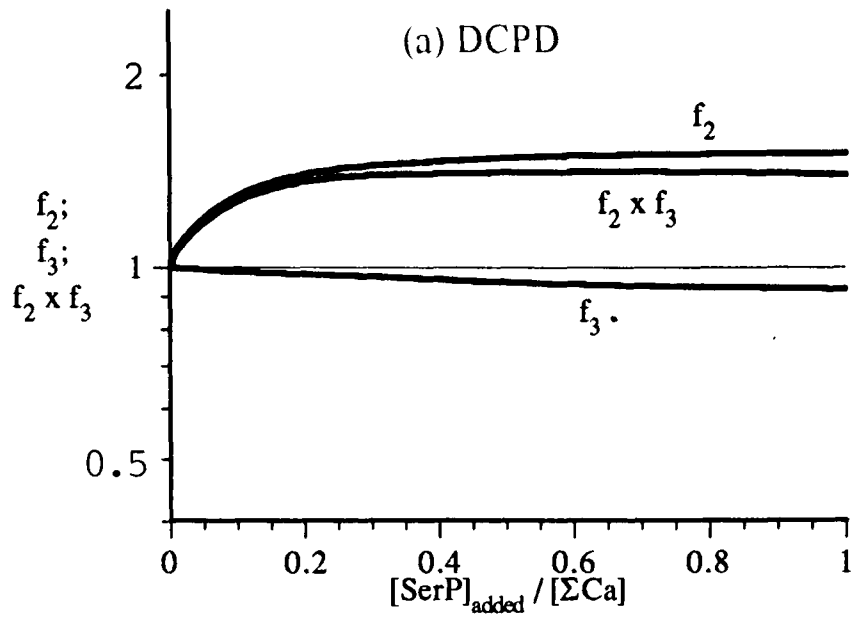

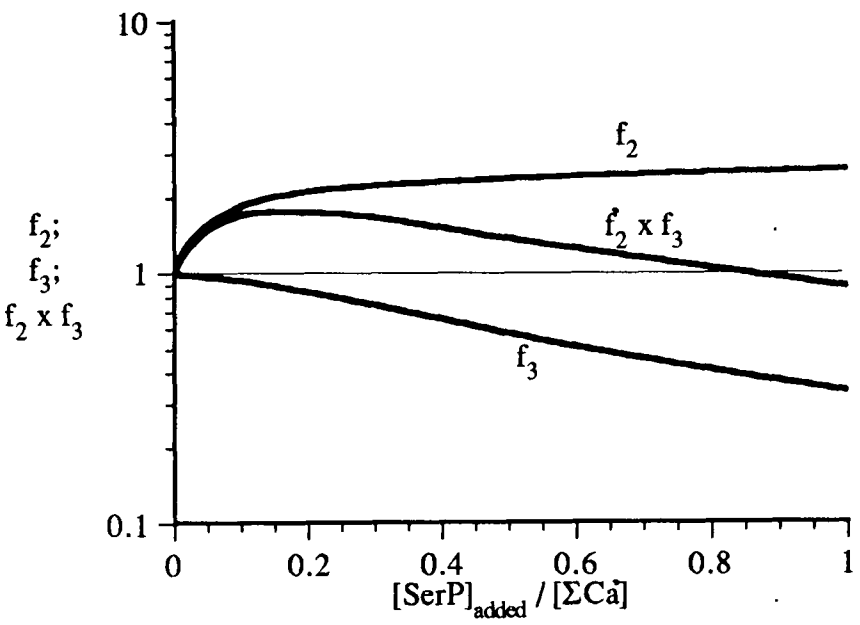

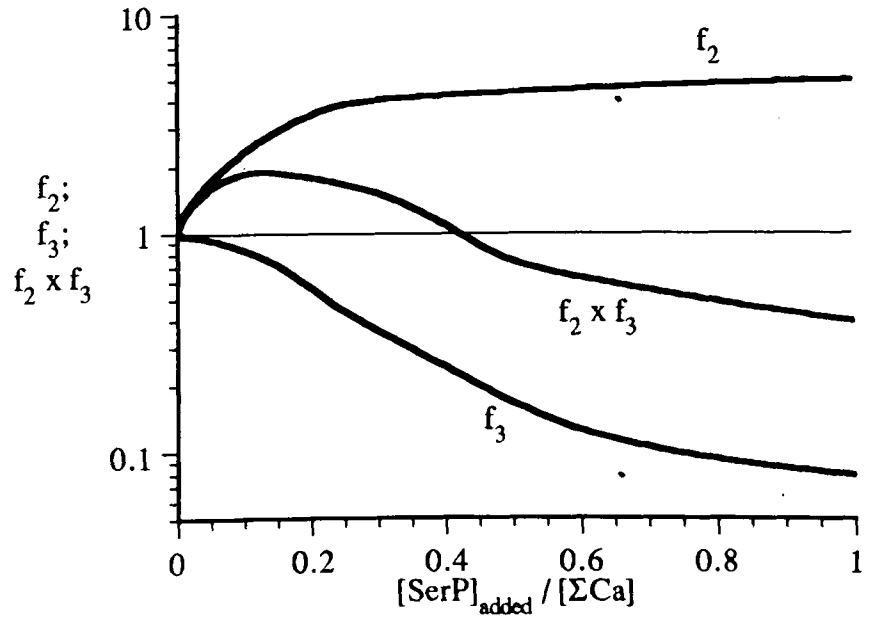

the physical distribution of precipitate as captured by scanning electron micrographs (Figures 7.22-7.28). It is clear that, in spite of the difference in transformation rates, nucleation was very effectively accelerated by small amounts of SerP addition and there is no sign of any decrease in nucleation rate at high SerP contents. On the other hand, the function f_3 (growth), as shown in Figure 7.33, decreases in a more uniform manner with increasing SerP content (Equation 7.12), an inclination which manifested itself through the decrease in crystal sizes with increasing amounts of SerP addition. Using f_2 and f_3, the optimum SerP concentrations for the formation of the various phases can be deduced from the combined function Z/Z° (Equation 7.10 and Figure 7.33). The predicted optima based on this modified Avrami model for the formation of OCP and HAP lie within the range of 10% to 25% mol/mol of SerP addition, which is consistent with the experimental findings.

As for the time exponent (n), it is found that its values are invariably in the upper region of the 3-4 range. This means that growth was again interface-controlled and that site-saturation did not take place. Thus, although the actual nucleation rate was influenced appreciably by the concentration of added SerP, the growth mechanism was not significantly affected. Referring to Figures 7.22-7.28, in spite of the different rates of precipitation and transformation, no major difference in the actual crystal morphology can be observed, agreeing with the relative constancy of the calculated values of n.

7.4 Conclusions

Constant-composition precipitation experiments were performed to assess whether the effects of a phosphorylated amino acid on calcification are dependent firstly on the nature of the side-chain to which the phosphoryl group is attached, and secondly on the concentration of the organic addition. It has been found that, regardless of the structure and the concentration of the phospho-amino acid, the preferred precursor was not affected - it was still determined predominantly by the overall $[\Sigma Ca] \times [\Sigma P]$ product of the calcifying medium. However, the precipitation and transformation rates were sensitive to changes in the organic additive.

From results of constant-composition precipitation studies using different phospho-amino acids, it becomes clear that both precipitation and phase transformation were facilitated by sterically

accessible organic molecules and by phosphoryl groups of enhanced electronegativity. These two contributing factors, however, are not of equal importance. Deduced from the inhibitory effects of TyrP and ArgP, the geometric consideration seems to exert a comparatively heavier effect in determining the promotional or inhibitory nature of a phospho-amino acid. Another point of interest is that, since the OCP-HAP transformation reaction was affected by the addition of different bio-chemicals in solution, the process must have involved surface reactions. This agrees with the assumed solvent-mediated mechanism of the phase transformation phenomenon.

When different amounts of SerP were added to the supersaturated solutions, the acceleration of both precipitation and phase transformation seemed to be maximised at an optimum concentration between 10% and 25% mol/mol. Although the presence of SerP is essential for the lowering of the activation energy, the complexation between Ca^{2+} and phospho-amino acid molecules essentially lowers the availability of free Ca^{2+} ions in any calcifying solution for the formation of growth of critical nuclei. Thus the existence of an apparent optimum corresponds to the point at which these two conflicting factors are best compromised to yield a maximum net promotional effect. Analysis of the system using the modified Avrami model has yielded values of optimum concentrations which are consistent with the experimental results. Parallel trends should also apply to other phosphorylated amino acids, since the complexation mechanism is more or less identical in all cases. However, at the same molar concentrations, phospho-amino acids with less bulky side-chains and a more charge-concentrated phosphoryl group should still induce a more prominent promotional effect on crystallisation and phase transformation, although the corresponding optima may differ.

The precipitation model developed in Chapter 5 has been appropriately modified to accommodate the presence of these bio-chemicals during calcification. Certain assumptions regarding the chemistry and the physical properties at the solid-liquid interface were made on this otherwise indeterminate system. The validity of these assumptions have been verified by comparing the resulting predictions to the actual events.

Using such a model, further information about the precipitation behaviour can be drawn. The complexation tendencies of different phospho-amino acids increase in the reverse order of molecular mass and steric accessibility. At a low concentration of organic addition, the change in the interfacial free energy is the determining factor for the increase or decrease in precipitation and

transformation rates. Precipitation was found to have involved interface-controlled growth without any saturation of potential nucleation sites.

When the concentration of the organic additive exceeds a certain level, the influence due to the reduction in supersaturation can no longer be completely overridden by the interfacial energy and the collision probability terms. In fact, both nucleation and growth are significantly affected by the diminished reservoir of free Ca^{2+} ions. This agrees with the existence of an optimum level of organic addition.

Chapter 8
CONCLUSIONS

Several aspects of the precipitation behaviour of calcium phosphate in aqueous media have been examined using different experimental techniques. The major findings of this study are summarised in the following sections.

8.1 Effects of solution composition and temperature on the rate of precipitation

By closely following the solution *p*H and the Ca^{2+} content as precipitation proceeded and by comparing these values obtained from experiments performed with different solution compositions and at different temperatures, the dependence of the rate of precipitation on these physical and chemical variables has been examined.

It has been found that precipitation was accelerated by: (i) an increase in calcium content; (ii) an increase in *p*H; and (iii) an increase in temperature. An increase in the first two system properties created an enhanced thermodynamic potential for precipitation to occur due to an increase in the supersaturation of the solution. A temperature increase, on the other hand, speeded up precipitation by improving the kinetics of the system.

8.2 Formation of precursors and their subsequent transformation to more stable phases

Similar to other sparingly soluble multi-phase inorganic salts, the formation of the thermodynamically most stable phase of calcium phosphate is often preceded by the precipitation of less supersaturated phases. Over the range of conditions covered by the experiments discussed in this thesis, HAP has invariably been the most supersaturated and the most stable phase. However, precipitate characterisation revealed that the formation of HAP always followed an induction period in which precursors such as DCPD and OCP were preferentially formed, with unique morphological properties. DCPD precipitated in the form of efflorescences whose characteristic geometry was most probably a result of a common $\{1\bar{1}0\}$ planes at the intersection of adjacent DCPD crystals. OCP crystals, on the other hand, did not show geometric features as pronounced as DCPD, but due to its crystallographic similarity to HAP, was found to deposit more uniformly on HAP substrates.

The formation of precursor phases is consistent with Ostwald's Rule of Stages. Although the thermodynamic driving force is smaller for less supersaturated phases, the presence of a larger amount of lattice ions in the solution improves the formation probability of nuclei, i.e. the favourable kinetic consideration overrides the thermodynamic potential. However, the precipitation of less supersaturated phases gives rise to an energetically metastable system. This instability is remedied through the remodelling and the transformation of the precursor phases into more stable phases. Thus, the sequence of the precipitated phases follows the reverse order of thermal stability (and hence degree of supersaturation). This sequence can be predicted as long as the degrees of supersaturation with respect to the various phases can be precisely calculated.

This has been done for calcium phosphate by considering the different physical and chemical parameters of the calcium phosphate system. The degrees of supersaturation were evaluated using the concentrations of the individual lattice ions and the thermodynamic solubility products of the various phases. These, in turn, required the assessment of the activity coefficients, the chemical equilibria among all the ions and complexes, the overall electroneutrality of the system, the ionic strength of the solution, and the temperature at which precipitation occurred. Having calculated the supersaturation with respect to each phase, the preferred precursor phase(s) under each set of experimental conditions could then be predicted.

8.3 Precipitation of calcium phosphate under constant-composition conditions

The formation and transformation of precursor phases has been carefully studied under constant-composition conditions to eliminate variations in the physical and chemical properties of the systems during experiments. A dedicated instrument has been specially designed and constructed for this application. In spite of some minor technical inadequacies of the equipment, the control and the maintenance of the solution composition has proved to be accurate and satisfactory.

Constant-composition experimental results suggested that both nucleation and growth, the two processes in precipitation, depended heavily on the degrees of supersaturation. Chemically, supersaturation determined the precursors; whereas physically, it affected the number of crystals per unit substrate surface area, the crystal size and the morphology of the solid precipitate.

8.4 Modelling of the precipitation and transformation behaviour

A model has been developed to describe the precipitation and phase transformation reactions in a typical calcification experiment. This model is based on the Avrami-Johnson-Mehl expression for three-dimensional nucleation and growth processes. The original expression has, however, been considerably altered to adapt to the present multi-ionic aqueous system, and in particular, certain approximations have been made on the nucleation terms which are related to the system geometry. The modified equation is used in conjunction with the appropriate expressions for the nucleation and growth with the aid of a number of justifiable assumptions about the reaction system. The resulting model is numerically expressed by Equations 5.13 and 5.14. Certain unknown parameters in the model were evaluated by fitting the predictions given by these two equations to constant-composition experimental results. The model was found to describe the actual precipitation process closely - it correctly predicted the sequence of phase formation, the induction time for step-wise phase transformations and the extent of transformation as a function of time. These predictions also suggested that the transformation reactions follows an interface-controlled growth mechanism without any saturation of nucleation site, and that the solution composition has little effect on the heterogeneity of the precipitation process. It confirmed that the degrees of supersaturation are the most influential factors governing the characteristics of the transformation reactions.

8.5 Effects of certain bone-specific bio-chemicals on calcium phosphate precipitation

Certain non-collagenous bone-specific bio-chemicals were introduced to supersaturated calcium phosphate solutions in order to assess their effects on *ex vivo* calcification. It has been found that, irrespective of the added organic compound and its concentration, the precursor phase to HAP formation at physiological *p*H and temperature was determined solely by the total ionic product of calcium and phosphate in the solution.

However, different bio-chemicals did exert rather different effects on other aspects of the precipitation process. SerP accelerated the overall precipitation rate and led to the formation of a large quantity of tiny plate-like OCP crystals. BPE, on the other hand, displayed the strongest inhibitory effects on mineralisation. PS and ONec significantly suppressed calcification, and caused the formation of quasi-cubic OCP precipitate with dimensions closely resembling the unit cell

parameters, implying that there was no directional preference for growth as was the case for blade- and plate-like crystals. In contrast to reports which suggest the active part played by ONec in binding apatite particles to collagen, the present study has provided evidence that in the absence of collagen, ONec did not exhibit any promotional effects on the growth of existing calcium phosphate mineral.

Compositional analyses showed that, except for the BSA-induced precipitate, the Ca/P atomic ratios of the precipitates were very close to the stoichiometry of perfect crystals, with a slight calcium deficiency. However, in the presence of BSA, the precipitate was highly deficient in calcium. This has been explained by the adsorption of BSA on the crystal surface and the consequent blockage of growth sites. Moreover, BSA also differed from the other organic compounds in that it was likely to be the only chemical which was actively consumed during the precipitation reaction. This was supported by changes in the XRD pattern and in the fracture behaviour of the crystals.

8.6 Effects of phosphorylated amino acids on the precipitation of calcium phosphate

The fact that SerP and PS exerted completely different influence on the calcification process, although they both comprise a phosphoserine backbone, implied a possible link between the aliphatic side-chains and the calcium-binding affinity of the phosphoryl group of the amino acid esters. Also, the effects of organic additives on the precipitation of calcium phosphate are likely to be dependent on the concentration of these compounds in the supersaturated media. These postulations have been verified by a series of constant-composition experiments using a variety of phosphorylated amino acids and at different concentrations.

Experimental results confirmed that both precipitation and phase transformation were facilitated by sterically accessible organic molecules and by phosphoryl groups of enhanced electronegativity, with the geometric consideration playing a more prominent rôle in the process. When different amount of organics were added to the calcifying media, the acceleration of both precipitation and phase transformation seemed to be maximised at an optimum concentration. (For SerP, the optimum lies between 10% to 25% by mole.) This has been explained by the competition for free Ca^{2+} ions by the complexation and the precipitation reactions.

The precipitation model mentioned earlier has been appropriately modified to accommodate the presence of these bio-chemicals during calcification, and has been found to accurately describe the actual event. Predictions made by this model suggested that at a low concentration of organic addition, the change in the interfacial free energy is the determining factor which governs the increase or decrease in precipitation and transformation rates. With increasing concentration, the reduction in supersaturation can no longer be overridden by changes in interfacial free energy and collision probability. The model also predicted an optimum level of organic addition which was consistent with the experimental results.

8.7 Suggestions for future work

Although this project has produced some results which have proved to be helpful in the understanding of the precipitation and transformation behaviour of calcium phosphate in aqueous media, there are still a number of areas which require further investigation. A few suggestions are listed below.

8.7.1 Precipitation experiments using collagen substrates

Although the precipitation behaviour of calcium phosphate on HAP substrates under physiological conditions is analogous to the growth of hard-tissue minerals within the body, the*de novo* formation of mineral on the collagen network is clearly of equal importance both for a more complete understanding of the physiological mineralisation process and for the manufacture of a good biomaterial for hard-tissue replacement. Unfortunately, using collagen as a substrate will introduce extra variables in the calcifying system. For example, the physical characterisation of collagen substrates will not be as straightforward as for HAP; and the well-established affinity of collagen for phosphate ions (Clarke 1991) will create further confusion in the collection of co-existing chemical equilibria in the system.

8.7.2 Further improvement of the constant-composition technique

The shortcomings and the inadequacies of the present technique has already been discussed. Although they have not presented significant difficulties under the conditions covered by the current

experiments, the inaccuracy they may give rise to under more extreme conditions cannot be overlooked.

8.7.3 Assessment of the transformation model through a mechanistic approach

Although the transformation model described in this work satisfactorily predicts and describes the precipitation behaviour, it has not been developed through rigorous mechanistic consideration. The physical significance of parameters such as the transformation coefficient ($\kappa\lambda$) has not been explicitly analysed. The model can be further enhanced if the sub-processes of precipitation and transformation, e.g. nucleation, growth and solvent-mediated redissolution, are studied in finer detail.

8.7.4 Precipitation in simulated body fluid

The introduction of single organic compounds into the reaction chamber is the first step towards the ultimate goal of actually imitating the physiological mineralisation process in which the supersaturated medium contains a variety of bio-chemicals. In order to achieve this, it is important that the effects of individual classes of bio-chemicals are fully understood before the combined effects of these compounds can be interpreted.

In brief, there are still many questions in the exciting field of calcium phosphate-related research waiting to be answered. Any success in reducing the uncertainty revolving around the subject provides for a fuller understanding of the bodily mineralisation process, but, more importantly, it is a further step in the pursuit of the ideal bone replacement material.

REFERENCES

Abbona, F.; Franchini-Angela, M. (1990): *J. Crystal Growth*, **104**, 661.

Abbona, F.; Madsen, H.E.L.; Boistelle, R. (1986): *J. Crystal Growth*, **74**, 581.

Abbona, F.; Madsen, H.E.L.; Boistelle, R. (1988): *J. Crystal Growth*, **89**, 592.

Abramson, M.B.; Katzman, R.; Gregor H.P. (1964): *J. Biol. Chem.* **239**, 70.

Amjad, Z. (1987): *Langmuir*, **3**, 1063.

Aoba, T.; Moreno, E.C. (1985): *J. Coll. Interf. Sci.*, **106**, 110.

Arends, J.; Christoffersen, J.; Christoffersen, M.R.; Eckert, H.; Fowler, B.O.; Herghebaert, J.C.; Nancollas, G.H.; Yesinowski, J.P.; Zawacki, S.J. (1987): *J. Crystal Growth*, **84**, 515.

Avrami, M. (1939): *J. Chem. Phys.*, **7**, 1103.

Avrami, M. (1940): *J. Chem. Phys.*, **8**, 212.

Avrami, M. (1941): *J. Chem. Phys.*, **9**, 177.

Bates, R.G. (1951): *J. Res. Nat. Bur. Stand.*, **47**, 127.

Bates, R.G.; Acree, S.F. (1943): *J. Res. Nat. Bur. Stand.*, **30**, 129.

Beevers, C.A. (1958): *Acta Crystal.*, **11**, 273.

Beertsen, W.; van den Bos, T. (1992): *J. Clin. Invest.*, **89**, 1974.

Berne, R.M.; Levy, M.N. (1988): in *Physiology*, 2nd ed., Mosby, St. Louis.

Betts, F.; Blumenthal, N.C.; Posner, A.S. (1981): *J. Crystal Growth*, **102**, 609.

Betts, F.; Posner, A.S. (1974): *Mat. Res. Bull.*, **9**, 907.

Blumenthal, N.C. (1989): *Clin. Orthop. Rel. Res.*, **247**, 279.

Blumenthal, N.C.; Posner, A.S. (1984): *Calcif. Tissue Int.*, **36**, 439.

Boistelle, R.; Lopez-Valero, I. (1990): *J. Crystal Growth*, **102**, 609.

Bonfield, W. (1987): *Met. Mat.*, **3**, 712.

Boskey, A.L. (1989): *Bone Min.*, **6**, 111.

Boskey, A.L.; Dick, B.L. (1991): *Calcif. Tissue Int.*, **49**, 193.

Boskey, A.L.; Posner, A.S. (1977): *Calcif. Tissue Res.*, **23**, 251.

Brečević, Lj.; Füredi-Milhofer, H. (1972): *Calcif. Tissue Res.*, **10**, 82.

Brown, W.E.; Lehr, J.R.; Smith, J.P.; Frazier, A.W. (1957): *J. Am. Chem. Soc.*, **79**, 5318.

Brown, W.E.; Mathew, M.; Tung, M.S. (1981): *Prog. Crystal Growth Charact.*, **4**, 59.

Brown, W.E.; Smith, J.P.; Lehr, J.R.; Frazier, A.W. (1962): *Nature*, **196**, 1048.

Butler, J.N. (1964): in *Ionic Equilibrium - A Mathematical Approach*, Addison-Wesley, Reading, Massachusetts.

Campbell, A.A.; Nancollas, G.H. (1991): *Coll. Surf.*, **54**, 33.

Christian, J.W. (1975): in *The Theory of Transformation in Metals and Alloys Part 1: Equilibrium and General Kinetic Theory*, 2nd ed., Pergamon Press, Oxford.

Christoffersen, J.; Christoffersen, M.R.; Kibalczyc, W.; Andersen, F.A. (1989): *J. Crystal Growth*, **84**, 767.

Clarke, K.I. (1991): *Investigation into the Properties of a Hydroxyapatite-Collagen Composite for Use as a Biomaterial*, Pt. II thesis, Dept. Mat., U. Oxford.

Cohen-Solal, L.; Lian, J.B.; Kossiva, D.; Glimcher, M.J. (1978): *Fed. Eur. Biochem. Soc. Lett.*, **89**, 107.

Dalas, E.; Ioannou, P.V.; Koutsoukos, P.G. (1989a): *Langmuir*, **5**, 157.

Dalas, E.; Koutsoukos, P.G. (1989b): *J. Chem. Soc. Faraday Trans. I*, **85(8)**, 2465.

Davies, C.W. (1962): in *Ion Association*, Butterworth, London.

Doi, Y.; Okuda, R.; Takezama, Y.; Shibata, S.; Moriwaki, Y., Wakamatsu, N.; Shimizu, N.; Moriyama, K.; Shimokawa, H. (1989): *Calcif. Tissue Int.*, **44**, 200.

Eanes, E.D.; Gillessen, I.H.; Posner, A.S. (1965): *Nature*, **208**, 365.

Eanes, E.D.; Posner, A.S. (1967): in *Proceedings of the Conference on Small Angle X-ray Scattering*, ed. Brumberger, H., Gordon Breach, New York, 493.

Eanes, E.D.; Posner, A.S. (1970): in *Biological Calcification*, ed. Schraer, H., Amsterdam, 1.

Ebrahimpour, A.; Zhang, J.; Nancollas, G.H. (1991): *J. Crystal Growth*, **113**, 83.

Endo, A.; Glimcher, M.. (1989): *Conn. Tissue Res.*, **21**, 179.

Fleisch, H.; Neuman, W.F. (1961): *Am. J. Physiol.*, **200**, 1296.

Fogg, D.N.; Wilkinson, N.T. (1958): *Analyst (London)*, **83**, 406.

Frèche, M.; Heughebaert, J.C. (1989): *J. Crystal Growth*, **94**, 947.

Fujisawa, R.; Kuboki, Y.; Sasaki, S. (1987): *Calcif. Tissue Int.*, **41**, 44.

Fuller, R.A.; Rosen, J.J. (1986): *Sci. Am.*, **255(4)**, 96.

Füredi-Milhofer, H.; Purgarić, B.; Brečević, Lj.; Pavković, N. (1971): *Calcif. Tissue Res.*, **8**, 142.

Glimcher, M.J. (1959): *Rev. Mod. Phys.*, **31(2)**, 359.

Glimcher, M.J. (1984): *Phil. Trans. Royal Soc. London*, **304B**, 479.

Glimcher, M.J.; Bonar, L.C.; Gryupas, M.D.; Landis, W.J.; Roufouse, A.H. (1981): *J. Crystal Growth*, **53**, 100.

Glimcher, M.J.; Hodge, A.J.; Schmidt, F.O. (1957): *Proc. Nat. Acad. Sci. USA*, **43**, 860.

Gregory, T.M.; Moreno, E.C.; Brown, W.E. (1970): *J. Res. Nat. Bur. Stand.*, **74A(4)**, 461.

Harned H.S.; Owen B.B. (1958): in *The Physical Chemistry of Electrolytic Solutions*, 3rd ed., Reinhold, New York.

Harper, R.A.; Posner, A.S. (1966): *Proc. Soc. Exp. Biol. Med.*, **122**, 137.

Heimke, G. (1989): *Adv. Mat.*, **1**, 7.

Hench, L.L.; Wilson, J. (1985): *Mat. Res. Soc. Symp. Proc.*, **55**, 65.

Hendrickson, H.S.; Fullington, J.G. (1965): *Biochem.*, **4**, 1599.

Heugheaert, J.C.; Nancollas, G.H. (1984): *J. Phys. Chem.*, **88**, 2478.

Heughebaert, J.C.; Zawacki, S.J.; Nancollas, G.H. (1990): *J. Coll. Interf. Sci.*, **135(1)**, 20.

Higashi, S.; Yamamuro, T.; Nakamura, T.; Ikada, Y.; Hyon, S.-H.; Jamshidi, K. (1986): *Biomat.*, 7, 183.

Hodge, A.J.; Petruska, J.A. (1963): in *Aspects of Protein Structure*, ed. Ramachandran, G.N., Academic Press, New York.

Jackson, S.A.; Cartwright, A.S.; Lewis, D. (1978): *Calcif. Tissue Res.*, **25**, 217.

Johnson, W.A.; Mehl, R.F. (1939): *Trans. Am. Inst. Min. (Metall.) Eng.*, **135**, 416.

Katthagen, B.-D. (1987): in *Bone Regeneration with Bone Substitutes - An Animal Study*, Springer-Verlag, Berlin.

Kay, M.I.; Young, R.A.; Posner, A.S. (1964): *Nature*, **204**, 1050.

Koch, W.; Pike, F.H. (1910): *J. Pharmacol.*, **2**, 245.

Koch, W.; Todd, C.C. (1911): *Proc. Am. Soc. Biol. Chem.* in *J. Biol. Chem.*, **9**, XV.

Lavernia, C.; Schönung, J.M. (1991): *Ceram. Bull.*, **70(1)**, 95.

Lundy, D.R.; Eanes, E.D. (1973): *Arch. Oral Biol.*, **18**, 813.

Marshall, R.W.; Nancollas, G.H. (1969): *J. Phys. Chem.*, **73**, 3838.

McDowell, H.; Gregory, T.M.; Brown, W.E. (1977): *J. Res. Nat. Bur. Stand.*, **81A(2/3)**, 273.

Miller, A. (1984): *Phil. Trans. Royal Soc. London*, **304B**, 455.

Mura-Galelli, M.J.; Voegel, J.C.; Behr, S.; Bres, E.F.; Schaaf, P. (1991): *Proc. Nat. Acad. Sci. USA*, **88**, 5557.

Nancollas, G.H. (1989): in *Biomineralization - Chemical and Biochemical Perspectives*, ed. Mann, S.; Webb, J.; Williams, R.J.P., VCH Verlags GmbH, Weinheim.

Nancollas, G.H.; Amjad, Z.; Koutsoukos, P. (1979): in *Chemical Modelling in Aqueous Systems*, Am. Chem. Soc., 475.

Nancollas, G.H.; Koutsoukos, P.G. (1980): *Prog. Crystal Growth Charact.*, **3**, 77.

Nancollas, G.H.; LoRe, M.; Perez, L.; Richardson, C.; Zawacki, S.J. (1989): *Anat. Rec.*, **224**, 234.

Nancollas, G.H.; Mohan, M.S. (1970): *Arch. Oral Biol.*, **15**, 731.

Nancollas, G.H.; Purdie, N. (1964): *Quart. Rev. Chem. Soc.*, **18**, 1.

Nancollas, G.H.; Tomažić, B. (1974): *J. Phys. Chem.*, **78(22)**, 2218.

Newseley, H. (1966): *Arch. Oral Biol.*, **6**, 174.

Oldberg, Å; Franzén, A.; Heinegård, D. (1986): *Proc. Nat. Acad. Sci. USA*, **83**, 8819.

Osborn, J.F. (1985): in *Implant Material Hydroxylapatite Ceramic - Basic Considerations and Clinical Applications*, Quintessenz-Verlags GmbH, Berlin.

Ostwald, W. (1879): *Z. Phys. Chem.*, **22**, 289.

Papahadjopoulos, D.; Hanahan, D.J. (1964): *Biochim. Biophys. Acta*, **90**, 436.

Pascoe, K.J. (1978): in *An Introduction to the Properties of Engineering Materials*, 3rd ed, Reinhold, Wokingham.

Porter, D.A.; Easterling, K.E. (1981): in *Phase Transformation in Metals and Alloys*, Reinhold, Wokingham.

Posner, A.S. (1978): *Bull. Hosp. Joint Dis.*, **39**, 126.

Posner, A.S.; Betts, F.; Blumenthal, N.C. (1980): *Prog. Crystal Growth Charact.*, **3**, 49.

Posner, A.S.; Blumenthal, N.C.; Boskey, A.L.; Betts, F. (1975): *J. Dent. Res.*, **54B**, 88.

Posner, A.S.; Perloff, A.; Diorio, A.F. (1958): *Acta Crystal.*, **11**, 308.

Robison, R. (1923): *Biochem. J.*, **24**, 1927.

Sillén, L.G.; Martell, A.E. (1971): in *Stability Constants (Supplement No. 1)*, Chem. Soc., London / Alden Press, Oxford.

Silverstone, L.M.; Wefel, J.S.; Zimmerman, B.F.; Clarkson, B.H.; Featherstone, M.J. (1981): *Caries Res.* **15**, 138.

Stryer, L. (1981): in *Biochemistry*, 2nd ed., Freeman, San Francisco.

Termine, J.D.; Belcourt, A.B.; Conn, K.M.; Kleiman, H.K. (1981a): *J. Biol. Chem.*, **256**, 10403.

Termine, J.D.; Eanes, E.D.; Conn, K.M. (1980): *Calcif. Tissue Int.*, **31**, 247.

Termine, J.D.; Kleinman, H.K.; Whitson, S.W.; Conn, K.M.; McGarvey, M.L.; Martin, G.R. (1981b): *Cell*, **26**, 99.

Termine, J.D.; Posner, A.S. (1967): *Calcif. Tissue Res.*, **1**, 8.

Thudichum, J.L.W. (1901): in *Die Chemische Konstitution des Gehrins des Menschen und der Tiere*, Pietzcker, Tübingen.

Tomson, M.B.; Nancollas, G.H. (1978): *Science*, **200**, 1059.

van Blitterswijk, C.A.; Hesseling, S.C.; Grote, J.J.; Koerten, H.K.; de Groot, K. (1990): *J. Biomed. Mat. Res.*, **24**, 433.

van Kemenade, M.J.J.M.; de Bruyn, P.L. (1989): *J. Coll. Interf. Sci.*, **129**, 1.

Vanderzee, C.E.; Quist, A.S. (1961): *J. Phys. Chem.*, **65**, 118.

Vaughan, J. (1981): in *The Physiology of Bone*, 3rd ed., Clarendon Press, Oxford.

Veis, A. (1988): in *1988 Cell and Molecular Biology of Vertebrate Hard Tissues*, Wiley, Chichester.

Williams, D.F. (1991): *Met. Mat.*, **7**, 24.

Winnand, L.; Dallemagne, M.J. (1962): *Nature*, **193**, 369.

Woodard, H.Q. (1962): *Physiol. Rev.*, **49**, 760.

Zawacki, S.J.; Heughebaert, J.C.; Nancollas, G.H. (1990): *J. Coll. Interf. Sci.*, **135(1)**, 33.

Zhang, J.-W.; Nancollas, G.H. (1990): *Rev. Mineral.*, **23**, 365.

Zhang, J.; Nancollas, G.H. (1992): *J. Crystal Growth*, **125**, 251.